Leishmania major promastigote entry of an autophagy-like compartment and amastigote escape from the parasitophorous vacuole

Dissertation

zur Erlangung des Grades
Doktor der Naturwissenschaften

am Fachbereich Biologie
der Johannes Gutenberg-Universität Mainz

Meike Thomas
geb. am 23.11.1985 in Freudenberg/Westfalen

Mainz, 2015

Dekan

1. Berichterstatter
2. Berichterstatter

Tag der mündlichen Prüfung: 21.05.2015

Summary

In this thesis, we investigated the interaction of the obligate intracellular parasite *Leishmania* (*L.*) *major* with two phenotypes of human monocyte derived macrophages (hMDMs). Thereby we focused on the development and maturation of the parasitophorous vacuole (PV) and could show that compartment development is dependent on the parasite stage.

Focusing on the ultrastructure of PVs containing axenic amastigotes, we demonstrated that the parasites are partially located in damaged PVs or in the cytoplasm of the host. Moreover, we visualized multiple amastigotes in a common PV 144 h p.i. in pro-inflammatory hMDM I but not in anti-inflammatory hMDM II indicating different PV development.

Regarding the promastigote form, we demonstrated a different uptake of viable and apoptotic *L. major* promastigotes by hMDMs. Viable promastigotes are predominantly taken up via the flagellum tip whereas apoptotic promastigotes enter the cells via the parasite body. Analyzing compartment maturation, we found that 20-30% of the PVs get positive for the early maturation markers PI3P and EEA1 independent of the viability of the parasites and unaffected by the human macrophage type. Subsequently, 25-40% of the parasites acquire the autophagy marker LC3 on their PV, what is independent of the viability of the parasites as well. We quantified this and in hMDM II less LC3-positive compartments formed compared to hMDM I. Analyzing the ultrastructure, we investigated that the compartments consist of a single-membrane PV characteristic for LC3-associated phagocytosis (LAP). Involvement of LAP was confirmed by demonstrating that the protein kinase ULK1 is dispensable for LC3-compartment formation around *Leishmania* PVs. Visualizing compartment dynamics in real time showed that apoptotic promastigotes are degraded in LC3-positve compartments, whereas viable promastigotes are able to get rid of LC3-protein on their PV suggesting an involvement in parasite development and survival. In this thesis, we established a lentiviral based fluorescent imaging technique that we combined with High-Pressure-Freezing (HPF) and high-resolution 3D electron microscopy. We visualized a promastigote in a LC3-compartment whose ultrastructure showed an opening of the PV to the outside. To identify new LAP markers involved in *Leishmania* infection, we established an immuno-magnetic isolation protocol for the purification of *Leishmania* containing compartments.

In conclusion, this study suggests that *L. major* compartment biogenesis and maturation in pro- and anti-inflammatory human macrophages is dependent on the parasite stage and is different between axenic amastigotes, viable promastigotes and apoptotic promastigotes. Understanding the development and maturation of *Leishmania* parasites in human host cells is important to control and combat the neglected disease leishmaniasis in the future.

Zusammenfassung

In der vorliegenden Arbeit wurde die Interaktion des obligat intrazellulären Parasiten *Leishmania (L.) major* mit zwei unterschiedlichen Phänotypen von humanen Makrophagen untersucht. Der Fokus lag dabei auf der Charakterisierung der Entwicklung und Reifung der parasitophoren Vakuole (PV) und es konnte gezeigt werden, dass die Lebensform des Parasiten einen Einfluss auf die Kompartimententwicklung in der Wirtszelle hat.

Die Untersuchung der Ultrastruktur der PV von axenischen *L. major* Amastigoten hat gezeigt, dass die Parasiten teilweise in beschädigten Kompartimenten oder im Zytoplasma der Wirtszelle lokalisiert sind. Zudem konnten in pro-inflammatorischen Makrophagen 144 h nach Infektion mehrere Amastigoten in einem gemeinsamen Kompartiment visualisiert werden, was auf eine unterschiedliche Entwicklung der PV in pro- und anti-inflammatorischen Makrophagen hindeutet.

Bezüglich der promastigoten Lebensform konnten wir darlegen, dass lebende Promastigoten überwiegend über ihre Geißel und apoptotische Promastigoten mit dem Parasitenkörper voran von humanen Makrophagen aufgenommen werden. Bei der Untersuchung der Kompartimentreifung haben wir herausgefunden, dass 20-30% der PV positiv für die frühen Maturationsmarker PI3P und EEA1 werden. Dies ist unabhängig von der Viabilität der Parasiten sowie vom Makrophagentyp. Anschließend erlangen, ebenfalls unabhängig von der Viabilität, 25-40% der Parasiten den Autophagiemarker LC3 auf ihrer PV. Quantifizierungen haben ergeben, dass sich in anti-inflammatorischen Makrophagen weniger LC3-positive Kompartimente bilden als in pro-inflammatorischen Makrophagen. Untersuchungen auf Ebene der Ultrastruktur haben zudem gezeigt, dass die Kompartimente aus einer Einzelmembran bestehen, die charakteristisch für LC3-assoziierte Phagozytose (LAP) ist. Die Beteiligung des LAP Signalweges konnte mit Hilfe der Proteinkinase ULK1, die nicht für die Rekrutierung von LC3-Proteinen zu *Leishmanien*-Kompartimenten benötigt wird, bestätigt werden. Mit Hilfe von *Live Cell Imaging* Experimenten wurde deutlich, dass apoptotische Promastigoten in LC3-positiven Kompartimenten abgebaut werden. Im Gegensatz dazu wird die PV von lebenden Promastigoten mit der Zeit LC3-negativ, ohne dass dabei der Parasit abgebaut wird, was auf eine Funktion während der Entwicklung des Parasiten hindeutet. Die in dieser Arbeit etablierte lentivirale Transduktion von primären Makrophagen als Tool für fluoreszenzmikroskopische Analysen des Infektionsprozesses, wurde mit der Methodik des Hochdruckgefrierens und mit 3D Elektronenmikroskopie kombiniert. Dabei konnte ein Parasit in einem LC3-positiven Kompartiment visualisiert werden, dessen PV in der Ultrastruktur einen Kanal zum extrazellulären Raum aufweist. Um neue LAP-Marker zu identifizieren, wurde ein immuno-magnetisches Isolationsprotokoll für die Aufreinigung von *Leishmanien* enthaltenen Kompartimenten etabliert.

Zusammenfassend legen die Ergebnisse dieser Dissertation nahe, dass die Entstehung und Reifung der *L. major* PV in pro- und anti-inflammatorischen humanen Makrophagen abhängig von der Lebensform des Parasiten ist und somit bei axenischen Amastigoten sowie lebenden und apoptotischen Promastigoten unterschiedlich vermittelt wird. Das Verständnis über die Entwicklung und Reifung von *Leishmanien* in humanen Wirtszellen trägt entscheidend dazu bei, die vernachlässigte Krankheit Leishmaniose in der Zukunft zu kontrollieren und bekämpfen zu können.

Table of contents

1 Introduction

1.1 Leishmaniasis

Leishmaniasis is a parasitic infection caused by protozoan vector-borne parasites of the genus *Leishmania* and is a WHO classified neglected tropical disease. It affects mainly poor people in developing countries and its mortality and morbidity rate show a worrying increasing trend.

1.1.1 Epidemiology and risk factors

According to the World Health Organization (WHO) 12 million people worldwide suffer from the disease, 1.3 million new cases are estimated to occur per year and 20.000-30.000 deaths are reported annually (WHO, 2015; World Health Organization, 2010). However, 350 million people are at risk of developing leishmaniasis since the disease is endemic in 88 countries, mainly in tropical and subtropical regions of the world (Figure 1). Thereby countries of the New World (Central and South America) and of the Old World (South Europe, North Africa, the Middle East and small parts of India and China) are affected (Global Medicine, 2015).

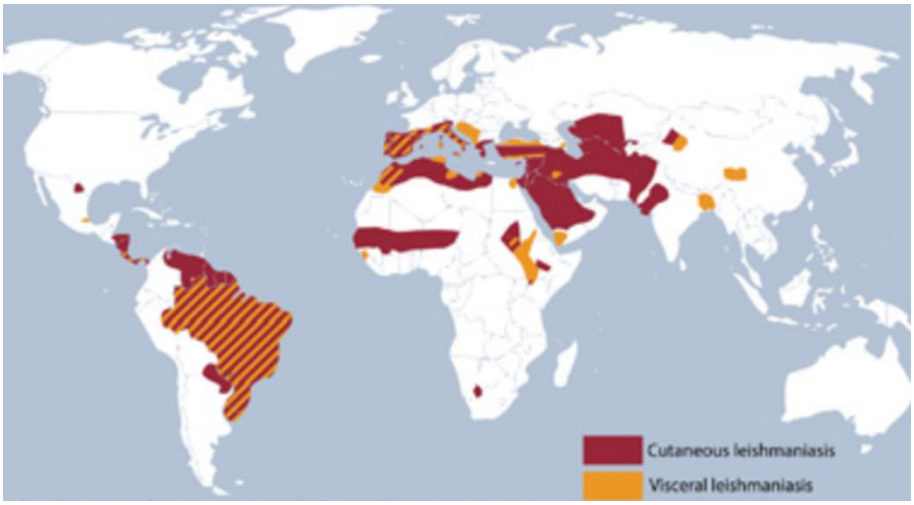

Figure 1: World map highlighting geographical distribution of cutaneous (red) and visceral (orange) leishmaniasis. (Global Medicine, 2015)

Leishmaniasis is associated with poverty and infection risk is mediated by poor housing, lack of healthcare access, malnutrition, a weak immune system and coinfection with other infectious diseases like human immunodeficiency virus (HIV) (Alvar et al., 2006). Additionally leishmaniasis is a climate-sensitive disease. The epidemiology of the disease depends on the occurrence of the female sand fly (*Phlebotomus* spp and *Lutzomyia* spp) because parasites are transmitted by the bite of the sand fly which is found throughout the intertropical and temperate regions of the world. Global warming is expected to change the epidemiology of leishmaniasis to regions that are currently free of it. Consequently, leishmaniasis could become a problem in Central Europe and Germany. There already were some observations of *Phlebotomus* species in Germany and Belgium (World Health Organization, 2010). In addition the Mediterranean area is endemic for infected dogs. Hence, leishmaniasis might evolve into a global health problem what emphasizes the importance of understanding the molecular mechanisms of the infection process to be prepared to prevent and control the disease.

1.1.2 Clinical manifestations

Leishmaniasis can be divided into three main clinical manifestations: a cutaneous, a mucocutaneous and a visceral form as well as some lesser prevalent syndroms. These forms are determined by over 20 different human pathogenic *Leishmania* species (WHO, 2015). Cutaneous leishmaniasis (CL) also known as Oriental Sore or Aleppo Boil is the most common but least severe form and is caused by several species such as *Leishmania* (*L*.) *major*, *L. tropica*, *L. mexicana*, *L. amazonensis* and *L. braziliensis* (Goto and Lauletta Lindoso, 2012). CL leads to skin infections present as singular ulcerative or nodular lesions (Figure 2 A) at the site of infection (McGwire and Satoskar, 2014). Usually they are found on uncovered areas of the body such as the face, arms and legs and spontaneously self-heal in a few months to a year regulated by infected macrophages themselves. The resolution of cutaneous lesions can be improved and accelerated by treatment.

Mucocutaneous leishmaniasis (MCL) starts with skin ulcers, which spread and metastize into mucocutaneous tissue causing chronic tissue damage of the nose, the mouth and the eyelids (Figure 2 B). It can occur months or years after resolution of primary infections and progress to hamper respiration and nutrition. MCL is caused by *L. braziliensis* and is found in South American countries (McGwire and Satoskar, 2014).

Visceral leishmaniasis (VL), also known as kala-azar or black fever, is the most serious form that results from the infection of phagocytes of the reticuloendothelial system. The parasites

or parasite-infected macrophages move from the initial site of infection to the liver, the spleen and the bone marrow leading to swelling of these organs (hepatosplenomegaly) (Figure 2 C) and bone marrow suppression. If left untreated the disease results in the death of the host by immunosuppression or secondary super-infections with other microbes. VL is caused mainly by the *L. donovani* complex but also by *L. infantum* or *L. tropica* (McGwire and Satoskar, 2014). Patients who are treated for VL and are asymptomatic for months to years can develop a so called post-kala-azar dermal leishmaniasis (PKDL) characterized by a rush of nodular lesions starting around the mouth. It occurs mainly in India and Sudan in patients infected with *L. donovani.* Probably PKDL acts as a reservoir for parasites but the pathogenesis is not fully understood (Zijlstra et al., 2003).

Figure 2: Clinical manifestations of leishmaniasis. A) CL lesion on the hand, B) MCL lesion of the mouth and nose (McGwire and Satoskar, 2014), C) VL patient with bleeding (©WHO).

1.1.3 Treatment

Depending on severity of the disease, treatment is needed. Treatment is performed using several anti-parasitic drugs such as pentavalent antimony, amphotericin B, paromomycin, pentamidine, imiquimod, miltefosine or azoles (McGwire and Satoskar, 2014). Miltefosine is reported to be the only effective oral treatment of leishmaniasis; the other drugs can only be administered by injection. However, new therapies are needed since chemical treatments can cause potentially lethal side effects and drug-resistant strains emerge rapidly. Cryotherapy applying liquid nitrogen directly on lesions (Negera et al., 2012) or radiofrequency-induced heat therapy of the lesions (Bumb et al., 2013) can be used to hasten resolution. Furthermore vaccinations using heat-killed *Leishmania* in combination with bacillus Calmette-Guerin (BCG) (Convit et al., 2004) or defined recombinant antigens together with GM-CSF (Badaro et al., 2001) have been tested in small patient numbers, but so far could not be successfully established.

1.2 The obligate intracellular parasite *Leishmania major*

At the end of the nineteenth century William Boog Leishman together with Charles Donovan and others, each independently identified the eukaryotic parasite causing leishmaniasis (World Health Organization, 2010). The parasites were finally named by Ronald Ross after Leishman, who developed a detection method for *Leishmania* in 1901 (Leishman, 1901).

1.2.1 Taxonomy

The unicellular, obligate-intracellular, protozoan parasite *Leishmania* belongs to the class of flagellates and the order of kinetoplastida, because of the existence of a large DNA-containing mitochondrium, the kinetoplast. Among kinetoplastida they are part of the family of trypanosomatida. Within the genus *Leishmania* one can distinguish between the subgenus *Vianna* with the complexes *L. braziliensis* and *L.guyanensis*. The subgenus *Leishmania* is divided into four species complexes: *L. major*, *L. donovani*, *L. tropica* and *L. aethiopica* (WHO, 2015; World Health Organization, 2010).

1.2.2 Life cycle

Leishmania have a biphasic life-cycle changing between two hosts, insects and mammals. The insects are sand flies of the genus *Phlebotomus* spp and *Lutzomyia* spp and the mammalian hosts are commonly humans, rodents and wild or domestic animals like dogs. The parasite exists in two morphologically different life stages: the motile flagellated promastigote and the non-flagellated amastigote form. Promastigotes exist and replicate in the midgut of the insect and develop from a non-virulent procyclic stage into highly infective metacyclic parasites by a process called metacyclogenesis (Giannini, 1974; Sacks and Perkins, 1984). Therefore typical environmental parameters of the sand fly midgut as alkaline pH and temperatures between 22°C and 28°C are necessary (Zilberstein and Shapira, 1994). Metacyclic promastigotes migrate to the anterior midgut and foregut and from there they are injected into the skin of their host during the blood meal of the sand fly. Thereby the fly inoculates about 100 - 3000 promastigotes into the skin (Warburg and Schlein, 1986). Most *Leishmania* promastigotes are rapidly killed in the extracellular tissue environment by complement mediated lysis (Sacks and Perkins, 1984), but some can escape and release a chemotactic factor called *Leishmania* chemotactic factor (LCF) (van Zandbergen et al., 2002). This leads to the recruitment of the first host phagocytes, the neutrophilic granulocytes (polymorphonuclear neutrophil granulocytes, PMN) (Laskay et al.,

2003; van Zandbergen et al., 2004). Two photon intravital imaging could demonstrate and confirm that PMNs are the early hosts for *L. major in vitro* (Peters et al., 2008). PMNs take up the metacyclic parasites that consist of viable and apoptotic promastigotes (Wanderley et al., 2009; van Zandbergen et al., 2006). The presence of apoptotic promastigotes in the virulent inoculum of *Leishmania* leads to increased intracellular survival rates of viable parasites inside PMNs (van Zandbergen et al., 2006). Infected PMNs produce the cytokine IL-8 (Laufs et al., 2002), accelerating the recruitment of neutrophils to the site of infection and facilitating the uptake of the parasites. It could be shown, that upon infection with *Leishmania* the apoptotic death program of PMN is delayed. However, after 42 hours the infected PMNs undergo apoptosis and this time point peaks with the migration of monocytes into the infected tissue attracted by chemotactic factors such as MIP1-β (macrophage inflammatory protein 1 beta, also known as CCL4). Hiding inside apoptotic PMNs, promastigotes are phagocytosed by macrophages (MFs) so that *Leishmania* are internalized by an indirect and "silently" way. This "Trojan horse" strategy is beneficial for *Leishmania* survival (Laskay et al., 2003; van Zandbergen et al., 2004). In addition engulfment of apoptotic promastigotes, characterized by phosphatidylserine (PS) on their surface, stimulate infected MFs to release the cytokine transforming growth factor beta (TGF-β) and interleukin-10 (IL-10), which create an anti-inflammatory milieu (Huynh et al., 2002; van Zandbergen et al., 2007). Inside the MFs the promastigotes end up in specialized compartments, the so called parasitophorous vacuole (PV). The PV represents an enclosed area that gets acidic by fusion with lysosomes. The combination of both a low pH (4.5-6) and high temperatures inside the warm-blooded mammalian host (32-37°C) contributes to the transformation of promastigotes into the amastigote form (Zilberstein and Shapira, 1994). The differentiation process already starts within 5-12 hours after phagocytosis and is finished depending on the infecting strain between 2 and 5 days (Courret et al., 2002). Promastigotes are protected to acidic environments and hydrolytic degradation by the glycosylinositolphospholipid lipophosphoglycan (LPG) through scavenging of oxygen radicals (Chan et al., 1989), modulation of nitric oxidase synthase expression (Proudfoot et al., 1996) and delay of phagolysosomal biogenesis (Desjardins and Descoteaux, 1997). Amastigotes are adapted to an acidic environment and in contrast to promastigotes are able to multiply inside MFs until the cell eventually bursts. They can infect further MFs and are responsible for disease propagation and appearance and maintenance of clinical manifestations. When the sandfly takes a blood meal from an infected host, it takes up MFs infected with amastigotes. The ingested parasites differentiate into the promastigote stage in the fly´s midgut, which then divide and migrate in direction of the proboscis, closing the life cycle. The biphasic life-cycle of *Leishmania* between an arthropod vector and a mammalian host is illustrated in Figure 3.

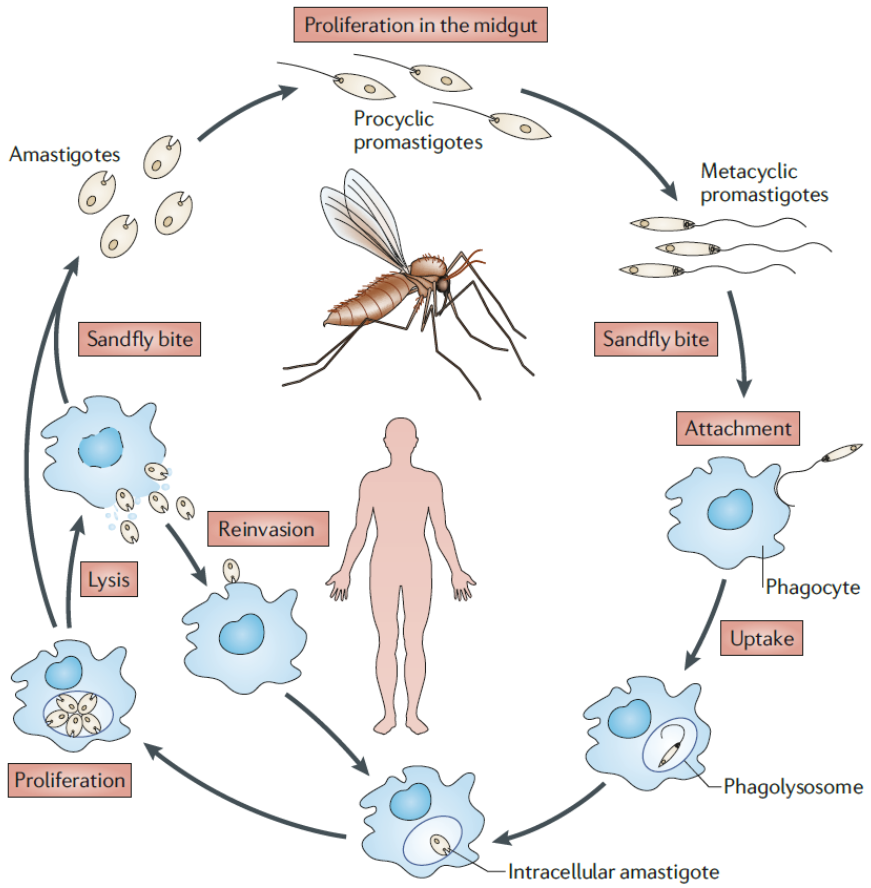

Figure 3: Biphasic life-cycle of *Leishmania* between an arthropod vector and a mammalian host. In the midgut of the female sandfly procyclic promastigotes differentiate into metacyclic promastigotes by simple division. Metacyclic promastigotes migrate to the pharyngeal valve and are transferred to the mammalian host during blood meal. They invade phagocytes (granulocytes, macrophages or dendritic cells) and transform into amastigotes. Amastigotes divide and leave infected cells for re-infection of further phagocytes. The transmission cycle is complete when during blood feeding amastigotes or amastigote infected cells are transferred into the midgut of the vector, where they convert into procyclic promastigotes. (Kaye and Scott, 2011)

1.3 Human macrophages and their role in innate and adaptive immunity

Macrophages (MFs) were discovered in 1882 by the Russian biologist Metchnikoff, who received the Nobel Prize in Medicine in 1908, shared with Paul Ehrlich, for his work on phagocytosis. MFs are key players in the immune system and are a prerequisite for protection of the host against infectious agents. Human MFs can be identified by the expression of specific markers like CD14, CD11b (CR3) (Leenen et al., 1994; Solovjov et al., 2005) and CD68 (Holness and Simmons, 1993). They evolve by differentiation of blood monocytes infiltrating infected tissues. The monocytes are attracted to the site of infection by chemotaxis and while entering the damaged tissue they undergo a series of changes induced by various cytokines (Adams and Hamilton, 1984; Nathan, 1987; Stout and Suttles,

2004) to become a differentiated macrophage. Furthermore there exist “fixed” MFs in the human body, which stay at strategic locations like mucosal surfaces and tissues of the lung, liver and spleen. MFs are, like dendritic cells and neutrophilic granulocytes, professional phagocytes, that remove apoptotic and necrotic cells and are able to internalize pathogens.

Since MFs serve as the first line of defense against infections, they are equipped with many effector functions to recognize attack and eliminate invading pathogens. They express pattern recognition receptors (PRRs) on their surface like Toll-like-receptors (TLRs), mannose-receptors and scavenger-receptors to detect infiltrating pathogens and trigger phagocytosis.

Research has focused on two human macrophage phenotypes – pro-inflammatory and anti-inflammatory macrophages (Goerdt et al., 1999; Mills et al., 2000), which differ in their morphology and their effector functions and therefore show opposite immune functions. *In vitro* these cells can be generated by culturing blood-derived monocytes, which subsequently are differentiated into monocyte-derived macrophages (MDMs) using lineage-determining cytokines. Pro-inflammatory stimuli such as Granulocyte-Macrophage colony-stimulating factor (GM-CSF) leads to the development of MDM type I (Mantovani et al., 2004; Verreck et al., 2004) with a rounded morphology (Figure 4 A) whereas the Macrophage colony-stimulating factor (M-CSF) results in the polarization of stretched MDM type II (Verreck et al., 2004) with a spindle-like shape (Figure 4 B). Depending on the type of macrophages, processed antigens lead to Th1 or Th2 responses and a different outcome of the disease (Mills et al., 2000).

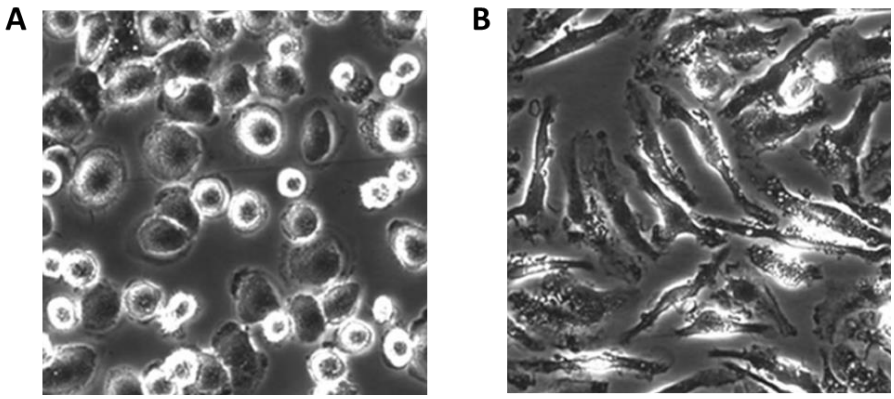

Figure 4: Morphology of differentiated macrophages. A) Macrophages differentiated with GM-CSF maintained a spherical shape during differentiation. B) Macrophages differentiated with M-CSF show an elongated shape. Modified from (Waldo et al., 2008).

Pro-inflammatory type I macrophages, also defined as “classically activated MF” (Goerdt et al., 1999), are potent effector cells that kill microorganisms. After stimulation they produce pro-inflammatory cytokines including tumor necrosis factor alpha (TNF-α), Interleukin-1 (IL-1), IL-6, IL-12 and IL-23 (Mosser and Edwards, 2008; Verreck et al., 2004, 2006). In addition, they produce antimicrobial effector molecules such as reactive oxygen intermediates (ROI) and nitrogen intermediates. Furthermore they express high levels of MHC class I and class II antigens on their surface (Cassol et al., 2010) and participate in the induction of polarized Th1 cells by priming the adaptive immune response (Mosser and Edwards, 2008). In turn, activated Th1 cells or NK cells secrete pro-inflammatory molecules (IFN-γ, TNF-α) that provoke differentiation of classically activated macrophages (Mantovani et al., 2004).

In contrast, anti-inflammatory type II macrophages (Smith et al., 1998) are defined as “alternatively activated MFs” and dampen the adaptive immune responses by driving Th2 responses and producing anti-inflammatory cytokines such as IL-10 or transforming growth factor beta (TGF-β). Furthermore they lack the production of pro-inflammatory cytokines like IL-6, TNF-α (Xu et al., 2006) and IL-12 (Verreck et al., 2004, 2006). Cytokines of the Th2 response like IL-4 and IL-13 lead to the induction and differentiation of type II macrophages (Gordon and Taylor, 2005). Alternatively activated macrophages have a higher phagocytic capacity than type I macrophages and retain their anti-inflammatory status after uptake of apoptotic cells (Xu et al., 2006, 2007). Beside phagocytosis of apoptotic cells (Xu et al., 2006) they are involved in immunoregulation, tissue-remodeling (Mantovani et al., 2004), wound healing, allergy and elimination of pathogens (Martinez et al., 2009). Therefore they are more heterogeneous than type I cells. A phenotypic characteristic of type II macrophages is the expression of the scavenger receptor CD163 on their cell surface, which is supposed to be upregulated by anti-inflammatory cytokines and down-regulated by pro-inflammatory mediators (Buechler et al., 2000).

1.4 Interaction of human macrophages with *Leishmania* parasites

Beside silent uptake of *Leishmania* parasites by human macrophages via phagocytosis of infected neutrophils, *Leishmania* are able to directly bind to surface receptors on macrophages and stimulate their phagocytosis. Promastigote stages are coated by a thick glycocalyx containing glycosylphosphatidylinositol (GPI)-anchored proteins (proteophosphoglycanes), the GPI-anchored phosphoglycane lipophosphoglycan (LPG), free GPI-anchored glycolipids termed glycoinositolphospholipids (GIPLs) (Naderer et al., 2004) and to a high extend glycoprotein 63 (gp63). LPG is an attachment-promoting factor on the cell surface of *Leishmania* but has only a minor role in macrophage invasion (Naderer et al.,

2004). The most prominent internalization mechanism includes the *L:* major surface glycoprotein gp63 also known as leishmaniolysin (Russell and Wilhelm, 1986), which is a metalloprotease that is upregulated in the metacyclic parasites and promotes parasite uptake by cleaving C3b to C3bi (Brittingham and Mosser, 1996; Brittingham et al., 1995). C3b, which is a component of the complement cascade, opsonizes the parasites, but is inactivated through cleavage to C3bi. C3bi binds with high affinity to the host cell receptors complement receptor (CR) 1 (CD35) (Rosenthal et al., 1996; da Silva et al., 1988) and CR3 (CD11b/CD18) (Russell and Wright, 1988) and thereby the metacyclic parasites gain access to the macrophage. Other identified macrophage receptors for promastigote uptake include the mannose-fucose receptor (Bogdan and Röllinghoff, 1998; Russell and Wilhelm, 1986; Wilson and Pearson, 1986) and the fibronectin receptor (Bogdan and Röllinghoff, 1998; Rizvi et al., 1988).

After the uptake of promastigotes by human macrophages, parasites end up in an intracellular compartment called parasitophorous vacuole (PV). Similar like endosomes or phagosomes this compartment undergoes modifications leading to the fusion with lysosomes. The acidified PV is characterized by a pH of 4.7-5.2 (Antoine et al., 1990), hydrolytic enzymes (Prina et al., 1990), the membrane markers LAMP1 and LAMP2 (Russell et al., 1992) and major histocompatibility complex (MHC) class II molecules (Lang et al., 1994a). In some extent pathogens are destructed in the harsh environment and peptides are presented in MHC class II molecules on the cell surface to activate the adaptive immune response. Together with cytokine secretion and expression of co-stimulatory molecules, a T cell response may be provoked (Bogdan et al., 1990). In turn, a Th1 response leads to the production of inflammatory cytokines such as INF-γ, IL-2, IL-12 and TNF-β, which activate the generation of reactive oxygen species (ROS) like hyperoxide anion (superoxide, O2·-) or hydrogen peroxide (H_2O_2) by the nicotinamide adenine dinucleotide phosphate-oxidase (NADPH oxidase) and superoxide dismutase (Kumar et al., 2002). Furthermore the expression of inducible nitric oxide synthase (iNOS) is induced (Liew et al., 1990) what results in stimulation of murine macrophages for improved intracellular killing (Bogdan and Röllinghoff, 1998). In humans the role of nitrogen oxide (NO) induction is controversial, but recently the involvement of the antimicrobial peptide cathelicidin (LL-37) in elimination of promastigotes could be demonstrated (Bank, 2012).

However, *Leishmania* promastigotes are protected from the acidic environment by their thick glycocalyx and partly are able to escape destruction and transform into multiplying amastigotes. Interestingly, amastigotes miss the dense glycocalyx on their surface, what correlates with a reduced LPG (McConville and Blackwell, 1991; Pimenta et al., 1991) and gp63 (Bahr et al., 1993) expression. Furthermore it was shown, that amastigotes express a

structurally different LPG than metacyclic promastigotes (Glaser et al., 1991; Turco and Sacks, 1991). Therefore amastigotes must invade new host cells by a different strategy than promastigotes. Microscopic data demonstrate engulfment of promastigotes by membrane ruffles forming at the flagellum tip whereas amastigotes appear to sink into the human macrophages. Experiments using axenic amastigotes showed that *L. major* amastigotes do not infect human neutrophils but are highly infective for human macrophages. In addition, amastigote uptake by macrophages is more efficient than promastigote engulfment (Wenzel et al., 2012). Further studies on amastigote internalization suggest an uptake via CR3 as well as Fc receptor mediated uptake after immunoglobulin opsonisation (Guy and Belosevic, 1993). Moreover, evaluating the expression of the pro-inflammatory cytokine TNF-α indicates that amastigotes in contrast to promastigotes enter human macrophages in a silent way resulting in growth (Wenzel et al., 2012). However, the knowledge of the exact mechanisms by which *Leishmania* promastigotes and amastigotes enter their host cells is still fairly limited. In addition most knowledge arises from studies using murine macrophages and relatively little is known about the interaction with human macrophages. Primary human macrophages offer an ideal cell model to study the human disease leishmaniasis, because in contrast to immortalized cell lines they retain important physiological properties and in contrast to mouse cells they closely mimic the *in vivo* conditions.

1.5 Uptake mechanisms of pathogens by human macrophages

1.5.1 Endocytosis

Endocytosis is a process by which a cell can absorb molecules such as proteins or pathogens. Depending on the cell type and the size of endocytozed particles one can distinguish between four main types of endocytosis: Clathrin-mediated endocytosis, Caveolar endocytosis, pinocytosis and phagocytosis (Figure 5) (Nichols, 2003).

By the clathrin-mediated endocytosis pathway or also called receptor-mediated endocytosis, ligands bind to receptors in the plasma membrane, what leads to intracellular coating of the membrane with clathrin and invagination of clathrin-coated vesicles. The vesicles are pinched off from the plasma membrane, uncoated and form a so-called early endosome (Owen, 2004).

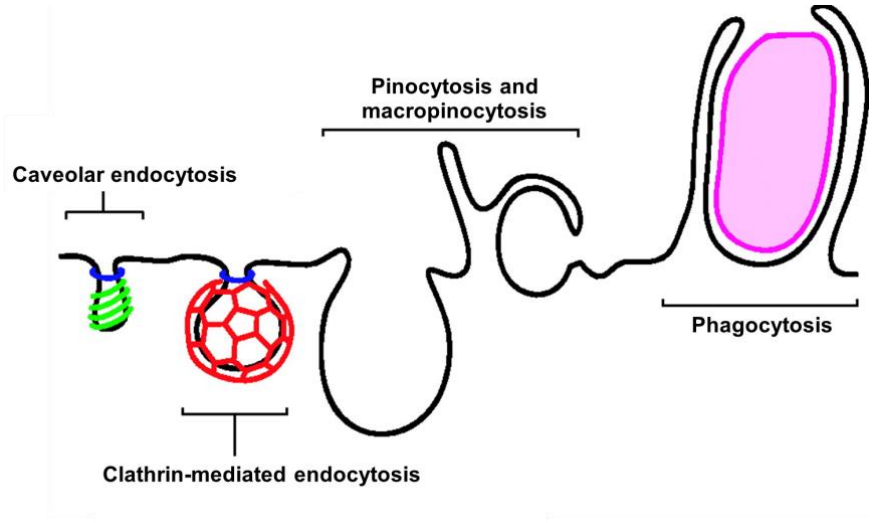

Figure 5: Different types of endocytosis. Four main types of endocytosis are shown. Modified from (Nichols, 2003).

The most common non-clathrin coated plasma membrane process is called caveolae-mediated endocytosis (Kiss, 2012). Caveolae are small invaginations of the plasma membrane which are rich in proteins like caveolin as well as lipids such as cholesterol and sphingolipids (Anderson, 1998). They are a special type of lipid rafts and have several functions in signal transduction and are usually not linked to uptake of pathogenic microorganisms, because such pathogens are too large for this engulfment pathway. However, it was demonstrated, that the engulfment of mycobacteria and *Plasmodium falciparum* (Lauer et al., 2000) are linked to caveolae-mediated endocytosis. Furthermore, it could be demonstrated, that *L. chagasi* promastigotes can be internalized by a caveolin-mediated endocytosis mechanism resulting in a delayed phagosome-lysosome fusion (Rodríguez et al., 2006).

1.5.2 Phagocytosis

Phagocytosis denotes the uptake of large particles (< 0.5 µm) and is an actin-based form of endocytosis (Chimini and Chavrier, 2000) which only occurs in specialized cells such as macrophages, dendritic cells and neutrophilic granulocytes. These cell types can take up cell debris, apoptotic cells and pathogenic organisms like microorganisms and parasites (Aderem and Underhill, 1999). Phagocytes are attracted by pathogens via chemotaxis, pathogen-associated molecular patterns (PAMPs) (Janeway, 1992) or opsonins such as C3b or antibodies. Phagocytosis of pathogens by macrophages initiates the innate immune response, which in turn orchestrates the adaptive immune response. In contrast,

phagocytosis of apoptotic cells takes place without activating pro-inflammatory responses. The macrophage receptors see a ligand on apoptotic cells that is not present on healthy cells such as phosphatidylserine in the outer leaflet of the membrane (Vieira et al., 2002).

During the phagocytic process cells change their shape by extending pseudopodia that surround the particle until membrane fusion occurs (Swanson and Baer, 1995). After engulfment the particle resides in a compartment called phagosome. Towards F-actin depolymerization the phagosome becomes accessible to early endosomes (Aderem and Underhill, 1999). The early endosomes mature to late endosomes and are then fused with lysosomes. The formation of a phagolysosome leads to degradation of the cargo proteins or pathogens, a process which can be oxygen-dependent or oxygen-independent. Oxygen-dependent degradation requires NADPH oxidase and reactive oxygen species (ROS) whereas during oxygen-independent degradation granules are released, which contain proteolytic enzymes such as defensins and lysozyme.

1.5.3 Autophagy

In eukaryotic cells two distinct mechanisms for large-scale degradation exist: the proteasome and autophagy, but only autophagy can degrade entire organelles. Autophagy means self-eating and occurs at basal levels in most tissues and contributes to the routine turnover of cytoplasmic components. It acts as a buffer against starvation by liberating building blocks from macromolecules. Autophagy can be induced by nutrient depletion, heat or oxidative stress and is also implicated in certain human diseases. Whether autophagy protects from or causes disease is still unclear. In addition, autophagy plays a role in innate and adaptive immunity (Levine and Deretic, 2007), as it can eliminate invasive pathogens such as viruses, parasites and bacteria, a process also referred to as xenophagy (Gomes and Dikic, 2014; Levine and Deretic, 2007).

There exist three types of autophagy: macroautophagy, microautophagy and chaperone-mediated autophagy, which are mechanistically different from each other. Here we will focus on macroautophagy, hereafter referred to as autophagy. During autophagy at first a so called phagophore or isolation membrane is formed (Figure 6). It enwraps cytosol or organelles to form a double-membrane vesicle; the autophagosome. The membrane source of the autophagosome is still heavily debated. The endoplasmic reticulum (ER) (Ylä-Anttila et al., 2009), mitochondria (Hailey et al., 2010), the Golgi apparatus (Ge and Schekman, 2014) and the plasma membrane (Cuervo, 2010; Ravikumar et al., 2010) have been shown to serve as sources for autophagosome formation. The closed autophagosome may fuse with the endosome and is then called amphisome. After fusion with the lysosome and the degradation

of the inner membrane, the autophagolysosome arises (Shintani and Klionsky, 2004). Autophagic vacuoles can be further classified into early or initial autophagic vacuoles (AVi), which contain morphologically intact cytosol or organelles and to late or degradative autophagic vacuoles (AVd), containing partially degraded cytoplasmic material (Dunn, 1990, 1994).

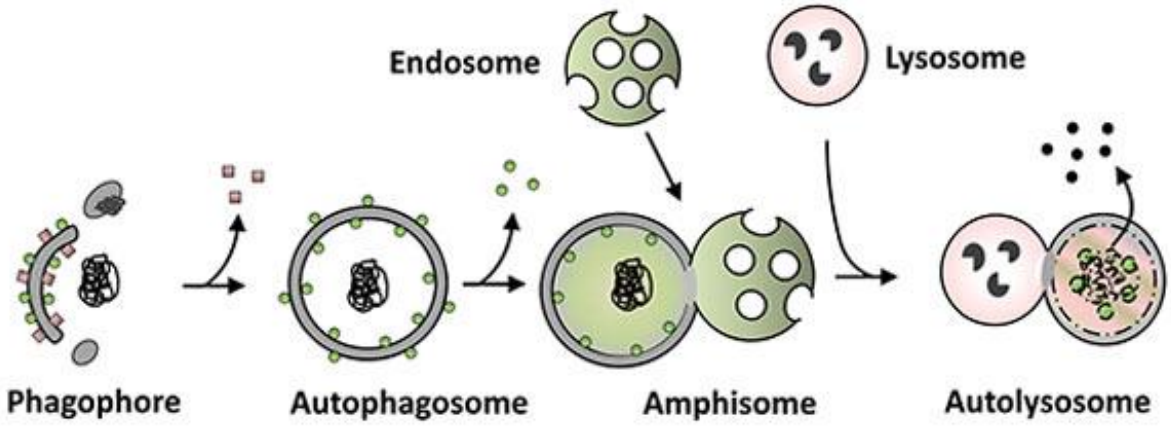

Figure 6: Autophagic sequestration process. Figure made by Pauline Isakson, Anne Simonsen group, University of Oslo.

The morphology of autophagy was first identified in the 1950s in mammalian cells and to date there are 31 autophagy-related genes (ATG) known, which were originally discovered in yeast (Huang and Klionsky, 2007). Autophagosome formation involves a nucleation step, where the unc-51 like autophagy activating kinase (ULK) complex and the class III phosphatidylinositol 3-kinase (PtdIns3K)/Vps34 complex are activated as well as an elongation step that involves two ubiquitin-like protein conjugation systems (Atg12 and LC3) (Figure 7). Usually, induction of autophagy in mammalian cells occurs by inhibition of the mammalian target of rapamycin (mTOR) through nutrient deprivation. Decreased mTOR activation leads to dephosphorylation and thereby translocation of the ULK1 complex to the isolation membrane. The ULK complex is composed of ULK1 (an Atg1 homolog), ULK2, mammalian Atg13 (mAtg13), Atg101 and the scaffold protein focal adhesion kinase (FAK)-interacting protein of 200 kDa (FIP200) (Hara et al., 2008; Hosokawa et al., 2009; Jung et al., 2009; Mizushima and Levine, 2010). Vesicle nucleation is initiated by the class III PtdIns3K complex, that includes the class III kinase hVps34, Beclin-1 (a homolog of Atg6), p150 (a homolog of Vps15) and Atg14L (Atg14-like protein) (Yang and Klionsky, 2010). Phosphatidylinositol-3-phosphate (PI3P) formed by hVps34 (Mehta et al., 2014) by phosphorylation of Phosphatidylinositol (PI), a plasma membrane lipid, leads to the recruitment of two ubiquitin-like conjugation systems that are part of the vesicle elongation process to build up the autophagosome.

In the one system Atg12 is covalently conjugated to Atg5 in a reaction that requires the E1-like enzyme Atg7 and the E2-like enzyme Atg10. The Atg12-Atg5 conjugate forms a complex with Atg16L, which oligomerizes to form a large multimeric complex called Atg16L complex (Levine and Deretic, 2007). The Atg16L complex is then localized to the isolation membrane and can act as a novel E3-like enzyme, determining the sites of LC3 lipidation (Fujita et al., 2008).

The second complex involves the microtubule-associated protein 1A/1B-light chain 3 (LC3) (known as Atg8 in yeast cells) conjugation system. The protease Atg4 cleaves LC3 at its C-terminal end to generate the cytosolic form LC3-I. Via a C-terminal glycine residue LC3-I is conjugated to phosphatidylethanolamine (PE) catalyzed by the E1-like enzyme Atg7 and the E2-like enzyme Atg3 (Kabeya et al., 2003). The lipidated form of LC3 (LC3-II) is attached to both sides of the double-membrane phagophor. After autophagosome formation, bound Atg proteins are ultimately removed from the outer membrane, but LC3 bound to the inner membrane is trapped inside the vesicle. As soon as the autophagosome is completed, it rapidly fuses with lysosomes in a Rab7 dependent manner (Jäger et al., 2004) leading to degradation of the inner membrane as well as LC3 protein. LC3 conjugation to membranes serves as a widely used specific marker to study autophagosome formation.

There exist different ways to chemically modulate autophagy. The best known autophagy inducer is the pharmacological agent rapamycin (sirolimus), an inhibitor of the serine/threonine protein kinase mTOR. It is a macrocyclic antibiotic produced by the bacterium *Streptomyces hygroscopicus* and was discovered in the soil of Easter Island as an antifungal agent (Ballou and Lin, 2008). Due to its immunosuppressive properties it was used as a drug after organ transplantations. Another potent mTOR inhibitor is AZD8055 that was developed for antitumor activity and is currently in phase I clinical trials (Chresta et al., 2010). It is an ATP-competitive inhibitor and in some cell lines treatment even leads to cell death (Sini et al., 2010).

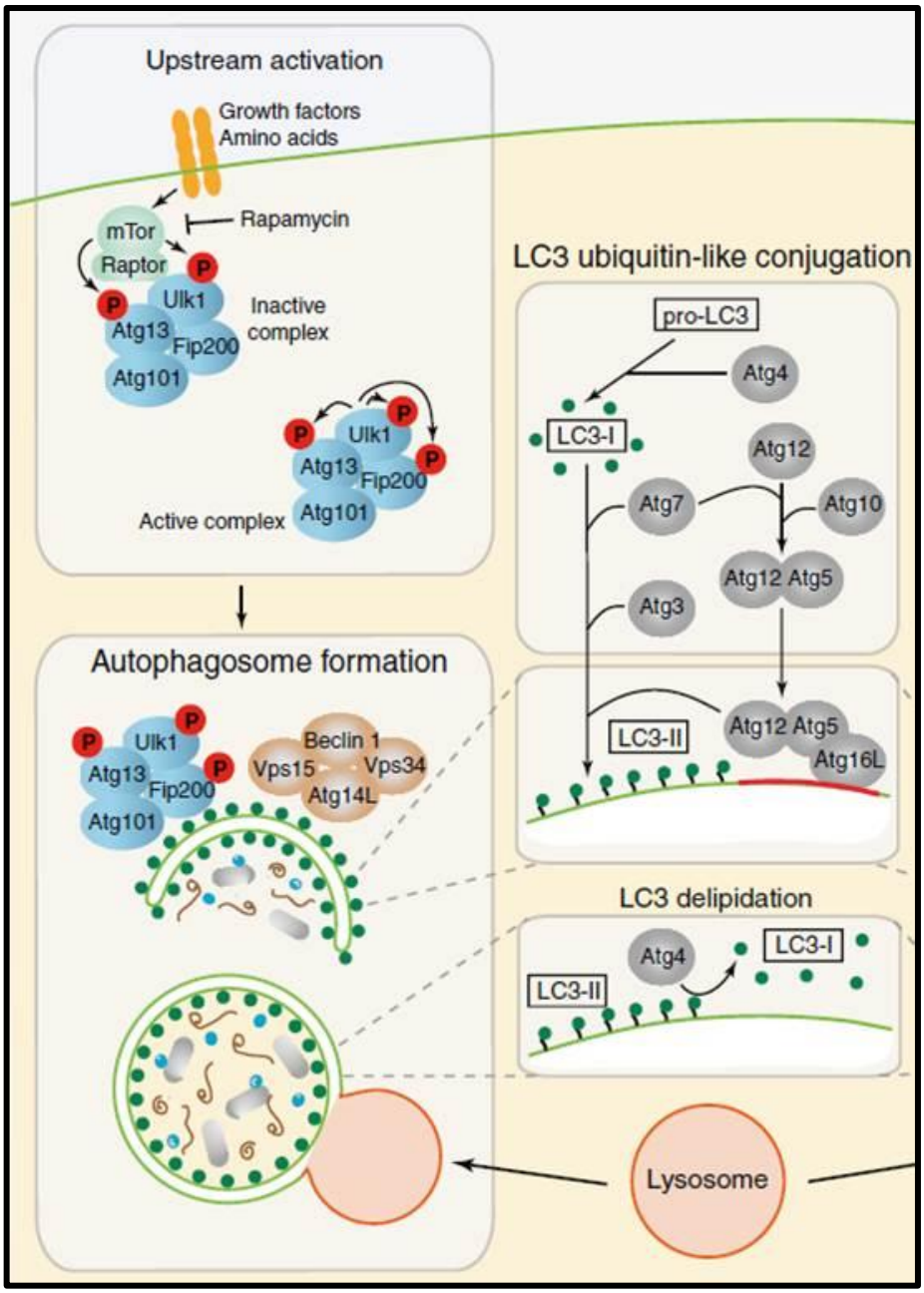

Figure 7: Molecular machinery of autophagosome formation. In the presence of growth factors or amino acids mTOR associates to and inhibits the ULK complex (ULK1/2, Atg13, Atg101, FIP200). Upon starvation the ULK complex localizes to the isolation membrane, what leads to the recruitment of the class III PtdIns3K complex (Vps34, Beclin1, Vps15, Atg14L). Vesicle elongation is mediated by two ubiquitin-like conjugation systems (Atg12 and LC3). Lipidated LC3 (LC3-II) is conjugated to arising double-membrane autophagosomes. Finally, lysosomal maturation leads to LC3 delipidation and recycling. Modified from (Florey and Overholtzer, 2012).

1.5.4 LC3-associated phagocytosis

Recently, it has been demonstrated that components of the autophagy machinery including LC3 can be recruited to phagosomes in a noncanonical form of autophagy termed LC3-associated phagocytosis (LAP). Similar like the canonical autophagy form xenophagy, LAP is involved in degradation of pathogens. Whereas xenophagy focuses on the degradation of pathogens that disable the phagolysosomal maturation or escape into the cytosol (Levine, 2005), LAP targets phagocytosed extracellular pathogens (Figure 8) (Mehta et al., 2014).

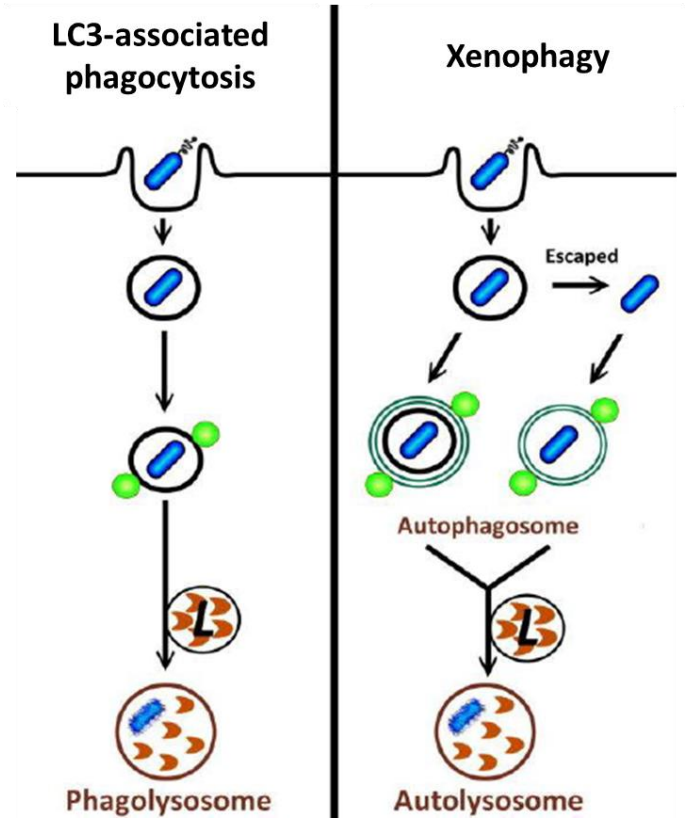

Figure 8: Pathogen destruction by LC3-associated phagocytosis (LAP) or xenophagy. LAP targets phagocytosed extracellular pathogens whereas xenophagy focuses on degradation of pathogens that disable phagosomal maturation or escape in the cytosol. Modified from (Lai and Devenish, 2012).

The exact mechanism of LAP initiation is still unknown. Several cell surface receptors have been reported to be involved in triggering LAP. Initially LC3 was found on phagosomes containing particles (zymosan, LPS- or PAM3CSK4-coated beads) that trigger Toll-like receptors (TLRs) like TLR1, TLR2 and TLR4 (Sanjuan et al., 2007). LC3 recruitment was shown to be a transient process starting within 15 min after phagocytosis and remaining for about 60 min (Sanjuan et al., 2007). TLR9 activation by DNA-containing immune complexes (DNA-IC) also requires LAP for secretion of type I interferons (IFNs) like IFN-α (Henault et al., 2012). In addition to TLRs, the innate immune receptor Dectin-1 recognizes β-glucan in

fungal cell walls (Goodridge et al., 2009) and is able to trigger lysosomal maturation (Mansour et al., 2013) in a LC3 dependent manner (Ma et al., 2014). LAP has also been associated with anti-inflammatory responses. The uptake and clearance of apoptotic cells by macrophages is mediated by the phosphatidylserine (PS) receptor T cell immunoglobulin domain and mucin domain protein-4 (TIM4) and induces LAP and the production of anti-inflammatory cytokines (Martinez et al., 2011). Moreover it has been shown, that LC3 is recruited more efficiently to IgG-opsonized particles than to uncoated or bovine serum albumin-coated beads indicating involvement of Fc receptors (FcR) in LAP (Huang et al., 2009). The activation of the NOX2 NADPH oxidase by FcRs or TLRs leads to production of microbiocidal reactive oxygen species (ROS) what results in the recruitment of LC3 to the phagosome (Huang et al., 2009).

In principle LAP involves the same molecular machinery as autophagy, but there are also some differences (Figure 9). The most significant difference distinguishes LAP from canonical autophagy on the ultrastructural level. Electron microscopic analysis showed that LAP occurs with the formation of a single-membrane compartment instead of a double-membrane autophagosome as it is characteristic for autophagy (Florey et al., 2011; Sanjuan et al., 2007). Furthermore it could be demonstrated that the mTOR regulated ULK1 pre-initiation complex composed of ULK1/2, mAtg13, Atg101 and FIP200 is dispensable for LAP (Florey et al., 2011; Henault et al., 2012; Martinez et al., 2011) and rapamycin treatment has no effect on LC3 positive phagosomes (Sanjuan et al., 2007). In contrast to that the class III PtdIns3K complex and the Atg12 conjugation system are dependent for LAP formation. Martinez and colleagues (Martinez et al., 2011) could show that Atg7-deficient macrophages fail to degrade dead cells. In concordance, Sanjuan and colleagues (Sanjuan et al., 2007) demonstrated the relevance of Atg5, Atg7, Beclin-1 and Vps34 for LC3 recruitment to phagosomes. For degradation of phagocytosed material, the phagosome matures and fuses with lysosomes. There is evidence, that LC3 covered phagosomes promote a more efficient and rapid lysosomal maturation and enhance phagosomal degradation (Mehta et al., 2014).

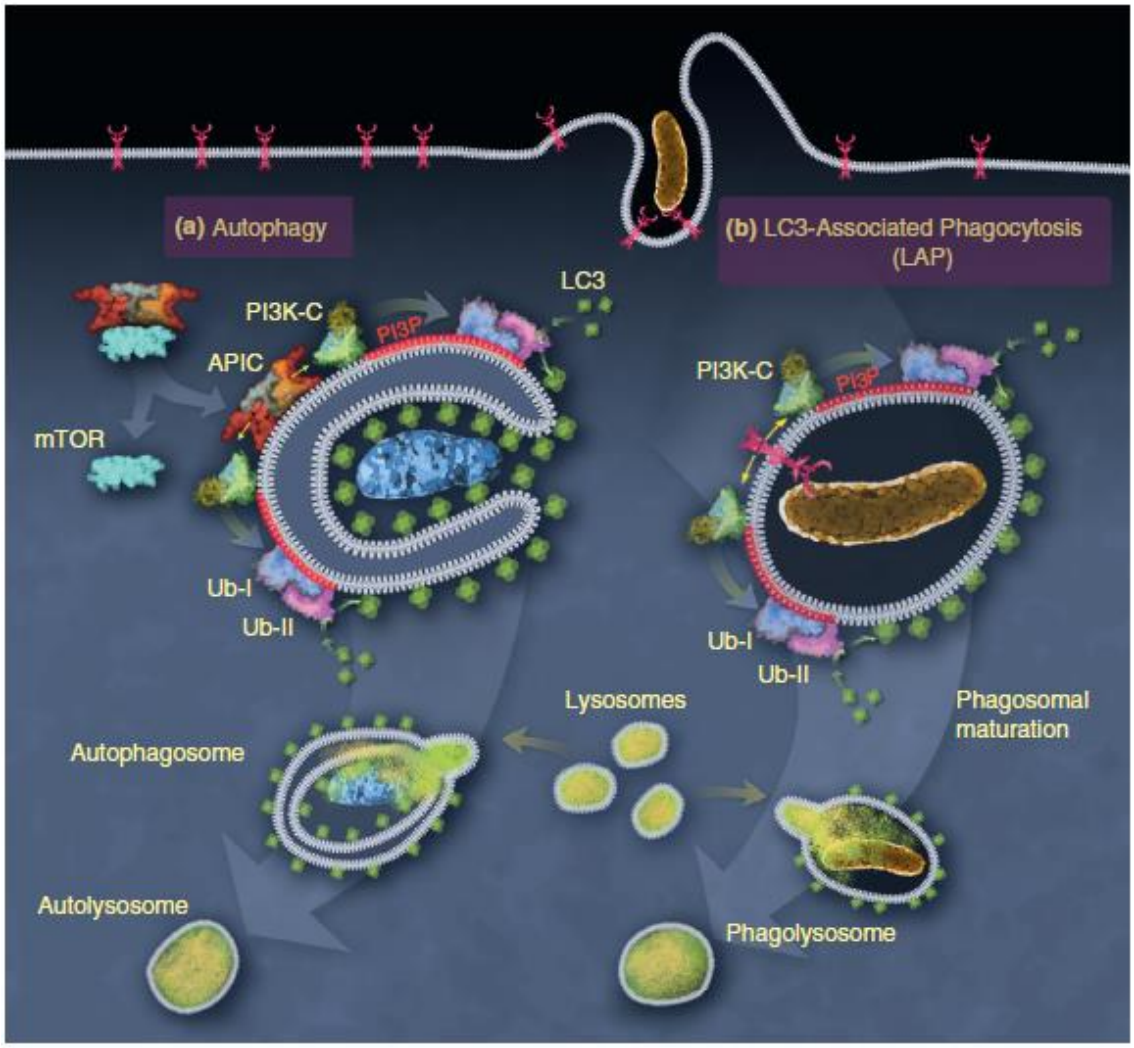

Figure 9: Autophagy versus LC3-associated phagocytosis (LAP). Autophagy initiates the formation of a double-membrane autophagosome whereas in LAP pathogens end up in a single-membrane phagosome. Both mechanisms use the same molecular machinery except of the mTOR regulated ULK pre-initiation complex (APIC) that is only involved in autophagosome formation. The class III PtdIns3K complex (PI3K-C) containing Vps34 catalyzes the formation of PI into PI3P which triggers the recruitment of two ubiquitin-like conjugation systems (Ub-I and Ub-II) that lead to conjugation of LC3-II to the membrane. Finally LC3-positive compartments fuse with lysosomes for degradation of uptaken material. Modified from (Mehta et al., 2014).

1.6 Compartment maturation of the *Leishmania*-harboring parasitophorous vacuole

L. major promastigotes are primarily phagocytosed by resident macrophages via CR3 (Von Stebut, 2007). The exact mechanisms of biogenesis and maturation of *Leishmania*-harboring PVs is still poorly understood. In principle, PV maturation follows a hierarchy like that of endosome or phagosome maturation. Nascent compartments fuse with early endosomes, late endosomes, and finally lysosomes thereby modifying the composition of their content

and membrane. Every step is characterized by the expression of different markers and an acidification of the compartments as shown in Table 1.

Table 1: Molecular markers and pH-values of maturing endosomal and phagosomal compartments. Modified from (Vieira et al., 2002).

Organelle	Markers	pH
Early endosome/ phagosome	EEA1, Rab5, PI3P, syntaxin 13, CD71, VAMP3	~ 6.0
Late endosome/ phagosome	Rab7, Rab9, mannose 6-phosphate receptor, syntaxin 7, LAMP1/2	5.5-6.0
Lysosome/ phagolysosome	LAMP1/2, cathepsins	4.5-5.5

It could be demonstrated that early *Leishmania* containing phagosomes are positive for the early-endosomal markers transferrin receptor (TfR, CD71), Rab5 and early endosome antigen 1 (EEA1) (Courret et al., 2002; Rodríguez et al., 2011). EEA1 is a hydrophilic peripheral membrane protein with a size of 180 kDa and was originally identified as a lupus erythrematosus autoantigen (Mu et al., 1995). Via the GTPase Rab5 it is recruited to endosomes and localizes on the cytoplasmic part of the membrane (Christoforidis et al., 1999). It is involved in vesicle trafficking and required for fusion of early endosomes with late endosomes or phagosomes. EEA1 functions in tethering thereby enabling docking of the vesicles by SNARE (soluble N-ethylmaleimide-sensitive-factor attachment receptor) proteins. Through its C-terminal FYVE-domain it can directly bind to phosphatidylinositol 3-phosphate (PI3P) (Gaullier et al., 1998; Patki et al., 1997) that is produced through phosphorylation of PI by PIns3K on phagosomes (Ellson et al., 2001) as well as on autophagosomes and LAP compartments (Figure 9). The FYVE zinc finger domain was identified in 1996 (Stenmark et al., 1996) and consists of about 70 conserved residues that specifically bind to PI3P with high affinity similar like the Phox homology domain (PX domain) of NADPH oxidase. It is named after four cysteine-rich proteins in which it has been found either as single finger or as tandem repeat: Fab1, YOTB, Vac1 and EEA1. The FYVE domain contains eight conserved cysteine-residues and two zinc-ions that stabilize the structure and enable binding to PI3P. Additionally three conserved amino-acid motives are involved in binding (Kutateladze, 2006). The FYVE protein structure is composed of two small beta hairpins followed by an alpha helix (Misra and Hurley, 1999). The distribution of PI3P on membranes in living cells can be measured by overexpression of two FYVE domains fused in tandem to GFP (Vieira et al., 2002).

The key event in maturation is acidification of the PV by fusion with lysosomes. Acidification is regulated by the vacuolar-type H^+-ATPase (V-ATPase) (Lukacs et al., 1990) that pumps

protons across the plasma membrane. The acidic pH is needed for hydrolytic enzyme activity of lysosomal hydrolyses including the proteases cathepsin B (Rodman et al., 1990), D and L (Tanida et al., 2005). Further marker proteins of acidic compartments are the so called lysosomal associated membrane proteins (LAMPs). LAMP1 (CD107a) and LAMP2 (CD107b), both belong to the family of lysosome-associated membrane glycoproteins (Hunziker and Geuze, 1996). They are highly similar and probably diverged from a common ancestor (Granger et al., 1990) and protect the lysosomal membrane from auto digestion. LAMP2 is a 120 kDa protein and was described to be critical for autophagy since LAMP2 deficient mice showed an accumulation of autophagic vacuoles what leads to a reduced degradation of long-lived proteins (Tanaka et al., 2000). Furthermore LAMP2-knockout in mice leads to impaired phagosomal maturation in PMNs that thus are unable to efficiently clear bacterial pathogens (Beertsen et al., 2008). The absence of functional LAMP2 in humans leads to an X-linked lysosomal disorder called Danon disease where patients suffer from hypertrophic cardiomyopathy, skeletal myopathy and mental retardation (Cottinet et al., 2011). Courret and colleagues showed the recruitment of lysosomal markers (LAMP1, cathepsin B and cathepsin D) to PVs containing *L. amazonensis* metacyclics in bone-marrow-derived macrophages (BMDM) pre-treated with IFN-γ (Courret et al., 2002). Infecting BMDMs with *L. infantum chagasi* parasites revealed that more amastigote PVs than promastigote PVs are positive for the marker LAMP1 after 1 h and 24 h of co-incubation (Rodríguez et al., 2011). Inhibition of phagoylsosomal biogenesis is one mechanism used by promastigotes to avoid microbicidal consequences. Earlier studies also showed that PVs progress differently depending on the parasite stage (promastigotes or amastigotes) (Desjardins and Descoteaux, 1997). *L. donovani* promastigotes are located in PVs which poorly fuse with late endocytic organelles (Desjardins and Descoteaux, 1997) whereas amastigote PVs rapidly fuse with late endocytic compartments (Dermine et al., 2000; Lang et al., 1994b). This observation could be associated with LPG that is only present on the surface of promastigotes (Desjardins and Descoteaux, 1997). In addition to delayed LAMP1 recruitment to promastigote PVs the V-ATPase is excluded for up to 24 h in *L. donovani* phagosomes (Vinet et al., 2009) enabling the parasites to differentiate into amastigotes. In contrast *Leishmania* amastigotes are adapted to the hydrolytic environment (Lewis and Peters, 1977) and are able to multiply within these compartments. Furthermore it seems as if different *Leishmania* species developed their own establishment strategies (Turco et al., 2001) and compartment morphologies. For *L. amazonensis* and *L. mexicana* amastigotes large communal PVs are reported (Real et al., 2008), whereas *L. major* and *L. donovani* parasites reside in tight individual PVs (Chang and Dwyer, 1978; Courret et al., 2002).

1.7 Aim of the study

Monocyte derived macrophages (MDMs) are the preferred and final host cell for the obligate intracellular parasite *Leishmania* (*L.*) *major*. Most of our knowledge about the molecular mechanisms of disease is based on studies using murine macrophages. The interaction of the parasites with human macrophages is still poorly understood. The dimorphic *Leishmania* parasites exist in a disease inducing promastigote life stage and a disease propagating amastigote form. So far it is unclear, whether promastigote and amastigote containing parasitophorous vacuoles (PVs) mature in a uniform way. Therefore in this study we focused on the development and composition of amastigote and promastigote PVs in two different phenotypes of human macrophages (pro- and anti-inflammatory macrophages) by analyzing the compartment ultrastructure in the EM and by evaluating the molecular machinery involved in compartment formation using siRNA knockdown and live cell imaging techniques. The project is guided by the following two hypotheses (Figure 10):

1.7.1 Hypothesis 1: Amastigotes re-infecting macrophages are able to escape the PV

Almost all our knowledge about disease propagation of *L. major* induced cutaneous leishmaniasis (CL) is based on promastigote research, because the infective promastigote stage can easily be cultured *in vitro* (Gupta et al., 2001). However, the amastigote stage is the disease propagating form in the mammalian host. Nevertheless direct amastigote infections could not be studied intensively, because this form was not available in adequate amounts so far. Recently our working group successful established an *in vitro* system for stable generation and culturing of axenic *L. major* amastigotes (Wenzel et al., 2012). In the first part of this thesis we therefore focused on the analysis of the *L. major* amastigote containing PV inside hMDMs on the ultrastructural level by electron microscopy (Figure 10).

Aim 1: Comparison of chemical fixation and HPF to find an appropriate sample preparation method for analyses of *L. major* amastigote containing compartments inside hMDMs by TEM.

Aim 2: Evaluation of parasite escape and PV integrity after direct infection of hMDMs with axenic *L. major* amastigotes to imitate re-infection of macrophages during disease development using HPF, TEM and STEM tomography.

1.7.2 Hypothesis 2: Apoptotic promastigotes enter a LC3-positive compartment, a process that might help the viable parasites to survive

In the second part of this study we focused on the *L. major* promastigote PV inside hMDMs (Figure 10). Metacyclic promastigotes consist of a highly infective mixture of viable and apoptotic parasites. Inside hMDMs different maturating compartments can contribute to either parasite survival or control. After infection, viable promastigotes enter a LAMP2-positive phagolysosome, where they transform into amastigotes, which are responsible for disease propagation. In contrast, it had been shown by immunofluorescence stainings, that apoptotic promastigotes, but not viable ones, are localized in a LC3-positive compartment (Crauwels et al., 2015). This compartment is visible already after 15 min, reaches its maximum after 3 h and almost disappears after 24 h (Gottwalt, 2011).

Aim 3: Analysis of the uptake of viable and apoptotic *L. major* promastigotes by pro- and anti-inflammatory macrophages using scanning electron microscopy (SEM) as well as light microscopy *real-time* imaging.

Aim 4: Characterization of the LC3-positive PV as an autophagy or LAP compartment by assessing the ultrastructure of the compartment membrane using electron microscopic analysis and LC3-immunogold microscopy and by examine the molecular machinery associated to the compartment by siRNA techniques targeting ULK1.

Aim 5: Establishment of lentiviral transduction of hMDMs to overcome immunofluorescence analysis of fixed samples and usage of transduced cells for quantification and dynamic visualization of LC3-compartment formation around parasites.

Aim 6: Performing correlative microscopy of promastigote PVs by combining fluorescence microscopy of LC3-transduced hMDMs with SEM analysis as well as with state of the art FIB/SEM that enables 3D imaging on the ultrastructural level.

Aim 7: Analysis of the recruitment of late (LAMP2) and early maturation markers (PI3P, EEA1) to *L. major* promastigote containing compartments and their role in parasite control using intracellular immunofluorescence stainings, lentiviral transduction and *real-time* fluorescence microscopy.

Aim 8: Immuno-magnetic isolation of *L. major* promastigote PVs from hMDMs to identify PV constituents involved in compartment biogenesis or suited to distinguish LAP from autophagy.

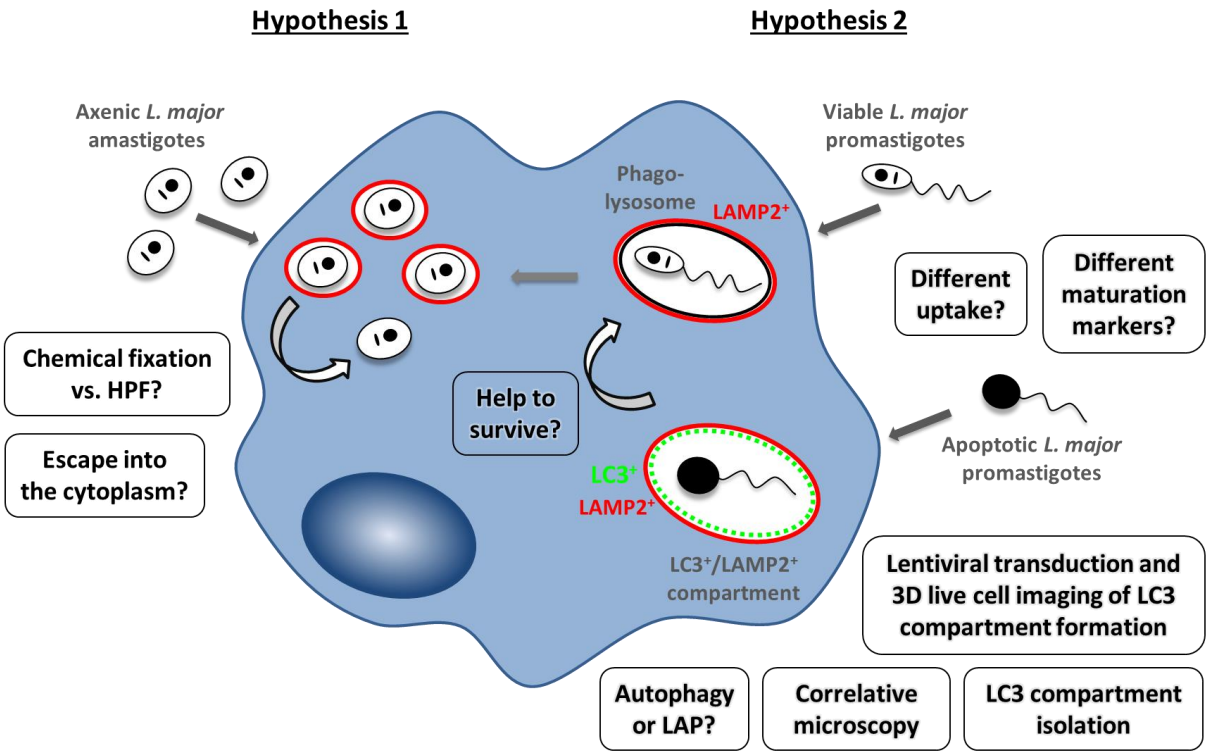

Figure 10: Hypotheses of the study. Hypotheis 1: During disease development *L. major* amastigotes escape from their compartment into the cytoplasm. Therefore we are interested in the PV integrity on the ultrastructural level. **Hypothesis 2**: Apoptotic *L. major* promastigotes enter a LC3-positive compartment and somehow help viable promastigotes to survive in the phagolysosome. In this context we are interested in analyzing the different uptake of viable and apoptotic parasites as well as different compartment maturation markers. Furthermore we want to isolate the apoptotic promastigote PV, distinguish it as an autophagy or LAP compartment as well as visualize the formation of the compartment using state of the art microscopic techniques.

2 Material and Methods

2.1 Material

2.1.1 Chemicals

Chemical	Manufacturer
2-propanol	VWR, Bruchsal, GER
β-Mercaptoethanol	Sigma-Aldrich, Deisenhof, GER
Acetic acid	Merck, Darmstadt, GER
Acetone	VWR, Bruchsal, GER
Acrylamide / Bisacrylamide solution 30%	Serva, Heidelberg, GER
Adenine	Sigma-Aldrich, Deisenhof, GER
Agarose, Type II	Sigma-Aldrich, Deisenhof, GER
Agarose, LE	Biozym Scientific GmbH, Oldendorf, GER
Agarose, Low Gelling (SeaPlaque)	FMC, Maine, USA
Ammonium chloride	Merck, Darmstadt, GER
Ammoniumpersulfat (APS)	Serva, Heidelberg, GER
Aqua bidest.	Medienküche PEI, Langen, GER
AZD8055	Selleckchem, Houston, USA
Benzil	Sigma-Aldrich, Deisenhof, GER
Benzonase ®	Novagen, Merck, Darmstadt, GER
Benzoyl Peroxide	Sigma-Aldrich, Deisenhof, GER
Biotin	Sigma-Aldrich, Deisenhof, GER
Boric acid	Merck, Darmstadt, GER
Bovine Serum Albumin (BSA)	Sigma-Aldrich, Deisenhof, GER AppliChem, Darmstadt, GER
Calciumchlorid ($CaCl_2$)	Sigma-Aldrich, Deisenhof, GER
Calcium chloride dehydrate ($CaCl_2$)	Merck, Darmstadt, GER
Casyton	Roche Innovatis AG, Reutlingen, GER
Chloroquine	Sigma-Aldrich, Deisenhof, GER
Colloidal gold particles (15 nm)	Aurion, Wageningen, NL
Cytochalasin D	Calbiochem, Merck, Darmstadt, GER
Diethyl pyrocarbonate (DEPC)	AppliChem, Darmstadt, GER
Developer G153 A+B	AGFA, Mortsel, BE
D-Glucose	Merck, Darmstadt, GER
Difco™ Brain Heart Infusion Agar	Becton Dickenson, Sparks, USA

Dimethylsulfoxid (DMSO)	Serva, Heidelberg, GER
Disodium Hydrogen phosphate (Na_2HPO_4)	Sigma-Aldrich, Deisenhof, GER
Dithiothreitol (DTT)	Sigma-Aldrich, Steinheim, GER
dNTP-Mix (10 mM each)	NEB, Frankfurt am Main, GER
Dulbecco´s Modified Eagle Medium (DMEM)	Lonza, Basel, CH
EDTA (Ethylenediaminetetraacetic acid)	Carl Roth, Karlsruhe, GER Merck, Darmstadt, GER
Ethanol (EtOH), absolut	VWR, Bruchsal, GER Carl Roth, Karlsruhe, GER
Fetal Calf Serum (FCS)	Sigma-Aldrich, Deisenhof, GER Lonza, Basel, CH
Formvar	Agar Scienific, Stansted, Essex, UK
Gelatin capsules	Plano GmbH, Wetzlar, GER
Glutaraldehyde (GA), 25% in H_2O	Sigma-Aldrich, Steinheim, GER
Glycerol (99 %)	Citifluor, London, UK
Glycine	Sigma-Aldrich, Steinheim, GER
Hemin	Sigma-Aldrich, Deisenhof, GER
HEPES (4-(2-hydroxyethyl)-1 -piperazineethanesulfonic acid)	AppliChem, Darmstadt, GER
High-purity water	Medienküche PEI, Langen, GER
Histopaque 1,077	Sigma-Aldrich, Deisenhof, GER
Histopaque® 1119	Sigma-Aldrich, Deisenhof, GER
Human recombinant Granulocyte Macrophage Colony Stimulating Factor (GM-CSF)	Bayer Healthcare Pharmaceutical, Leverkusen, GER
Human recombinant Macrophage Colony Stimulating Factor (M-CSF)	R&D Systems, Minneapolis, USA
Human Serum Type AB	Lonza, Walkersville, USA
Hydrochloric acid (HCl), 1 N	AppliChem GmbH, Darmstadt, GER
Hydrochloric acid (HCl), 25%	Merck, Darmstadt, GER
Hydrochloric acid (HCl), 37%	VWR, Bruchsal, GER
Immersion oil (Immersol™ 518F)	Carl Zeiss, Jena, GER
LB Agar	Merck, Darmstadt, GER
LB Bouillon (Miller)	Carl Roth, Karlsruhe, GER
Lead citrate	Serva Electrophoresis GmbH, Heidelberg, GER
L-glutamine	Biochrom AG, Berlin, GER
Lipobiotin	EMC microcollections GmbH, Tübingen, GER
Lipofectamine™ LTX Reagent	Invitrogen, Darmstadt, GER
Lymphocyte Separation Medium (LSM) 1077	PAA, Pasching, AUT

Magnesiumchlorid ($MgCl_2$)	Merck, Darmstadt, GER
Magnesium chloride hexahydrate ($MgCl2*6H_2O$)	Merck, Darmstadt, GER
Medium 199	Sigma-Aldrich, Deisenhof, GER
Methanol	Merck, Darmstadt, GER
Methylcellulose	Sigma-Aldrich, Deisenhof, GER
Milk powder Sucofin	TSI GmbH & Co. KG, Zeven, GER
Molecular sieve	Sigma-Aldrich, Deisenhof, GER
Mowiol 4-88	Carl Roth, Karlsruhe, GER
Natrium chloride (NaCl)	Sigma-Aldrich, Deisenhof, GER
OptiMEM® I Reduced Serum Medium	Invitrogen, Darmstadt, GER
Osmiumtetroxid (OsO_4)	Sigma-Aldrich, Deisenhof, GER ChemPur, Karlsruhe, GER
Pancoll human 1.077g/L	PAN Biotec, Aidenbach, GER
Paraformaldehyde (PFA)	Sigma-Aldrich, Deisenhof, GER
Penicillin/Streptomycin	Biochrom AG, Berlin, GER
Poly-L-lysine	Sigma-Aldrich, Deisenhof, GER
Polyvinylpyrolidone (PVP)	Sigma-Aldrich, Deisenhof, GER
Potassium chloride (KCl)	Merck, Darmstadt, GER
Potassium dihydrogen orthophosphate (KH_2PO_4)	Merck, Darmstadt, GER
Precast Gel Mini-PROTEAN TGX Gels 4-20%, 10-well	Bio-Rad, München, GER
ProLong® Gold antifade reagent	Invitrogen, Darmstadt, GER
Protease inhibitor cocktail	Roche Applied Science, Mannheim, GER
Rabbit, Blood, defibrinated	Elocin-Lab GmbH, Gladbeck, GER
Rapamycin	Cayman Chemical Company, Ann Arbor, USA
Rapid Fixer	AGFA, Mortsel, BE
RNase AWAY	VWR, Darmstadt, GER
RNase-free water	Medienküche PEI, Langen, GER
Roswell Park Memorial Institute (RPMI) 1640 Medium	Sigma-Aldrich, Deisenhof, GER
Saponin from *Quillaja bark*	Sigma-Aldrich, Steinheim, GER
SOB-Medium	Carl Roth, Karlsruhe, GER
Sodium azide (NaN_3)	Sigma-Aldrich, Steinheim, GER
Sodium chloride (NaCl)	Merck, Darmstadt, GER
Sodium dihydrogen phosphate (NaH_2PO_4)	Merck, Darmstast, GER
Sodium Dodecyl Sulfate (SDS)	Merck, Darmstadt, GER
Sodium hydroxide (NaOH) solution (10M)	Merck, Darmstadt, GER
Sodium sulfate (Na_2SO_4), waterfree	Carl Roth, Karlsruhe, GER

Sucrose	Sigma-Aldrich, Deisenhof, GER
Sulfuric acid (H_2SO_4)	Merck, Darmstadt, GER
Tannin	Carl Roth, Karlsruhe, GER
TEMED (N, N, N´,N´-tetramethylethylenediamine)	Serva, Heidelberg, GER
Triethanolamine	Sigma-Aldrich, Steinheim, GER
Tris(hydroxylmethyl)-aminomethan (Tris)	Sigma-Aldrich, Deisenhof, GER Merck, Darmstadt, GER
Tris(hydroxymethyl)-aminomethan hydrochlorid	Merck, Darmstadt, GER
Trypsin 250	Merck, Darmstadt, GER
Tween 20	Sigma-Aldrich, Steinheim, GER
Uranyl acetate (UAc)	Merck, Darmstadt, GER
Water, sterile filtered	Sigma-Aldrich, Deisenhof, GER

2.1.2 Buffers and solutions

Buffer/solution	**Composition**
Ammoniumchloride solution	0.15 M Ammoniumchloride Aqua bidest.
Auto MACS-buffer pH 7.2	1x PBS without Ca^{2+} and Mg^{2+} pH 7.1 2 mM EDTA 0.5% BSA (w/v)
Blocking solution	TBS/T + 5% milk powder (w/v)
Blotting buffer	50 mM Tris 40 mM Glycin 0.0375% SDS (w/v) 2.5% Methanol (v/v) Aqua bidest.
CASY ton	Roche Innovatis AG, Reutlingen, GER
DEPC-H_2O	0.1% DEPC Aqua bidest.
DNA loading dye (6x)	25 mM EDTA 20% glycerol (v/v) 0.025% bromphenol blue dye (w/v)
Dulbecco PBS	136.9 mM sodium chloride 2.68 mM potassium chloride 0.5 mM magnesium chloride hexahydrate 1.47 mM potassium dihydrogen orthophosphate 8.1 mM sodium dihydrogen phosphate 0.9 mM calcium chloride dehydrate Aqua bidest.

FACS-buffer	1x PBS without Ca^{2+} and Mg^{2+} pH 7.1 1% FCS (v/v) 1% BSA (w/v) 1% human serum (v/v) 0.45 µm sterile filtered
FACS-Fix	1x Dulbecco PBS 1% PFA (w/v) 0.1% NaN_3 (v/v) 0.45 µm sterile filtered
FACS-Wash	1x PBS without Ca^{2+} and Mg^{2+} pH 7.1 1% FCS (v/v) 0.1% NaN_3 (v/v) 0.45 µm sterile filtered
Hank´s Balanced Salt solution (HBSS) without Ca^{2+} and Mg^{2+}, with phenol red	Biochrom AG, Berlin, GER
HBS buffer (2x)	281 mM NaCl 100 mM HEPES-buffer 1.5 mM Na_2HPO_4 pH adjusted to 7.12 0.22 µm sterile filtered
HEPES buffer (1M) pH 7.2	Biochrom AG, Berlin, GER
Homogenization buffer	15 mM HEPES 0.5 mM MgCl2 25 mM Sucrose pH 7.2-7.4, 0.02 µm sterile filtered
MACS-buffer I	Ringer solution 0.5% BSA (w/v)
MACS-buffer II	1x PBS without Ca^{2+} and Mg^{2+} pH 7.1 0.5% BSA (w/v)
Laemmli-Buffer (6x)	500 mM Tris/HCl pH 6.8 38% Glycerol (v/v) 10% SDS (w/v) 600 mM DTT 0.01% bromphenol blue dye (w/v) Aqua bidest.
Lysis-Buffer (5x) (Borstel)	125 mM Tris-HCl pH 7.8 50% Glycerol (v/v) 10% SDS (w/v) 1% β-Mercaptoethanol (v/v) (add fresh)
PBS without Ca^{2+} and Mg^{2+} pH 7.1 (1x)	136.9 mM sodium chloride 2.68 mM kalium chloride 1.47 mM potassium dihydrogen orthophosphate 8.1 mM sodium dihydrogen phosphate Aqua bidest.

PBS/EDTA solution	1x PBS without Ca^{2+} and Mg^{2+} pH 7.1 1 mM EDTA
Ringer solution	B. Braun Melsungen AG, Melsungen, GER
Running buffer (5x)	125 mM Tris 1.25 M Glycine 0.5% SDS (w/v) Aqua bidest.
Separating gel buffer pH 8.8 (4x)	1.5 M Tris-HCl pH 8.8 0.4% SDS (w/v) Aqua bidest.
Stacking gel buffer pH 6.8 (4x)	0.5 M Tris-HCl pH 6.8 0.4% SDS (w/v) Aqua bidest.
Stripping buffer	25 mM Glycine 1% SDS (w/v) Aqua bidest. pH 2.0 with HCl
TAE buffer (20x)	0.8 M Tris-HCl pH 8.0 20 mM EDTA 2.25% acetic acid Aqua bidest.
TBE buffer (10x)	0.89 M Tris-HCl pH 8.0 0.89 M boric acid 20 mM EDTA Aqua bidest.
TBS buffer (10x)	50 mM Tris-HCl pH 7.4 150 mM NaCl Aqua bidest.
TBS/T solution	1x TBS buffer 0.5% Tween 20 (v/v)
Tris/EDTA buffer pH 8.0	10 mM Tris-HCl pH 8.0 1 mM EDTA
Tris-HCl (0.5 M) pH 6.8	460 mM Tris(hydroxymethyl)-aminomethan hydrochlorid 40 mM Tris(hydroxymethyl)-aminomethan Aqua bidest. pH 6.8 adjusted with 1 N HCl
Tris-HCl (1.5 M) pH 8.8	1.5 M Tris(hydroxymethyl)-aminomethan Aqua bidest. pH 8.8 adjusted with 25% HCl
Trypsin/EDTA solution	1x PBS without Ca^{2+} and Mg^{2+} pH 7.1 0.05% Trypsin 0.7 mM EDTA
Washing-buffer	1x PBS without Ca^{2+} and Mg^{2+} pH 7.1 5% complete-medium (v/v)

2.1.3 Media

Medium	Composition
AAM (Alex-Amastigote-Medium)	500 mL RPMI-1640 10% FCS (v/v) 3 mM L-glutamine 100 U/mL Penicillin 100 µg/mL Streptomycin pH 5.5 adjusted with 38% HCl 0.22 µm sterile filtered
Leishmania medium	500 mL RPMI-1640 5% FCS (v/v) 2 mM L-glutamine 50 µM β-Mercaptoethanol 100 U/mL Penicillin 100 µg/mL Streptomycin 10 mM HEPES buffer
Lm suspension medium	500 mL Medium 199 10% FCS (v/v) 100 U/mL Penicillin 100 µg/mL Streptomycin 20 mM HEPES buffer 5 mL 10 mM Adenine in 50 mM HEPES-buffer 1 mL 0.25% Hemin (w/v) in 50% Triethanolamine 0.5 mL 0.1% Biotin (w/v) in 95% Ethanol
Lysogeny Broth (LB) medium (Miller) pH 7.0	2.5% LB Bouillon (Miller) Aqua bidest.
Macrophage Complete-Medium	500 mL RPMI-1640 10% v/v FCS 2 mM L-glutamine 50 µM β-Mercaptoethanol 100 U/mL Penicillin 100 µg/mL Streptomycin 10 mM HEPES buffer
Macrophage culture medium (Borstel)	500 mL RPMI-1640 10% v/v FCS 1% L-glutamine
Novy-McNeal-Nicolle Blood Agar	50 mL defibrinated rabbit blood 20.8 g Difco™ Brain Heart Infusion (BHI) agar 400 mL high-purity water 100 mL 1x PBS without Ca^{2+} and Mg^{2+} pH 7.1 66.2 U/mL Penicillin 66.2 µg/mL Streptomycin
Selective Agar Plates	3.7% LB Agar Aqua bidest. + 100 µg/mL Ampicillin/Kanamycin
S.O.C. medium	2.66% SOB-Medium 20 mM D-Glucose, Aqua bidest.

2.1.4 *Leishmania* strains

Leishmania major isolate MHOM/IL/81/FEBNI:
Originally isolated from a skin biopsy of an Israeli patient and kindly provided by Dr. Frank Ebert (Bernhard Nocht Institute for Tropical Medicine, Hamburg, Germany)

Leishmania major isolates MHOM/IL/81/FEBNI DsRed and eGFP*:*
MHOM/IL/81/FEBNI isolates genetically transfected with the red fluorescent DsRed gene (from *Discosoma*) or green fluorescent eGFP gene (from *Aequorea victoria*) together with a hygromycin phosphotransferase as selection marker (Mißlitz et al., 2000).

2.1.5 Human primary cells

Human peripheral blood mononuclear cells (PBMCs) were obtained from buffy coats of healthy donors from the DRK-Blutspendedienst in Frankfurt. Subsequently, cells were isolated as described in 2.2.4.

2.1.6 Cell lines

Cell line	Cell type	Source
293 T/17 cells	human embryonic kidney cells (HEK), genetically engineered to express the large T-antigen from the polyomavirus SV40, adherent cell growth	ICLC HTL04001
HT-1080	human fibrosarcoma cell line, epithelial-like cells, adherent cell growth	ATCC CCL-121

2.1.7 Bacterial strains

Strain	Manufacturer
One Shot® TOP10 Chemically Competent *E. coli*	Invitrogen, Darmstadt, GER

2.1.8 Plasmids

Nr.	Name	Resistence	Source
TvL0006	pEGFP-C3-LC3	Kan, Amp	Addgene, Cambridge, USA
TvL0009	pcDNA3-mCherry (6B)	Amp, Neo	Addgene, Cambridge, US
TvL0010	pHIV-1 SEW	Amp	Matthias Schweizer lab, PEI, originally from Manuel Grez, Georg-Speyer-Haus
TvL0011	pPBj SEW	Amp	Matthias Schweizer lab, PEI (Kloke et al., 2010)
TvL0015	pcDNA3-LAMP2-mCherry	Amp	this thesis
TvL0017	pPBj-SW-eGFP-LC3	Amp	this thesis
TvL0018	pPBj-SW-LAMP2-mCherry	Amp	this thesis
TvL0019	pHIV-1-SW-eGFP-LC3	Amp	this thesis
TvL0020	pHIV-1-SW-LAMP2-mCherry	Amp	this thesis
TvL0028	pMD.G2 (VSV-G)	Amp	Matthias Schweizer lab, PEI, originally from D. Trono, Tronolab, CH
TvL0029	pCMVdeltaR.9	Amp	Matthias Schweizer lab, PEI, originally from U. Blömer, University Hospital Kiel (Zufferey et al., 1997)
TvL0030	pPBj-pack (SIVsmmPBj packaging)	Amp	Matthias Schweizer lab, PEI (Wolfrum et al., 2007)
TvL0031	pVpxPBjsyn	Amp	Matthias Schweizer lab, PEI (Kloke et al., 2010)
TvL0032	pEGFP-2xFYVE	Amp	Max Gutierrez, Helmholtz-Zentrum f. Infektionsforschung, Braunschweig
TvL0033	pPBj-SW-eGFP-2xFYVE	Amp	this thesis

2.1.9 Oligonucleotides

All primers were obtained from Eurofins MWG Operon (Ebersberg, GER) with HPSF purified grade and a synthesis scale of 0.01 µmol.

Primer	5´-3´ sequence	Restriction site
CMV_seq for (MT9)	CGCAAATGGGCGGTAGGCGTG	
EGFP-2xFYVE for (MT42)	TAAACTAGTATGGTGAGCAAGGGCGAGG	SpeI
EGFP-2xFYVE rev (MT43)	AAACCTGCAGGTATTATCCTTGCAAGTCATTGA	SbfI
eGFP-LC3 for (MT1)	ATAACTAGTATGGTGAGCAAGGGCGAG	SpeI
eGFP-LC3 rev (MT2)	AAACATATGTCAGTTATCTAGATCCGGTGG	NdeI
EGFP_mid_seq for (MT17)	CCTGGGGCACAAGCTGG	
GAPDH fwd	GAGTCAACGGATTTGGTCGT	
GAPDH rev	TTGATTTTGGAGGGATCTCG	
LAMP2 for (MT5)	TTTGGTACCATGGTGTGCTTCCGCCTC	KpnI
LAMP2 rev (MT6b)	TATAATATTAAATTGCTCATATCCAGCATGAT	SspI
LAMP2_end_seq for (MT19)	CTCAGCTACTGGGATGCC	
LAMP2-mCherry for (MT7)	ATAACTAGTATGGTGTGCTTCCGCCTC	SpeI
LAMP2-mCherry rev (MT8)	TTTCATATGCTACTTGTACAGCTCGTCC	NdeI
LAMP2_mid_seq for (MT18)	CCAAGGCAGCATCTAC	
LC3_seq rev (MT11)	CAGGTACAAGGAACTTTG	
mCherry_seq rev (MT20)	GATGAACTCGCCGTCCTG	
PBj-SEW for (MT3)	ATACATATGCGCGACTCTAGAGTCGAC	NdeI
PBj-SEW rev (MT4)	AAAACTAGTGACCGGTGGATCCCCC	SpeI
pcDNA3_seq for (MT12)	GGCTAACTAGAGAACCCACTG	
pcDNA3_seq rev (MT13)	GGCAACTAGAAGGCACAGTC	
SFFV_seq for (MT15)	CAGATGGTCCCCAGATATGG	
ULK1 for (MT36)	AGCACGATTTGGAGGTCGC	
ULK1 rev (MT37)	GCCACGATGTTTTCATGTTTCA	
WPRE_seq for (MT16)	CCACGTTGCCTGACAACG	

siRNA	Manufacturer
AllStars Negative Control siRNA SI03650318	Qiagen, Hilden, GER
ULK1 1 siRNA SI00053060	Qiagen, Hilden, GER
ULK1 4 siRNA SI00053081	Qiagen, Hilden, GER
ULK1 5 siRNA SI02223270	Qiagen, Hilden, GER
ULK1 6 siRNA SI02223277	Qiagen, Hilden, GER

2.1.10 Enyzmes

Enzyme	Manufacturer
Calf Intestinal Alkaline Phosphatase (CIP) (10 U/µL)	NEB, Frankfurt am Main, GER
Phusion® High-Fidelity DNA polymerase (2 U/µL)	NEB, Frankfurt am Main, GER
PfuUltra High-Fidelity DNA polymerase (2.5 U/µL)	Agilent, Santa Clara, USA
Recombinant DNase I (10 U/µL)	Roche, Mannheim, GER
Recombinant RNaseOut™ Ribonuclease Inhibitor (40 U/µL)	Invitrogen, Darmstadt, GER
Recombinant RNasin® Ribonuclease Inhibitor (20-40 U/µL)	Promega, Mannheim, GER
Restriction enzyme BamHI (10 U/µL)	Promega, Mannheim, GER
Restriction enzyme EcoRI (10 U/µL)	Promega, Mannheim, GER
Restriction enzyme KpnI (20 U/µL)	NEB, Frankfurt am Main, GER
Restriction enzyme NdeI (20 U/µL)	NEB, Frankfurt am Main, GER
Restriction enzyme SbfI (20 U/µL)	NEB, Frankfurt am Main, GER
Restriction enzyme SpeI (20 U/µL)	NEB, Frankfurt am Main, GER
Restriction enzyme SspI (20 U/µL)	NEB, Frankfurt am Main, GER
T4 DNA Ligase (400 U/µL)	NEB, Frankfurt am Main, GER
Taq-polymerase (5U/µL)	NEB, Frankfurt am Main, GER

2.1.11 Antibodies

All primary Western Blot (WB) antibodies were diluted in 5% BSA/TBST + 0.01% NaN_3 and were incubated overnight. Secondary HRP-coupled Western Blot antibodies were diluted in 5% milk powder/TBST for 1h at RT. Immunofluorescence antibodies (IF) were diluted in PBS + 0.5% saponin/1% BSA/1% FCS/1% human serum. Immunogold labeling (IG) and FACS stainings were done in PBS + 1% BSA/1% FCS/1% human serum.

Primary Antibodies	**Use**
β-Actin mouse monoclonal antibody (8H10D10), Cell Signaling (3700)	WB 1:1000
CD14 mouse monoclonal antibody, clone M5E2, Pacific Blue conjugated, IgG2aκ, BD (558121), 200 µg/mL	FACS 1 µL/100.000 cells
CD163 mouse monoclonal antibody, clone GHI/61, PE conjugated, IgG1κ, BD (556018)	FACS 10 µL/100.000 cells
Cox4 rabbit polyclonal antibody, Cell Signaling (4844)	WB 1:1000
EEA1 mouse monoclonal antibody, FITC conjugated, IgG1κ, BD (612006), 250 µg/mL	IF 1:130
GFP rabbit polyclonal antibody, Abcam (ab290)	WB 1:2000
LC3 rabbit polyclonal antibody, MBL International Corporation (PD015), 6 mg/mL	IF 1:100, IG 1:100
LC3B rabbit polyclonal antibody, Cell Signaling (2775), 19 µg/mL	IG 1:50, WB 1:1000
Leishmania metacyclic mouse serum Meta+/Meta-	WB 1:500
Leishmania metacyclic mouse serum Meta+ 1:100 in PBS + 1% FCS + 1% BSA	IF 10 µL/100.000 cells
Nucleoporin p62 mouse monoclonal antibody, IgG2bκ, BD (610497)	WB 1:500
Polyclonal 2nd boost rabbit-anti-SLA *L.major* vom 20.02.2013, 1:100 in PBS + 1% FCS + 1% BSA, Uwe Ritter, Regensburg	IF 5 µl/100.000 cells
ULK1 rabbit polyclonal antibody (H-240), Santa Cruz (sc-33182), 200 µg/mL	WB 1:500

Isotype controls	**Use**
Mouse IgG1 isotype control, PE conjugated, BD (555749)	FACS 10 µL/100.000 cells
Mouse IgG1κ isotype control, FITC conjugated, BD (555909)	IF 1:130

Mouse IgG2aκ isotype control, Pacific Blue conjugated, clone G155-178, BD (558118), 200 µg/mL	FACS 1 µL/100.000 cells
Mouse serum isotype control, Daniela Sprügel, PEI	IF 10 µL/100.000 cells of 1:100
Prä-Serum rabbit-anti-SLA *L.major* vom 02.11.2012, 1:100 in PBS + 1% FCS + 1% BSA, Uwe Ritter, Regensburg	IF 5 µl/100.000 cells
Rabbit serum isotype control, Roland Plesker, PEI, 5-10 mg/mL	dependent on primary Ab

Secondary antibodies	**Use**
Chicken anti-rabbit IgG (H+L), AF647 conjugated, Invitrogen (A-21443), 2 mg/mL	IF 1 µL/100.000 cells
Chicken anti-mouse IgG (H+L), AF 488 conjugated, Invitrogen (A-21200), 2 mg/mL	IF 1 µL/100.000 cells
EM Goat F(ab)2 anti-Rabbit IgG: 10 nm Gold BBI International, The Immunogold Specialist (EM.GFAR10)	1:50
Goat anti-rabbit IgG, conjugated with 10 nm gold particles Aurion (810.011)	1:50, 1:25
Goat anti-mouse IgG (H+L), HRP conjugated, Thermo Scientific (31430)	WB 1:5.000-1:20.000
Goat anti-rabbit IgG (H+L), HRP conjugated, Thermo Scientific (31460), 800 µg/mL	WB 1:5.000-1:10.000
Goat anti-rabbit IgG, HRP conjugated, Santa Cruz Biotechnology (sc-2004), 400 µg/mL	WB 1:1000

2.1.12 Antibiotics

Antibiotic	**final conc.**	**Manufacturer**
Hygromycin B, solution	20 ng/mL	Invitrogen, San Diego, USA
Ampicillin (1000x in water)	100 µg/ml	AppliChem GmbH, Darmstadt, GER
Kanamycin (1000x in water)	30 µg/ml	AppliChem GmbH, Darmstadt, GER

2.1.13 Dyes and magnetic particles

Dye / magnetic particle	Manufacturer
AlexaFluor 647 coupled Succinimidylesters (NHS-AF647) (10 mg/mL)	Molecular Probes, California, USA
AnnexinV Fluos	Roche Applied Science, Mannheim, GER
Bionized nanoferrite (BNF)-Dextran beads conjugated with lipobiotin	micromod Partikeltechnologie GmbH, Rostock, GER
Bromphenol blue dye	Serva, Heidelberg, GER
DAPI (5 µg/mL)	Molecular Probes, California, USA
Diff-QUIK®	Medion Diagnostics, Düdingen, CH
Ethidium bromide solution (1% in water)	Merck, Darmstadt, GER
Streptavidin-AF647 (1 mg/mL)	Life Technologies GmbH, Darmstadt, GER
Streptavidin-Cy3 (1 mg/mL)	Life Technologies GmbH, Darmstadt, GER
Streptavidin-conjugated magnetic nanoparticles	MagCellect™, R&D Systems, Wiesbaden, GER
Trypan Blue staining solution	Lonza, Basel, CH

2.1.14 Ready-to-use-kits

Kit	Manufacturer
Amersham ™ ECL ™ Western Blotting Analysis System	GE Healthcare, Buckinghamshire, UK
AnnexinV MicroBead Kit	Miltenyi Biotec, Bergisch Gladbach, GER
CD14 MicroBead Kit, human	Miltenyi Biotec, Bergisch Gladbach, GER
Epoxy Embedding Medium Kit	Sigma-Aldrich, Steinheim, GER
Im Prom-II Reverse Transkription System	Promega, Mannheim, GER
LR-Gold	Agar Scientific, Essex, UK
MESA Blue qPCR MasterMix Plus for SYBR Assay No Rox	Eurogentec, Köln, GER
MinElute® Gel Extraction Kit	Qiagen, Hilden, GER
Pierce™ BCA Protein Assay Kit	Thermo Scientific, Dreieich, GER
Pure Yield™ Plasmid Maxiprep System	Promega, Mannheim, GER
Qiaprep® Spin Miniprep Kit	Qiagen, Hilden, GER
QIAquick® PCR Purification Kit	Qiagen, Hilden, GER

RNeasy Plus Mini Kit	Qiagen, Hilden, GER
Stemfect™ RNA Transfection Kit	Stemgent, San Diego, USA
Venor®GeM-OneStep-mycoplasma Detection Kit	MinervaBiolabs, Berlin, GER

2.1.15 Size marker

Marker	Manufacturer
1 kb DNA ladder	NEB, Frankfurt am Main, GER
100 bp DNA ladder	NEB, Frankfurt am Main, GER
Full-Range Rainbow Molecular Weight Marker	GE Healthcare, Buchinghamshire, UK
PageRuler Prestained Protein Ladder	Fermentas, Thermo Scientific, Dreieich, GER

2.1.16 Laboratory supplies

Consumable	Manufacturer
8-well µ-Slide, ibidi-treat	ibidi GmbH, Planegg / Martinsried, GER
10-well microscope slides	Dunn Labortechnik, Asbach, GER
CASY cups	Roche Innovatis AG, Reutlingen, GER
Cell culture flasks with filter (25 cm^2, 75 cm^2 and 175 cm^2)	BD labware Europe, Le Pont de Claix, FRA
Cell culture petri dish (10 cm diameter)	Sarstedt, Nümbrecht, GER Greiner Bio-One, Kremsmünster, AT
Cell culture plates (6-well, 24-well)	BD labware Europe, Le Pont de Claix, FRA
Cell culture plates (96-well flat-/v-bottom)	Sarstedt, Nümbrecht, GER
Cellfunnel (single, double)	Tharmac GmbH, Waldsolms, GER
Cellspin filter cards (one/two hole/s)	Tharmac GmbH, Waldsolms, GER
Cell Scraper, 16 cm	Sarstedt, Nümbrecht, GER
Centrifuge tubes (0.2 mL)	PE Applied Biosystems, Norwalk, USA
Centrifuge tubes (1.5 mL, 2.0 mL)	Eppendorf, Hamburg, GER
Centrifuge tubes PCR Tube Multiply® Pro (0.5 mL)	Sarstedt, Nümbrecht, GER

Chamberslide, 12-well, ibidi-treat	ibidi GmbH, Planegg / Martinsried, GER
Cover Slide (24x50 mm)	VWR, Darmstadt, GER
Cryogenic vial, internal thread (2 mL)	Greiner Bio-One GmbH, Frickenhausen, GER
Cryogenic vial, external thread (1 mL)	Nunc, Thermo Scientific, Dreieich, GER
Cytocentrifuge Slides one circle, uncoated	Tharmac GmbH, Waldsolms, GER
ECL films (Hyperfilm™ ECL)	GE Healthcare, Buckinghamshire, UK
FACS microtubes (2 mL)	Micronic, Lelystad, NL
FACS tubes (5 mL) with snap-cap	BD labware Europe, Le Pont de Claix, FRA
Falcons (15 mL, 50 mL)	BD labware Europe, Le Pont de Claix, FRA
Gold spacer ring (50 µm thick, 3 mm diameter)	Plano GmbH, Wetzlar, GER
Grids (nickel, copper, 200 mesh)	Athene, Agar Scientific, Essex, UK
Grids (copper, 300 mesh)	Plano GmbH, Wetzlar, GER
Light Cycler 96-well plates with foil, white	Roche Applied Science, Darmstadt, GER
MACS LD column or LS column	Miltenyi Biotec, Bergisch Gladbach, GER
Manufix sensitive gloves	B. Braun Melsungen AG, Melsungen, GER
Microscope slide, 10-well, glass	Dunn Labortechnik GmbH, Asbach, GER
Microplate, 96 well, PS, F-bottom	Greiner Bio-One GmbH, Frickenhausen, GER
MidiMACS separator	Miltenyi Biotec, Bergisch Gladbach, GER
Millipore Express® PLUS Membrane Filters, polyethersulfone, 0.22 µm; 0.45 µm	Merck Millipore, Billerica, USA
Multichannel pipette (Research® Plus)	Eppendorf, Hamburg, GER
Nalgene™ Mr. Frosty Freezing Container	Thermo Scientific, Dreieich, GER
Nitril gloves	Ansell Healthcare, Brussels, BE
Nitrocellulose membrane (Hybond ECL blot membrane)	GE Healthcare, Buchinghamshire, UK
Neubauer improved cell counting chamber (depth 0.1 mm, 0.02 mm)	VWR, Darmstadt, GER
Pasteur pipette, glass	VWR, Darmstadt, GER
Paseur pipette, plastic	Sarstedt, Nümbrecht, GER
Petri dish (3 cm diameter)	Greiner Bio-One, Kremsmünster, AT
Pipette controller (accu-jet® pro)	BRAND, Wertheim, GER

Pipette filter tips (1-10 µL; 10-200 µL, 100-1000 µL)	Nerbe plus, Winsen/Luhe, GER
Pipettes (Research® plus: 0.5-10 µL; 10-100 µL, 20-200 µL, 100-1000 µL)	Eppendorf, Hamburg, GER
Pipette tips (0.5-10 µL; 2-200 µL; 50-1000 µL)	Eppendorf, Hamburg, GER
Polyallomer Centrifuge Tubes	Beckmann Coulter GmbH, Krefeld, GER
Polypropylene (PP) Tubes, round bottom, 14 mL	Greiner Bio-One, Kremsmünster, AT
Polystyrene Lids, PS, High profile	Greiner Bio-One GmbH, Frickenhausen, GER
Sapphire discs (160 µm thick, 3 mm diameter)	Engineering Office M. Wohlwend GmbH, Sennwald, CH
Serological pipettes, sterile (2.5 mL; 5 mL; 10 mL; 25 mL)	Greiner Bio-One, Kremsmünster, AT
Sterile filter (0.22 µm, 0.45 µm)	VWR, Darmstadt, GER
Syringe (20 mL, 50 mL)	BD labware Europe, Le Pont de Claix, FRA
Teflon bag	Süd Laborbedarf, Gauting, GER
Transfer pipette (3.5 mL)	Sarstedt, Nümbrecht, GER
Whatman paper gel blotting	VWR, Darmstadt, GER

2.1.17 Instruments

Device	**Manufacturer**
Centrifuges	
Avanti J-26XP with JE-5.0 Elutriator Rotor	Beckman Coulter, Krefeld, GER
Beckman J2-MC	Beckman Coulter, Krefeld, GER
Beckman J6-HC + JA-14 and JA-20 rotor	Beckman Coulter, Krefeld, GER
BIOLiner Buckets (75003670; 7500368)	Thermo Scientific, Dreieich, GER
Bioshield 1000 A swing-out rotor	Thermo Scientific, Dreieich, GER
Bench top centrifuges 5430 and 5430R	Eppendorf, Hamburg, GER
Bench top centrifuge	Hettich Rotanta, Hamburg, GER
Cytocentrifuge Cellspin II Universal 320R	Tharmac GmbH, Waldsolms, GER
Heraeus Megafuge 40R	Thermo Scientific, Dreieich, GER
Multifuge 3SR	Heraeus, Hanau, GER

Optima™ L-70k Ultracentrifuge	Beckman Coulter, Krefeld, GER
Sprout Mini-Centrifuge	Biozym, Hamburg, GER
Ultracentrifuge Buckets, Type SW28	Beckman Coulter, Krefeld, GER
Ultracentrifuge Rotor, Type SW28	Beckman Coulter, Krefeld, GER

Compartment isolation

Branson Sonifier 450 II Classic	Heinemann, Schwäbisch-Gmünd, GER
Collecting device	HOOCK GmbH, Kiel, GER
Free-flow magnetic chamber HOKImag	HOOCK GmbH, Kiel, GER
Flow column	HOOCK GmbH, Kiel, GER
Peristaltic pump (Minipulse 3)	Gilson, Middleton, WI, USA
Speed control module R2	Gilson, Middleton, WI, USA

Electron microscopy supplies

300 kV field Emission STEM (Titan)	FEI company, Hillsboro, OR, USA
Carbon evaporator CED030	Balzers, Wartenberg-Angersbach, GER
EM 109 transmission electron microscope	Zeiss, Jena, GER
EM Trim-Specimen	Leica, Solms, GER
Glow discharge machine (Linion CTA 010)	Balzers, Wartenberg-Angersbach, GER
Helios Nanolab 600 FIB/SEM	FEI company, Hillsboro, OR, USA
HPF 01 apparatus (High-pressure freezer)	Engineering Office M. Wohlwend GmbH, Sennwald, CH
JEM-1400 transmission electron microscope	Jeol, Tokyo, Japan
KnifeMaker	Reichert-Jung/Leica, Solms, GER
Polymerization oven	Advantage Lab GmbH, Darmstadt, GER
Rotation Wheel	PELCO®/PLANO GmbH, Wetzlar, GER
Scanning electron microscope S-5200	Hitachi Ltd. Corporation, Tokyo, Japan
Ultramicrotome Ultracut E / UCT	Reichert-Jung/Leica, Solms, GER
Ultramicrotome Ultracut E + FC 4E	Reichert-Jung/Leica, Solms, GER

Electrophoresis and Blotting

Development machine Curix 60	AGFA, Mortsel, BE
Horizontal electrophoresis equipment	Biotec-Fischer, Reiskirchen, GER
Mini-PROTEAN® Tetra Cell	Bio-Rad, München, GER
Power Supply “PowerPac™ 200/2.0”	Bio-Rad, München, GER
Semi-Dry Transfer Unit TE 77 PWR	Amersham Biosciences, Freiburg, GER
UV-Transilluminator GenoView	VWR International, Darmstadt, GER

Flow Cytometry

Flow Cytometer LSR II	Becton Dickinson, Heidelberg, GER
Flow Cytometer LSR II SORP	Becton Dickinson, Heidelberg, GER
Flow Cytometer FACS Canto II	Becton Dickinson, Heidelberg, GER

Imaging (all Carl Zeiss, Jena, GER)

Microscope Primo Star	
Microscope Axio Vert.A1	
Microscope AxioPhot	equipped with a color camera AxioCam IC and a mercury vapor lamp HBO50
Microscope Observer Z.1	equipped with an ApoTome, an AxioCam MRM, an illuminator HXP120C, reflectors DIC TL, 38 HE GFP, 43 HE DsRed, 49 DAPI, 50 Cy5, 64 HE mPlum, objectives LD Achro Pln 20x/0.4 Ph2 DICIII, LD Achro Plan 40x/0.6 Ph2, Pln Apo 20x/0.8 DICII, PlnN 10x/0.3 Ph1 DICI, EC PlnN 40x/1.3 Oil DICIII, Pln Apo 63x/1.4 Oil DICIII
Microscope LSM 7 *Live*	Observer Z.1 equipped with a line scanner, four laser lines (405 nm, 488 nm, 561 nm and 635 nm), an AxioCam MRM, an illuminator HXP120C, a piezo z-controller 24V80CAP (piezo system jena), an incubation chamber (PECON), reflectors Pol TL, 26 AF660, 38 HE GFP, 43 DsRed, 49 DAPI, objectives Pln Apo 63x/1.4 Oil DICIII, Pln Apo 40x/0.95 DICIII

Incubators

CO_2-Incubator Forma Series II Water Jacket	Thermo Scientific, Marietta, USA
CO_2 incubator, Heraeus Auto Zero	Thermo Scientific, Dreieich, GER
Heracell 240i CO_2 Incubator	Thermo Scientific, Marietta, USA
Heraeus Instruments CO_2 Incubator	Thermo Scientific, Dreieich, GER
Recirculating cooler	Julabo, Seebach, GER

Lamina air flow

Workbench MSC-Advantage	Thermo Scientific, Dreieich, GER
Steril Gard III Advance	The Baker Company, Sanford, USA
Steril Gard Hood	The Baker Company, Sanford, USA

PCR Thermo Cycler

LightCycler® 480 System	Roche Applied Science, Mannheim, GER
Personal Cycler	Biometra, Göttingen, GER
S1000™ Thermal Cycler	Bio-Rad, München, GER

Others

AutoMACS Pro separator	Miltenyi Biotec, Bergisch Gladbach, GER
Autoclave Systec vx-150	Systec, Wettenberg, GER
Analytical balance KB BA 100	Sartorius, Göttingen, GER
AutoMACS Pro separator	Miltenyi Biotec, Bergisch Gladbach, GER
Innova® 44	New Brunswick, Eppendorf, Hamburg, GER
CASY Modell TT	Roche Innovatis AG, Reutlingen, GER
ELISA Reader Synergy2	BioTek, Bad Friedrichshall, GER
Ice machine AF 1000	Scotsman, Pogliano Milanese, IT
Freezer (-20°C)	Bosch, Stuttgart, GER
Freezer U725-G (-80°C)	New Brunswick, Eppendorf, Hamburg, GER
Nitrogen container “Chronos”	Messer, Bad Soden, GER
Magnetic stirrer IKA® C-MaG HS7	IKA®-Werke, Staufen, GER
Microwave	Bosch, Gerlingen, GER
pH Meter PB-11	Sartorius, Göttingen, GER

Refrigerator	Bosch, Stuttgart, GER
Thermomixer 5437 (1.5 mL)	Eppendorf, Hamburg, GER
Thermomixer comfort (1.5 mL)	Eppendorf, Hamburg, GER
Ultrasonic bath Sonorex Super RK103H	Bandelin, Berlin, GER
UV-Vis Spectrophotometer NanoDrop 2000c	PeqLab, Erlangen, GER
Vortex mixer VV3	VWR International, Darmstadt, GER
Water bath	Köttermann VWR International, Darmstadt, GER

2.1.18 Software

Software	Manufacturer
Axio Vision Rel. 4.8	Carl Zeiss, Jena, GER
Auto Slice & View.G1	FEI company, Hillsboro, OR, USA
BD Diva Software (V6.1.3)	Becton Dickinson, Heidelberg, GER
Cygwin	Open Source
FlowJo Vx	Miltenyi Biotec GmbH, Bergisch Gladbach, GER
Gen5™ Software	BioTek, Bad Friedrichshall, GER
GraphPad Prism 6	GraphPad Software, Inc., La Jolla, USA
ImageJ and FiJi	Open Source
Imod (V4.5.7)	Open Source
Light Cycler software LC480 (v1.5.0 SP4)	Roche Applied Science, Mannheim, GER
Mendeley Desktop	Mendeley Ltd., London, UK
Microsoft® Office 2010	Microsoft, Redmont, US
NCBI Nucleotide Blast® (blastn)	National Library of Medicine, Bethesda, USA
Vector NTI (V11.5)	Invitrogen, Dan Diego, USA
Zen 2012 (blue edition, black edition)	Carl Zeiss, Jena, GER

2.2 Eukaryotic Cell Culture

Eukaryotic cell culture was carried out under sterile conditions and in an endotoxin-free environment under a laminar air flow. Media, buffer and flasks needed for cultivation of eukaryotic cells were autoclaved for 20 min at 121°C. Cells were cultivated in a humidified atmosphere with 5% CO_2 and incubation temperatures of 27°C, 33°C or 37°C. To allow optimal growth conditions, bicarbonate-buffered salt solutions containing vitamins and amino acids were used as basic cell culture media supplemented with fetal calf serum (FCS), L-glutamine and antibiotics.

2.2.1 Cultivation of *Leishmania major* promastigotes

Leishmania (L.) major promastigotes were cultured in NNN modified medium. NNN medium was developed by Novy, McNeal and modified by Nicolle. It is a biphasic blood-based medium consisting of a blood agar slope and a highly nutritious overlay medium. For passaging, 3 wells of a 7 days old *Leishmania* culture were collected in 3 mL liquid *Leishmania*-medium (*Lm*-medium) and counted (2.2.12.1). Promastigotes were adjusted to a final concentration of $1x10^6$/mL ($12x10^6$ promastigotes in 12 mL medium) and $1x10^5$ promastigotes per well (= 100 µL) were transferred to a new blood agar plate using a multi-channel pipette. The plate was incubated at 27°C and 5% CO_2 for 6-8 days until stationary phase promastigotes were used for infection experiments. Parasites were cultured up to 8 serial passages until they were discarded. For the passage of eGFP and DsRed genetically modified promastigotes *Lm*-medium was supplemented with 20 ng/mL hygromycin B to keep selection pressure.

2.2.1.1 Preparation of blood agar plates

For cultivation of *L. major* promastigotes on NNN biphasic blood agar medium, the blood agar was prepared in a 96-well plate. At first 20.8 g Brain Heart Infusion (BHI) agar was dissolved in 400 mL water and autoclaved for 15 min at 121°C. 100 mL PBS was pre-warmed to 42°C in a petri dish with a diameter of 25 cm prior to addition of the cooled BHI agar (~55°C). 4 mL penicillin/streptomycin (P/S) and finally 50 mL aseptically collected defibrinated rabbit blood were added. Flat-bottom 96-well plates were put in a 45° angle and 60 µL blood agar was filled in with a multi-channel pipette to achieve sloped blood agar. As soon as the blood agar became solid, plates were sealed and stored at 4°C for up to 4 months.

2.2.1.2 Long-time storage of *L. major* promastigotes

For long-time storage of *L. major* promastigotes, cells were pelleted at 2400 xg for 8 min and resuspended in ice-cold *Lm*-medium supplemented with 20% FCS. 500 µL *Lm*-suspension containing between $100x10^6$ and $200x10^6$ parasites were transferred into cryo tubes and mixed with 500 µL *Lm*-medium containing 20% FCS and 20% dimethylsulfoxid (DMSO). Cells were cooled down overnight in a Mr. Frosty freezing container at -80°C prior to storage in liquid nitrogen.

For thawing, the parasites were warmed at 37°C and added drop wise to *Lm*-medium to dilute the DMSO. After pelleting, promastigotes were resuspended in 12 mL *Lm*-medium and 100 µL of the suspension were transferred to a new blood agar plate per well. The culture was not used until parasites were passaged the first time.

2.2.2 MACS separation of viable and apoptotic *L. major* promastigotes

During early events of apoptosis phosphatidylserine (PS) is translocated from the inner side to the outer side of the plasma membrane. AnnexinV is a 35 kDa phospholipid-binding protein with high affinity to PS under physiological concentrations of calcium (Ca^{2+}). Similar as for human cells, one characteristic of apoptotic promastigotes is the externalization of PS to the cell surface.

Separation of viable from apoptotic *L. major* promastigotes was done by magnetic activated cell sorting (MACS) using AnnexinV MicroBeads (Miltenyi). MicroBeads are 50 nm large super paramagnetic particles that do not activate cells due to their small size. First of all stationary phase promastigotes were counted (2.2.12.1). $250x10^6$ parasites were pelleted (2400 xg, 8 min, 4°C) and washed once with 10 mL ringer-solution + 0.5% BSA (MACS-buffer I) containing Ca^{2+}. Next, cells were pelleted and resuspended in 400 µL MACS-buffer I. 75 µL AnnexinV MicroBeads (Miltenyi) were added, mixed well and incubated for 15 min in the refrigerator. In the meantime a MACS LS column designed for positive selection and containing ferromagnetic spheres was calibrated three times with 3 mL MACS-buffer I. After incubation 10 mL MACS-buffer I was added to the parasites, cells were centrifuged, pellet was resuspended in 500 µL MACS-buffer I and cell suspension was applied onto the column for 5 min. Flow-through containing unlabeled cells was collected in a 15 mL tube. The column was washed three times with 3 mL MACS-buffer I to collect PS-negative (PS-) promastigotes, here termed the viable promastigotes. For elution of PS-positive (PS+) promastigotes, here termed the apoptotic promastigotes, the column was washed three times with 3 mL MACS-buffer II without Ca^{2+} (PBS + 0.5% PBS). Purity of both fractions was

counted in a counting chamber (2.2.12.1). To improve purity of PS- fraction, viable promastigotes were separated via a second column, this time a LD column designed for negative selection that means depletion of labeled cells. Therefore $100x10^6$ pre-separated viable promastigotes were resuspended in 160 µL MACS-buffer I and 20 µL AnnexinV MicroBeads. In principle separation procedure was the same as described above. Washing- and elution volumes were reduced to 1.5 mL, because of a slower flow rate of ~ 0.2 mL/min instead of ~ 2 mL/min. In addition to counting, purity was determined using AnnexinV Fluos staining and flow cytometry (2.6.7, 2.7.1).

2.2.3 Generation and cultivation of *L. major* amastigotes *in vitro*

To prepare a promastigote pre-culture, 16 wells of a logarithmic growth phase *L. major* promastigote culture (3-4 days old) were mixed with 20 mL *Lm*-suspension-medium and 2 mL FCS. Afterwards 5 mL of this *Lm*-suspension was put into a culture flask (25 cm^2) and was incubated at 27°C. After 3 days amastigote pre-culture was prepared. Parasites were pelleted at 2400 xg for 8 min and washed twice with 10 mL AAM. Then the pellet was resuspended in 40 mL AAM for counting and viable promastigotes were adjusted to $20x10^6$/mL. $100x10^6$ parasites were again seeded in 25 cm^2 culture flasks and incubated for 7-14 days at 33°C and 5% CO_2. For isolation of the amastigotes a discontinuous Histopaque® 1119 density gradient was used. The amastigote pre-culture was harvested and centrifuged at 2400 xg for 8 min. The pellet was resuspended in 2.5 mL prewarmed 50% Histopaque® 1119 (density of 1.0595 g/mL) and layered on a discontinuous gradient to separate the amastigotes from dead parasites and remaining promastigotes. From bottom to top the gradient consisted of 3 mL 100% Histopaque (1.119 g/mL), 2 mL 90% Histopaque (1.1071 g/mL), 3 mL 80% Histopaque (1.0952 g/mL) and 2 mL 70% Histopaque (1.0833 g/mL). The gradient was centrifuged for 35 min at 2400 xg with minimal acceleration and deceleration. The interphase between 80% and 90% layers was collected and washed twice in AAM. Amastigotes were adjusted to $20x10^6$/mL and seeded in a 25 cm^2 culture flask with 5 mL per flask. 70% to 80% interphase also contains amastigotes, but remaining promastigotes, too. 90% to 100% interphase contains amastigotes and some remaining dead cells. The purity of isolated amastigotes was screened by Diff QUIK® staining of cytospins. Purified amastigotes are stable for 7 days when they are incubated at 33°C and 5% CO_2. *L. major* amastigotes can be transformed back into promastigotes by culturing amastigotes on NNN blood agar medium. By retransformation of amastigotes one can ensure the virulence of the parasites.

2.2.4 Isolation of peripheral blood mononuclear cells by density centrifugation

Peripheral blood mononuclear cells (PBMC) were isolated from Buffy Coats of healthy donors, obtained from the DRK Blutspendedienst in Frankfurt. 30-50 mL blood were diluted with prewarmed sterile PBS to a final volume of 100 mL and 25 mL of this dilution was layered carefully on top of 15 mL prewarmed leukocyte separation medium (LSM) 1077 in a 50 mL tube. Tubes were centrifuged at 545 xg for 30 min at room temperature (RT) without acceleration and deceleration. Centrifugation led to separation of the different blood cells and the formation of a density gradient. Red blood cells, granulocytes and dead cells were pelleted at the bottom of the tube, followed by the LSM layer and the PBMC interphase containing monocytes and lymphocytes. On top, the plasma containing the thrombocytes was located. The PBMCs were harvested from the interphase using a 25 ml pipette, distributed into 6 new tubes and filled with washing-buffer (PBS without Ca^{2+} and Mg^{2+} + 5% complete-medium) till a final volume of 50 mL for the following washing steps. Cells were centrifuged first at 1024 xg, then at 545 xg and finally at 135 xg for 8 min and RT to remove residual LSM, cell debris and small cells like erythrocytes and thrombocytes. The last washing step was repeated until the supernatant was clear. If the pellet was still red, erythrocytes were lysed by incubation with 10 mL ice-cold 0.15 M ammonium chloride (in H_2O) for 10-15 min. Subsequently, the cells were washed twice with washing-buffer (135 xg, 8 min) and pooled in one tube for counting using a CASY cell counter (2.2.12.3). Isolation of monocytes from the PBMCs was either achieved by plastic adherence (2.2.5) or CD14 MACS separation (2.2.6).

2.2.5 Generation of hMDMs by plastic adherence

For generation of human monocyte derived macrophages (hMDMs) by plastic adherence, $40x10^6$ freshly prepared PBMC were seeded in 5 mL complete-medium + 1% human serum in a 25 cm^2 culture flask. Cells were incubated at 37°C and 5% CO_2 for 1.5 hours (h) to let the monocytes adhere to the bottom of the plastic. Non-adherent cells, mainly lymphocytes, residual erythrocytes and thrombocytes were removed by gently washing the flasks two times with prewarmed washing-buffer. For differentiation of monocytes growth factors were added. For generation of hMDM type I, cells were incubated with 5 mL complete-medium supplemented with 10 ng/mL GM-CSF. hMDM type II cells were incubated in 4 mL culture medium with 30 ng/mL M-CSF. Macrophages differentiated during 5-7 days at 37°C and 5% CO_2.

2.2.6 Generation of hMDMs by CD14 MACS

2.2.6.1 CD14 isolation using an AutoMACS separator

$100x10^6$ PBMC were washed once with 10 mL MACS-buffer (300 xg, 8 min, RT) and the pellet was resuspended in 400 µL MACS-buffer. 100 µL CD14 MicroBeads were added and the mixture was incubated for 15 min in the refrigerator. Subsequently, the cells were washed again with 10 mL MACS-buffer (300 xg, 8 min, RT) and the pellet was resuspended in 500 µL MACS-buffer. The labeled cells were put into an AutoMACS separator and CD14 cells were isolated by positive selection via two columns. After separation purified monocytes were counted using a CASY cell counter and $4x10^6$ monocytes were seeded into 6-well plates in a final volume of 2.5 mL. To differentiate the monocytes the complete-medium was supplemented with 10 ng/mL GM-CSF (hMDM I) or 30 ng/mL M-CSF (hMDM II) and cells were incubated at 37°C and 5% CO_2 for 5-7 days. After 3 days medium was exchanged and growth factors were refreshed. Therefore 2 mL medium was removed and pooled with same conditions. Cells in the supernatant were centrifuged (300 xg, 8 min, RT), resuspended in fresh medium containing growth factors for the total volume (2.5 mL) and put back in the 6-well plate.

2.2.6.2 CD14 isolation using a MidiMACS separator

PBMC were washed once with 50 mL MACS-buffer (300 xg, 8 min, RT) and pellet was resuspended in 95 µL MACS-buffer per $100x10^6$ cells. 5 µL of CD14 MicroBeads were added per $100x10^6$ cells, mixed well and incubated for 15 min in the refrigerator. Mixture was shaken gently from time to time. Cells were washed twice by adding at least 20 times the volume of the labeling buffer. In the meantime a MACS LS column designed for positive selection was rinsed two times with 5 mL MACS-buffer. The cell pellet was resuspended in 3 mL MACS-buffer and cell suspension was applied onto the column. Unlabeled cells were collected in a 50 mL tube and column was rinsed three times with 3 mL MACS-buffer to let the negative cells pass through. Subsequently, the column was removed from the separator and placed on a 15 mL tube. CD14 positive labeled cells were eluted by pipetting 5 mL MACS-buffer onto the column and flushing out the cells using the supplied plunger. Purified monocytes were counted using a CASY cell counter and $4x10^6$ monocytes were seeded into 6-well plates in a final volume of 2.5 mL. Differentiation of the monocytes was done as described before (2.2.6.1).

2.2.7 Harvesting differentiated hMDMs

5-7 days old hMDM I or hMDM II were checked under the microscope for shape, adherence and cell count. Afterwards flasks were put on ice for 15-30 min to detach macrophages from the plastic. Macrophages were harvested with a cell scraper and pooled in a 50 mL tube. Culture flasks were washed with 3-4 mL cold washing-buffer (PBS without Ca^{2+} and Mg^{2+} + 5% complete-medium) and the buffer was added to the tube. Subsequently, tubes were centrifuged for 8 min and 300 xg. Depending on the size of the pellet cells were resuspended in 1-10 mL complete-medium and counted using a CASY cell counter (2.2.12.3).

2.2.8 Isolation of peripheral blood mononuclear cells, isolation of monocytes by elutriation and generation of hMDMs in teflon bags

For isolation of *L. major* containing compartments from infected hMDMs (2.5.3) different protocols for isolation of PBMC and monocytes and generation of macrophages were used since experiments were performed in another laboratory. 10 mL prewarmed pancoll (1.077 g/L) was transferred into a 50 mL tube. Next, 250 mL fresh blood was diluted 1:1 with prewarmed sterile PBS and 40 mL of this dilution was layered carefully on top of the pancoll. Tubes were centrifuged at 1024 xg for 40 min at RT without acceleration and deceleration. Centrifugation led to separation of the different blood cells and the formation of a density gradient. Red blood cells, granulocytes and dead cells were pelleted at the bottom of the tube, followed by the pancoll layer and the PBMC interphase containing monocytes and lymphocytes. On top, the plasma containing the thrombocytes was located. First of all the plasma was discarded. Cold PBS was transferred into a 50 mL tube, put on ice and interphase was harvested using a Pasteur pipette. The interphase of three gradients was pooled and tubes were filled with cold PBS till a final volume of 50 mL prior to centrifugation for 10 min at 545 xg and 4°C. Supernatant was discarded, three pellets were resuspended in 20 mL cold PBS and again centrifuged for 10 min at 545 xg and 4°C. Finally pellets were resuspended in culture medium (RPMI 1640 + 10% FCS + 1% L-glutamine) and counted using a counting chamber. For elutriation cells were resuspended in HBSS (Hank´s Balanced Salt solution) (+ 1% BSA) with a concentration of $5x10^6$cells/mL. After elutriation 20-$25x10^6$ monocytes were resuspended in differentiation medium (RPMI 1640 + 2% FCS + 1% L-glutamine + 1% P/S + 10 ng/mL M-CSF) and seeded in a teflon bag (Menck et al., 2014; Reiling et al., 2001), which was flushed two times with 50 mL PBS using a 50 mL syringe. Cells were incubated at 37°C and 5% CO_2 for 7 days. For harvesting differentiated type II hMDMs, teflon bags were placed on ice for 1 h and by pulling the bags over the edge of the bench hMDM II were detached from the bag. Cell suspension was transferred into a 50 mL

tube and centrifuged for 10 min at 545 xg and 4°C. Supernatant was discarded and cells were resuspended in culture medium prior to counting and seeding $10x10^6$ hMDM II in a volume of 10 mL in a petri dish with a diameter of 10 cm.

2.2.9 Transduction of hMDMs using lentiviral vector particles

2.2.9.1 Transduction of monocytes prior to differentiation to hMDMs

CD14 isolated monocytes (2.2.6.1) were either seeded in a 6-well plate ($3x10^6$ in 4mL medium) for FACS analysis or in ibidi slides for microscopic analysis. $5x10^5$ cells in 300 µL medium were seeded in 8-well µ-slides or $1x10^6$ monocytes in 700 µL medium in a 4-well µ-slide. Medium was discarded and monocytes were transduced with lentiviral vector particles with a MOI of 1, 0.5 or 0.1 for 4 h at 37°C and 5% CO_2. To retain semi-adherent monocytes partially medium change was performed or plates were centrifuged (300 xg, 5 min, RT) prior to medium change if possible. After washing the cells twice, complete-medium supplemented with 10 ng/mL GM-CSF (hMDM I) or 30 ng/mL M-CSF (hMDM II) was added and cells were incubated for 5-7 days at 37°C and 5% CO_2.

2.2.9.2 Direct transduction of differentiated hMDMs

hMDM I or hMDM II were harvested (2.2.7) and adjusted to a concentration of $1x10^6$ cells/mL. $2x10^5$ macrophages in a total volume of 200 µL were seeded in an ibidi µ-slide 8-well for microscopic analysis. For generation of Western blot samples $1x10^6$ cells were seeded in a 24-well plate. hMDMs were left to adhere either for 1 h or overnight at 37°C and 5% CO_2. Lentiviral vector particles were added with a MOI of 0.1 or 0.2 for 4 h prior to a complete medium change. After 5-7 days transduced hMDMs were directly analyzed or co-incubated with *L. major* parasites (2.2.10.3).

2.2.10 Co-incubation of hMDMs and *L. major* parasites

2.2.10.1 Co-incubation in cell culture plates

For co-incubation of macrophages and parasites in cell culture plates, macrophages were adjusted to a cell concentration of $1x10^6$ cells/mL. Depending on the size of the plate, different amounts of macrophages were seeded. $1x10^5$ cells/well were seeded in a 96-well plate or a chamberslide, $2x10^5$ cells/well in an ibidi µ-slide 8-well and $1x10^6$ cells/well in a 24-

well plate. The cells were left to adhere in the cell culture plates for 1-1.5 h or overnight at 37°C and 5% CO_2. Non-adherent cells were removed by discarding the supernatant. *L. major* promastigotes or amastigotes were adjusted to $10x10^6$ parasites/mL and added to the macrophages with a multiplicity of infection (MOI) of 10. The plates were incubated at 37°C and 5% CO_2 for at least 3 h. For analysis of parasite and compartment development after longer infection times (24 h, 48 h, 72 h, 144 h) extracellular parasites were removed after 3 h by rinsing the cells two to three times with prewarmed washing-buffer (PBS without Ca^{2+} and Mg^{2+} + 5% complete-medium).

2.2.10.2 Co-incubation in centrifuge tubes

For co-incubation of macrophages and parasites in centrifuge tubes, macrophages were adjusted to a cell concentration of $10x10^6$ cells/mL. 100 µL of this cell suspension ($1x10^6$ macrophages) were transferred into a 1.5 mL reaction tube. *L. major* promastigotes or amastigotes were added to the macrophages with a MOI of 10 in a tenfold smaller volume ($10x10^6$ parasites/10 µL). After 3 h of co-incubation at 37°C and 5% CO_2, complete-medium was added ad 1 mL. Infected cells were either directly harvested after 3 h by centrifugation at 300 xg for 8 min or after an infection time of 24 h, 48 h, 72 h or 144 h prior to further analyses.

2.2.10.3 Co-incubation of transduced hMDMs and *L. major* parasites

Co-incubation of transduced hMDMs and *L. major* parasites was performed in a cell culture plate as described in 2.2.10 with an MOI of 10, 20 or 50. Western blot analysis was done in a 24-well plate and cells and parasites were co-incubated for 1 h. For microscopy cells were seeded in an ibidi µ-slide 8-well and co-incubation was performed for either 1 h prior to washing and fixation or transduced cells were directly analyzed under the microscope.

2.2.11 Cultivation of mammalian cell lines

2.2.11.1 Cultivation of 293 T/17 cells

293 T/17 cells (ICLC HTL04001) are human embryonic kidney (HEK) cells with adherent growth and a star-shaped or rounded morphology. The cells contain the gene for the large T-antigen from the polyomavirus SV40, which is required for its high transfectability. Cells were grown in DMEM (Dulbecco´s Modified Eagle Medium) supplemented with 10% FCS, 4 mM L-

glutamine and 1 % P/S and incubated at 37°C and 5% CO_2. They were subcultured twice a week in a 175 cm^2 culture flask by splitting them in a ratio of 1:3. Therefore culture medium was discarded and cells were washed with 10 mL prewarmed PBS. To detach the cells 3 mL trypsin/EDTA was added and incubated for 5 min. Trypsinization was stopped with 9 mL culture medium. 4 mL of this cell suspension was mixed with 20 mL fresh culture medium and transferred into a new 175 cm^2 flask.

2.2.11.2 Cultivation of HT-1080 cells

HT-1080 (ATCC CCL-121) is a fibrosarcoma cell line created from tissue taken in a biopsy of a fibrosarcoma present in a 35 year old human male. They are epithelial-like adherent cells growing as monolayers with a doubling time of 30 h. Cells were grown in DMEM supplemented with 10% FCS, 4 mM L-glutamine and 1 % P/S and incubated at 37°C and 5% CO_2. They were subcultured twice a week in a 75 cm^2 culture flask by splitting them in a ratio of 1:10. Therefore culture medium was discarded and cells were washed with 10 mL prewarmed PBS. To detach the cells 2 mL PBS/EDTA (PBS w/o Ca^{2+} and Mg^{2+} pH 7.1 + 1 mM EDTA) was added and incubated for 5 min at 37°C. Then 8 mL culture medium was added and 1 mL of this cell suspension was transferred into a new 75 cm^2 flask containing 20 mL fresh culture medium.

2.2.11.3 Long-time storage of adherent mammalian cell lines

For long time storage 293 T/17 cells were resuspended in DMEM + 20% FCS + 4 mM glutamine + 10% DMSO and $2x10^6$ cells were transferred into cryo tubes. In case of HT-1080 cells, $4x10^6$ cells were resuspended in DMEM + 20% FCS + 10% DMSO for freezing. Cells were cooled down overnight in a Mr. Frosty freezing container at -80°C prior to storage in liquid nitrogen.

For thawing, the cells were warmed at 37°C and added drop wise to culture medium to dilute the DMSO. After pelleting, cells were resuspended in 20 mL culture-medium and transferred into a 75 cm^2 flask.

2.2.11.4 Testing for mycoplasmas

We used a PCR-kit (MinervaBiolabs) for analyzing cell culture contaminations by mycoplasmas. PCR was performed according to the manufacturer´s instructions using the supernatant of the cells or supplied negative and positive controls as template.

2.2.12 Counting eukaryotic cells

2.2.12.1 Counting *L. major* parasites

Leishmania parasites were counted using a neubauer improved counting chamber with a depth of 0.02 mm. 5 µL of the cell suspension was added to the chamber and at least 16 small squares were counted. When counting promastigotes, both viable and apoptotic parasites were counted except for starting a growth curve or transferring log-phase promastigotes into AAM during generation of amastigotes. For these two exceptions only viable promastigotes were counted. For calculation of cell concentrations per mL, amount of calculated parasites were divided through the amount of counted squares and multiplied by 16 and the chamber factor ($5x10^4$).

2.2.12.2 Counting mammalian cell lines

Mammalian cell lines (293 T/17 and HT-1080) were counted using a neubauer improved counting chamber with a depth of 0.1 mm. Depending on the size of the cell pellet cells were diluted with culture medium and mixed with trypan blue in a ratio of 1+1 to stain dead cells. 10 µL of the cell suspension was added to the chamber and 4 big squares each consisting of 16 small squares were counted. Cell concentrations per mL were calculated by multiplying counted cell amount per one big square with the chamber factor ($1x10^4$) and the dilution.

2.2.12.3 Counting PBMC, monocytes and hMDMs

Primary cells were counted using an automatic CASY cell counter (Roche) that is based on the non-invasive Electrical Current Exclusion (ECE) principle using a 150 µm capillary. Therefore, 10 µL of the cell suspension were added to 10 mL CASY ton in a CASY cup. The program for determination of cell numbers had to be adjusted once and individually for every cell type. The cell counter determines cell concentration, cell viability, cell volume and cell debris as well as cell aggregation. The aggregation factor (AF) indicates clumping of the

cells, so the cell concentration was divided by the AF, if it was > 1.00. When counting PBMC the AF was not considered, because PBMC are a mixture of different cell types.

2.2.13 Cytocentrifuging eukaryotic cells

1-2x10^6 *Leishmania* parasites or 1x10^5 hMDMs were resuspended in 100-200 µL medium or buffer. Cells were centrifuged on glass slides in a cytocentrifuge (Tharmac GmbH) at 500 xg for 10 min for *Leishmania* parasites and at 75 xg and 5 min for hMDMs. Subsequently, slides were air-dried and either Diff QUIK® stained (2.6.6) or mounted in ProLong® Gold antifade reagent for further analysis.

2.2.14 Autophagy modulation

There exist different mechanisms to regulate and modulate autophagy. Beside autophagy inhibition one can induce autophagy. We used the chemical autophagy inducer Rapamycin or also called sirolimus that binds to the mammalian target of rapamycin (mTOR). In addition we used the mTOR inhibitor AZD8055 for autophagy induction.

Autophagy modulation was performed with eGFP-LC3 transduced cells (2.2.9.2) in 24-well plates as wells as with ULK1 knockdown cells (2.4.3) in 1.5 mL centrifuge tubes. hMDMs were stimulated with rapamycin (1 µM, 10 µM) or AZD8055 (10 µM) for 40 min at 37°C. After incubation the cells were washed once with complete-medium. Therefore cells in centrifuge tubes were centrifuged at 300 xg for 8 min. Finally cells were resuspended in 1x Laemmli buffer for Western blot analysis (2.5.2).

2.3 Bacterial Cell Culture

Microbial culture is a tool used extensively in molecular biology. In this thesis bacterial cell culture was used for cloning experiments and the production of lentiviral vector particles in terms of plasmid amplification and production. Media, buffer and flasks needed for cultivation of bacteria were autoclaved for 20 min at 121°C. Bacterial cell culture was performed under sterile conditions in a laminar air flow.

2.3.1 Transformation of bacteria

Transformation of bacterial cells was discovered in 1928 by the bacteriologist Griffith (Griffith, 1928) and is a standard laboratory procedure in molecular biology. Transformation allows replication and amplification of plasmid DNA in bacterial cells. First of all One Shot® Chemically Competent *E. coli* were thawed on ice and split up on two centrifuge tubes. 1 µL to 5 µL of plasmid DNA (10 pg to 100 ng) or 5 µL ligation reaction (2.4.9.7) were added to the centrifuge tube and mixed gently. The tubes were incubated for 30 min on ice. Subsequently, the cells were heat-shocked at 42°C for 1 min without shaking and placed on ice for 2 min. 250 µL prewarmed S.O.C. medium was added aseptically to each tube. Cells were shaken for 45-60 min at 37°C and 300 rpm in a shaking incubator. 20 µL and 200 µL of each transformation reaction were spread on a prewarmed selective agar plate. The plates were inverted and incubated over night at 37°C. Remaining transformation mix was stored at 4°C. The next day single colonies were selected for isolation of plasmids (2.3.2). Transformed colonies are stable for up to two months on selective agar plates when stored at 4°C.

2.3.2 Plasmid preparation

For plasmid preparation TOP10 *E. coli* cells were grown in LB medium (Bertani, 1951) at 37°C and 180 rpm overnight. Depending on the carried plasmid, the LB-medium was supplemented with 100 µg/mL ampicillin or 30 µg/mL kanamycin. Bacteria carrying lentiviral plasmids were grown at 25°C for two days. For purification of low amounts of DNA (Miniprep) 5 mL liquid culture was inoculated with a single colony, grown over night in 14 mL polypropylene-tubes and pelleted at 5300 xg for 10 min. Plasmid preparation was performed using the Qiaprep® Spin Miniprep Kit according to the manufacturer´s protocol. For extraction of larger amounts of DNA (Maxiprep) 5 mL LB medium was inoculated in the morning, transferred into a 250 mL liquid culture in the afternoon and grown over night. Alternatively 10 µL of the glycerol stock was added to 250 mL LB medium and incubated overnight. Bacteria broth was centrifuged at 5000 xg for 10 min and resulting pellets were used for the preparation of plasmid DNA according to the manufacturer´s instructions of the Pure Yield™ Plasmid Maxiprep System using a vacuum pump and a vacuum manifold. Finally, plasmid DNA concentrations were determined photometrically measuring the absorption (A) at a wavelength of 260 nm using a NanoDrop 2000c.

2.3.3 Preparation of a glycerol stock

After validation of the plasmid sequence by restriction analysis (2.4.9.6) and sequencing (2.4.9.8) transformed bacteria were archived for long-time storage. 500 µL of an overnight culture was diluted with 500 µL 80% sterile glycerol and transferred into cryo-tubes. Glycerol stocks were stored at -80°C and used for inoculation of LB medium for plasmid preparations (2.3.2).

2.4 Molecular biology methods

Nucleic acid techniques can be performed with deoxyribonucleic acid (DNA) and ribonucleic acid (RNA). DNA was dissolved in double distilled water or Tris/EDTA buffer pH 8.0 and stored at -20°C. RNA was dissolved in RNase-free water and stored at -80°C.

2.4.1 Determination of nucleic acid concentration

In this thesis nucleic acid concentrations were determined using a NanoDrop 2000c UV-Vis spectrophotometer. 0.5-2 µL of the sample were pipetted on the quartz cell and concentration was measured at a wavelength of 260 nm in duplicates. For blanking appropriate buffers, in which samples were dissolved, were used.

2.4.2 Agarose gel electrophoresis

Separation of nucleic acids in an agarose gel matrix was established in 1964 and first described by Tsanev (Tsanev, 1965). Depending on the size of expected fragments, different amounts of agarose (Table 2) were added in TBE buffer for analytical gels or in TAE buffer for preparative gels and dissolved by heating in a microwave. Ethidium bromide solution was added and the gel solution was casted into a gel tray. Ethidium bromide intercalates into DNA strands and can be visualized under UV light. A comb was applied before polymerization of the matrix. DNA samples were mixed with 6x DNA loading dye prior to gel loading. As size marker a 1 kb DNA ladder or a 100 bp DNA ladder were used. The DNA fragments were separated by applying 90-100 V for 45-90 min in a horizontal electrophoresis chamber using TBE- or TAE buffer, respectively. Afterwards DNA fragments were visualized on a transilluminator and were either documented or extracted for purification.

Table 2: Separation range of agarose gels.

% Agarose (w/v)	DNA fragment size (kb)
0.5	1.0 – 30.0
0.7	0.8 – 12.0
1.0	0.5 – 7.0
1.2	0.4 – 6.0
1.5	0.2 – 3.0
2.0	0.1 – 2.0

2.4.3 Transfection of hMDMs with siRNA

hMDMs for siRNA transfection were generated by CD14 MACS separation (2.2.4 and 2.2.6.1). For the transfection of siRNA into eukaryotic cells the Stemfect™ RNA Transfection Kit (Stemgent) was used. Therefore $4x10^6$ cells were seeded in 6-well plates, the medium was aspirated and the cells were washed with 1 mL RPMI 1640 medium without supplements prior to transfection. Transfection was carried out in 1 mL RPMI 1640 medium without supplements. The Stemfect RNA Transfection Reagent and the Stemfect Transfection Buffer were warmed to RT and mixed (solution A, Table 3). A second solution (B) was prepared (Table 3) by mixing the Stemfect Transfection Buffer with 20 µM thawed siRNA (2.1.9). Solution A and B were mixed together within 5 min and the siRNA transfection complex was incubated at RT for 15 min. The entire siRNA transfection complex solution was added drop wise to the cells and the plate was gently rocked to ensure even distribution within the well. The final concentration of siRNA was approximately 20 nM. Cells were incubated at 37°C and 5% CO_2 for 7 h prior to a complete medium change. Therefore cells were washed once with complete-medium and finally 2.5 ml complete-medium was added per well. 2 days after siRNA transfection, hMDMs were harvested (2.2.7), counted using a CASY cell counter (2.2.12.3) and used for RNA isolation (2.4.4), preparation of Western blot samples (2.5.2) and infection experiments (2.2.10). Testing different ULK1 siRNAs was done in a smaller volume using $1.3x10^6$ hMDM in a 12-well plate. Buffer and siRNA volumes were scaled down according to the plate area (Table 3).

Table 3: siRNA transfection protocol.

	Target siRNA [10 µM/µL]		Non-target siRNA [20 µM/µL]	
	6-well	12-well	6-well	12-well
Solution A				
Stemfect Transfection Buffer	20 µL	6.7 µL	20 µL	6.7 µL
Stemfect RNA tranfection reagent	4.6 µL	1.5 µL	4.6 µL	1.5 µL
Solution B				
Stemfect Transfection Buffer	20 µL	6.7 µL	20 µL	6.7 µL
siRNA [final 20 µM]	2 µL	0.7 µL	1 µL	0.35 µL

2.4.4 RNA isolation

RNA was isolated using the RNeasy Plus Mini Kit according to the manufacturer´s protocol. Therefore 0.5-1x10^6 hMDMs were washed with cold PBS and pelleted at 1024 xg for 8 min at RT. The pellet was lysed in 350 µL RLT-buffer by resuspending, homogenized lysate was transferred to a gDNA eliminator spin column and centrifuged (15300 xg, 30 s, RT) to get rid of genomic DNA. 350 µL 70% ethanol were added to the flow-through and the mixture was loaded to an RNeasy Mini Column prior to centrifugation (15300 xg, 30 s, RT). The flow-through was discarded and the column was washed once with 700 µL buffer RW1 and twice with 500 µL RPE buffer (15300 xg, 30 s, RT). The column was transferred into a new collection tube and dried by centrifugation (1800 xg, 1 min, RT). Subsequently, RNA was eluted from the column with 30 µL RNase-free water in a fresh 1.5 mL centrifuge tube by centrifugation (15300 xg, 30 s, RT). The isolated RNA was treated with DNase I (2.4.5) to eliminate remaining genomic DNA. RNA concentration was measured (2.4.1) and samples were either placed on ice or stored at -80°C.

2.4.5 DNase I digestion of isolated RNA

Up to 10 µg of isolated RNA was incubated with 1 µL recombinant DNase I (10 U/µL) and 1 µL recombinant RNaseOut™ Ribonuclease Inhibitor (40 U/µL) for 20 min at 37°C. Enzymes were heat-inactivated for 10 min at 75°C. DNase digestion was performed twice to get rid of all residual genomic DNA.

2.4.6 Test-PCR of isolated RNA

To check the isolated RNA for genomic DNA contaminations a Test-PCR was performed using human GAPDH primer (2.1.9) and the isolated RNA as template. Additionally a positive control with cDNA as template and a negative control without template were prepared. A master-mix without the template was pipetted (Table 4) and distributed to the PCR tubes. Subsequently, the template was added and the PCR was run (Table 5). Samples were analyzed on a 2% TAE agarose gel (2.4.2). Only the positive control should show a PCR-product with a length of 300 bp.

Table 4: Reaction protocol for Test-PCR of isolated RNA.

Reagents	Volumes	Final amount
RNA or cDNA	X µL	100 ng
NEB Taq-buffer [10x]	5 µL	1x
Forward Primer [10 µM]	1 µL	0.2 µM
Reverse Primer [10 µM]	1 µL	0.2 µM
dNTP-Mix [2 mM each]	5 µL	0.2 mM
NEB Taq-polymerase [5 U/µL]	0.25 µL	1.25 U
ddH_2O	ad 50 µL	

Table 5: Amplification protocol for Test-PCR of isolated RNA.

Step	Temperature	Time
Initial denaturation	95°C	30 s
Denaturation	95°C	30 s
Annealing	60°C	30 s
Elongation	68°C	30 s
	30 cycles of amplification	
Final Elongation	68°C	10 min
Cooling	4°C	∞

2.4.7 Reverse Transcription / cDNA synthesis

Reverse transcriptase (RT) is a RNA-dependent DNA polymerase, which allows generation of complementary DNA (cDNA) from a RNA template. This enzyme was found in retroviruses in 1970 by two independent researchers (Baltimore, 1970; Temin and Mizutani, 1970). For cDNA synthesis the kit Im Prom-II Reverse Transkription System was used. In general, 100 ng RNA were transcribed using 0.5 µg random hexamer primer according to the

manufacturer´s instructions (Table 6). In addition a negative control in the absence of reverse transcriptase was produced to check for DNA contamination of the samples. Reverse transcription was carried out in 0.2 mL centrifuge tubes and samples were incubated in a PCR cycler (BioRad). cDNA concentrations were measured (2.4.1) and samples were stored at -20°C.

Table 6: Reverse transcription protocol.

Reagents	Volumes	Final amount
RNA	x µL	100 ng
Random hexamer primer [0.5 µg/µL]	1 µL	0.5 µg
Nuclease-free H_2O	ad 5 µL	
	Denaturation: 5 min 70°C Cooling: 5 min 4°C	
Nuclease-free H_2O	6.5 µL	
ImProm-II™ Reaction Buffer [5x]	4 µL	1x
dNTP-Mix [10 mM each]	1 µL	0.5 mM
$MgCl_2$ [25 mM]	2 µL	2.5 mM
Recombinant RNasin® Ribonuclease Inhibitor [20-40 U/µL]	0.5 µL	10-20 units
ImProm-II™ Reverse Transcriptase	1 µL	
	Annealing: 5 min 25°C Reverse transcription: 60 min 42°C Inactivation: 15 min 70°C Cooling: ∞ 4°C	

2.4.8 Quantitative real-time PCR

Quantitative real-time PCR (qPCR) is a technique to amplify DNA and in contrast to classical PCR the arising DNA amounts can be determined and quantified during analysis. Quantification was carried out using the fluorescent dye SYBR Green, which intercalates in dsDNA. In this thesis we used the “MESA Blue qPCR MasterMix Plus for SYBR Assay No Rox” according to the manufacturer´s instructions. For quantification of ULK1 mRNA levels, specific primers listed in (2.1.9) were used. qPCR reactions were applied as described in Table 7 in duplicates in a 96-well plate. As negative controls a “water-control” without cDNA and a “-RT-control” (cDNA synthesis of RNA without the reverse transcriptase) were included. Amplification was done using a light cycler LC480 from Roche running the program depicted in Table 8. Evaluation of generated data was performed with the applied software LC480 (version 1.5.0 SP4) analyzing the so-called CT-value (cycle threshold), which indicates the cycle in which the fluorescence signal significantly exceeds the background signal for the first time.

To find suitable primer for amplification four different primer-pairs were tested for efficiency. Therefore qPCR reactions were prepared as described in Table 7 using serial dilutions of cDNA (undiluted, 1:10, 1:100, 1:1000). cDNA dilution was plotted semi logarithmical against obtained CT-values and the efficiency (E) was calculated (E = ((10^(-1/slope))-1)*100). Primer efficiencies should be between 90% and 110%. Higher values indicate that the reaction was performed in a non-linear range.

Relative gene expression was evaluated by the $2^{-\Delta\Delta CT}$ method according to Livak and Schmittgen (Livak and Schmittgen, 2001). Following amplification, a melting curve analysis was performed to detect the formation of unspecific products or primer dimers, which have a different melting temperature compared to the specific PCR product. Additionally, the PCR products were checked for size and purity on an agarose gel (2.4.2).

Table 7: qPCR reaction protocol.

Reagent	Volumes	Final amount
Mesa Blue qPCR MasterMix [2x]	10 µL	1x
DEPC-H_2O	6 µL	-
Forward primer [10 µM]	1 µL	0.5 µM
Reverse primer [10 µM]	1 µL	0.5 µM
cDNA (undiluted)	2 µL	

Table 8: qPCR amplification profile.

Step	Temperature [°C]	Time	°C/s
Taq Activation	95	10 min	4.4
Denaturation	95	10 s	4.4
Annealing	60	10 s	2.2
Elongation	72	15 s	4.4
	45 cycles of amplification		
Final Elongation	85	10 s	4.4
Melting Curve	60-99	Continuous	0.11
Cooling	40	20 min	2.2

2.4.9 Cloning of lentiviral vector plasmids

In the following chapter cloning of lentiviral transfer plasmids is described.

2.4.9.1 Cloning strategy of the lentiviral transfer plasmid pPBj-SW-eGFP-LC3

For overexpression of eGFP-LC3 protein in primary human cells the lentiviral transfer plasmid pPBj-SW-eGFP-LC3 was constructed. As vector backbone the plasmid pPBj-SEW was used (Figure 11 B, (Kloke et al., 2010)), that was amplified by PCR (2.4.9.4) using sequence specific primer (2.1.9) introducing the restriction sites NdeI and SpeI at 5´- and 3´-ends. Thereby the whole plasmid was amplified deleting only the eGFP sequence (E) between the SFFV promotor (S) and the WPRE element (W). The insert eGFP-LC3 was amplified (2.4.9.4) from the commercially available plasmid pEGFP-C2-LC3 (Figure 11 A), thereby introducing the restriction sites SpeI and NdeI at 5´- and 3´- ends. By restriction digestion (NdeI, SpeI) of purified PCR products sticky ends were generated, that were needed for ligation of vector and insert (Figure 11 C). After transformation of *E.coli* bacteria (2.3.1), accuracy of prepared plasmids was analyzed by restriction analysis (2.4.9.6), sequencing (2.4.9.8) and overexpression (2.4.9.9).

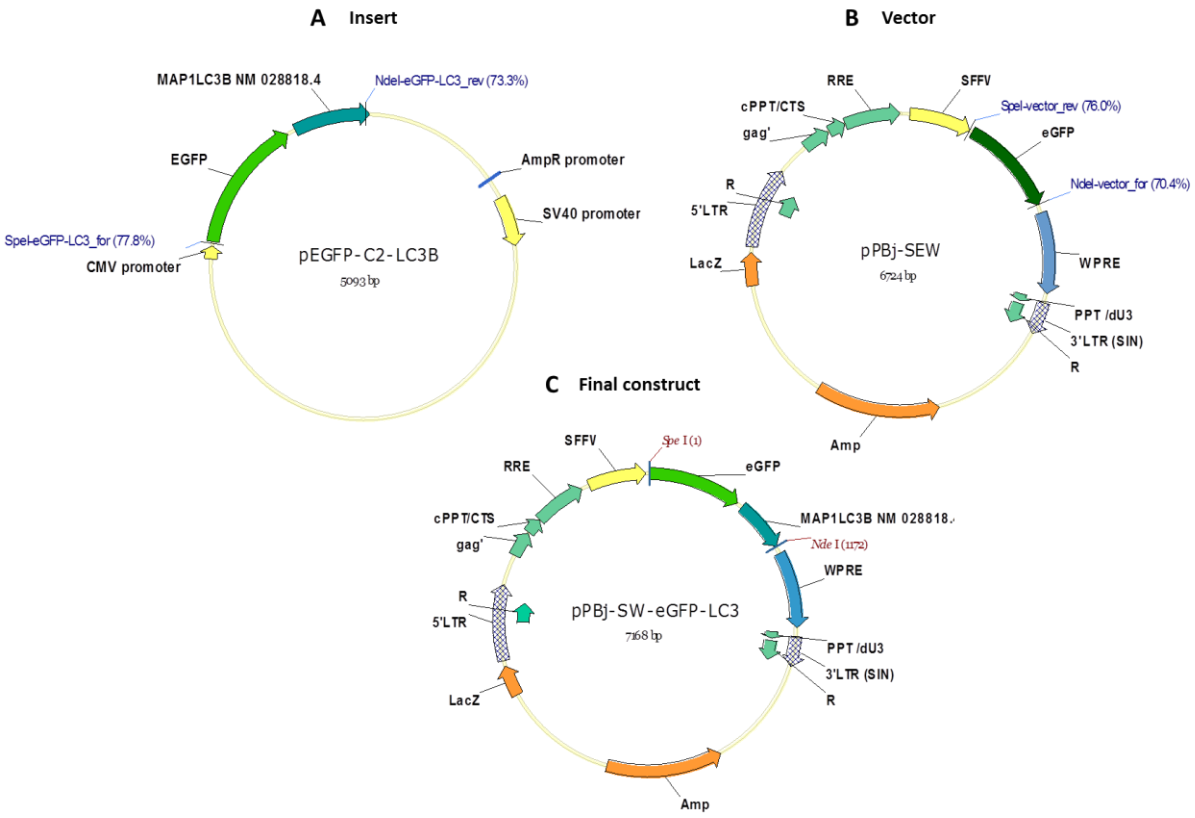

Figure 11: Cloning strategy of the lentiviral transfer plasmid pPBj-SW-eGFP-LC3.

2.4.9.2 Cloning strategy of the lentiviral transfer plasmid pPBj-SW-LAMP2-mCherry

For cloning of a LAMP2 (CDS of NM_002294.2) carrying lentiviral vector plasmid, RNA was isolated from hMDM I (2.4.4), cDNA was constructed (2.4.7) and used for amplification of the LAMP2 sequence. Amplification was done using a forward primer with a KpnI restriction site and a reverse primer with an SspI restriction site. The reverse primer was designed to delete the stop codon of the LAMP2 sequence to attach a fluorescent marker at the N-terminal site. By restriction digestion (KpnI, SspI) the amplified LAMP2 sequence was cloned into the vector backbone pcDNA-mCherry. Subsequently the resulting plasmid pcDNA-LAMP2-mCherry (Figure 12 A) was amplified by PCR using a LAMP2-specific forward primer with a SpeI restriction site and a mCherry specific reverse primer carrying an NdeI restriction site. Similar as for the pPBj-SW-eGFP-LC3 cloning strategy (2.4.9.1), the vector pPBj-SEW was amplified by PCR using primer with NdeI and SpeI restriction sites, respectively. Amplified insert and vector sequences were digested prior to ligation thereby constructing the plasmid pPBj-SW-LAMP2-mCherry (Figure 12 B).

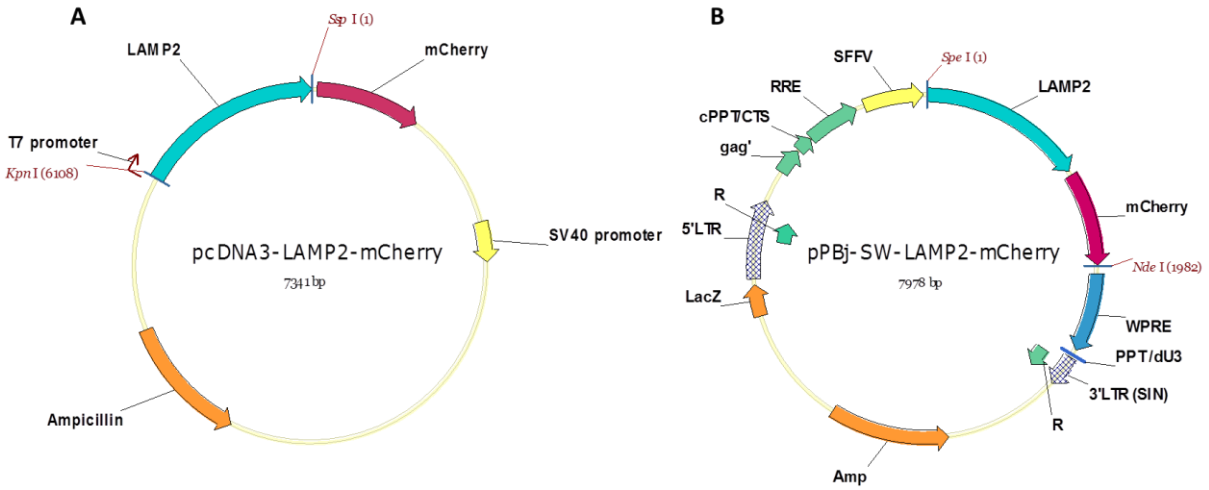

Figure 12: Cloning strategy of the lentiviral transfer plasmid pPBj-SW-LAMP2-mCherry.

2.4.9.3 Cloning strategy of the lentiviral transfer plasmid pPBj-SW-eGFP-2xFYVE

For cloning of the lentiviral transfer plasmid pPBj-SW-eGFP-2xFYVE we achieved a plasmid carrying the tandem FYVE-sequence coupled to an eGFP-sequence (pEGFP-2xFYVE) under the control of a CMV promotor from our cooperation partner Max Gutierrez (National Institute for Medical Research, London, UK). After sequencing the plasmid (2.4.9.8) using primer that bind to the CMV promotor and the eGFP-sequence we were able to design a SpeI-forward primer and a SbfI-reverse primer for amplification of the eGFP-2xFYVE

sequence. This time the plasmid pPBj-SW-eGFP-LC3 was used as vector backbone that was directly digested with the restriction enzymes SpeI and SbfI without prior amplification. Thereby the eGFP-LC3 sequence was deleted to introduce the eGFP-2xFYVE sequence at the same position (Figure 13).

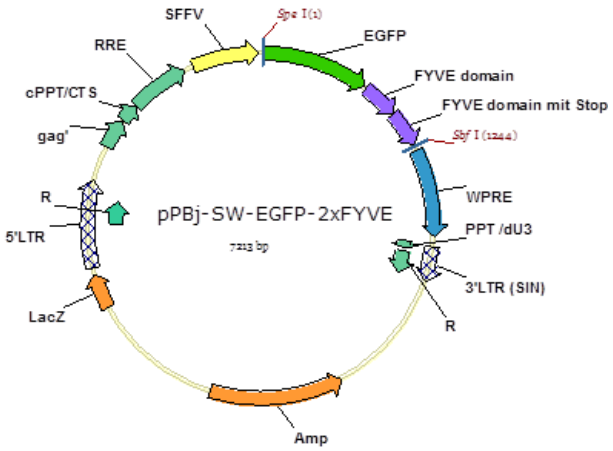

Figure 13: Cloning strategy of the lentiviral transfer plasmid pPBj-SW-eGFP-2xFYVE.

2.4.9.4 PCR of vector and insert

For cloning processes we first of all amplified the vector and the insert by PCR to introduce appropriate restriction sites. To design a PCR primer it is important to consider the reading frame of the amplified sequence. Moreover the primer should have a similar length, similar melting points (Tm) and a GC-content between 40% and 60%. It is of advantage, if the primers do not form secondary structures like hairpins or self-annealing. When restriction sites are introduced, three additional bases should be introduced on the 5´-end of the restriction site, because some restriction enzymes are not able to cut directly at the end of a strand. Used polymerases should have a proof-reading capacity to prevent mutations e.g. Phusion® High-Fidelity DNA polymerase or PfuUltra High-Fidelity DNA polymerase. PCR reaction protocol is shown in Table 9. Running a gradient PCR enables to test different annealing temperatures to find optimal conditions (Table 10). Small aliquots of the PCR products were analyzed on a TBE agarose gel (2.4.2).

Table 9: PCR reaction protocol for Phusion and PfuUltra DNA polymerases.

	Volumes		Final amount	
Reagent	**Phusion**	**PfuUltra**	**Phusion**	**PfuUltra**
Template	X µL		100 pg	50-100 ng
Forward primer [10 µM]	2.5 µL		0.5 µM	
Reverse primer [10 µM]	2.5 µL		0.5 µM	
dNTP-Mix [10 mM each]	1 µL		200 µM each	
Polymerase-buffer [5x, 10x]	10 µL	5 µL	1x	
Phusion™ High-Fidelity DNA polymerase [2U/µL]/ PfuUltra High-Fidelity DNA polymerase [2.5U/µL]	0.5 µL	1 µL	1 U	2.5 U
H_2O	ad 50 µL			

Table 10: Amplification program for Phusion and PfuUltra DNA polymerases.

	Phusion		PfuUltra	
Step	**Temperature**	**Time**	**Temperature**	**Time**
Initial denaturation	98°C	30 s	95°C	2 min
Denaturation	98°C	10 s	95°C	30 s
Annealing	Primer Tm ± 3°C	10-30 s	Primer Tm ± 5°C	30 s
Elongation	72°C	15-30 s / kb	72°C	1 min / kb
	35 cycles of amplification			
Final Elongation	72°C	10 min	72°C	10 min
Cooling	4°C	∞	4°C	∞

2.4.9.5 Purification of DNA

PCR products were first of all analyzed on an analytical agarose gel. If there was only one specific PCR-product, PCR-reaction was purified using the QIAquick® PCR Purification Kit. If there were side products, the PCR-product was electrophoretically separated on a preparative TAE-gel, the band of interest was cut out of the gel and was purified using the MinElute® Gel Extraction Kit. The same holds true for restricted DNA fragments. If only few nucleotides were cut off, fragments were directly purified. If bigger fragments dropped out, digested DNA had to be purified via an agarose gel.

2.4.9.6 Restriction digest of DNA

Restriction enzymes were first discovered in the 1970s (Danna and Nathans, 1971; Smith and Welcox, 1970) and to date there are several hundred enzymes commercially available. For cloning experiments and analytical restriction several restriction enzymes were used, which are listed in 2.1.10. Restriction enzymes from New England Biolabs (NEB) or Promega were used according to the manufacturer´s instructions (Table 11). For a preparative restriction up to 5 µg and for an analytical restriction 500 ng DNA were used. Digestion reactions were incubated for up to 2.5 h at 37°C in a thermoblock followed by a heating step to denature the enzymes. In case of a double digest the optimal buffer for the double digest was chosen to the manufacturer´s instructions. To prevent re-circularization of the vector during the ligation reaction, the vector was incubated for 1 h with 2.5 µL Calf Intestinal Alkaline Phosphatase (CIP) to remove 5´-phosphate. Samples were analyzed on an agarose gel (2.4.2) prior to purification (2.4.9.5) and measuring DNA concentrations at the Nano Drop (2.4.1).

Table 11: Standard restriction digest.

	Vector	**Insert**	**Analytical digest**
DNA	5 µg	1-5 µg	500 ng Vektor
Buffer [10x]	1x	1x	1x
BSA [10x] (optional)	1x	1x	1x
Enyzme 1 [20 U/µL]	0.5 µL/µg	0.5 µL/µg	0.5 µL/µg
Enzyme 2 [20 U/µL]	0.5 µL/µg	0.5 µL/µg	0.5 µL/µg
H_2O	ad 50 µL	ad 50-150 µL	ad 10 µL
	2.5 h 37°C Heat inactivation: 20 min 65°C / 80°C Vector + 25 U CIP [10 U/µL] 1 h 37°C		

2.4.9.7 Ligation of DNA fragments

During ligation the T4 DNA ligase catalyzes the formation of a phosphodiester bond between the 5´-phosphate of one DNA fragment and the 3´-hydroxy group of a second DNA fragment under consumption of ATP (Pheiffer and Zimmerman, 1983). For the ligation reaction digested plasmid DNA or amplified DNA with the same restricted ends (sticky-end or blunt-end) was used. Vector and insert were mixed in a ratio of 1:2, 1:3, 1:5 or 1:7. Per ligation reaction 50 ng vector was used. The amount of insert was calculated with the help of the following link: http://www.insilico.uni-duesseldorf.de/Lig_Input.html. The reaction-mix was either incubated at 16°C overnight or for 1-4 h at room temperature in a thermoblock (Table

12). Subsequently, ligase was heat-inactivated at 65°C for 10 min and stored at -20°C until transformation of *E. coli* bacteria (2.3.1).

Table 12: Standard ligation reaction.

Reagent	Ligation reaction
DNA Ligase-buffer [10x]	1.5 µL
Vector	50 ng
Insert	1:2, 1:3, 1:5, 1:7
T4 DNA Ligase	1 µL
H_2O	ad 15 µL
	16°C overnight Heat inactivation: 10 min 65°C

2.4.9.8 DNA sequencing

DNA sequencing reactions were performed at the company Eurofins MWG Operon. Samples were prepared according to the company´s instructions. 50-100 ng/µL purified plasmid DNA was mixed in a 1.5 ml centrifuge tube with 1.5 µL 10 µM primer in a total volume of 15 µL. Each sequencing primer had to be mixed with the plasmid in a separate tube. Samples were marked using prepaid labels and sent via regular mail to the company. Sequencing results could be downloaded from the web page. Analyses and verification of plasmid sequences were performed using either VectorNTI (Invitrogen) or Nucleotide Blast (blastn, NCBI).

2.4.9.9 Transient transfection of cells using Lipofectamine to test transgene expression of cloned lentiviral transfer plasmids

To validate cloned lentiviral transfer plasmids for transgene expression, 293 T/17 cells were transfected using Lipofectamine™ LTX Reagent (Invitrogen), which is a liposome-based DNA delivery reagent. $2.5x10^5$ 293 T/17 cells were seeded in a 12-well plate in 1 mL culture medium (DMEM + 10% FCS + 4 mM L-glutamine + 1% P/S) the day before transfection. Cell density should be 50-80% confluent on the day of transfection. For each well 1 µg plasmid DNA was diluted in 200 µL OptiMEM® I Reduced Serum Medium (Invitrogen) without supplements and mixed gently with 2.5 µL Lipofectamine. The mixture was incubated for 30 min at RT to form DNA-Lipofectamine complexes. In the meantime growth medium was removed and replaced with 1 mL fresh culture medium. Subsequently, 200 µL of the DNA-Lipofectamine complexes were added to each well and mixed gently by rocking the plate back and forth. Cells were incubated at 37°C and 5% CO_2 for 18-24 h and assayed for transgene expression by fluorescence microscopy.

2.4.10 Production and concentration of lentiviral vector particles

Lentiviruses integrate their viral genome into the genome of the host. They belong to the retroviridae family of viruses and have two positive-strand RNA copies. Lentiviruses have the unique ability among retroviruses to efficiently transduce non-dividing cells like monocytes and macrophages. In 1996 the first lentiviral vector was constructed by Naldini and others (Naldini et al., 1996) and since then, lentiviral vector particles have been modified in order to improve efficiency and safety. Necessary viral elements are separated on different plasmids to render the produced vectors replication-incompetent. The RNA to be packaged into the lentiviral vector particles is encoded on a transfer construct (pPBj-trans). The lentiviral transfer vector encodes for the transgene mRNA under control of the internal SFFV (spleen focus-forming virus) promotor and for two long-terminal-repeats (LTR) necessary for integration. The U3 region of the 3´-LTR was deleted to generate self-inactivating (SIN) lentiviral vectors (Miyoshi et al., 1998; Zufferey et al., 1998). The woodchuck hepatitis virus posttranscriptional regulatory element (WPRE) downstream of the transgene stabilizes the mRNA through secondary structures and thereby improves transgene expression (Hlavaty et al., 2005; Zufferey et al., 1999).

The packaging construct (pPBj-pack) carries the structural genes (*gag*, *pol*), which are important for the particle formation itself, with the exception of the envelope protein. The structural genes encode the sequences for the enzymes Reverse Transcriptase (RT) and integrase (IN), which are involved in early steps of replication.

The envelope construct (pMD.G2) is coding for the envelope-encoding sequence in this case the vesicular stomatitis virus G (VSV-G) protein (Naldini et al., 1996). VSV-G pseudotyping allows transduction of a wide range of target cells and redirects vector entry through the endocytic pathway (Aiken, 1997).

We generated simian immunodeficiency derived particles of the PBj strain from sooty mangabeys (Cercocebus atys) (SIVsmm) (Fultz et al., 1989). The original two-plasmid system lentivector SIVsmmPBj enables transduction of primary human monocytes (Mühlebach et al., 2005) and was later enhanced to a three-plasmid system, including the envelope construct pMD.G2, the packaging-construct pPBj-pack and the transfer vector pPBj-SEW (Kloke et al., 2010). The ability to transduce monocytes was found to be connected to the viral accessory protein Vpx (Wolfrum et al., 2007), so that for generation of lentiviral vectors the plasmid pVpxPBjsyn was included. The accessory protein Vpx is only encoded by viruses of the HIV-2/SIVsmm/SIVmac lineage and is also required for an efficient virus replication in macrophages and in dendritic cells (Fletcher et al., 1996; Hirsch et al., 1998; Srivastava et al., 2008). It could be demonstrated that Vpx targets the host cell

restriction factor SAMHD1 to proteasomal degradation what enables successful infection of myeloid cells with HIV-2 and related SIV viruses (Hrecka et al., 2011; Laguette et al., 2011). Furthermore, Vpx-mediated SAMHD1 degradation rendered primary monocytes highly susceptible to HIV-1 infection (Berger et al., 2011), although HIV-1 normally fails to transduce myeloid cells because of lacking Vpx.

Lentiviral vector particles were generated by transient transfection of 293 T/17 cells (Figure 14). After transfection the supernatant, containing the lentiviral vector particles, was harvested and concentrated by ultracentrifugation through a sucrose cushion. Vector titers were calculated by titration of the concentrated particles on HT-1080 cells.

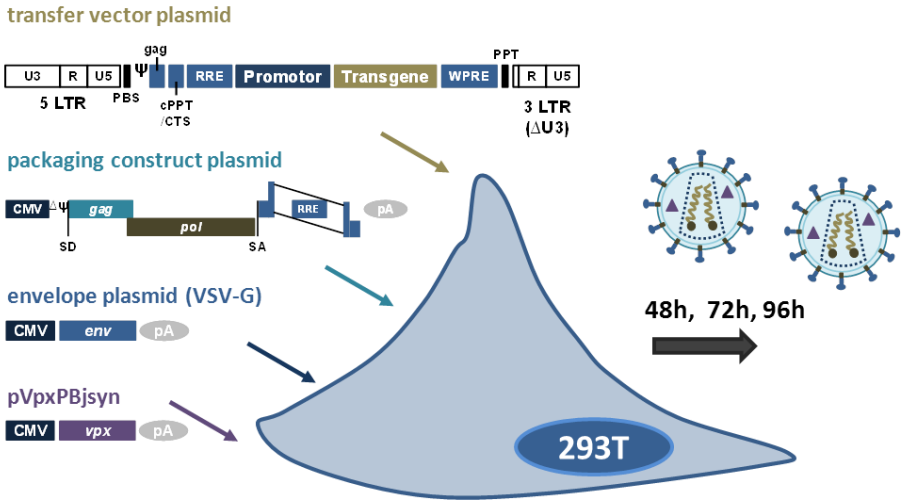

Figure 14: Production and concentration of lentiviral vector particles. Necessary viral elements, separated on different plasmids, are transiently transfected into 293 T/17 cells. 48 h, 72 h and 96 h post transfection, vector particles are harvested and concentrated by ultracentrifugation. Modified from (Kloke, 2009).

2.4.10.1 Large scale calciumphosphate transfection of cells

293 T/17 cells were transiently transfected with a four plasmid lentiviral vector system (2.4.10) using calcium phosphate transfection. In this technique a HEPES-buffered saline (HBS) containing sodium phosphate is drop wise mixed with a calciumchlorid ($CaCl_2$) solution containing the DNA. Thereby DNA:calciumphosphate precipitates are formed, which adhere to the cell surface and are taken up by the cell, presumably by endocytosis. The slower the two solutions are mixed the smaller are the formed precipitates. An excess of calcium ions leads to an altered permeability of the membrane, so the transfection has to be performed in serum-free medium to prevent penetration of serum proteins into the cytoplasm. DNA:calciumphosphate precipitates are given drop wise to the cells.

Three days before transfection, $4.5x10^6$ 293 T/17 cells were seeded into a T175 flask in 20 mL culture medium (DMEM + 10% FCS + 4 mM L-glutamine + 1% P/S). For a large scale experiment 24 flasks were prepared. 1 h before transfection the medium was replaced by 5 mL pre-warmed culture medium without P/S supplemented with 25 µM chloroquine. Chloroquine increases transduction efficiency by neutralizing the pH-value within the vesicles and thereby inhibiting lysosomal DNases. The four different plasmids were mixed in a particular ratio (Table 13), were diluted with H_2O (Sigma) and 250 mM $CaCl_2$ was added (Table 13). For twenty-four T175 flasks a total volume of 36 mL was prepared in a 50 mL tube and afterwards split to three tubes. The same volume 2x HBS-buffer was added drop wise while aspirating the DNA-$CaCl_2$ solution with a pipette. Subsequently, the precipitate was added drop wise to the cells (3 mL/flask). After 8 h and 24 h medium was replaced by 20 mL and 9 mL fresh culture medium with P/S.

Table 13: Plasmid and buffer amounts needed for large scale calcium phosphate transfection.

	Ratio	1x T175	24x T175
pPBj-pack	1	25 µg	600 µg
pPBj-trans	0.2	5 µg	120 µg
pMD.G2	0.33	8.25 µg	198 µg
pVpxPBjsyn	0.165	4.125 µg	99 µg
$CaCl_2$ [2.5M]	final 250 mM	150 µL	3.6 mL
H_2O [Sigma]		ad 1.5 mL	ad 36 mL
HBS-buffer [2x]		1.5 mL	36 mL

2.4.10.2 Concentration of lentiviral vector particles by ultracentrifugation

48 h after transfection (2.4.10.1) supernatant, containing the pseudotyped lentiviral vector particles, was harvested and replaced by 9 mL fresh culture medium. The supernatant of four flasks was pooled in one 50 mL tube and centrifuged for 10 min at 1200 rpm and 4°C to get rid of non-adherent cells and cell debris. Afterwards supernatant was put on ice and purified through a 0.45 µM filter (Millipore) using a vacuum pump. 30 mL of the filtered supernatant was added in a polyallomer centrifuge tube, sublayered with 5 mL 20% (w/v) sucrose and concentrated by ultracentrifugation at 25.000 rpm and 4°C for 2 h. A small aliquot (1 mL) of unconcentrated particles was stored at -80°C. Finally supernatant was discarded and pellet was resuspended in 50-200 µL RPMI without supplements. Pellets were dissolved by shaking at 4°C for 15 min prior to pooling them in a 2 mL tube and centrifugation (9000 rpm, 1 min, 4°C). Lentiviral vector particles were frozen in 25 µL and 50 µL aliquots at -80°C and can be stored up to three years. The vectors were harvested and prepared the same way after 72 h and 96 h post transfection.

2.4.10.3 Titration of concentrated lentiviral vector particles by transduction of HT-1080 cells

For titration of lentiviral vector particles HT-1080 cells were transduced and analyzed by flow cytometry (2.7.2). HT-1080 cells are suited for titration, because in FACS they appear as two distinct peaks for untransduced and transduced cells. One day before transduction $5x10^4$ cells were seeded in a 24-well plate to reach a confluence of 75-90% at the day of transduction. Concentrated as well as unconcentrated vector particle stocks were serially diluted with culture medium (HT-1080) (Table 14). The old medium was removed from the cells and 250 µL of the dilution was added per well. Cells were incubated for 4 h at 37°C and 5% CO_2 and the medium was exchanged by 1 mL fresh culture medium. After 3-4 days titers were calculated by determining the percentage of fluorescent cells by flow cytometry (2.7.2). For vector titer calculation, dilutions, in which 4-20% of the cells were transduced, were chosen. Higher transduction efficiencies indicate double-positive cells. Titers were calculated according to the following equation: Titer [TU/mL] = % transduced cells / 100 % x seeded cell number x dilution factor x 4 (to obtain transducing units per mL).

Table 14: Serial dilutions for titration of concentrated and unconcentrated supernatant on HT-1080 cells.

Concentrated supernatant		Unconcentrated supernatant	
dilution	**Volume supernatant/medium**	**dilution**	**Volume supernatant/medium**
1:10	40 µL / 360 µL	undiluted	
1:50	100 µL / 400 µL	1:5	100 µL / 400 µL
1:100	200 µL / 200 µL	1:10	200 µL / 200 µL
1:500	100 µL / 400 µL	1:50	100 µL / 400 µL
1:1000	200 µL / 200 µL	1:100	200 µL / 200 µL
1:5000	100 µL / 400 µL	1:500	100 µL / 400 µL

2.5 Protein techniques

2.5.1 SDS-PAGE

SDS-PAGE (Sodium Dodecyl Sulfate PolyAcrylamide Gel Electrophoresis) is a technique used to separate denatured proteins according to their electrophoretic mobility. 15% SDS-polyacrylamide gels were prepared to a standard protocol (Table 15) and polymerized between two glass plates. To improve sharpness of separated proteins pH was shifted between stacking and separating buffer conditions (Tulchin et al., 1976). Alternatively precasted 4-20% gradient gels (BioRad) were used. For sample preparation $0.5x10^6$ hMDMs or $5x10^6$ *L. major* parasites were pelleted (300 xg, 8 min, RT for hMDMs and 2400 xg, 8 min,

RT for *L. major*) and lysed in 20 µL 1x Laemmli-Buffer by heating at 95°C for 10 min. Isolated compartment samples (2.5.3) were mixed with 5x lysis buffer (Laemmli) containing 1% β-mercaptoethanol. Either 20 µL of the lysates or 12.5 µg of total protein (2.5.3) were loaded on the gel and for control a prestained size marker was added. Electrophoresis was performed in a Mini-PROTEAN® Tetra cell (Bio-Rad) in 1x running-buffer for constant 80 Volt (V) until samples reached the separating gel (~ 15-20 min). Henceforth gel was run at 100 V for 1.5-2 h.

Table 15: Protocol for preparation of 4 SDS-gels.

Chemicals	Separating gel [15%]	Stacking gel [~4%]
ddH_2O	4.5 mL	2.5 mL
Separating gel buffer pH 8.8 [4x]	4.5 mL	-
Stacking gel buffer pH 6.8 [4x]	-	1 mL
Acrylamide/bisacrylamide solution [30%]	9 mL	0.5 mL
TEMED	40 µL	5 µL
APS [10%]	180 µL	20 µL

2.5.2 Western Blot analysis and band detection

The Western blot method was originated in 1979 in the laboratory of Harry Towbin (Towbin et al., 1979). Western blot is used to transfer electrophoretic separated proteins from a polyacrylamide gel onto a membrane made of nitrocellulose or PVDF (PolyVinyliDene Fluoride). Subsequently immobilized proteins can be probed with specific antibodies and visualized by chemo-luminescence.

After SDS-PAGE (2.5.1) the proteins were transferred to a nitrocellulose membrane for 1 h at constant 1.5 mA/cm^2. Transfer was done by semi-dry blot. Afterwards the membrane was blocked for 1 h in 5% milk powder in TBS/T at RT or alternatively at 4°C overnight to avoid unspecific binding of the antibody to the membrane. The membrane was washed with TBS/T prior to adding the primary antibody, which was incubated over night at 4°C by gently agitation on a shaker. The next morning the membrane was washed 3 times for 10 min with TBS/T and incubated with a horseradish peroxidase (HRP)-coupled secondary antibody for 1 h at RT. Primary and secondary antibodies used in this thesis are depicted in 2.1.11. After another 3 washing steps for 10 min at RT, protein bands were detected using the Amersham ECL™ substrate according to the manufacturer´s protocol. High performance ECL films were exposed to the membrane for 30 s to 30 min in the dark depending on the detected protein. ECL films were developed and to visualize several proteins with similar molecular weight, blots were treated with a mild stripping-buffer for 30 min at RT to remove primary and

secondary antibodies. After 3 washing steps with TBS/T for 10 min at RT, the membrane was again blocked in milk powder solution prior to antibody incubation as described above.

2.5.3 Immuno-magnetic isolation of *L. major* promastigote containing compartment proteins

Following protocol is modified from an isolation protocol for isolation of mycobacteria-containing phagosomes using a free-flow magnetic chamber system (Steinhäuser et al., 2013, 2014).

For immuno-magnetic isolation of apoptotic *L. major* promastigote containing compartment proteins first of all promastigotes were separated by Annexin V MACS (2.2.2) in the evening and labeled with BNF-Dextran lipobiotin beads overnight (2.6.12). The next day $10x10^6$ hMDM II (2.2.8) were seeded in 10 mL culture medium (RPMI + 10% FCS + 1% L-glutamine) in a petri dish with a diameter of 10 cm. For one isolation experiment two petri dishes were prepared.

2.5.3.1 Harvesting the cells

hMDM II were co-incubated with magnetically-labeled apoptotic promastigotes with a MOI of 10 for 1 h at 37°C and 5% CO_2. For compartment isolation hMDM II were rinsed carefully with 10 mL culture medium to remove extracellular parasites. Subsequently, cells were harvested by adding 10 mL ice-cold homogenization-buffer containing 0.2% EDTA (Ethylenediaminetetraacetic acid) per petri-dish and putting the cells on ice for 10-15 min. Cells were detached using a rubber cell scraper and collected in a 50 mL tube. Petri dishes were rinsed with 10 mL homogenization-buffer containing 0.2% EDTA and cells were pelleted at 310 xg and 4°C for 10 min. The cell pellet was resuspended in 500 µL homogenization-buffer supplemented with protease inhibitor (1:25), Cytochalasin D (5 µg/mL) and Benzonase Nuclease (25 U/mL) and transferred into a 1.5 mL screw cap centrifuge tube. As a first control (sample I: total lysate), 50 µL of the solution was collected and diluted with 50 µL homogenization-buffer supplemented with protease inhibitor, Cytochalasin D and Benzonase Nuclease. 80 µL of this sample was stored for Western blot analysis (2.5.2) at -20°C. The other 20 µL were mixed with 20 µL buffer and put on ice for BCA-test (2.5.4).

2.5.3.2 Homogenization of the cells

In a next step macrophage cell membrane was disrupted using a Branson Sonifier 450 II Classic sonification device equipped with a cup-resonator. A 1:1 ethanol/water mixture (supplemented with 0.1% dishwashing liquid) was applied as ultrasound transmitter and cooling medium (4°C) at the same time. The success of this step relies on one´s ability to lyse the macrophages without damaging the phagosomal membrane (Chakraborty et al., 1994). The cells were sonicated two to three times for 2 min (Duty cycle: constant, Output control: 1-1.5). After each sonification step the sample was centrifuged (500 xg, 2 min, 4°C) and the cloudy supernatant containing the compartments was collected in a tube. Supernatant and pellet had to be removed carefully to avoid contaminations, because the pellet was not very tightly packed due to the gentle centrifugation. In total not more than 700 µL supernatant should be collected because only 650 µL volume can be loaded in the magnetic chamber. The supernatant was incubated at 37°C for 5 min. The DNase (Benzonase) present in the buffer leads to degradation of the DNA which may lead to clumping of intracellular compartments (Lee et al., 2010). Cytochalasin D inhibits the actin-polymerization and thereby destructs the actin-filaments and destroys the cytoskeleton. 50 µL of the supernatant were collected (sample II: homogenizate), diluted and stored like sample I for later biochemical analysis.

2.5.3.3 Magnetic isolation of the compartments

The magnetic chamber is constructed with a high-intensity magnetic field (2 Tesla) (Schütze et al., 2003) and a free-flow separation column in a small refrigerator for cooling the samples under a fume hood. After application of the homogenizate, magnetically labeled phagosomes are attracted to the walls of the column. The advantage of this system is that the column does not contain ferromagnetic material, so that a lysate of any density or even samples tending to spontaneously aggregate (Steinhäuser et al., 2013; Tchikov and Schütze, 2008; Tchikov et al., 2014) can be separated. Prior to loading the sample, the system was rinsed and the column was completely filled with homogenization buffer containing protease inhibitor until a drop formed under the separation column. The tube containing 650 µL homogenizate was put under the column. Subsequently, the sample was loaded by pumping (flow rate of 250 µL/min) and exposed to the magnetic field for at least 30 min. Afterwards the column was washed for 5 min by pumping (250 µL/min) homogenization buffer containing protease inhibitor and the non-magnetic fraction was collected in a 15 mL tube. 100 µL of the non-magnetic fraction (sample III) were collected and split up for Western blot analysis (80 µL) and BCA-test (20 µL + 20 µL homogenization buffer containing protease inhibitor,

Benzonase, Cytochalasin D). The column was rinsed for another 10 min to increase purity and the flow-through was discarded.

2.5.3.4 Elution of the magnetic fraction

In order to collect the magnetic fraction a fresh 1.5 mL centrifuge tube was put under the separation column that was afterwards removed from the magnetic chamber by disrupting it from the pump. A successful magnetic isolation is visible by light brown or white stripes on the wall of the column. Most of the magnetic fraction was released spontaneously from the column. By using a plunger of a 1 mL syringe the walls of the column were scraped off. Eluted magnetic fraction (sample IV) was centrifuged for 10 min at 15000 xg and 4°C. Due to the magnetic beads the pellet should have a brown color. It was resuspended in 50-100 µL homogenization buffer (supplemented with protease inhibitor, Benzonase, Cytochalasin D) and split up for Western blot analysis (40/80 µL) and BCA-test (10/20 µL + 10/20 µL homogenization buffer containing protease inhibitor, Benzonase, Cytochalasin D).

2.5.4 BCA-test

To analyze protein concentrations during isolation of *L. major* containing compartments (2.5.3) a BCA Protein Assay Kit was used according to the manufacturer´s instructions. To prepare BCA-reagent, first of all 6 mL of solution A were mixed with 120 µL of solution B. BSA (2 mg/mL) was serially diluted in a 1:2 ratio and 10 µL of the standard or the unknown sample, respectively, were transferred to a 96-well plate with a flat bottom. Samples were prepared in duplicates. Subsequently 200 µL BCA-reagent were added per well and incubated for 30 min at 37°C (without CO_2) in the dark. Colorimetric reaction was measured by analyzing optical density at 562 nm using an ELISA Reader.

2.6 Staining and labeling of hMDMs and *L. major* parasites

2.6.1 EEA1 immunofluorescence staining of *L. major* infected hMDMs in chamber slides

The Early Endosome Antigen 1 (EEA1) is an endosomal marker protein involved in endosomal trafficking and the fusion of endosomes with phagosomes. Through its C-terminal FYVE domain it directly binds to the phospholipid phosphatidylinositol 3-phosphate (PI3P)

that is synthesized in cell membranes upon stimulation. The human intracellular protein EEA1 was analyzed by immunofluorescence staining after co-incubation of hMDMs with stationary phase *L. major* promastigotes or purified PS+ parasites (2.2.2).

$1x10^5$ hMDMs were seeded per well in a 12-well chamberslide (ibidi) in 100 µL complete medium and incubated for 30 min at 37°C and 5% CO_2 to let the cells adhere to the plastic. Chamberslides provide a convenient tissue chamber for incubation of the cells with small amounts of antibody, which can be removed so that the remaining slide containing stained cells can be prepared for microscopic analysis. Co-incubation of hMDMs with *Leishmania* was performed with an MOI of 50 for 15 min at 37°C and 5% CO_2. After incubation cells were washed two times with prewarmed washing buffer to remove extracellular parasites. To fix the cells 100 µL 4% paraformaldehyde (PFA) /PBS was added and incubated for 15 min on ice in the dark. PFA is a fixing reagent that chemically reacts amongst others with proteins forming covalent inter- and intra-molecular cross-linking. It mainly reacts with amino groups to form methylene bridges. The supernatant was removed to wash the cells with 100 µL buffer I (PBS + 1% BSA, 1% FCS, 1% human serum). Afterwards 100 µL buffer II (PBS + 0.5% saponin, 1% BSA, 1% FCS, 1% human serum) was added to permeabilize the cell membrane so that the antibodies have access to the inside of the cells and can bind to their antigens. Saponin is a detergent derived from Q*uillaja bark* and influences membrane permeability by complexing cholesterin. Other detergents like Triton X-100 interact unspecifically and are able to dissolve proteins out of the cell membrane (Jamur and Oliver, 2010). Both buffers contain high amounts of proteins to block unspecific binding of the antibodies to the cells. To leave out a separate blocking step antibodies were diluted in buffer II. The primary antibodies (EEA1-FlTC antibody, anti-*Leishmania* rabbit serum) or the isotype controls (2.1.11), respectively, were diluted in 100 µL buffer II per well and incubated for 30 min on ice in the dark. Unbound antibodies were removed by rinsing the well with 100 µL buffer II. Secondary antibodies (2.1.12) were mixed with 2 µL DAPI (5 µg/mL) in 100 µL buffer II and incubated for 30 min on ice. Subsequently, stained cells were rinsed once with 100 µL buffer II followed by 100 µL buffer I. Residual buffer was removed carefully by tapping the slide on cellulose paper. The incubation chamber was erased and the slide was dried before it was mounted in ProLong® Gold Antifade Reagent. The cover slip (24 x 50 mm) was sealed with nail polish and the slide was stored at 4°C in the dark until microscopic analysis.

2.6.2 LC3 immunofluorescence staining of *L. major* infected hMDMs using Tokuyasu technique fixation conditions

Microtubule-associated protein 1A/1B-light chain 3 (LC3) is the homologue of the yeast protein ATG8 and is an important marker and effector of autophagy (1.5.3).

For LC3 immunofluorescence staining, $1x10^5$ hMDMs were seeded in a 12-well chamberslide in a total volume of 300 µL and slides were incubated for 30 min at 37°C and 5% CO_2 to let the cells adhere. Afterwards cells were infected with stationary phase *L. major* promastigotes for 3 h and a MOI of 10 (2.2.10.1). After 3 h cells were washed twice with prewarmed washing-buffer to remove extracellular parasites. Following steps were performed as described in 2.6.1 with exception of the fixation step that was done for 30 min on ice with a mixture of 4% paraformaldehyde (PFA) and 1% glutaraldehyde (GA). GA is the fixative of choice in electron microscopy. Like PFA, GA is a chemical fixation reagent that is even more effective at forming cross-linking between molecules and therefore effectively preserves the ultrastructure of cells. Used primary (polyclonal rabbit LC3 antibody, MBL or anti-*Leishmania* mouse serum) and secondary antibodies as well as appropriate isotype controls are listed in 2.1.11.

2.6.3 LC3 immunofluorescence staining of cryo sections

Cryo sections (2.8.5.7) were collected on a 10-well microscope slide and washed first for 10 min in PBS and then for 5 min in buffer I (PBS + 1% BSA, 1% FCS, 1% human serum). The microscope slide was put in a humidified chamber and cells were incubated for 30 min at 4°C with 20 µL primary antibodies (polyclonal rabbit LC3 antibody, MBL or anti-*Leishmania* mouse serum) or the isotype controls (rabbit serum or mouse serum) diluted in buffer I. The slide was rinsed with PBS and then washed once in PBS for 5 min. 20 µL secondary antibody diluted in buffer I (2.1.2) was incubated for 30 min at 4°C. After washing the slide with PBS, cells were mounted in mowiol and analyzed by fluorescence microscopy (2.8.2).

2.6.4 LC3 immunogold labeling of cryo sections

Cryo sections (2.8.5.7) were collected on nickel grids and placed in a humidified chamber. Beside antibody incubations that were performed in a humidified chamber by incubating the grids on small droplets all following steps were carried out in petri dishes. The grids were carefully transferred to the next solution or buffer using a loop. First of all grids were incubated for 15 min in PBS, followed by incubation in fresh PBS for 3 min twice. For

blocking and staining the grids were incubated for 15 min at 4°C with the primary antibody (polyclonal rabbit LC3 antibody, MBL) or subsequent isotype control (rabbit serum) that both were diluted (1:100) in buffer I (PBS + 1% BSA, 1% FCS, 1% human serum). After five washing steps with PBS for 3 min, the grids were incubated for 1 h at RT with a 10 nm gold-particle conjugated secondary antibody (2.1.11) that was diluted 1:50 in PBS. The grids were washed again five times for 3 min with PBS and then twice for 3 min with Aqua dest. to wash away the phosphate. For contrasting and embedding of the samples, cryo sections were incubated for 10 min in 0.2% uranyl acetate (UAc)/ 2% methyl cellulose in Aqua dest..

2.6.5 LC3 immunogold labeling of LR-Gold embedded samples

LR-Gold embedded samples were collected on copper grids (300 mesh) and were blocked for 10 min in PBS containing 1% BSA, 1% FCS and 1% human serum. All incubation steps were carried out by putting the grids on small droplets in a humidified chamber. All solutions were centrifuged at 10.000 rpm for 2 min prior to incubation to avoid dust particles. After blocking, the primary antibody (polyclonal rabbit LC3 antibody, Cell Signaling) was diluted 1:25 and 1:50 in blocking-buffer and incubated for 30 min. Grids were incubated six times with PBS for 2 min. Subsequently, gold-particle labeled secondary antibody (goat anti-rabbit conjugated with 10 nM gold particles, Aurion) was incubated for 30 min. After washing the grids with PBS (6x for 2 min), samples were fixed for 5 min in 1% glutaraldehyde solution (in PBS). Prior to contrasting of the samples for 5 min in 1% UAc (in H_2O), sections were kept four times in Aqua dest. for 2 min. Finally grids were rinsed with Aqua dest. by consecutively dunking them into three beaker glasses and afterwards they were dried using filter paper. LC3 immunogold-labeled samples were analyzed by transmission electron microscopy (TEM) (2.8.6).

2.6.6 Diff QUIK® staining

Diff QUIK® staining is a histological staining that is based on a modification of the Wright Giemsa stain pioneered by Bernard Witlin in 1970. Used Diff QUIK® kit consists of three solutions. First of all air-dried cytospin slides (2.2.13) were fixed for 2 min in fixation solution (blue) containing methanol (MeOH). Afterwards cells were incubated for 2 min in Staining-solution I (orange), an eosinophilic solution. The xanthene dye eosin is an acid dye with negative charge that stains basic components of the cell in red like the cytoplasm or collagen. Staining solution II (violet) was also incubated for 2 min. This basophilic staining solution contains thiazine dyes with a positive charge that stains negatively charged

molecules like the DNA of the nucleus or the kinetoplast in violet. The slides were rinsed with tap water and air-dried for microscopically analysis using an AxioPhot microscope (Zeiss) with a color camera (2.8.1).

2.6.7 Annexin V staining of *L. major* parasites

The human vascular anticoagulant, annexin V, is a Ca^{2+}-dependent phospholipid-binding protein that has high affinity for phosphatidylserine (PS). Apoptotic *L. major* promastigotes are able to bind AnnexinV suggesting externalization of PS, similar as with apoptotic cells. In 1995 Vermes and colleagues developed a new flow cytometric assay for measuring apoptosis using fluorescein labeled AnnexinV (Vermes et al., 1995). Based on this assay AnnexinV conjugated to a fluorophore was used to identify apoptotic *L. major* promastigotes by flow cytometry (2.7.1).

$2x10^6$ parasites (promastigotes or amastigotes) were put in duplicates in a v-shaped 96-well plate. The plate was centrifuged (300 xg, 4 min, 4°C) and the medium was discarded by turning and hitting the plate on cellulose. The pellets were washed (300 xg, 4 min, 4°C) in 100 µL Ringer-solution containing calcium (330 mg/mL) and finally were resuspended either in 100 µL Ringer-solution as negative control or 100 µL staining solution containing 100 µL Ringer-solution + 0.5 µL AnnexinV Fluos. The plate was incubated for 20 min at 4°C and washed once with 100 µL Ringer-solution to wash away unbound AnnexinV. At last pellets were resuspended in 100-150 µL Ringer-solution and transferred into FACS microtubes.

2.6.8 DAPI staining of *L. major* parasites

Leishmania are able to take up 4´,6-diamido-2-phenylindole (DAPI) from the growth medium. In addition DAPI can pass through intact cell membranes, but less efficiently. DAPI is a fluorescent stain that binds strongly to A-T rich regions in DNA. Thereby the DNA-containing nucleus and kinetoplast of the parasites are stained.

$10x10^6$ *L. major* promastigotes were pelleted (2400 xg, 8 min, RT) and resuspended in 100 µL *Lm*-medium. 5 µL DAPI-solution (5 µg/mL) was added and parasites were incubated for at least 30 min at 27°C and 5% CO_2. If parasites were needed for live cell imaging experiments, they were washed two times with complete-medium as the DAPI stain is toxic for hMDMs in high concentrations. For short-time infection experiments (up to 3 h) parasites were directly used without washing.

2.6.9 Succinimidylester-AF647 staining of apoptotic *L. major* promastigotes

AlexaFluor 647 coupled Succinimidylester (NHS-AF647) was used for staining of purified apoptotic promastigotes. Succinimidylester bind to primary amines ($R\text{-}NH_2$) of peptides, proteins or amine-modified oligonucleotides. One can conjugate amine-reactive reagents with virtually any protein or peptide. Amine-reactive reagents react with non-protonated aliphatic amine groups including the amine terminus of proteins and the ε-amino group of lysines. They show little reactivity with aromatic amines, alcohols and phenols. Produced carboxamide bonds are as stable as peptide bonds.

$10x10^6$ purified PS+ *L. major* promastigotes were pelleted in a 1.5 mL centrifuge tube for 8 min at 2400 xg. Pellet was resuspended in 100 µL NHS-AF647 solution (6.25 µg/mL) and apoptotic parasites were incubated for 1 h at 27°C and 5% CO_2. NHS-AF647 stock was prepared with a concentration of 5 mg/mL in DMSO and stored at -80°C. After incubation parasites were washed two times with 1 mL *Lm*-medium (2400 xg, 8 min, RT) and finally pellet was resuspended in 100 µL complete-medium for infection of hMDMs and microscopic analyses (2.8.2).

2.6.10 Lipobiotin/Streptavidin-AF647 labeling of apoptotic *L. major* promastigotes

The biotinylated lipopeptide termed Lipobiotin (LB, PHCKKKKK(Aca-Aca-Biotin) x 3 TFA, N-Palmitoyl-S-(1,2-bishexadecyloxycarbonyl) ethyl-[R]-cysteinyl-[S]-lysyl-[S]-lysyl-[S]-lysyl-[S]-lysyl -[S]-lysine(ε-aminocaproyl-ε-aminocaproyl-biotinyl) x 3 CF3COOH) (Figure 15) is able to integrate in cell membranes by its lipopeptide part. It seems to integrate preferential in apoptotic membranes (Steinhäuser et al., 2014). Using fluorescent coupled streptavidin, which has a high affinity for biotin, lipobiotin labeling can be visualized. The binding of biotin to streptavidin is one of the strongest non-covalent interactions that is even resistant to organic solvents, denaturants, detergents, proteolytic enzymes and extreme temperature and pH variations.

$10x10^6$ purified PS+ promastigotes were resuspended in 100 µL RPMI without supplements in a 0.5 mL centrifuge tube and centrifuged at 3800 xg and 10°C for 6 min. In the meantime Lipobiotin-stock (1 mg/mL in H_2O) was vortexed and diluted 1:100 or 1:500 in RPMI. Parasites were resuspended in 100 µL diluted Lipobiotin-solution and incubated for 1 h on ice. After incubation parasites were washed once with 100 µL RPMI (3800 xg, 6 min, 10°C) prior to incubation with 100 µL Streptavidin-AF647 (1:100 in RPMI, stock 1 mg/mL in PBS) on ice for 1 h in the dark. Parasites were again washed once in 100 µL RPMI and finally

resuspended in 100 µL RPMI. For flow cytometry analysis unstained parasites or parasites only incubated with Streptavidin-AF647 were prepared as controls. In addition labeled promastigotes were cytocentrifuged on slides (2.2.13) and analyzed by microscopy or they were used for infection experiments of transduced cells (2.2.10.3).

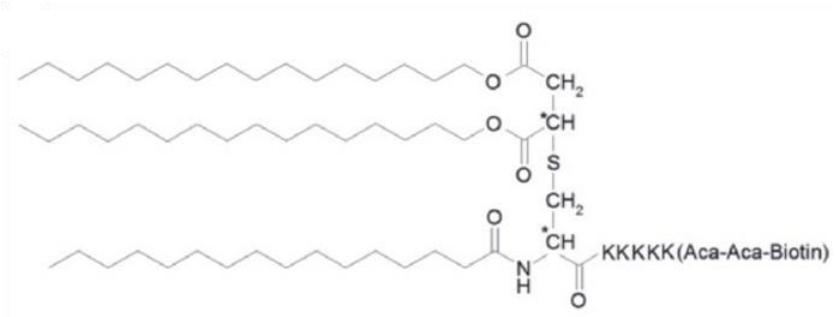

Figure 15: Chemical structure of synthesized triacylated, biotinylated Lipobiotin (Steinhäuser et al., 2013)**.**

2.6.11 Magnetic labeling of apoptotic *L. major* promastigotes using Lipobiotin and Streptavidin-conjugated magnetic nanoparticles

Magnetic nanoparticles (also known as ferrofluids) have no magnetic memory and do not need mixing during the binding reaction. They have a diameter of ~150 nm and a high ligand binding capacity per mass.

$100x10^6$ purified PS+ promastigotes were resuspended in 1mL RPMI without supplements in a 1.5 mL centrifuge tube and centrifuged at 3800 xg and 10°C for 6 min. In the meantime Lipobiotin-stock (1 mg/mL in H_2O) was vortexed and diluted 1:500 in RPMI. Parasites were resuspended in 1 mL diluted Lipobiotin-solution and incubated for 1 h on ice. After incubation parasites were washed once with 1 mL RPMI (3800 xg, 6 min, 10°C) prior to incubation with Streptavidin-conjugated magnetic nanoparticles (5 µL in 100 µL RPMI) on ice for 20 min in the dark. Labeled promastigotes were used for subsequent compartment isolation procedure (2.5.3).

2.6.12 Magnetic labeling of apoptotic *L. major* promastigotes using Lipobiotin-beads

For isolation of *L. major* containing compartments, parasites were magnetically labeled using bionized nanoferrite (BNF)-Dextran beads harboring lipobiotin on their surface. They can be ordered at micromod Partikeltechnologie GmbH and are prepared with a core of 75-80%

(w/w) magnetite and a shell of dextran. The beads exhibit a size of 150 nm and are available as suspension in water with a concentration of 10 mg/mL. For labeling $180x10^6$ purified PS+ promastigotes were pelleted (3800 xg, 6 min, 10°C) and resuspended in 1.8 mL RPMI without supplements. 18 µL BNF-Dextran lipobiotin beads (final concentration of 100 ng/mL) were added and incubated at 4°C overnight. The next morning parasites were centrifuged (3800 xg, 6 min, 10°C), resuspended in 200 µL medium and transferred into 10 mL macrophage culture medium. $20x10^6$ hMDM II were infected with the labeled parasites with a MOI of 9 for 1 h at 37°C and 5% CO_2.

To analyze labeling efficiency $2x10^6$ labeled parasites were washed once with 20 µL RPMI without supplements (3800 xg, 6 min, 10°C) prior to incubation in 20 µL Streptavidin-Cy5 (1:200 in RPMI) for 30 min at 4°C. After incubation parasites were again washed with 20 µL RPMI without supplements and resuspended in 100 µL PBS for flow cytometry (2.7.1).

2.7 Flow cytometry

Flow cytometry or also called Fluorescence activated cell sorting (FACS) describes a technique to measure cell characteristics like size, granularity and fluorescence. Fluorescent-labeled cells are suspended to a single cell solution and in a stream of fluid they pass several lasers emitting scattered light. Data were analyzed with FlowJo software from MiltenyiBiotec.

2.7.1 Flow cytometry analysis of *L. major* parasites

Annexin V binding (2.6.7) to apoptotic *L. major* promastigotes as well as Lipobiotin/Streptavidin-AF647 labeling (2.6.10) and BNF-Dextran lipobiotin magnetic beads labeling (2.6.12) were assessed by flow cytometry. Parasites were analyzed with a threshold of 200 and logarithmic scaled axes for FSC, SSC and the fluorescent dyes.

2.7.2 Flow cytometry analysis of transduced HT-1080 cells

For titration of lentiviral vector particles HT-1080 cells were transduced (2.4.10.3) and analyzed by flow cytometry. Therefore, 3-4 days after transduction cells were washed first with 1 mL PBS and then 200 µL PBS/EDTA (1 mM) was added for 3-5 min to detach cells from the plastic. Cells were transferred in FACS-tubes containing 800 µL FACS-Wash and were centrifuged for 5 min at 230 xg. Supernatant was discarded and pellet was

resuspended in 300-500 µL FACS-Fix. FACS-tubes were vortexed and stored at 4°C prior to determination of the percentage of fluorescent cells by flow cytometric analysis. HT-1080 cells were analyzed with a threshold of 5000 and linear scaled axes for FSC and SSC as well as logarithmic scaled axes for the fluorescent dyes.

2.7.3 Flow cytometry analysis of transduced and (infected) monocytes/hMDMs

Stainings were carried out in v-shaped 96-well plates in the dark and on ice. $1x10^5$ eGFP-transduced hMDMs were washed once in FACS-buffer and were incubated with CD163-PE or CD14-PacBlue antibodies or matched isotype controls for 30 min on ice. Antibody concentrations used for stainings are depicted in 2.1.11. As a control for eGFP-transduced monocytes or hMDMs untransduced cells were prepared. For analysis of infection rates, hMDMs were infected with *L. major* DsRed promastigotes in centrifuge tubes (2.2.10.2) prior to antibody incubation. Cells were washed in FACS-buffer (300 xg, 4 min, 4°C), resuspended in 200-400 µL FACS-buffer and transferred into FACS microtubes. hMDMs were analyzed with a threshold of 5000 and linear scaled axes for FSC and SSC as well as logarithmic scaled axes for the fluorescent dyes.

2.8 Microscopic techniques

2.8.1 Transmitted light microscopy

Light microscopy is commonly used in cell culture for analysis of cell growth (Axio Vert.A1) or counting of cells (Primo Star). For evaluation of Diff QUIK® stained samples we used a Zeiss AxioPhot microscope equipped with a high quality color camera (AxioCam IC) and AxioVision 4.8. software (Zeiss).

2.8.2 Fluorescence microscopy

For analysis of LC3 immunofluorescence staining methods (2.6.2, 2.6.3, 2.6.4) we used a fluorescence microscope (Zeiss Observer Z.1 with a HXP120C) equipped with a black and white camera (AxioCam MRM) and an ApoTome to create optical sections by structured illumination. With the help of a grid that can be moved into the beampath at three different positions, the system calculates an optical section. In the end only the focal plane is visualized in the image what leads to a higher contrast and a better resolution.

2.8.3 Confocal laser scanning microscopy

Transduced cells (2.2.9.2) and EEA1 stained cells (2.6.1) were analyzed on a confocal laser scanning microscope. In 1957 Marvin Minsky patented the principle of confocal imaging, which uses optical sectioning to achieve better resolution of fluorescent images. Thereby a pinhole is placed at the confocal plane of the lens to eliminate out-of-focus light. The disadvantage of the increased resolution is decreased signal intensity and long exposure times, since the fluorescence light from the sample is partly blocked at the pinhole. We used a LSM 7 *Live* (Zeiss) confocal laser scanning microscope that is equipped with a slit instead of a conventional pinhole. Accordingly the sample is illuminated in a line instead of a single point. The spatial resolution of the LSM 7 *Live* is not as high as for point-scanning confocal microscopes, but the system is much faster. The line scanner enables the system to image samples in high-speed with up to 1010 frames per second. Furthermore the system is equipped with four laser lines (405 nm, 488 nm, 561 nm and 635 nm) and a black and white camera (AxioCam MRM) allowing multicolor fluorescence acquisition combined with transmitted light. To perform live cell imaging experiments the system is encased by an incubation chamber providing optimal culturing conditions (37°C, 5% CO_2) for the cells.

Optical sectioning makes confocal laser scanning microscopes suitable for 3D imaging of the samples. Depicted 3D profiles were created with either Zen Black 2012 or Zen Blue 2012 Software (Zeiss).

2.8.4 Live cell imaging

Live cell imaging experiments were performed on a LSM 7 *Live* (Zeiss) confocal laser scanning microscope (2.8.3) in 8-well µ-Slides with a coverslip-like bottom suitable for high resolution microscopy. hMDMs were transduced (2.2.9.2) and co-incubated with DAPI-stained (2.6.8) or NHS-AF647 stained (2.6.9) parasites. Depending on the analyzed target and cellular process, the time interval for data acquisition differed between 1 and 15 min. Wide field images (3.3.1.4) were recorded with an AxioCam MRM (Zeiss).

2.8.5 Electron microscopic sample preparation

2.8.5.1 Chemical fixation and sample preparation

Fixation of the cells

For chemical fixation 5-10x10^6 hMDM were co-incubated with *L. major* amastigotes at a MOI of 10 in a 15 mL or a 50 mL tube for 3 h. Medium was increased to 5 mL or 10 mL and cells were centrifuged (1024 xg, 8 min, RT) and resuspended in 2.5% glutaraldehyde (in Dulbecco PBS) for 45 min at RT. Glutaraldehyde treatment is a classical method for chemical fixation because it leads to protein cross-linking and thereby fixation of the samples. In contrast to paraformaldehyde (PFA) the ultrastructure is well preserved, but it shows higher auto fluorescence levels. After fixation cells were washed twice with 25 mL PBS w/o Ca^{2+} and Mg^{2+} and were stored at 4°C in PBS supplemented with 0.1% sodium azide (NaN_3) to prevent microbial growth.

Agarose embedding and contrasting of the cells using heavy metal staining

Fixed cell suspension was transferred to glass centrifuge tubes with a v-shaped bottom and centrifuged at 1024 xg for 8 min. Supernatant was discarded and residual buffer was removed using a glass pasteur pipette. The tube containing the cell pellet was put in a 50°C water bath, a few drops liquid agarose (3% in H_2O) were added and mixed. To harden the agarose the tube was put on ice for 10 min. Afterwards the agarose block was cut in small cubes and transferred into small vials with snap-on caps filled with Dulbecco´s PBS. Following steps were performed under a fume hood wearing gloves. PBS was aspirated with a plastic pasteur pipette prior to incubation with 1% osmium tetroxide (OsO_4) for 1 h on ice. Contrasting of electron microscopic samples with osmium tetroxide was introduced in 1934 by Ladislaus Marton. Osmium tetroxide, that is diluted in Dulbecco´s PBS, normally is colorless, but due to OsO_2 impurities it often has a yellow-brown color (Girolami, 2012). It primary reacts with lipids and thereby fixes and contrasts the cell membrane. After incubation osmium tetroxide was discarded and agarose blocs were washed three times for 5 min with Dulbecco´s PBS. At the same time 0.1% tannic acid was prepared by diluting 0.01 g tannin in 500 µL 1 M HEPES-buffer pH 7.4 and 9.5 mL H_2O. The tannic acid was incubated for 1 h at RT. Tannic acid was introduced for EM purposes by Futaesaku et al. 1972 and acts as a mordant and fixative by creating conditions for enhancing electron density of protein materials. It has been demonstrated that tannic acid binds electrostatically to amino acids in collagen (Meek and Weiss, 1979) and also to carbohydrate complexes (Sannes et al., 1978). To wash out the tannic acid the samples were washed two times with 1% sodium sulfate (Na_2SO_4) in 0.05 M HEPES-buffer and three times with ddH_2O. Subsequently the samples were contrasted by adding 2% uranyl acetate through a 0.2 µm sterile filter and incubation of

the vials for 1 h at RT in the dark. Uranyl acetate is a heavy metal salt that is slightly radioactive and toxic. Uranyl acetate is photosensitive and should be suspended in HEPES-buffer or ddH_2O, but should not be diluted in a phosphate buffer like PBS, because it reacts with phosphate groups. However, uranyl ions bind to phosphate groups of nucleic acids, to lipids, to proteins and to sialic acid carboxyl groups. Finally agarose blocks were washed twice for 5 min with ddH_2O and stored in the refrigerator overnight.

Dehydration of the samples and epon embedding

To enable sample embedding in a resin, which is in turn necessary for preparation of thin sections, agarose embedded samples were dehydrated. Dehydration was achieved by the replacement of water with organic solvents such as ethanol (EtOH). Therefore ddH_2O was replaced by 30% EtOH using a plastic pasteur pipette and agarose pieces were incubated for 30 min by rotation on a wheel. EtOH concentrations were increased to 50%, 70%, 80%, 90% and 96% and samples were rotated for 30 min, respectively. Finally agarose pieces were incubated twice in water-free absolute EtOH for 15 min. To filter out the water, the EtOH is kept on a molecular sieve. During the 80% EtOH incubation step the resin epon was prepared using an Epoxy Embedding Medium Kit (Sigma). Amounts indicated in Table 16 are sufficient for 3-4 samples. For epon preparation it is recommended to wear nitrile gloves and the accelerator should be added under a fume hood. Water-free EtOH was mixed with freshly prepared epon in three different ratios (2+1, 1+1, 1+2). EtOH/epon solutions were successively incubated for 30 min, thereby increasing epon concentrations. Pure epon was incubated for 1 h with an open cap, was removed and finally added again for an overnight incubation.

Table 16: Protocol of an epon preparation for 3-4 samples.

Reagent	Density	Amount
Epon 812/Epoxy Embedding Medium	1.22 g/L	23 g
Hardener DDSA (2-Dodecenylsuccinic anhydride)	1.00 g/L	10.5 g
Hardener MNA (Methylnadic anhydride)	1.23 g/L	13.9 g
Accelerator DPM-30 (2,4,6-Tris(dimethylaminomethyl)phenol)	-	400 µL

Shake bottle until the mixture gets orange
Shake bottle from time to time

The next morning epon was again exchanged and incubated for 3-4 h. Agarose pieces were transferred to the lower end of gelatin capsules and filled up with epon. To polymerize the epon, gelatin capsules were incubated at 60°C for 48 h in an oven (Advantage Lab). After two days gelatin capsules were dissolved in a 60°C warm water bath. Washing procedure was repeated twice to obtain the pure epon block.

2.8.5.2 High-Pressure-Freezing and freeze substitution

High-Pressure-Freezing (HPF) is a form of cryofixation that is used to prepare samples for electron microscopy. Cryofixation of biological samples always bears the risk of distortion at the ultrastructural level by the formation and growth of ice crystals, because the volume of water increases when it freezes. With HPF, the cells are frozen in a physiologically defined state under liquid nitrogen for cooling of the sample and under high pressure (around 2000 bar) to lower the freezing point of water and thereby to inhibit crystallization. For HPF we used light transparent sapphire specimens and a freeze substitution protocol for contrasting of the membranes (Höhn et al., 2011).

Preparation of sapphire discs

Sapphire carriers had a diameter of 3 mm and were 160 µm thick. Before they could be used for cell growth they had to be cleaned and coated with carbon. Therefore sapphire discs in a small vial with snap-on cap were incubated for 15 min in 60% sulfuric acid (H_2SO_4) in an ultrasonic bath before they were rinsed three times with Aqua dest. Afterwards they were cleaned in the ultrasonic bath with dishwashing liquid and were again rinsed three times in Aqua dest.. After incubation in 96% denatured ethanol (EtOH) in the ultrasonic bath for 5-15 min, sapphire discs were coated with a thin carbon film (10-20 nm) by electron beam evaporation (Carbon evaporator CED030, Balzers) and a “2” was scratched in for orientation of the upper side (Figure 16). Subsequently, they were dried in an oven at 180°C for 12 h to increase the stability of the carbon and stored at RT. Shortly before they were used in an experiment, they were glowed hydrophilic using air as gas (Linion CTA 010, Balzers). During a glow discharge, electrons are ionized between two electrons with direct or alternating voltage under low gas pressure (0.15 mbar) and the charge carrier deposits on the sapphire discs. To sterilize the discs, they were put under UV-light of a laminar air-flow for 15 min.

High-pressure freezing

Four sapphire discs were put into a 24-well plate or an 8-well µ-Slide containing 200 µL or 50 µL complete-medium. hMDMs were adjusted to a final concentration of $2x10^6$ cells/mL and subsequently $1x10^6$ or $2x10^5$ cells were added per well. Complete medium was added to a final concentration of $1x10^6$ cells/mL and cells were incubated for 30 min at 37°C and 5% CO_2 to let the macrophages adhere to the carbon-coated sapphire discs. hMDMs were infected with 12-13 days old *L. major* promastigotes or *L. major* amastigotes with a MOI of 10. Extracellular parasites were removed after 3 h of co-incubation by washing the cells twice with complete medium. Living cells were either directly fixed by HPF or further incubated for 24 h, 48 h or 144 h. HPF was done with a Wohlwend HPF Compact 01 high-pressure freezer (Engineering Office M. Wohlwend GmbH, Sennwald, Switzerland). A 50 µm gold spacer ring

was mounted in between two 160 µm thick sapphire discs and these sandwiches were high-pressure frozen (Figure 16) and stored in liquid nitrogen until freeze substitution and epon embedding (Hawes et al., 2007; Höhn et al., 2011).

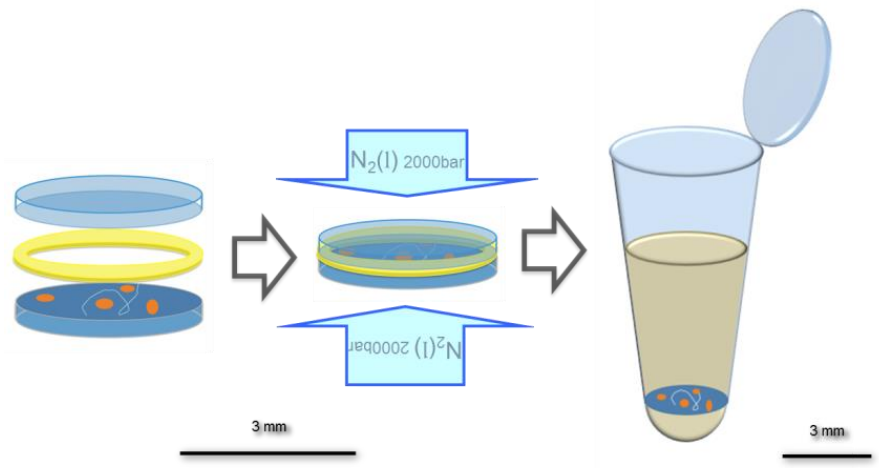

Figure 16: Schematic representation of High-Pressure Freezing. Two 160 µm thick sapphire discs and a 50 µm thick gold ring as spacer were mounted as a sandwich prior to HPF under high pressure and liquid nitrogen. Frozen samples were freeze substituted and embedded in epon. Adapted from (Villinger et al., 2012).

Freeze substitution and epon embedding

Freeze substitution was performed as described in Walther und Ziegler 2002 (Walther and Ziegler, 2002). The substitution medium was dissolved by sonification for 10 min and then 500 µL were added into a 1.5 mL centrifuge tube to precool the substitution medium in liquid nitrogen to -90°C. Sapphire discs were transferred from liquid nitrogen into substitution medium consisting of acetone with 0.1% uranyl acetate (UAc), 0.2% osmium tetroxide (OsO_4) and 5% water for a good contrast of the membranes. Freeze substitution was performed overnight (16-17 h) and the temperature was exponentially raised from -90°C to 0°C. During freeze substitution the sample is simultaneously dehydrated, chemically fixed and contrasted. After substitution the samples were kept for 1 h on ice and subsequently for 1 h at RT to enhance contrasting. Sapphire discs were washed three times with acetone and stepwise embedded in epon. First of all samples were incubated for 6 h in an epon-aceton mixture (1:1) and then overnight in 100% epon prior to polymerization at 60°C within 72 h.

Freeze substitution and LR-Gold embedding

Freeze substitution was performed in the same substitution medium as described above. Temperature was exponentially raised from -90°C to -20°C overnight and subsequent working steps were performed at -20°C. Sapphire discs were transferred into precooled

propanol to wash away the acetone of the substitution medium. Since propanol gets solid at -90°C it is not suitable as substitution medium. Samples were embedded in LR-Gold resin supplemented with 1 mg/mL benzoyl peroxide and 1 mg/mL benzil. The embedding mixture is photosensitive, oxygen sensitive and polymerizes already at RT. Sapphire discs were incubated for 1 h at -20°C in a LR-Gold-propanol mixture and then 1 h at -20°C in LR-gold. For polymerization centrifuge tubes containing sapphire discs in LR-Gold were put in a mixture of glycerol and 2-propanol inside liquid nitrogen to lead off the thermal energy and were irradiated with UV-light overnight.

2.8.5.3 Trimming

Epon embedded samples were trimmed before sectioning using either a razor blade or a Leica EM Trim-Specimen. Thereby the edges of the resin block were milled to generate a quadratic or trapezoid cutting area. Before trimming, sapphire discs were removed from the resin, so that the cells remained at the surface of the epon block.

2.8.5.4 Sectioning

Samples were cut with a Reichert-Jung Ultracut E (or Ultracut UCT) ultramicrotome using a diamond knife (Diatome) to thin sections of 70 nm thickness for transmission electron microscopy (TEM). For STEM (Scanning transmission electron microscopy) tomography semi-thin sections with a thickness of 500 nm or 1 µm were prepared. The sections were collected either on formvar-coated or bare copper grids.

For tomography (Höhn et al., 2011) the sections were attached to poly-L-lysine (10% in water)-coated grids and warmed on a heating table to 60°C to flatten the sections. To attach the 15 nm colloidal gold particles that serve as fiducial markers for the calculation of the tomograms, the sections were again coated with poly-L-lysine. Afterwards the sections were carefully coated with 5 nm carbon from both sides by electron beam evaporation to increase electrical conductivity and mechanical stability in the microscope. Improving electrical conductivity helps to reduce mass loss caused by ionization due to inelastic scattering (Walther et al., 1995).

2.8.5.5 Additional contrasting

Ultra-thin sections on copper grids were additionally contrasted prior to microscopic analysis. Therefore grids were incubated for 7 min in 2% uranyl acetate (UAc in absolute EtOH) in the dark and washed seven times with Aqua dest.. Afterwards grids were incubated for 2 min in 0.2% lead citrate to stain proteins. To prevent crystallization of lead citrate, grids were rinsed two times in 10 M sodium hydroxid solution (NaOH) and five times in Aqua dest..

2.8.5.6 Sample preparation for Scanning electron microscopy

To prepare samples for SEM, hMDMs were co-incubated with stationary phase *L. major* promastigotes in 8-well µ-Slides for 1 h and a MOI of 10 (2.2.10.1). Extracellular parasites were washed away by rinsing the well twice with 300 µL complete-medium. Cells were fixed with a mixture of 4% PFA and 1% GA prior to critical point drying (CPD).

2.8.5.7 Preparation of cryo sections using Tokuyasu method

Tokuyasu method is named after its inventor Tokuyasu, who developed in 1973 (Tokuyasu, 1973) an immunogold labeling procedure on ultrathin cryo sections. In this technique sucrose is infused into chemically fixed samples to prevent ice crystals and to control the sectioning consistency.

To prepare cryo sections using Tokuyasu technique $4x10^6$ hMDMs were seeded in 400 µL culture medium in a 15 mL tube and were co-incubated with stationary phase *L. major* DsRed promastigotes ($10x10^6$/10 µL) for 3 h and a MOI of 15. After incubation cells were washed twice with 5 mL complete medium (135 xg, 8 min, RT) and were fixed in 1 mL 4% PFA/1% GA (in PBS) for 45 min in the refrigerator. Subsequently, cells were washed with 14 mL PBS (545 xg, 8 min, RT), the pellet was resuspended in 2 mL PBS and cells were stored at 4°C until preparation of cryo sections. For freezing, the cells were embedded in 3% Low Gelling Agarose and small pieces were placed in 1.8 M Sucrose with 20% Polyvinylpyrolidone (PVP) overnight at 4°C. The next day the agarose pieces were sticked to the head of a pin using 1.8 M Sucrose with 20% PVP. Cells were frozen by direct immersion in liquid nitrogen. Before cryo sectioning, agarose blocks were trimmed using a metal thorn. Sectioning was performed using an ultramicrotome with a cryokit attachment. For cooling, the sectioning chamber was flushed with liquid nitrogen and 100 nm thin sections were cut using a glass knife. The sections were collected with a sucrose-filled loop and transferred either on a microscopic slide for immunofluorescence staining (2.6.3) or on Formvar coated

nickel grids for immunogold labeling (2.6.4). To prevent drying of the sucrose, the samples were deposited in a humidified chamber.

2.8.6 Transmission electron microscopy (TEM)

Samples were imaged with a Zeiss EM 109 transmission electron microscope at an acceleration voltage of 80 kV and a magnification between 5.000x and 30.000x. LR-Gold embedded samples (2.8.5.2) were analyzed on a Jeol JEM-1400 transmission electron microscope at a magnification between 1.000x and 50.000x.

2.8.7 Scanning electron microscopy (SEM)

The scanning electron microscope creates an image by scanning across the sample with a focused electron beam. The displayed image maps the specimen surface, such as its topography and compositions. Samples were analyzed on a Hitachi S-5200 scanning electron microscope with a magnification between 2.500x and 18.000x.

2.8.8 Scanning transmission electron microscopical tomography (STEM tomography)

In general, electron microscopy creates two-dimensional images of a three-dimensional sample. With scanning transmission electron microscopical (STEM) tomography a three-dimensional data-set can be acquired by gradually tilting the sample in the electron beam. At every tilt angle an image is recorded and this image series is reconstructed into a three-dimensional model. The tilt series (-72° to +72° with a 2° increment) of semi-thin sections was recorded with a 300 kV field emission STEM (Titan) as described in Höhn et al. (Höhn et al., 2011). Tomograms were reconstructed either automatically or with the help of the colloidal gold particles as fiducial markers using the standard settings of the IMOD software package (Kremer et al., 1996).

2.8.9 Focused ion beam/scanning electron microscopy tomography (FIB/SEM tomography)

Focused ion beam/scanning electron microscopy (FIB/SEM) tomography is a novel approach for the acquisition of three-dimensional datasets. FIB/SEM tomography is also called “slice and view”, because the resin embedded sample is first milled with the FIB and the produced surface in then imaged by SEM (Figure 17). These processes can be repeated over large volumes allowing a 3D analysis of whole eukaryotic cells. The epon block containing cells of interest was sawed with a jigsaw to a height of 1 mm and mounted on an SEM specimen. The epon block was imaged using the FEI Helios Nanolab 600 FIB/SEM. Depending on the accelerating voltage the contours of the embedded cells were visible what helps to find the area of interest. Finally slicing and viewing was performed using the software module Auto Slice & View.G1 from FEI.

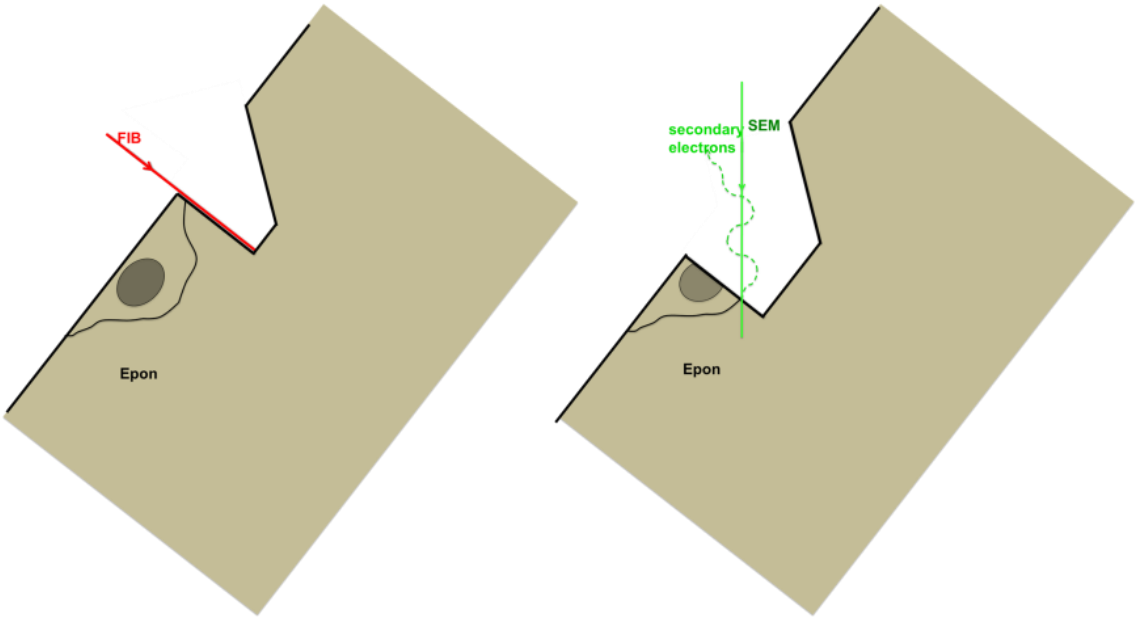

Figure 17: Theoretical mechanism of FIB/SEM tomography. Epon embedded sample is repeatedly milled with the focused ion beam (FIB) and then imaged by scanning electron microscopy (SEM). Adapted from (Villinger et al., 2012).

2.8.10 Correlative fluorescence and electron microscopy

The term correlative microscopy refers to imaging of structures with at least two imaging modalities. This commonly combines fluorescence and electron microscopy. Fluorescent probes provide the ability to follow special targets on or in living cells. However, fluorescence microscopy is limited in the resolution. By traditional electron microscopy higher resolution can be revealed enabling to image the ultrastructure of cells like organelles, membranes or macromolecules. By combining both imaging techniques, cellular processes in living cells can now be followed up at high resolution at the ultrastructural level. This makes correlative microscopy a new powerful research tool (Giepmans, 2008).

For correlative fluorescence and electron microscopy transduced and infected hMDMs (2.2.10.3) were at first analyzed on a fluorescence microscope (Zeiss Observer Z.1, HXP120C) prior to HPF, freeze substitution and epon-embedding (2.8.5.2). Afterwards cells were analyzed by FIB/SEM (2.8.9) to visualize them on the ultrastructural level. Alternatively cells were prepared for and analyzed by SEM (2.8.5.6, 2.8.7).

2.9 Statistical analysis

Data are depicted as mean values ± standard deviation (SD). Microsoft Excel 2010 software was used to determine SD. Statistical significance of the data was analyzed using unpaired or paired student´s t-test (two-tailed distribution) with GraphPad Prism software. Values of $p< 0.05$ (*), $p< 0.01$ (**) and $p< 0.005$ (***) were considered significant.

3 Results

3.1 Interaction of human monocyte derived macrophages (hMDMs) with *Leishmania (L.) major* parasites

In leishmaniasis macrophages are known to be the final host cell for the parasite *L. major* and in the human body there exist different types of macrophages (1.3). Our research has focused on two macrophage phenotypes, which among others differ in their morphology (Figure 18). Pro-inflammatory human monocyte derived macrophages type I (hMDM I) show a rounded morphology (Figure 18 A), whereas anti-inflammatory hMDM type II appear with a longish shape (Figure 18 C). Both macrophage types can be infected with *L. major* promastigotes (Figure 18 B and E), but the parasite burden, in this case the amount of parasites per macrophages, is higher in hMDM II than in hMDM I. The same is true for *L. major* amastigote infected macrophages (Figure 18 C and F). Beside this, amastigote infection results per se in a higher parasite burden than promastigote treatment. This data is in concordance with previous findings from our group (Wenzel et al., 2012).

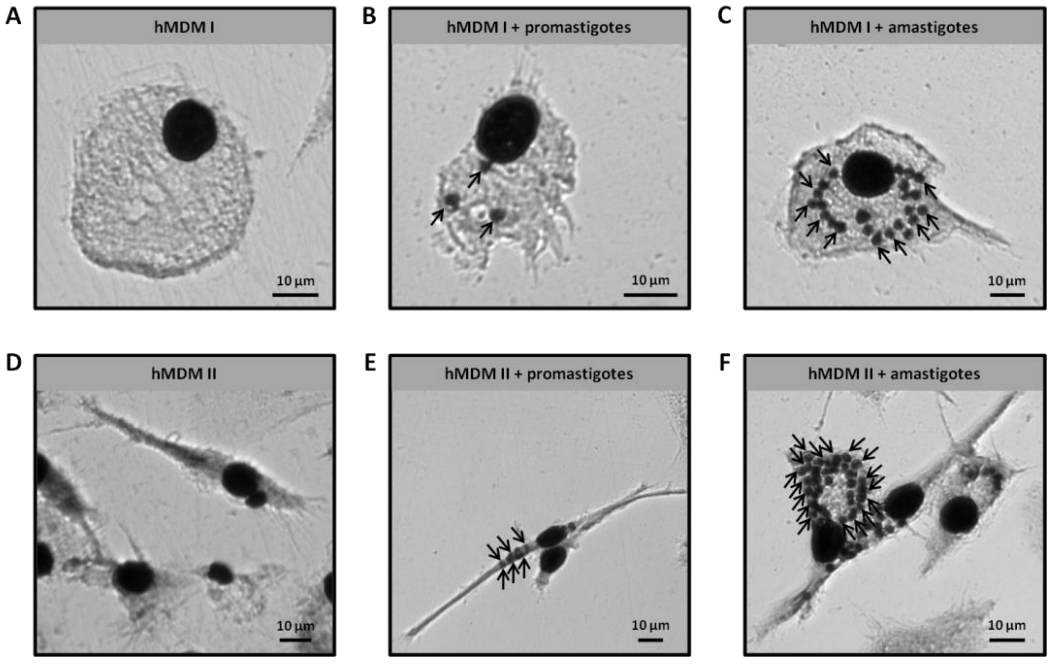

Figure 18: Different hMDM types and their interaction with *L. major* promastigotes and amastigotes. hMDMs were co-incubated with *L. major* parasites. Extracellular parasites were removed 3 h p.i. and 72 h p.i. the cells were stained with Diff QUIK. A) pro-inflammatory hMDM I B) hMDM I co-incubated with stationary phase *L. major* promastigotes C) hMDM I co-incuabted with axenic *L. major* amastigotes D) anti-inflammatory hMDM II E) hMDM II co-incubated with stationary phase *L. major* promastigotes F) hMDM II co-incubated with axenic *L. major* amastigotes. Representative micrographs were taken on a Zeiss Axio Observer Z1. Black arrows indicate intracellular parasites. Magnification: 40x objective with 10x ocular. Scale bar: 10 µm.

3.2 Part 1: Analysis of the amastigote containing parasitophorous vacuole

In the first part of this thesis we focused on the analysis of the *L. major* amastigote containing parasitophorous vacuole inside hMDMs, because we hypothesize that after re-infection of macrophages during disease development, amastigotes are able to escape from their compartment into the cytoplasm.

3.2.1 Comparison of chemical fixation and High-Pressure-Freezing for ultrastructural analysis of *L. major* containing compartments

To validate whether *L. major* amastigotes are able to escape the parasitophorous vacuole after re-infection of human macrophages, we first of all had to find appropriate methods for analysis. We set out to apply state of the art ultrastructural compartment analyses; therefore we first compared two different sample preparation methods for transmission electron microscopy (TEM). We prepared samples either with chemical fixation or with High-Pressure-Freezing (HPF) and subsequent freeze substitution. Both preparation methods resulted in clearly contrasted samples of *L. major* amastigote infected macrophages. In both cases we were able to identify the amastigotes and characteristic parasite structures like the nucleus (N), the kinetoplast (KP), the flagellum pocket (FP) and microtubular structures (M) below the parasite membrane (Figure 19). Quantifying the structural integrity of the host macrophage PV membrane and parasite lipid bilayer we found the phagosomal and parasite membrane to be interrupted after chemical fixation, both in hMDM I and hMDM II (Figure 19 A and C). In contrast to that amastigotes were surrounded by an intact phagosomal membrane after HPF (Figure 19 B and D).

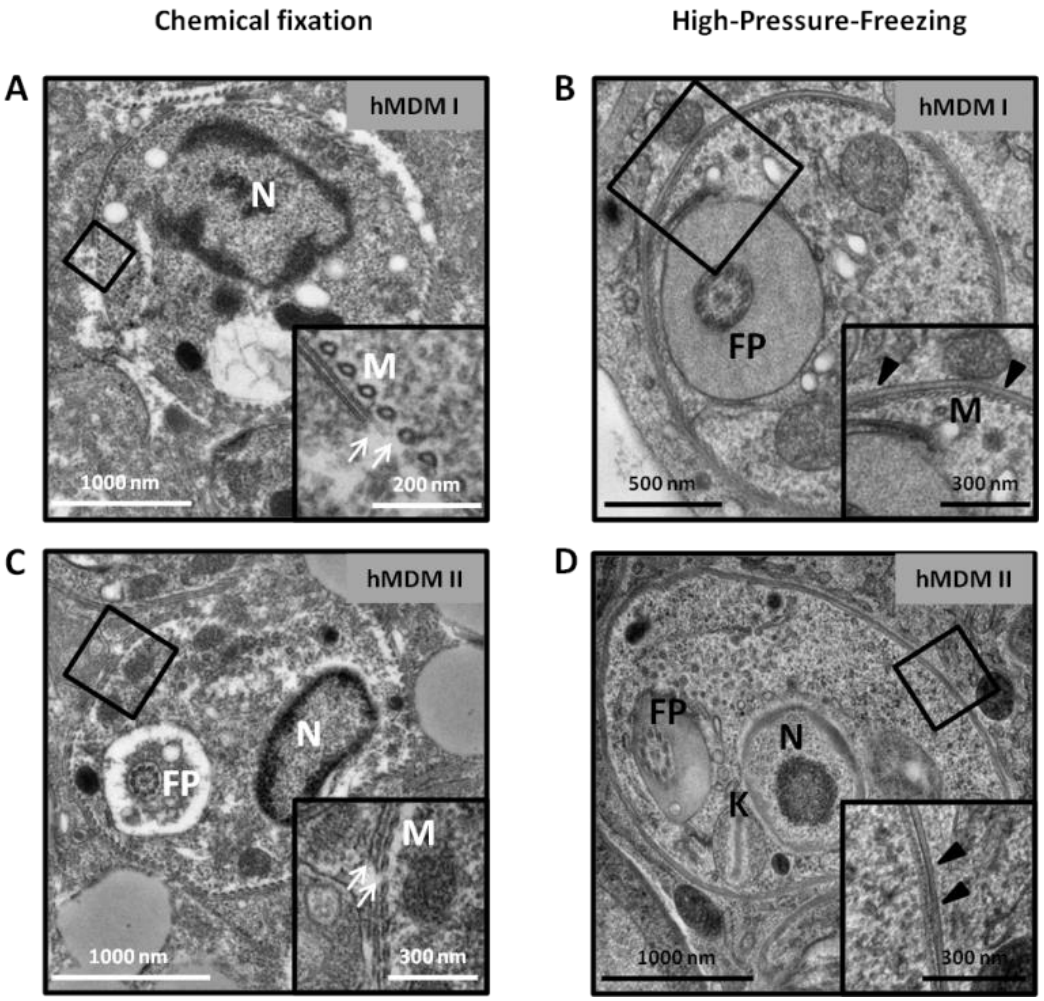

Figure 19: HPF in contrast to chemical fixation results in a better preserved ultrastructure. hMDMs were co-incubated with axenic *L. major* amastigotes for 3h. Extracellular parasites were removed and cells incubated for 48h prior to either chemical fixation with glutaraldehyde or High-Pressure-Freezing (HPF) and subsequent preparation for electron microscopy. Ultra-thin sections were analyzed by transmission electron microscopy (TEM). A) Amastigote infected hMDM I after chemical fixation. B) Amastigote infected hMDM I after HPF. C) Amastigote infected hMDM II after chemical fixation. D) Amastigote infected hMDM II after HPF. Representative EM micrographs of at least three independent experiments were taken on a Zeiss EM 109 transmission electron microscope. Magnification: between 5.000x and 30.000x. White arrows indicate interrupted lipid bilayers. Arrowheads indicate intact compartment membranes. N=nucleus, KP=kinetoplast, FP=flagellum pocket, M=microtubular structure. Scale bar: as indicated.

3.2.2 Axenic *L. major* amastigotes reside in an interrupted parasitophorous vacuole and in the cytoplasm

Since HPF resulted in a better preserved ultrastructure of membranes (3.2.1) we used this method for investigation of *L. major* amastigote compartment membrane integrity. We co-incubated hMDM I (Figure 20 A) and hMDM II (Figure 20 B) with axenic *L. major* amastigotes for different time points (3h, 24h, 48h, 144h) and analyzed HPF fixed samples by TEM. For all time points we found interrupted compartment membranes shown in the enlargements of TEM micrographs in Figure 20 A and B indicated by the black arrows. In some cases there were only small interruptions (Figure 20 A, 24h and 48h p.i.), other membranes looked more like they were bursted (Figure 20 B, 3h and 48h p.i.) or there were only small patches of compartment membranes left around the parasite (Figure 20 A, 144h p.i.).

Quantification of amastigotes laying in interrupted PVs using EM micrographs (Figure 20 C and D) suggests that the amount of damaged compartments increases with the time of infection. This could be shown for hMDM I and hMDM II. It has to be noted, that for some time points only one donor (instead of two) could be analyzed because of fixation problems.

Beside analysis of ultra-thin sections by TEM we generated semi-thin sections of high-pressure frozen samples and analyzed them by scanning transmission electron microscopic tomography (STEM tomography). During STEM tomography the sample is tilted in the electron beam and a picture is taken at every angle, so that a tomographic 3D model can be calculated. Representative sections of EM tomograms of *L. major* infected hMDM II are shown in Figure 21. The parasites can be clearly identified by characteristic structures like the nucleus (N), the flagellum pocket (FP) and the subpellicular microtubular structure (M) associated with the parasite membrane (PM). Black and white arrowheads indicate the parasite membrane (PM). Figure 21 A shows an interrupted parasitophorous vacuole (PV), that is still intact in the first section, but gets more and more disrupted in the other two sections indicated by the black arrows. Using EM tomography we even found an amastigote without a PV laying in the cytoplasm of the host (Figure 21 B). The PV was absent in all analyzed sections.

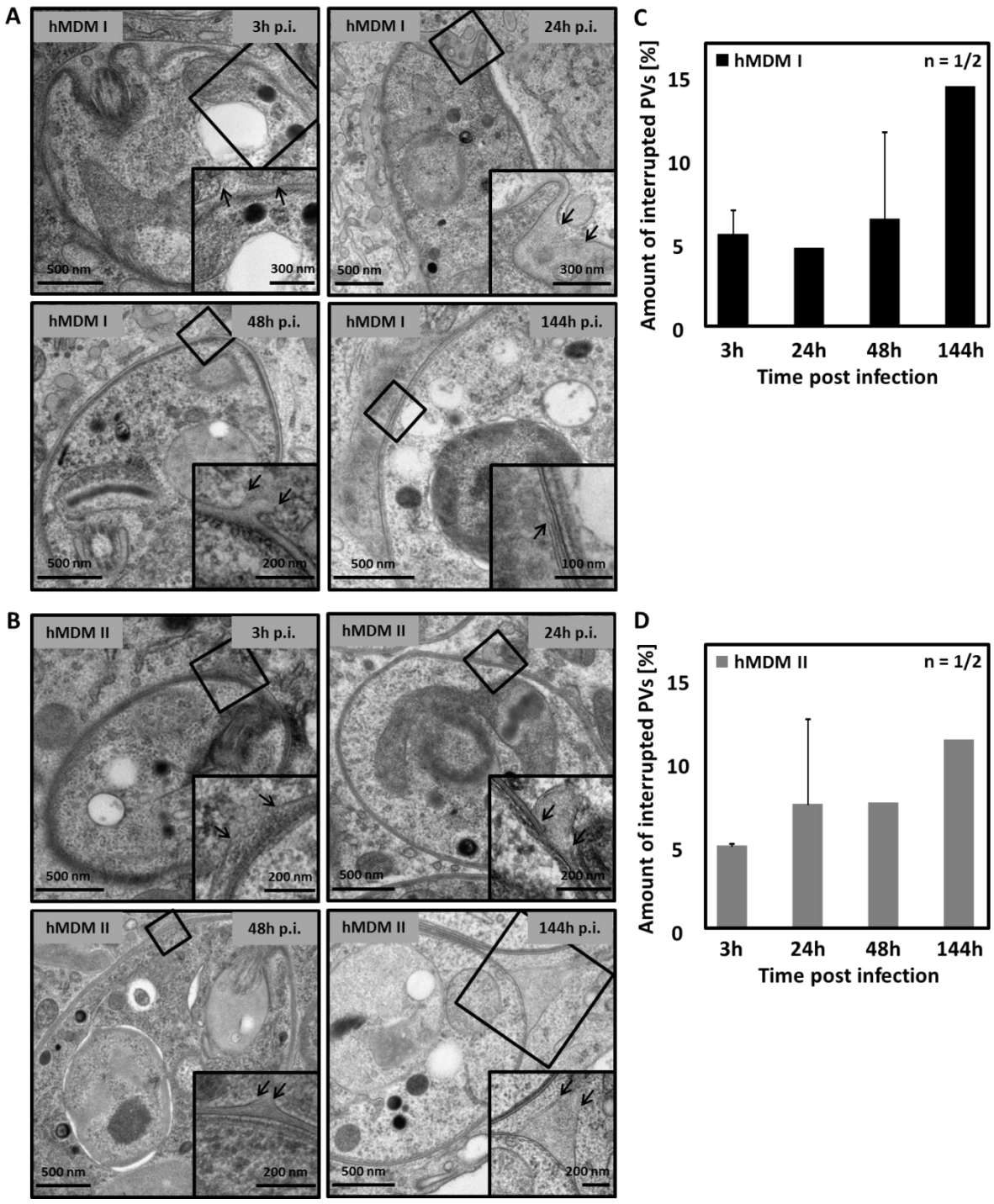

Figure 20: Axenic *L. major* amastigotes reside in an interrupted PV. hMDMs grown on sapphire disks were co-incubated with axenic *L. major* amastigotes for 3h. Extracellular parasites were removed and cells either directly fixed by HPF or incubated for given time points prior to HPF and subsequent preparation for electron microscopy. Ultra-thin sections were analyzed by TEM. A) Amastigotes in interrupted PVs inside hMDM I. B) Amastigotes in interrupted PV inside hMDM II. C) and D) Quantification of amastigotes with an interrupted PV membrane using TEM micrographs shown in (A) and (B). Representative EM micrographs were taken on a Zeiss EM 109 transmission electron microscope. Magnification: between 5.000x and 30.000x. Black squares indicate enlarged region. Black arrows in the enlargement show interrupted parasitophorous vacuoles (PVs). Scale bar: as indicated.

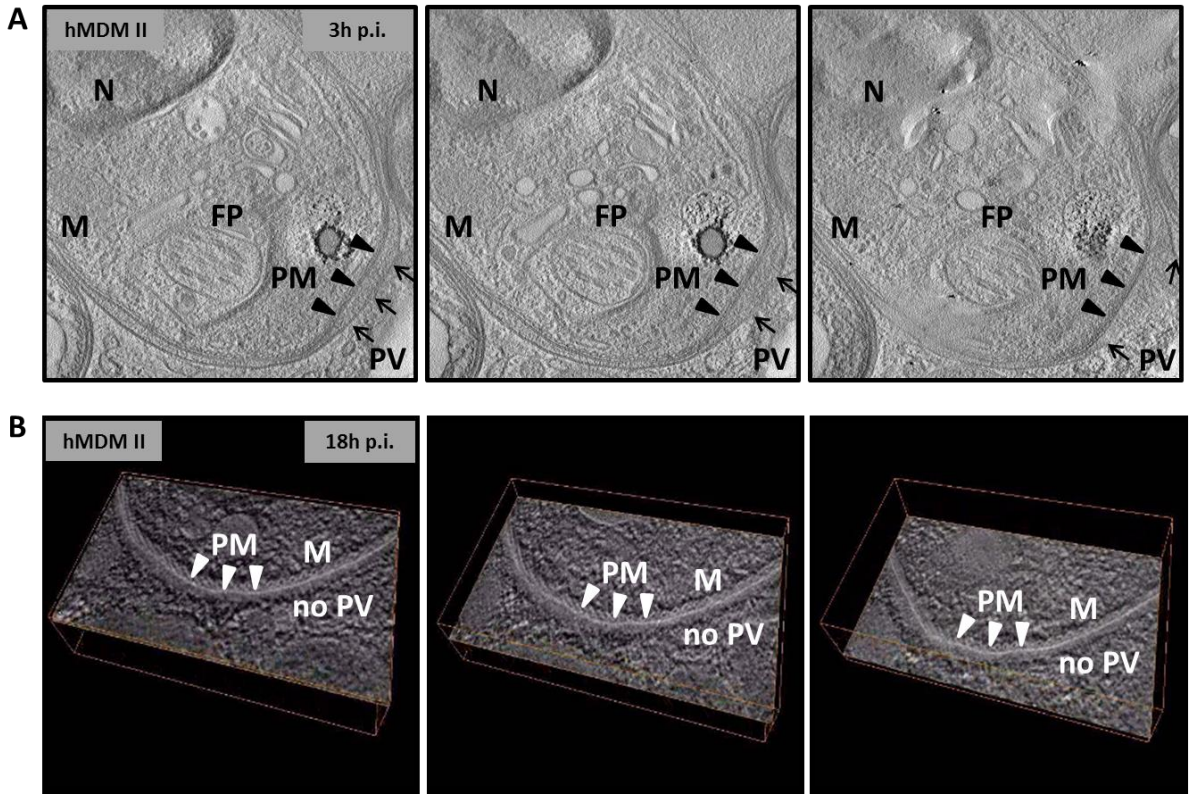

Figure 21: *L. major* amastigotes in an interrupted PV and in the cytoplasm visualized by HPF and STEM tomography. hMDM II grown on sapphire disks were co-incubated with axenic *L. major* amastigotes for 3h. Extracellular parasites were removed and cells either directly fixed by HPF (A) or incubated for 18h (B) prior to HPF and subsequent preparation for electron microscopy. Semi-thin sections were analyzed by STEM tomography on a FEI Titan (S)TEM equipped for electron tomography. A) Amastigote in an interrupted PV. B) Amastigote laying in the cytoplasm of the host. Arrows indicate the parasitophorous vacuole (PV). Arrowheads indicate the parasite membrane (PM). N=nucleus, FP=flagellum pocket, M=microtubular structure.

3.2.3 Axenic *L. major* amastigotes inside abnormal parasitophorous vacuoles

While analyzing *L. major* amastigote compartment integrity we discovered several abnormally PVs when macrophages were infected for longer time periods with amastigotes. Usually single *L. major* amastigotes are surrounded by one tight PV as it is shown in Figure 22 A and Figure 23 A. We were able to detect multiple amastigotes in one PV (Figure 22 B-D). For instance we found two amastigotes in one common PV both for hMDM II (Figure 22 B) and hMDM I (data not shown) after 144h of infection. Interestingly in hMDM I but not hMDM II we found big PVs containing four or even more amastigotes (Figure 22 C and D) without a compartment membrane in between the parasites. These common PVs harboring multiple amastigotes, we also found in chemical fixed samples 120h p.i. (data not shown).

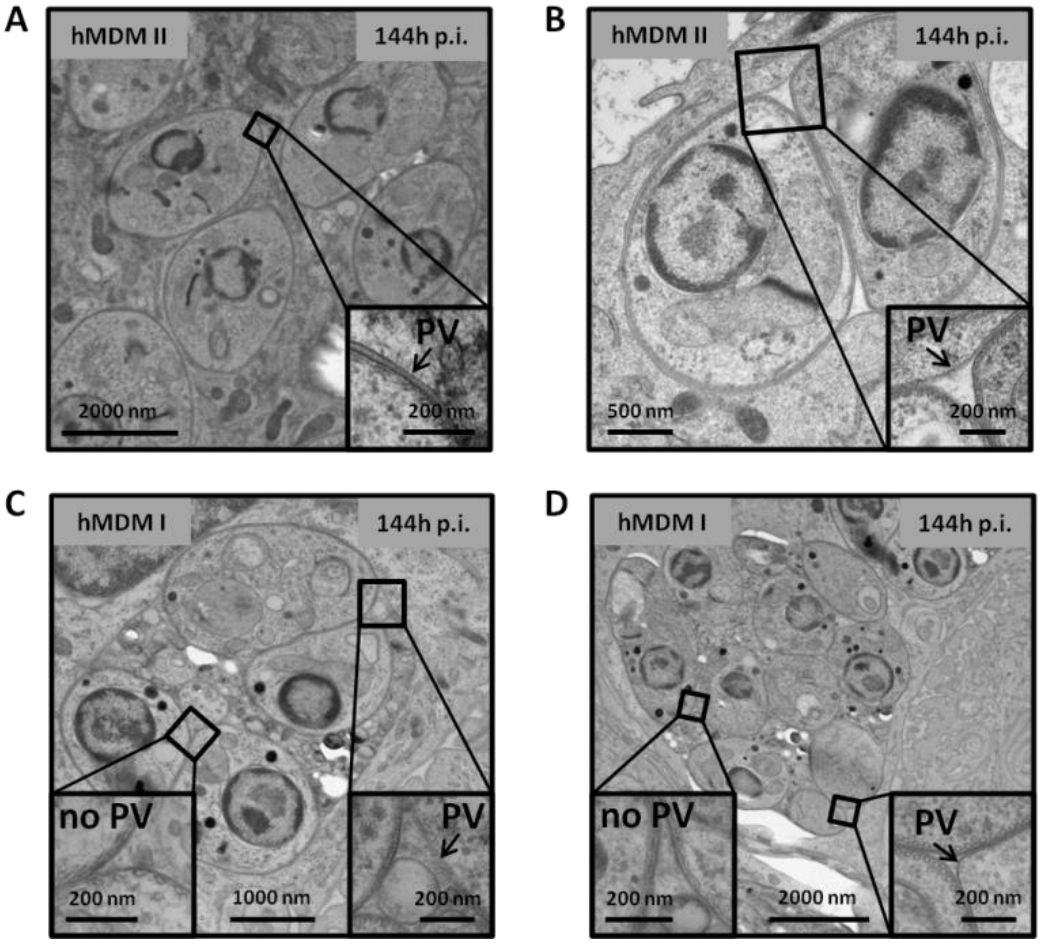

Figure 22: Multiple axenic *L. major* amastigotes in a common PV 144h post infection. hMDM II (A and B) and hMDM I (C and D) grown on sapphire disks were co-incubated with axenic *L. major* amastigotes for 3h. Extracellular parasites were removed and cells incubated for 144h prior to HPF and subsequent preparation for electron microscopy. Ultra-thin sections were analyzed by TEM. A) Amastigotes in a single PV. B) Two amastigotes in one common PV. C) Four amastigotes in one common PV. D) Multiple amastigotes in one common PV. Representative EM micrographs of one donor were taken on a Zeiss EM 109 transmission electron microscope. Magnification: between 5.000x and 30.000x. Black squares indicate enlarged region. Black arrows in the enlargement show the parasitophorous vacuole (PV). Scale bar: as indicated.

In addition we detected amastigotes in abnormal large compartments after early and late time points like 3h, 24h and 48h (data not shown) and after very late time points like 144h (Figure 23 B). Moreover we found few micrographs showing digested amastigotes demonstrated in Figure 23 C. Beside the parasitophorous vacuole and the parasite membrane the nucleus and some residual microtubular structures can still be clearly identified.

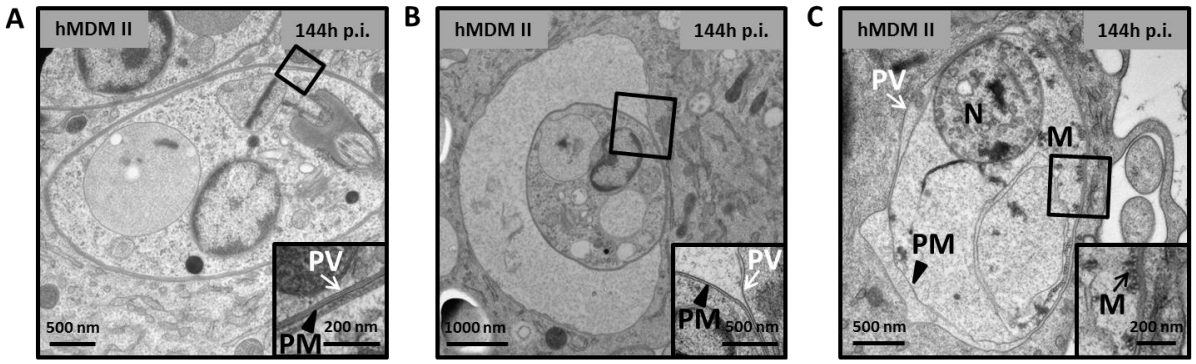

Figure 23: Axenic *L. major* amastigote in a single tight PV or a large PV and a digested amastigote. hMDM II grown on sapphire disks were co-incubated with axenic *L. major* amastigotes for 3h. Extracellular parasites were removed and cells incubated for 144h prior to HPF and subsequent preparation for electron microscopy. Ultra-thin sections were analyzed by TEM. A) Amastigote in a normal single tight PV. B) Amastigote in an abnormal large PV. C) Digested amastigote. Preliminary representative EM micrographs were taken on a Zeiss EM 109 transmission electron microscope. Magnification: between 5.000x and 30.000x. Black squares indicate enlarged region. White arrows in the enlargement show the parasitophorous vacuole (PV). Black arrowheads show the parasite membrane (PM). Black arrow shows microtubular structures (M). Scale bar: as indicated.

3.3 Part 2: Development and maturation of the *L. major* promastigote containing parasitophorous vacuole

In the second part of this study we focused on the *L. major* promastigote containing parasitophorous vacuole inside hMDMs. On the one hand we looked for differences between viable and apoptotic promastigotes concerning the parasite uptake by hMDMs as well as the compartment composition and on the other hand we were interested in the development and maturation of the promastigote containing compartment in general.

3.3.1 Differences between viable and apoptotic *L. major* promastigotes and their uptake by hMDMs

The virulent inoculum of *L. major* promastigotes consists of a mixture of viable and apoptotic parasites (van Zandbergen et al., 2006). In vitro they are represented by stationary phase promastigotes, which are grown in biphasic Novy-McNeal-Nicolle (NNN) blood agar medium for 6 to 8 days. In the infectious inoculum about 50% of the parasites are viable or apoptotic respectively and show different morphological characteristics.

3.3.1.1 Morphological characteristics of viable and apoptotic *L. major* promastigotes

Morphological characteristics of *in vitro* cultured viable and apoptotic stationary phase promastigotes were analyzed by light microscopy after Diff QUIK staining and by scanning electron microscopy (SEM). Viable promastigotes show an elongated parasite body with a length of 10 to 20 µm, a diameter of 1 to 2 µm and one flagellum at the apical end for active movement (Figure 24 A). Apoptotic promastigotes reveal different morphologically features like rounding and shrinkage of the parasite body (Figure 24 B). The parasite body decreases in size having a length of 5 to 10 µm and a diameter of 3 to 5 µm. Apoptotic promastigotes usually have one external flagellum at the apical end, but sometimes they even show a second shorter flagellum (Figure 24 B, right panel). Apoptotic promastigotes are not able to actively move using their flagellum (as observed by cell culture light microscopy).

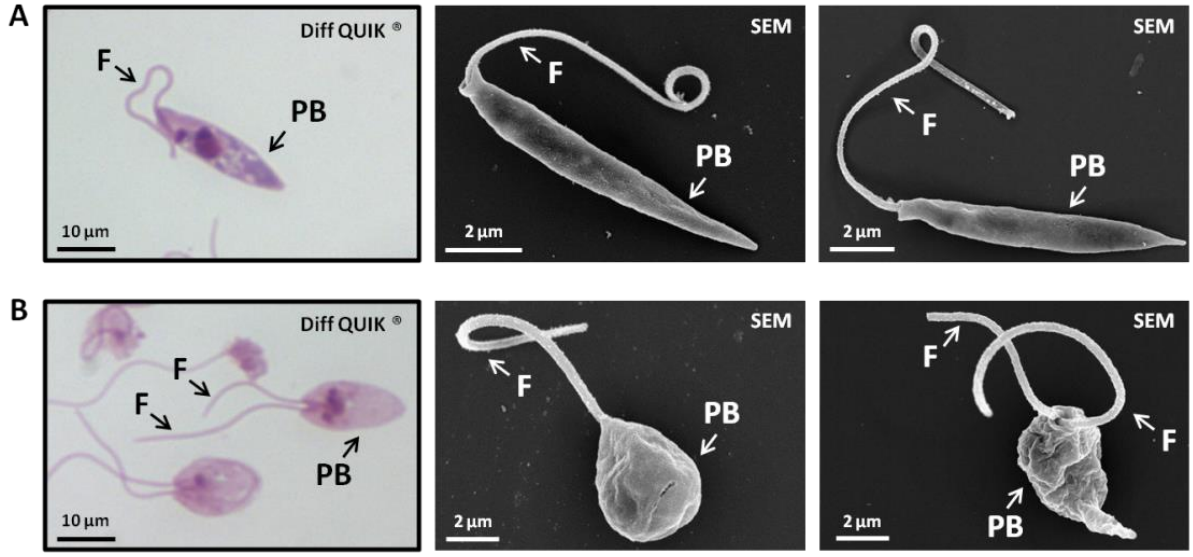

Figure 24: Different morphology of viable and apoptotic *L. major* promastigotes. Stationary phase *L. major* promastigotes were either cyto-centrifuged, Diff QUIK stained and analyzed by light microscopy or fixed and prepared for scanning electron microscopy (SEM). A) Morphology of viable stationary phase promastigotes. B) Morphology of apoptotic stationary phase promastigotes. Representative light microscopy photographs were taken on a Zeiss Axiophot with a 100x oil objective and a 10x ocular. Representative SEM micrographs were taken on a Hitachi S-5200 scanning electron microscope. Magnification: between 11.000x and 18.000x. Arrows indicate parasite body (PB) or flagellum (F). Scale bar: as indicated.

In addition we analyzed the different shape of the parasites by TEM (Figure 25). If the section of the parasite is longitudinal, one can clearly differentiate between the longish parasite body (PB) of the viable promastigotes and the rounded shape of the apoptotic parasite body. Moreover we observed further ultrastructural differences between viable

(Figure 25 A) and apoptotic (Figure 25 B) *L. major* promastigotes. The nucleus (N) of viable promastigotes is characterized by a central nucleolus and chromatin associated with the nuclear envelope. Furthermore viable promastigotes show a single kinetoplast (KP), which is a region of the mitochondrion containing concentrated DNA. The subpellicular microtubular structures (M) are equally arranged under the parasite membrane (Figure 25 A). In comparison to that apoptotic parasites show disordered microtubular structures, a swollen kinetoplast presenting disorganization of mitochondrial cristae and k-DNA and a loss of nuclear organization, characteristic of apoptosis (Figure 25 B) and in concordance with Aliança et al. (Aliança et al., 2014).

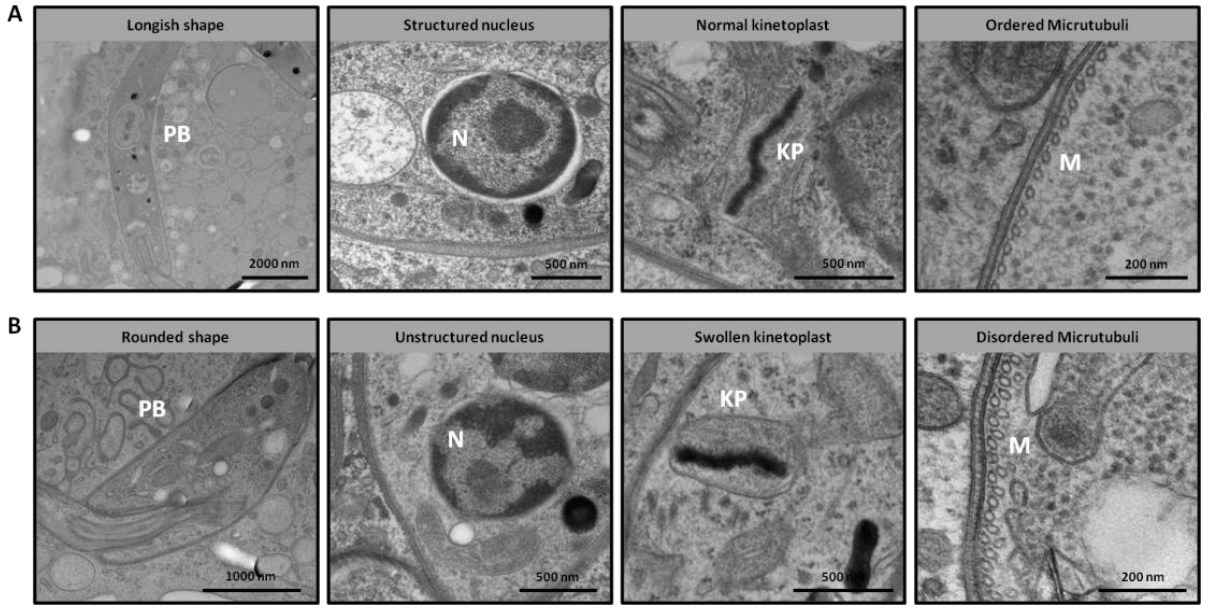

Figure 25: Ultrastructural differences of viable and apoptotic *L. major* promastigotes. hMDMs grown on sapphire disks were co-incubated with 12-13 days old *L. major* promastigotes for 3h. Extracellular parasites were removed and cells were fixed using HPF and prepared for electron microscopy. Ultra-thin sections were analyzed by TEM. A) Ultrastructural characteristics of viable promastigotes. B) Ultrastructural characteristics of apoptotic promastigotes. Representative EM micrographs were taken on a Zeiss EM 109 transmission electron microscope. Magnification: between 5.000x and 30.000x. PB=parasite body, N=nucleus, KP=kinetoplast, M=microtubular structures. Scale bar: as indicated.

3.3.1.2 Separation of viable and apoptotic *L. major* promastigotes by Annexin V binding to phosphatidylserine

Another characteristic of apoptotic promastigotes is their ability to bind annexin V, suggesting externalization of phosphatidylserine (PS), similar as with apoptotic cells. The human vascular anticoagulant, annexin V, is a Ca^{2+}-dependent phospholipid-binding protein that has high affinity for PS. Annexin V labeled with a fluorophore can identify apoptotic *L. major* promastigotes by flow cytometry. Furthermore, for magnetic separation of apoptotic from viable promastigotes superparamagnetic-particles that are conjugated to annexin V can be used. Stationary phase promastigotes were separated by positive selection using an AnnexinV MicroBead Kit from Miltenyi. After this separation procedure the purity of the PS-positive (PS+) and PS-negative (PS-) fractions as well as the initial population were quantified using a counting chamber (Table 17). Stationary phase day 8 promastigotes were found to consist of 55.5% ± 5.8 PS+ parasites. After separation, the PS+ fraction, here termed the apoptotic parasites, had a purity of about 95.0% ± 3.1. In the PS- fraction, which should contain the viable parasites, there were still over 25.5% ± 3.5 PS-positive parasites left. A second separation step of the PS- fraction using negative selection, which is designed for depletion of labeled cells, improved the purity to around 11.2% ± 3.8 (established by a Master student: Henner Zirpel). Moreover the purity of the different fractions was assessed by AnnexinV Fluos staining and flow cytometry. Representative FACS histograms are shown in Figure 26.

Table 17: Quantification of viable and apoptotic *L. major* promastigotes during MACS separation. Stationary phase day 8 (d8) promastigotes were incubated with AnnexinV MicroBeads for separation via magnetic columns prior to counting the parasites of the different fractions and the initial population in a counting chamber. Depicted are percentages of viable and apoptotic promastigotes. Data are shown as means ± SD. n=12 except last column n=4.

	stationary phase d8 parasites [%]	d8 PS+ fraction LS column [%]	d8 PS- fraction LS column [%]	d8 PS- fraction LD column [%]
Viable *L. major* promastigotes	44.5 ± 5.8	5.0 ± 3.1	74.5 ± 3.5	88.8 ± 3.8
Apoptotic *L. major* promastigotes	55.5 ± 5.8	95.0 ±3.1	25.5 ± 3.5	11.2 ± 3.8

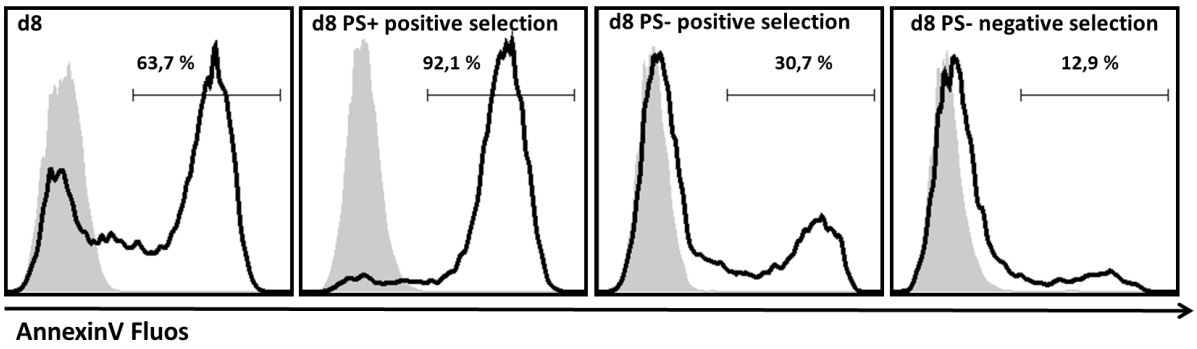

Figure 26: AnnexinV staining of separated *L. major* promastigotes. Stationary phase day 8 (d8) promastigotes were incubated with AnnexinV MicroBeads, separated via magnetic columns, stained for phosphatidylserine using AnnexinV Fluos and analyzed by flow cytometry. A) Representative FACS histogram of one experiment out of four independent experiments. Filled area shows unstained parasites, solid black line AnnexinV Fluos stained parasites. Percentages indicate PS+ parasites inside marked gate. Kind of fraction is indicated in the upper left side.

3.3.1.3 Different uptake of viable and apoptotic *L. major* promastigotes by hMDMs

Since viable and apoptotic promastigotes show different morphological characteristics we wanted to know whether they show also differences in the uptake by hMDMs. Therefore we co-incubated hMDMs with stationary phase promastigotes and prepared samples for SEM analysis. Preliminary experiments show that in both macrophage type's viable promastigotes are taken up via the flagellum tip (Figure 27 left panel of A and B). We did not observe apoptotic promastigote uptake starting at the flagellum. However we found one flagellum or a double flagellum, characteristic for apoptotic promastigotes, looking out of the macrophages (Figure 27 right panel of A and B), indicating apoptotic promastigote uptake with the parasite body first.

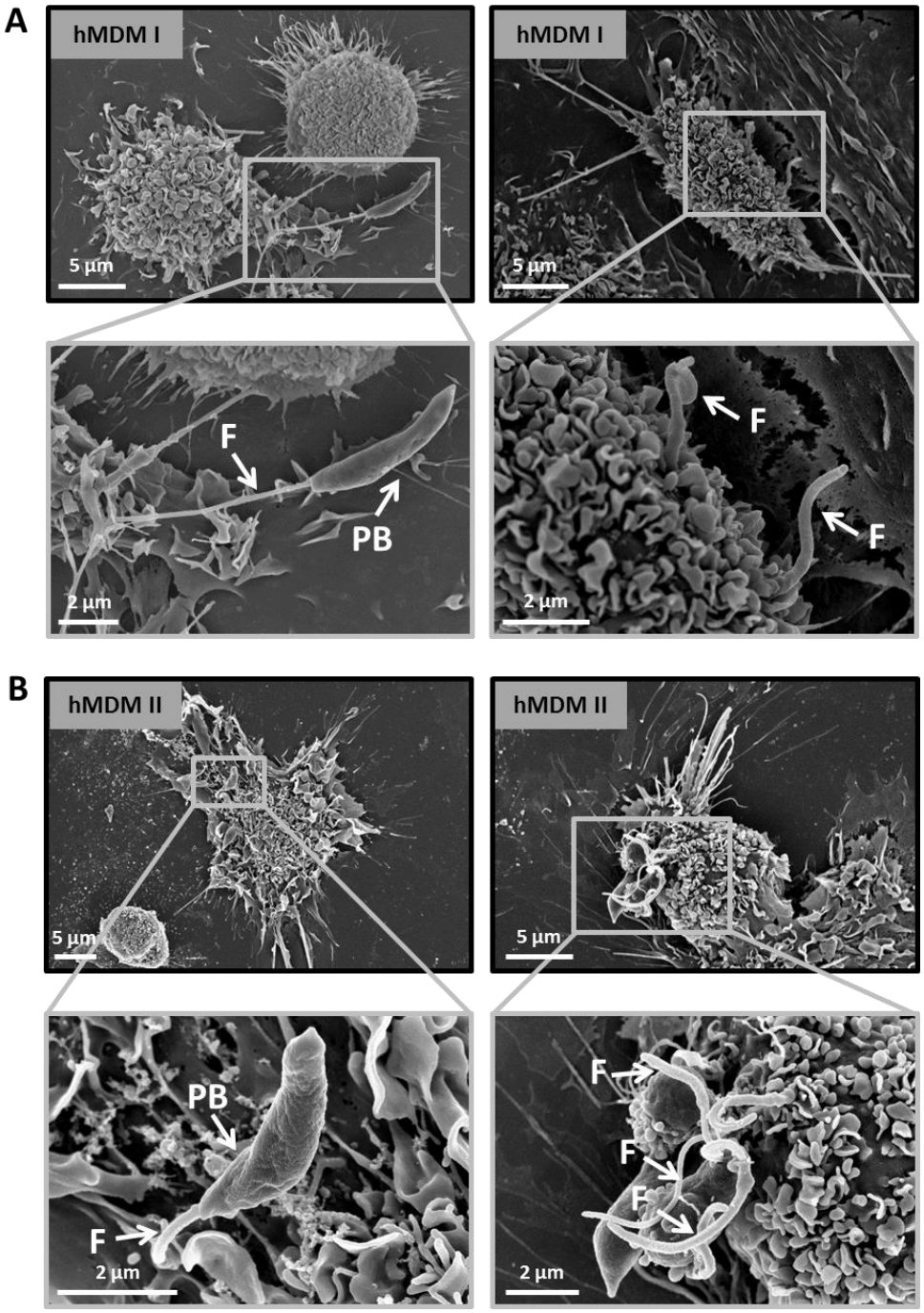

Figure 27: Different uptake of viable and apoptotic promastigotes by hMDMs. hMDM I (A) and hMDM II (B) were co-incubated with stationary phase *L. major* promastigotes for 1 h. Extracellular parasites were removed and cells were fixed for subsequent preparation for scanning electron microscopy (SEM). Left panels show hMDM I (A) and hMDM II (B) taking up a viable promastigote via the flagellum tip. Right panels show apoptotic promastigotes invading hMDM I (A) and hMDM II (B) with the parasite body first. SEM micrographs (n=1) were taken on a Hitachi S-5200 scanning electron microscope. Magnification: between 2.500x and 18.000x. Arrows indicate parasite body (PB) or flagellum (F). Scale bar: as indicated.

3.3.1.4 Live cell imaging of viable and apoptotic *L. major* promastigotes entering hMDMs

As mentioned above we found viable and apoptotic stationary phase *L. major* promastigotes entering hMDMs differently. Using live cell imaging of the uptake process we wanted to confirm our results. We co-incubated hMDM I and stationary phase promastigotes and with light microscopy time lapse imaging we focused on the invasion of a longish shaped viable promastigote (Figure 28). The overall uptake process took about 20 min. In the beginning of the movie (0 min) the parasite attached via the flagellum tip to the hMDM. During the first 10 min the parasite body was strongly moving in all directions with the flagellum tip staying attached to the macrophage. By membranes extruding from the macrophage, the flagellum was more and more ingested until it was completely covered after 18 min. From now the uptake process proceeded very fast. Already after 21 min the whole parasite was inside the macrophage.

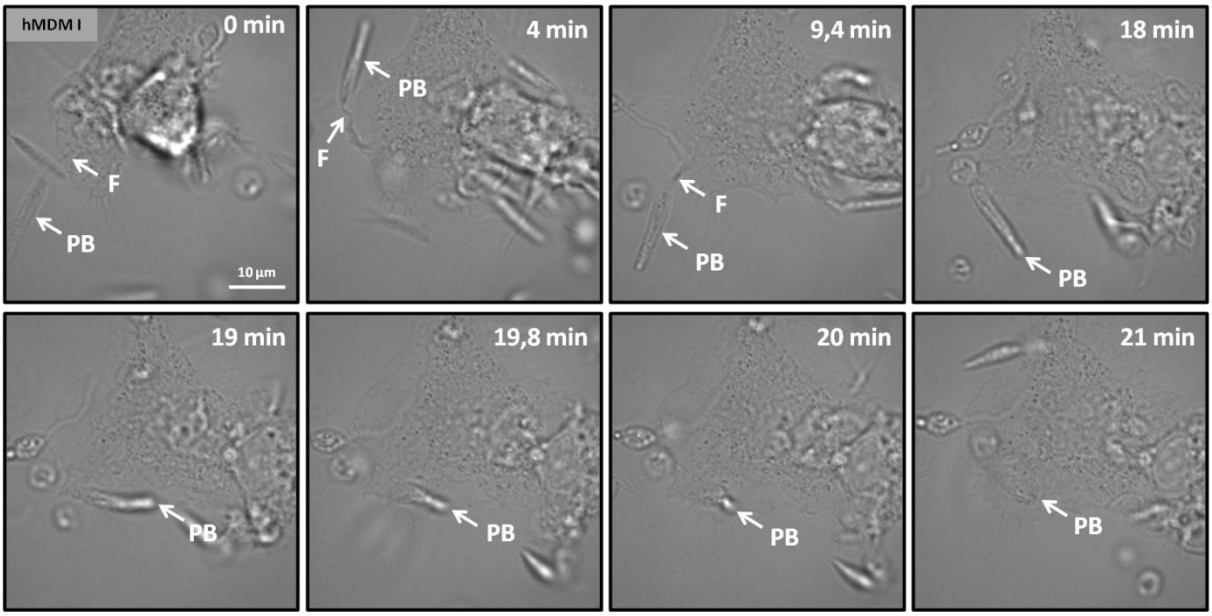

Figure 28: Live imaging of a viable promastigote entering a hMDM I. hMDM I were co-incubated with stationary phase *L. major* promastigotes and were directly analyzed by time lapse imaging using light microscopy. hMDM I taking up a viable promastigote via its flagellum tip is shown in time. Time lapse movie (n=1) was generated on a Zeiss LSM7 *Live* confocal laser scanning microscope with a 63x oil objective and a 10x ocular. Arrows indicate parasite body (PB) or flagellum (F). Scale bar: as indicated.

Similar like for a viable promastigote we were able to visualize the uptake of an apoptotic promastigote. We co-incubated hMDM I with PS+ purified apoptotic promastigotes and imaged the uptake process using time lapse light microscopy (Figure 29). The overall uptake

process took about 12 min and was faster than it was observed for viable promastigotes. In the beginning of the movie the apoptotic parasite slightly attached via the flagellum to the macrophage shown at the left side of the pictures. For the first 4 min one got the impression that this macrophage will take up the parasite. Another 4 min later a second macrophage on the right side was moving inside the picture getting in contact with the parasite body. Within the next 5 min the apoptotic promastigote disappeared inside the right macrophage with the parasite body first.

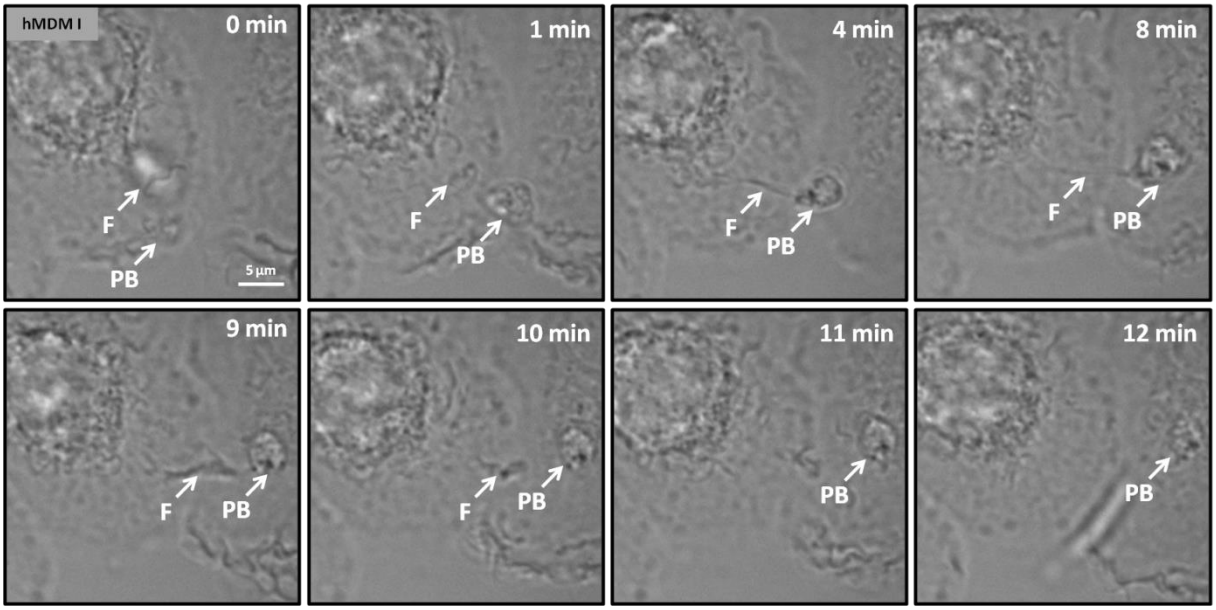

Figure 29: Live imaging of an apoptotic promastigote entering a hMDM I. hMDM I were co-incubated with PS+ purified apoptotic stationary phase *L. major* promastigotes and were directly analyzed by time lapse imaging using light microscopy. hMDM I taking up an apoptotic promastigote with the parasite body first is shown in time. Time lapse movie was generated on a Zeiss LSM7 *Live* confocal laser scanning microscope with a 63x oil objective and a 10x ocular. Arrows indicate parasite body (PB) or flagellum (F). Scale bar: as indicated.

3.3.2 Ultrastructural analysis of the *L. major* promastigote parasitophorous vacuole inside hMDMs to distinguish between autophagy and LC3-associated phagocytosis

As described before human macrophages take up viable and apoptotic *L. major* promastigotes by different mechanism (3.3.1.3). Now we were interested, whether thereby the parasites also end up in different compartments. As mentioned in the introduction (1.7) it is already known that apoptotic but not viable *L. major* promastigotes enter LC3-positive compartments inside hMDMs. The protein LC3 is the classical marker for autophagy and double-membrane autophagosomes, but it can also be recruited to single-membrane phagosomes, a process called LC3-associated phagocytosis (LAP). To investigate which of the two processes, autophagy or LAP, plays a role during uptake of *L. major* promastigotes by hMDMs, we analyzed the ultrastructure of the PV using several microscopically techniques like TEM, STEM tomography and immunogold labeling.

3.3.2.1 Apoptotic *L. major* promastigotes reside in a single-membrane compartment

First of all we examined the appearance of the *L. major* promastigote PV using HPF and TEM. Therefore we co-incubated hMDMs with 12-13 days old promastigote cultures, containing over 70% of apoptotic promastigotes. Figure 30 shows TEM micrographs of apoptotic promastiogtes inside hMDM I (A) and hMDM II (B). Interestingly in all cases the parasite membrane (PM) was surrounded by a single lipid bilayer (PV) as it is indicated in the enlargements. Quantification of TEM micrographs of three different donors revealed, that in hMDM I 97.1% ± 3.2 (Figure 30 C) and in hMDM II 96.1% ± 3.6 (Figure 30 D) of the apoptotic promastigotes appear in a single compartment membrane characteristic for LAP (Crauwels et al., 2015). In total we examined 350 parasites. Approximately one third of these parasites showed fixation artefacts or were already digested and were therefore excluded from this quantification.

In addition to TEM analysis of the ultrastructure we scanned the same samples by STEM tomography and found apoptotic *L. major* promastigotes inside single-membrane compartments in all visualized sections (Figure 31). STEM tomography illustrates in a three-dimensional manner, that there is only one lipid bilayer (PV) around the parasite membrane (PM).

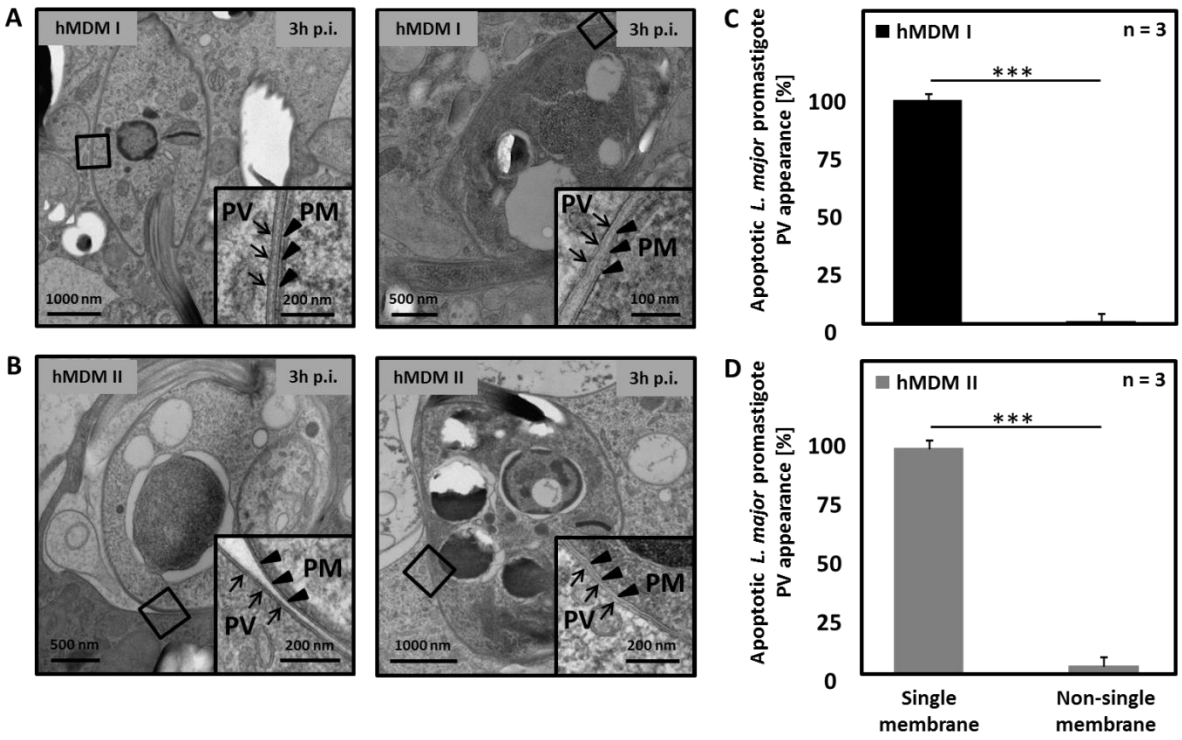

Figure 30: Apoptotic *L. major* promastigotes reside in a single-membrane compartment. hMDMs grown on sapphire disks were co-incubated with 12-13 days old *L. major* promastigotes for 3h. Extracellular parasites were removed and cells were fixed using HPF and prepared for electron microscopy. Ultra-thin sections were analyzed by TEM. A) Apoptotic promastigotes in a single-membrane compartment inside hMDM I. B) Apoptotic promastigotes in a single-membrane compartment inside hMDM II. C+D) Quantification of apoptotic *L. major* promastigote PV appearance in hMDM I (C) and hMDM II (D) using TEM micrographs shown in (A) and (B). Representative EM micrographs were taken on a Zeiss EM 109 transmission electron microscope. Magnification: between 5.000x and 30.000x. Black squares indicate enlarged region. Black arrows in the enlargement show single-membrane parasitophorous vacuoles (PVs). Black arrowheads indicate parasite membrane (PM). Scale bar: as indicated. Data of the bar charts are shown as means ± SD, n=3.

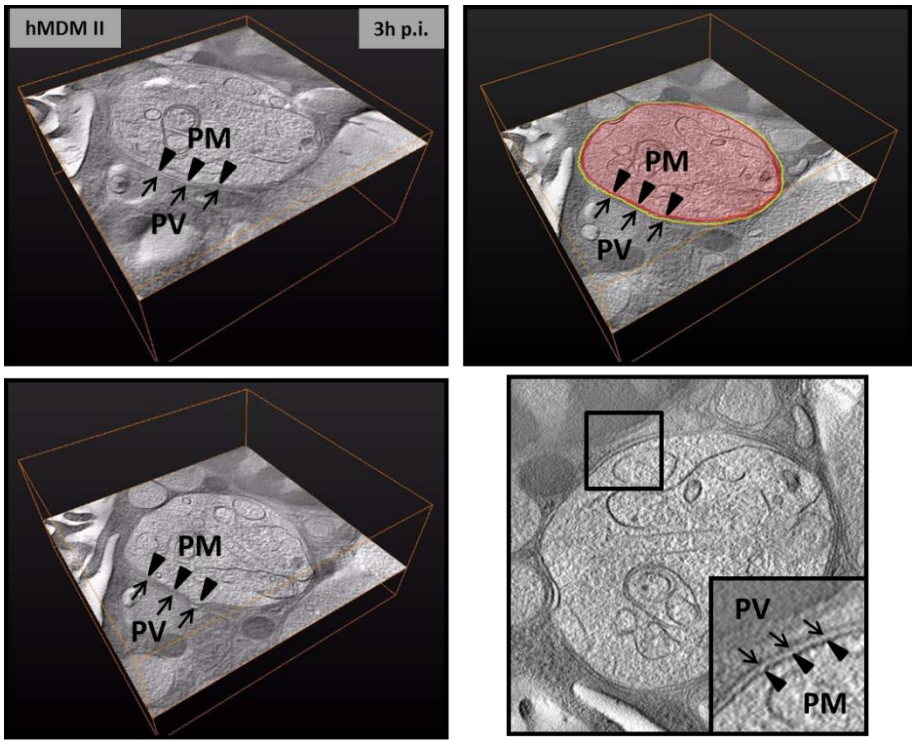

Figure 31: STEM tomography of an apoptotic *L. major* promastigote inside a single-membrane compartment. hMDM II grown on sapphire disks were co-incubated with 12-13 days old *L. major* promastigotes for 3h. Extracellular parasites were removed and cells were fixed using HPF and prepared for electron microscopy. Semi-thin sections were analyzed by STEM tomography on a Titan. Representative STEM micrographs of 3 independent experiments illustrate different sections showing an apoptotic promastigote inside a single-membrane compartment. Light red area marks the parasite. Arrowheads indicate the red colored parasite membrane (PM). Arrows indicate the single yellow colored parasitophorous vacuole (PV).

3.3.2.2 LC3-immunogold labeling of apoptotic *L. major* promastigote containing single-membrane compartments

After we could show that apoptotic *L. major* promastigotes reside in a single-membrane compartment, suggesting that dying promastigotes are not in a classical autophagy compartment, we wanted to directly visualize LC3 protein on the PV. Therefore we tried to establish LC3-immunogold labeling. We co-incubated macrophages with parasites and stained LR-Gold embedded samples with a LC3 antibody (Cell Signaling) and a gold-particle conjugated secondary antibody respectively. Unfortunately we could only observe unspecific binding of the secondary antibody to the macrophage nucleus (Figure 32 A and B), the parasite nucleus (Figure 32 C) and the parasite kinetoplast (Figure 32 B). We could not observe gold particles along the PV.

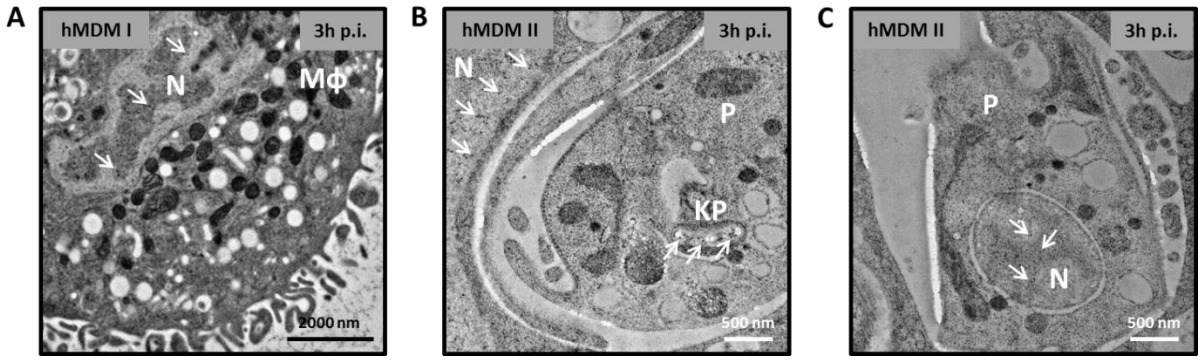

Figure 32: LC3 immunogold labeling of apoptotic *L. major* single PVs. hMDM I and hMDM II grown on sapphire disks were co-incubated with 13 days old *L. major* promastigotes for 3h. Extracellular parasites were removed and cells were fixed using HPF, embedded in LR-Gold and prepared for immunogold labeling. Ultra-thin sections were stained with a polyclonal rabbit anti-LC3 antibody from Cell Signaling and a gold-particle labeled secondary antibody and analyzed by TEM. A) Unspecific binding of the secondary antibody to the nucleus (N) of the macrophage (Mφ). B) Unspecific binding of the secondary antibody to the parasite´s (P) kinetoplast (KP). C) Unspecific binding of the secondary antibody to the parasite´s (P) nucleus (N). EM micrographs were taken on a Jeol JEM-1400 transmission electron microscope. Magnification: between 1.000x and 50.000x. White arrows indicate gold particles. Scale bar: as indicated.

Since the first try of LC3-immunogold labeling was not specific, subsequently we used another antibody and a different method for immunolabeling as suggested by Dr. M. Gutierrez (National Institute for Medical Research, London, UK). First of all we tested the suggested polyclonal rabbit LC3 antibody from MBL in immunofluorescence analysis to test whether fixation conditions needed for Tokuyasu technique (4% PFA + 1% GA) in principle enable a successful LC3 antibody staining. Immunofluorescence analysis (Figure 33) revealed that the staining was effective as the parasites stained in green are in the same area like the autophagy marker LC3 shown in red. Transmitted light visualization of the macrophages and DAPI staining of the macrophage nucleus confirmed that the parasites are inside the cells. These results are true for hMDM I (Figure 33 A) as well as for hMDM II (Figure 33 B).

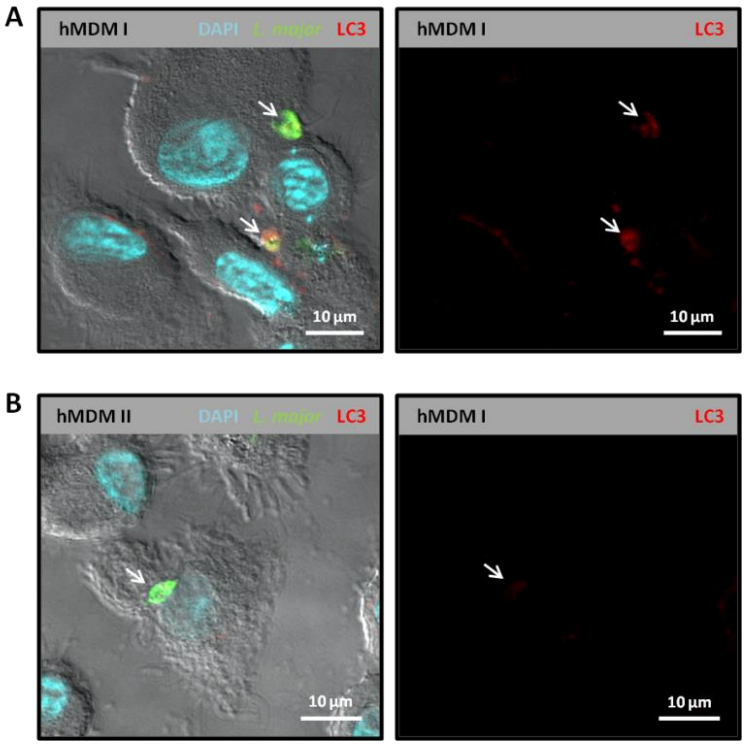

Figure 33: LC3 immunofluorescence analysis using Tokuyasu technique fixation conditions and a new LC3 antibody. hMDMs were co-incubated with stationary phase *L. major* promastigotes for 3h and fixed with 4% PFA + 1% GA prior to immunofluorescence staining using a polyclonal rabbit LC3 antibody (MBL) with an Alexa Fluor 568 labeled secondary antibody (red) as well as a *Leishmania* specific mouse serum with an Alexa Fluor 488 labeled secondary antibody (green). Macrophages are visualized by transmitted light and DAPI staining of the nucleus. Depicted are micrographs of hMDM I (A) and hMDM II (B) infected with a rounded promastigote typical for apoptotic parasites. Representative micrographs of at least three independent experiments were taken on a Zeiss Axio Observer Z1. White arrows indicate intracellular parasites. Magnification: 63x oil objective with 10x ocular. Scale bar: 10 µm.

In the next step during improvement of the immunogold-labeling protocol we tested the LC3 antibody (MBL) on Tokuyasu technique prepared cryo thin sections using immunofluorescence staining (Figure 34). Although we found only few cells we could obviously identify DAPI stained intact macrophages, green stained parasites and a red LC3 fluorescence. To conclude, the LC3 staining was successful on cryo sections in infected hMDM I (Figure 34 A) and hMDM II (Figure 34 B).

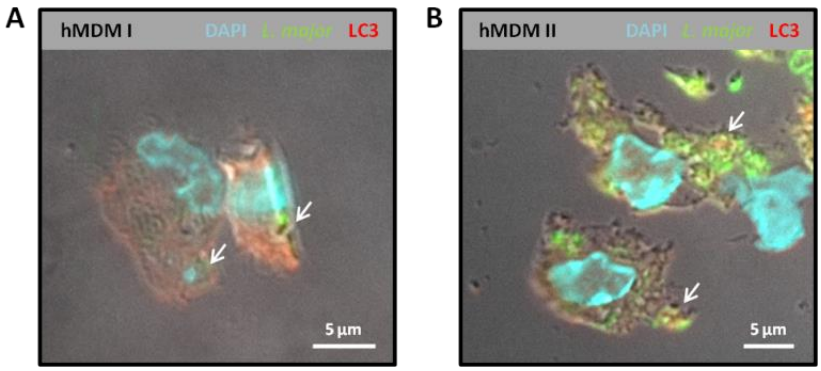

Figure 34: LC3 immunofluorescence analysis of cryo sections. hMDMs were co-incubated with stationary phase *L. major* DsRed promastigotes for 3h and fixed with 4% PFA + 1% GA prior to preparation of cryo sections and immunofluorescence staining using a polyclonal rabbit LC3 antibody (MBL) with an Alexa Fluor 568 labeled secondary antibody (red) as well as a *Leishmania* specific mouse serum with an Alexa Fluor 488 labeled secondary antibody (green). Macrophages are visualized by transmitted light and DAPI staining of the nucleus. Depicted are micrographs of infected hMDM I (A) and hMDM II (B). Representative micrographs were taken on a Zeiss Axio Observer Z1. White arrows indicate LC3 stained intracellular parasites. Magnification: 63x oil objective with 10x ocular. Scale bar: 5 µm.

Finally we performed LC3 immunogold labeling of Tokuyasu technique prepared cryo thin sections of infected hMDM I and hMDM II. The isotype control of infected hMDM I (Figure 35 A) showed little, equal distributed unspecific bound gold particles (black arrow). LC3 staining of infected hMDM I revealed some unspecific bound gold-particles (black arrows), but also some gold-particles that were ordered in a chain and associated with the PV (black arrowheads). Altogether the gold particles were equally distributed over the cell, but appeared to form aggregates. Similar results were obtained from infected hMDM II (Figure 35 B). We found some unspecific bound gold-particles in the isotype control as well as in the LC3 specific staining (black arrows). Furthermore few gold particles associated with the compartment membrane (black arrowheads) in the LC3 stained sample. hMDM II showed overall less gold-particles than hMDM I. Although first results looked very promising, we were not able to reproduce these results using different donors or even within the same sample. We found PVs associated with gold-particles in the isotype control and PVs without gold-particles in the LC3 specific staining (Figure 35 C). Above all with Tokuyasu technique it was impossible to distinguish between viable and apoptotic promastigotes.

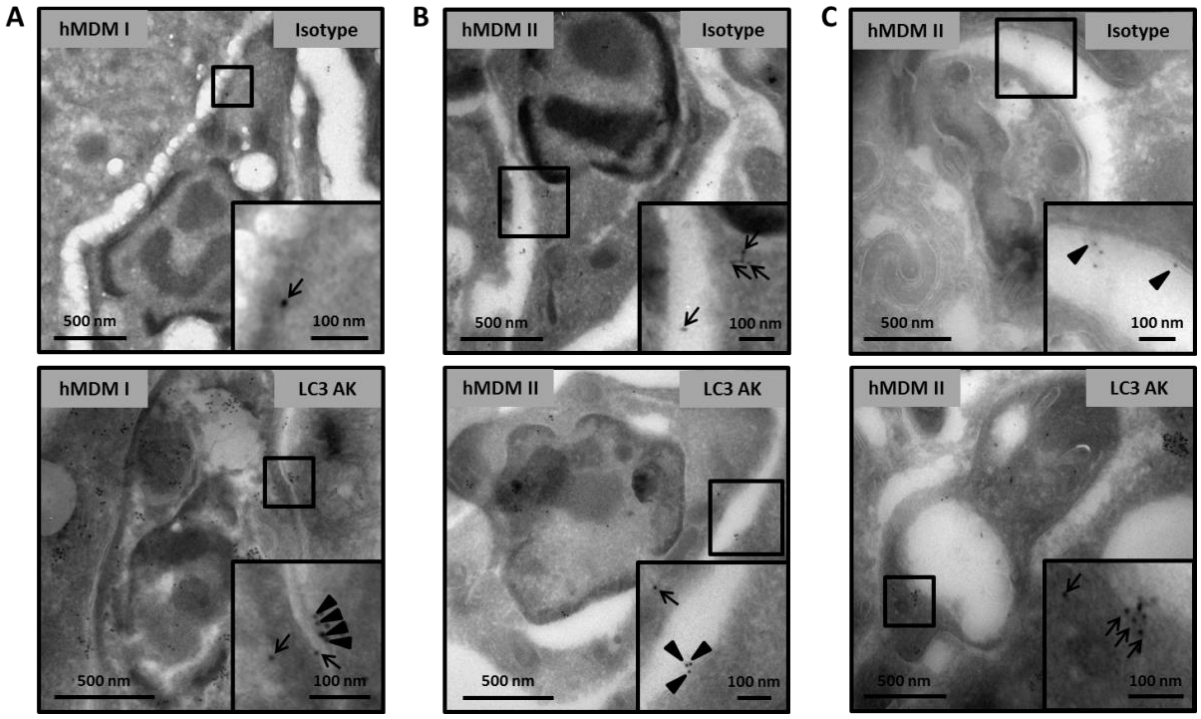

Figure 35: LC3 immunogold labeling of *L. major* single PVs using Tokuyasu method. hMDMs were co-incubated with stationary phase *L. major* DsRed promastigotes for 3h. Cells were extensively washed to remove extracellular parasites and fixed with 4% PFA + 1% GA. Tokuyasu technique prepared cryo thin sections were incubated with polyclonal rabbit LC3 antibody (MBL) or appropriate isotype control and a gold-particle conjugated secondary antibody prior to TEM analysis. Depicted are EM micrographs of infected hMDM I (A) and hMDM II (B+C). Micrographs were taken on a Zeiss EM 109 transmission electron microscope. Magnification: between 5.000x and 30.000x. Black squares indicate enlarged region. Black arrows show unspecific bound gold-particles. Black arrowheads indicate PV-associated gold-particles. Scale bar: as indicated.

3.3.3 ULK1 siRNA knockdown in hMDMs to discriminate between autophagy and LC3-associated phagocytosis

Next we looked for another method to distinguish between autophagy and LAP. The serine/threonine protein kinase Unc-51 like autophagy activating kinase 1 (ULK1) is known to play an important role during induction of autophagy (1.5.3). LAP activation is independent of ULK1. To discriminate between autophagy and LAP after *L. major* promastigote infection of macrophages, we focused on ULK1 using siRNA knockdown techniques. First of all we tested four different ULK1 siRNAs or the mixture of the four ULK1 siRNAs for knockdown efficiency (Figure 36 A). In comparison to a non-target siRNA, two single siRNAs (# 5 and # 4) as well as the siRNA mix reduced endogenous ULK1 mRNA levels up to 90% in hMDM I and hMDM II. In addition, evaluation of protein levels revealed reduced ULK1 protein levels after knockdown with siRNA # 5, siRNA # 4 and the siRNA mix (Figure 36 B). Based on these results, for further experiments we used ULK1 siRNA # 5.

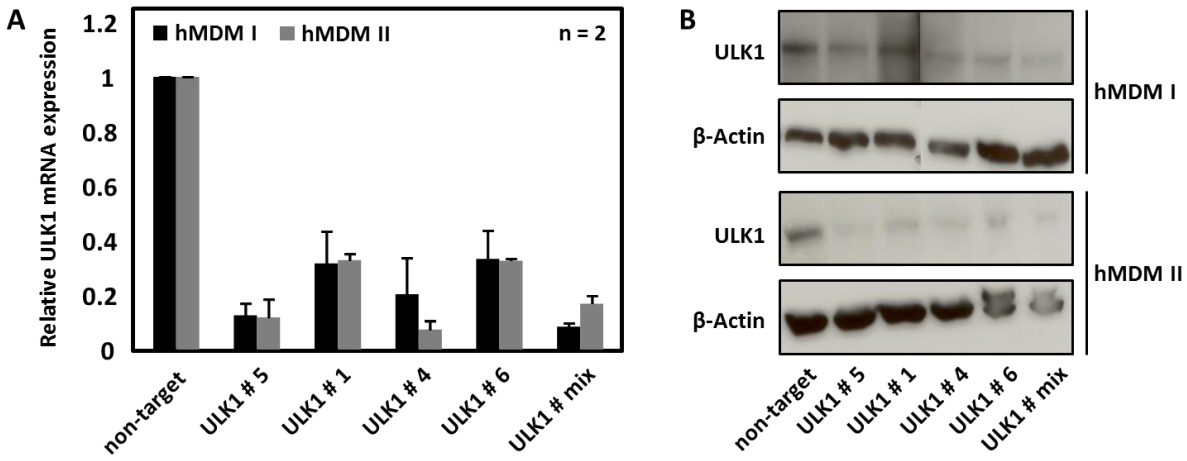

Figure 36: Testing different ULK1 siRNAs for knockdown efficiency on mRNA and protein level. hMDM I and hMDM II were treated with different ULK1 siRNAs or a non-target siRNA and subjected to quantitative real time PCR or Western Blot analysis. A) Relative ULK1 mRNA expression after knockdown. Data are shown as means ± SD, n=2. B) ULK1 protein expression after knockdown. Endogenous ULK1 protein was detected using a polyclonal rabbit ULK1 antibody (Santa Cruz) and β-Actin as loading control was visualized with a monoclonal mouse antibody (Sigma). Representative Western blots are shown. The ULK1 siRNA mix as well as the single siRNAs #5 and #4 showed efficient knockdown on mRNA and protein level.

To discriminate between autophagy and LAP, we again treated hMDM I with ULK1 siRNA # 5 and analyzed ULK1 mRNA expression levels in comparison to non-target cells after either *Leishmania* or rapamycin treatment (Figure 37 A). ULK1 mRNA expression was significantly reduced to 0.15 fold change ± 0.10, representing about 85% knockdown efficiency. Quantification of ULK1 protein expression showed a relative reduction to 0.29 ± 0.19 indicating 70% of reduction (Figure 37 B). Next we evaluated, whether LC3-I to LC3-II conversion is impaired by ULK1 knockdown (Figure 37 C). Both, autophagy and LAP induction can be visualized by LC3-I to LC3-II conversion. As expected, Western Blot analysis and densitometry quantification of rapamycin treated samples showed significantly increased LC3 conversion in non-target cells, but not in ULK1 knockdown cells meaning, that ULK1 is needed for rapamycin induced autophagy. Parasite infection resulted in increased LC3 conversion in non-target as well as in ULK1 knockdown cells, indicating that ULK1 protein is not essential for *L. major* promastigote induced LAP, although LC3-I to LC3-II conversion was not significant. However, in another project focusing on T-cell proliferation, significant induction of LC3 conversion in *Leishmania* treated hMDMs could already be demonstrated (Crauwels et al., 2015).

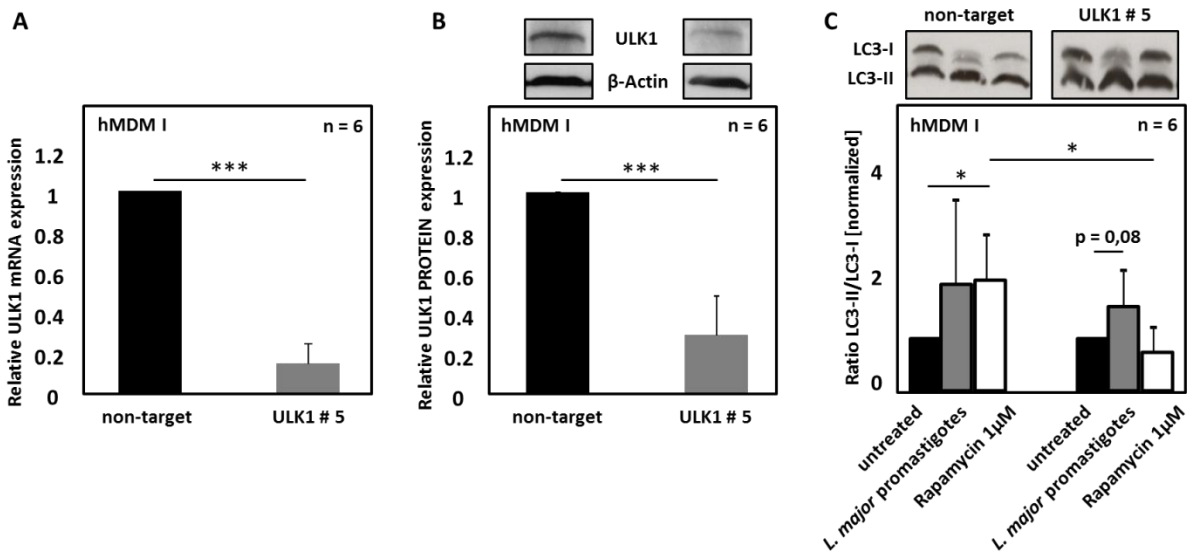

Figure 37: ULK1 siRNA knockdown to discriminate between *Leishmania*-induced autophagy or LAP. hMDM I were treated with ULK1 siRNA #5 or a non-target siRNA and subjected to quantitative real time PCR or Western blot analysis. A) Relative ULK1 mRNA expression after ULK1 knockdown. B) Western blot quantification of ULK1 protein expression after ULK1 knockdown. C) Western blot quantification of LC3-I to LC3-II protein conversion after treatment of non-target and knockdown cells with parasites or rapamycin. ULK1 is not needed for LC3 conversion of parasite treated knockdown cells indicating LAP. Representative Western blots are shown. Quantifications were performed using ImageJ software. Data are shown as means ± SD, n=6. * P-value < 0.05, *** P-value < 0.001.

3.3.4 Establishment of a LC3 lentiviral vector system for transduction of hMDMs

Using Live Cell Imaging we wanted to dynamically image the development of LC3 positive compartments around apoptotic parasites. For overexpression of fluorescent-labeled LC3 inside hMDMs we used a lentiviral vector system.

3.3.4.1 Testing of different lentiviral vector particles suitable for transduction of hMDMs

For transduction of primary human macrophages we tested two different lentiviral vector particles containing eGFP as a marker gene. The first one was the simian immunodeficiency derived particle PBj-SEW (Kloke et al., 2010). The second lentiviral vector particle was HIV-1 derived and designated HIV-1-SEW.

We transduced monocytes, subsequently generated macrophages and analyzed eGFP expression as well as macrophage-specific cell surface marker expression with flow cytometry (Figure 38). Examining eGFP fluorescence (Figure 38 A) revealed about 72% PBj-

SEW (green line) transduced hMDM I and hMDM II. For HIV-1-SEW particles (blue line) the transduction efficiency was around 100% for both macrophage types.

Analyzing CD14 (Figure 38 B), a marker mainly expressed on monocytes, macrophages and dendritic cells, we found high expression levels for untransduced (black line), PBj-SEW (green line) and HIV-1-SEW (blue line) transduced hMDM II (96.4%, 92.1% and 80.2%). Analyzing CD14 expression of HIV-1-SEW (blue line) transduced hMDM I we measured only 9% CD14 positive cells. 85.5% of PBj-SEW (green line) transduced hMDM I and 49.4% of untransduced (black line) hMDM I cells expressed CD14.

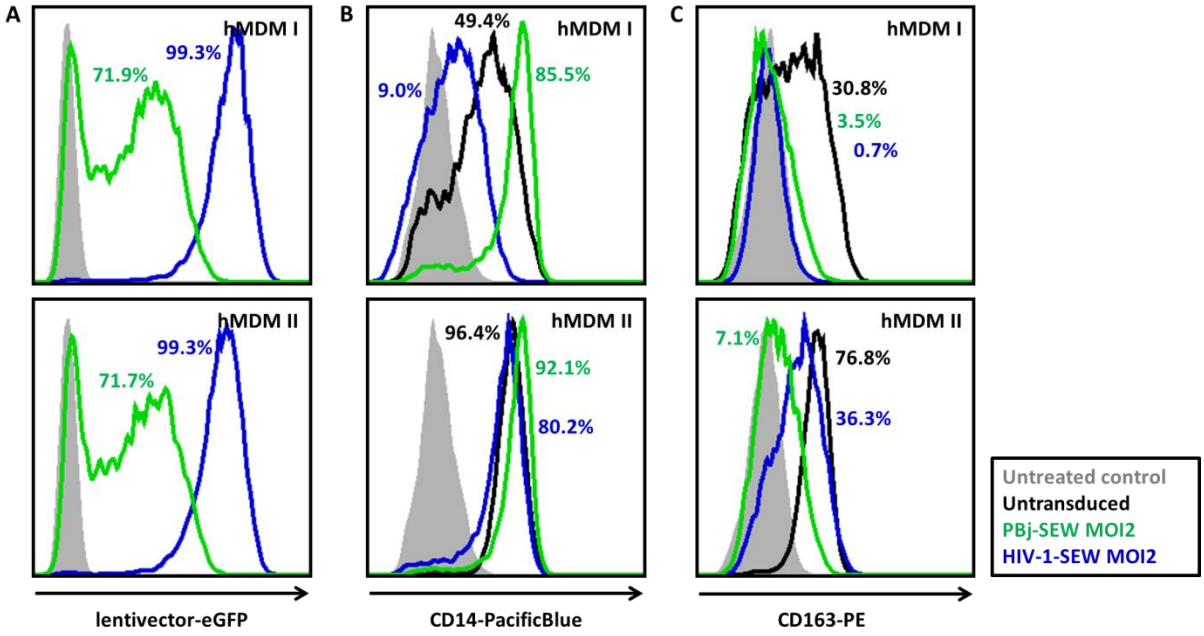

Figure 38: Testing different lentiviral vector particles for transduction of monocytes prior to differentiation into macrophages. Primary human monocytes were either directly transduced with PBj-SEW particles (green line) containing the accessory protein Vpx (MOI 2) or pre-incubated with virus-like-particles (VLPs) containing Vpx (MOI 1) prior to transduction with HIV-1-SEW particles (blue line) (MOI 2) or were left untransduced (black line). Four hours post transduction medium was exchanged against medium containing growth factors for differentiation of monocytes into hMDM I (upper panels) or hMDM II (lower panels). After five days transduction efficiency and macrophage-specific cell surface marker expression was analyzed by flow cytometry. A) Transduction efficiency of the lentivectors measured by eGFP overexpression. B) CD14 surface expression stained with a PacificBlue-conjugated mouse anti-CD14 antibody. C) CD163 surface expression stained with a PE-conjugated mouse anti-CD163 antibody. Preliminary FACS histograms are shown (n=2).

Beside this, we analyzed the expression of the scavenger receptor CD163 (Figure 38 C), which is a specific marker for anti-inflammatory hMDM II and plays a role in the resolution of inflammation (Moestrup and Møller, 2004; Onofre et al., 2009). As expected, in general we found higher expression levels on hMDM II than on hMDM I cells. 76.8% of untransduced

(black line) hMDM II were positive for CD163 compared to 30.8% of hMDM I. HIV-1-SEW transduced cells (blue line) revealed 36.3% hMDM II cells expressing CD163, whereas on hMDM I we could not detect CD163 at all (0.7%). In PBj-SEW transduced cells (green line) the expression level of CD163 was slightly higher in hMDM II (7.1 %) than in hMDM I (3.5%), but these cells showed an overall reduced CD163 expression.

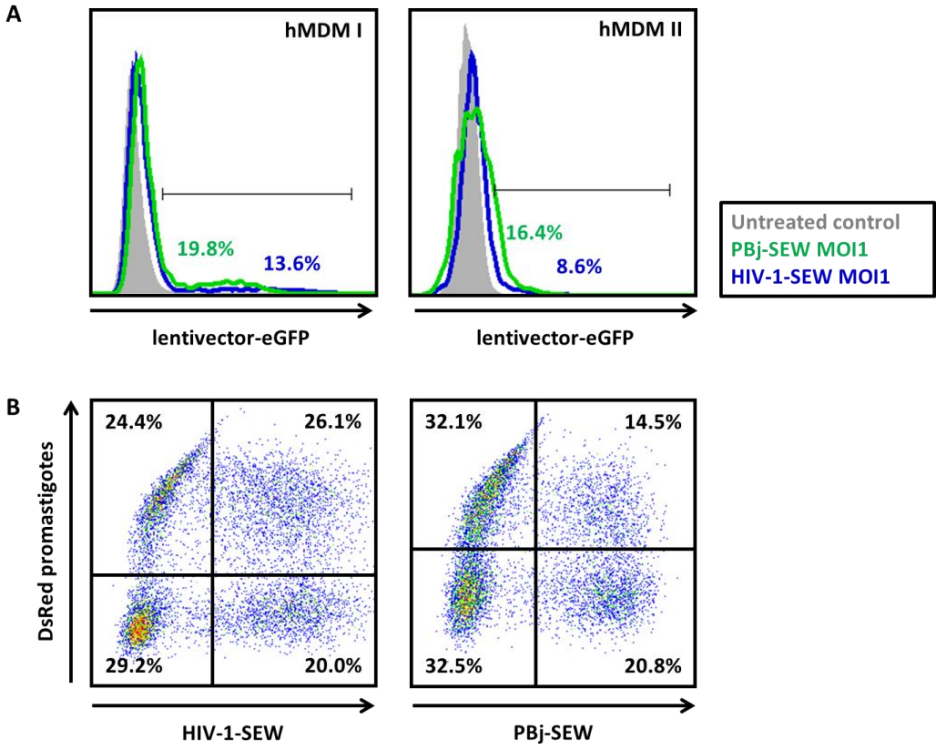

Figure 39: Testing different lentiviral vector particles for transduction of macrophages and subsequent *L. major* promastigote infection. hMDM I and hMDM II were either transduced with PBj-SEW particles (green line) containing the accessory protein Vpx (MOI 1) or with HIV-1-SEW particles (blue line) (MOI 1) or were left untransduced (grey area). Four hours post transduction medium was exchanged and cells incubated for three days. A) Transduction efficiency of the lentivectors determined by measuring eGFP overexpression using flow cytometry. Preliminary FACS histograms are shown (n=2). B) EGFP-transduced cells were co-incubated with stationary phase *L. major* DsRed promastigotes for 72h and analyzed by flow cytometry. Preliminary FACS density plots are shown (n = 1). Displayed are the percentages of transduced and/or infected cells.

The ability to transduce monocytes using these lentiviral vector particles was already demonstrated (Kloke et al., 2010; Mühlebach et al., 2005; Wolfrum et al., 2007). In addition, we tried to directly transduce macrophages (Figure 39 A). Even though the transduction efficiency for PBj-SEW (green line) and HIV-1-SEW (blue line) with 19.8% and 13.6%, was lower as compared to monocyte transduction efficiencies (Figure 38 A) we anyhow were able to transduce hMDM I cells. 16.4% of hMDM II cells were transduced with PBj-SEW particles

and 8.6% with the HIV-1-derived vector. Furthermore we successfully infected transduced hMDM I and hMDM II cells with *L. major* promastigotes expressing the fluorescent protein DsRed (Figure 39 B). 26.1% of HIV-1-SEW transduced hMDM I and 14.5% of PBj-SEW transduced hMDM I were infected with parasites after 3 days of co-incubation.

3.3.4.2 Cloning of LC3 transfer vector constructs

For overexpression of fluorescent proteins in primary human macrophages we cloned the eGFP-LC3 cDNA sequence into the transfer vector pPBj-SEW. We decided to use the PBj vector backbone for cloning, because HIV-1 lentiviral particles resulted in higher copy numbers of overexpressed protein than PBj-SEW particles (Figure 38 A) and accumulation of transgenic proteins in the cell leads to artificial conditions.

First, we amplified the eGFP-LC3 cDNA sequence, the insert, from the commercially available plasmid pEGFP-C2-LC3 by polymerase chain reaction (PCR) (Figure 40 A), thereby introducing the restriction sites SpeI and NdeI at 5´- and 3´- ends. The specific PCR-product with a length of 1182 basepairs (bp) resulted at every tested annealing temperature (Figure 40 A). Additionally we observed an unspecific side product with a length of 300 bp. Therefore we excised the eGFP-LC3 DNA fragment from the agarose gel with a clean scalpel and purified it using the Qiagen gel extraction Kit.

The vectors were also amplified by PCR to insert NdeI and SpeI restriction sites at 5´- and 3´- ends. Using a temperature gradient we tested different annealing temperatures. Annealing temperatures of 62.9°C and 66.2°C resulted in successful amplification of the pPBj vector (Figure 40 B). Subsequently, the PBj DNA fragments were purified by gel extraction, too.

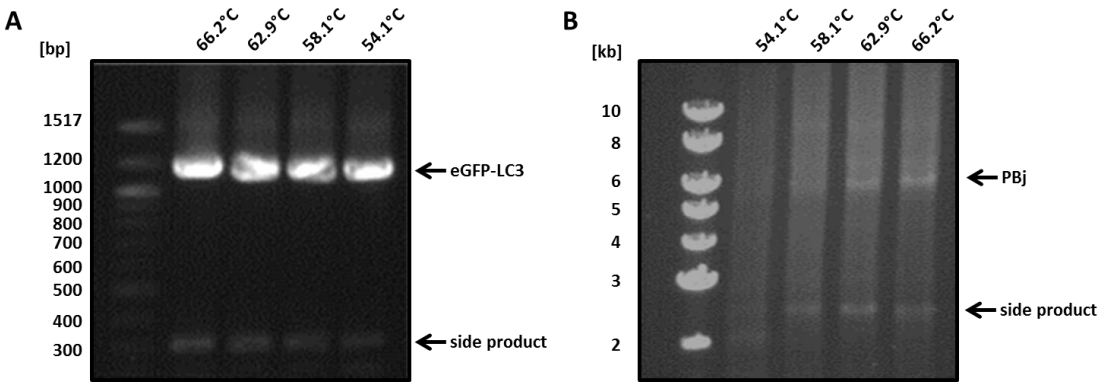

Figure 40: Amplification of insert and vector for cloning of LC3 transfer vector constructs. Insert eGFP-LC3 (1182 bp) (A) and vector PBj (6010 bp) (B) were amplified by PCR using different annealing temperatures. The restriction enzymes NdeI and SpeI were introduced by PCR. PCR products were separated by gel electrophoresis on a 0.8% (A) or 0.5% (B) agarose gel.

Purified eGFP-LC3 and PBj DNA fragments were digested using the restriction enzymes NdeI and SpeI. Both enzymes generated sticky ends enabling the ligation of the two fragments. The ligation mix was used for transformation of *E.coli* bacteria and resulted in bacterial clones carrying the pPBj-SW-eGFP-LC3 transfer plasmid. These plasmids were purified by plasmid purification and analyzed by three different methods (Figure 41) to confirm correct cloning. As expected, restriction analysis (Figure 41 A) using the same enzymes as for cloning (NdeI and SpeI) excised the eGFP-LC3 insert with a size of ~1 kb. Incubating the pPBj-SW-eGFP-LC3 construct with BamHI and EcoRI restriction enzymes produced three fragments of different sizes that were exactly the same as generated *in silico* using vector NTI software.

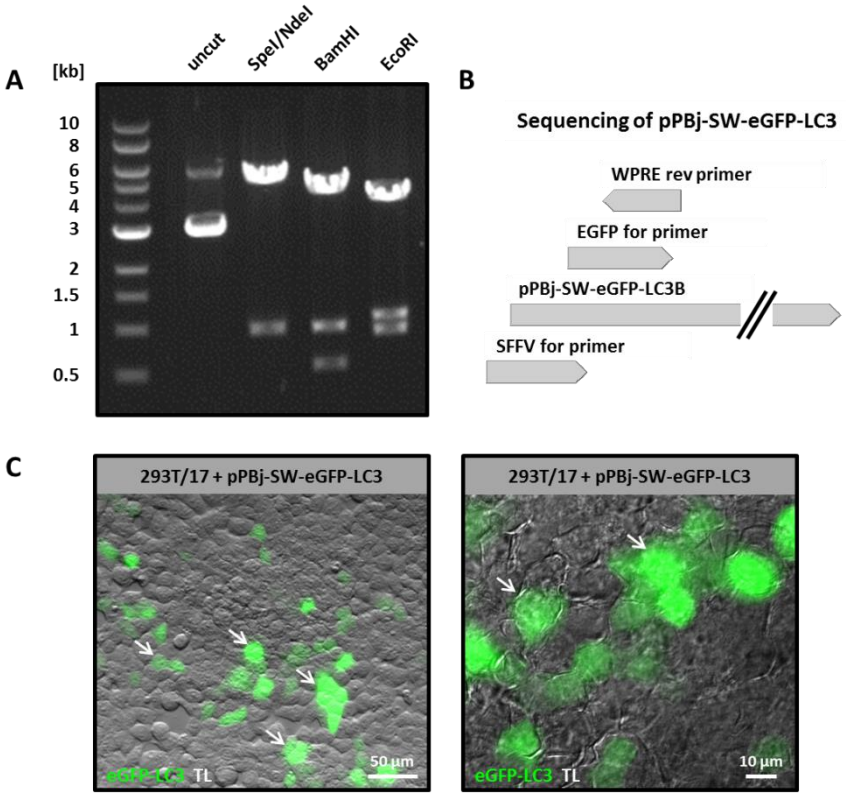

Figure 41: Verification of cloned pPBj-SW-eGFP-LC3 transfer vector constructs. The ligation plasmid pPBj-SW-eGFP-LC3 was analyzed by three different methods to verify the cloned transfer vector sequence. A) pPBj-SW-eGFP-LC3 was digested using NdeI/SpeI, BamHI or EcoRI restriction enzymes and separated by gel electrophoresis on a 0.5% agarose gel. B) Primer overlap for sanger sequencing of the construct pPBj-SW-eGFP-LC3. C) 293T/17 cells were transiently transfected with pPBj-SW-eGFP-LC3 using Lipofectamine and eGFP-LC3 overexpression was analyzed by fluorescence microscopy. Representative micrographs were taken on a Zeiss Axio Observer Z1. White arrows indicate transfected cells. Magnification: 20x (left) and 63x oil (right) objective with 10x ocular. Scale bar: as indicated.

Thereafter the construct was sent for sequencing to exclude mutations in relevant parts meaning introduced eGFP-LC3 sequence (Figure 41 B). One sequencing reaction enables screening of up to 800 bp, but is often inaccurate at the beginning and the end of the reaction. Therefore sequencing primers were designed expecting an overlap in mentioned regions. Sequencing verified correct cloning of pPBj-SW-eGFP-LC3 (data not shown).

To check, whether eGFP-LC3 protein is overexpressed in human cells, 293T/17 cells were transiently transfected with the newly generated plasmid (Figure 41 C) and evaluated by fluorescence microscopy. As indicated by the green cells (Figure 41 C) eGFP-LC3 overexpression was successful.

3.3.4.3 Generation of lentiviral vector particles and vector titer calculation

For generation of eGFP-LC3 lentiviral vector particles (2.4.10) the transfer vector pPBj-SW-eGFP-LC3 was used. Vector particles were harvested on three consecutive days, concentrated by ultracentrifugation, titrated by HT1080 cell transduction (2.4.10.3) and analyzed by flow cytometry (Figure 42).

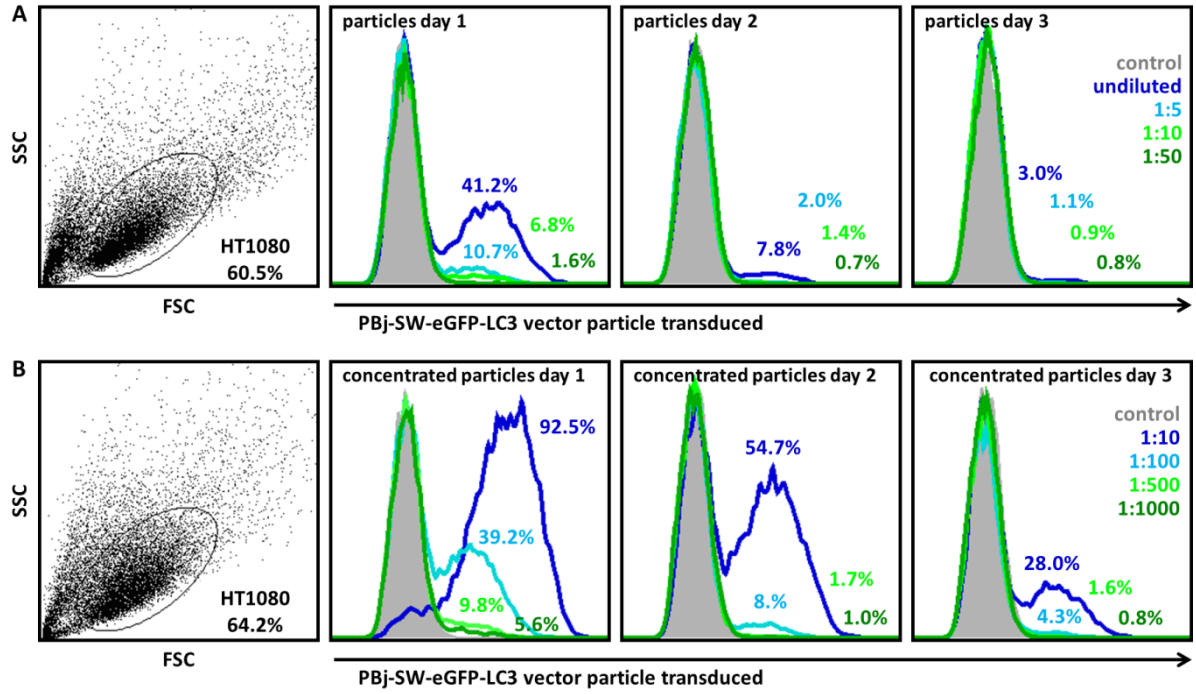

Figure 42: Titration of generated eGFP-LC3 lentiviral vector particles by HT1080 cell transduction. HT1080 cells were transduced with PBj-SW-eGFP-LC3 particles containing the accessory protein Vpx. Transduction efficiency was determined by measuring eGFP-LC3 overexpression using flow cytometry. A) Transduction efficiency of a dilution series of unconcentrated particles, which were harvested at three consecutive days. B) Transduction efficiency of a dilution series of concentrated particles, which were harvested at three consecutive days. Representative FACS dot plots and histograms of three independent experiments are shown. Serial dilutions are indicated in the right plots. Displayed are the percentages of transduced HT1080 cells.

Titration of unconcentrated particles is shown in Figure 42 A. Undiluted particles that were harvested on day 1 transduced 41.2% of the HT-1080 cells. As expected, dilution of the particles (1:5, 1:10, 1:50) decreased the transduction efficiency (10.7%, 6.8%, 1.6%). Same tendency can be observed with day 2 and day 3 vector particles although the overall transduction efficiency is decreased in comparison to day 1 particles.

In principle the same holds true for concentrated vector particles. By diluting the particles and dependent on the day they are harvested the transduction efficiency is decreased (Figure 42 B). Nevertheless with concentrated vector particles we observed an increased transduction of HT-1080 cells compared to unconcentrated ones. Whereas unconcentrated, undiluted particles transduced 41.2% of the cells on day 1, similar results were obtained with a 1:100 dilution of concentrated particles (39.2%). Using a 1:10 dilution of day 1 concentrated particles we achieved transduction efficiencies of up to 92.5% (Figure 42 B).

For vector titer calculation (2.4.10.3), dilutions, in which about 4-20% of the cells were transduced, were chosen. Beside eGFP-LC3 lentiviral vector particles we generated LAMP2-mCherry and eGFP-2xFYVE vector particles for analysis of further maturation markers. Lentiviral particles produced on the PBj vector backbone resulted in titers as depicted in Table 18.

Table 18: Titers of PBj-derived lentiviral vector particles reached on HT1080 transduced cells.

	date	titer
PBj-eGFP-LC3 VSV-G vpx	15.05.2013	$9{,}3 \times 10^6$ TU/ml
	16.05.2013	$1{,}6 \times 10^6$ TU/ml
	17.05.2013	$6{,}5 \times 10^5$ TU/ml
PBj-LAMP2-mCherry VSV-G vpx	17.07.2013	$8{,}2 \times 10^6$ TU/ml
	18.07.2013	$1{,}3 \times 10^6$ TU/ml
	19.07.2013	$6{,}5 \times 10^5$ TU/ml
PBj-eGFP-LC3 VSV-G vpx A	30.10.2013	$1{,}4 \times 10^6$ TU/ml
	31.10.2013	$3{,}0 \times 10^6$ TU/ml
PBj-eGFP-LC3 VSV-G vpx B	30.10.2013	$2{,}2 \times 10^6$ TU/ml
	31.10.2013	$2{,}0 \times 10^6$ TU/ml
PBj-eGFP-2xFYVE VSV-G vpx	28.05.2014	$1{,}9 \times 10^7$ TU/ml
	29.05.2014	$2{,}5 \times 10^6$ TU/ml

3.3.4.4 Macrophage transduction efficiency of the lentiviral vector particle PBj-SW-eGFP-LC3

After generation of the vector particle PBj-SW-eGFP-LC3 we measured macrophage transduction efficiency by flow cytometry and microscopy. PBj-SW-eGFP-LC3 monocyte transduction with a MOI of 1 prior to hMDM I differentiation resulted in 53.1% of transduced cells (Figure 43 A). Since for monocyte transduction large amounts of vector particles were needed, we directly transduced hMDM I with a MOI of 0.1 to reduce vector particle amounts, and achieved a transduction efficiency of 9.6% (Figure 45 B), which is sufficient for subsequent microscopic analysis. Similar results were obtained for hMDM II (data not shown).

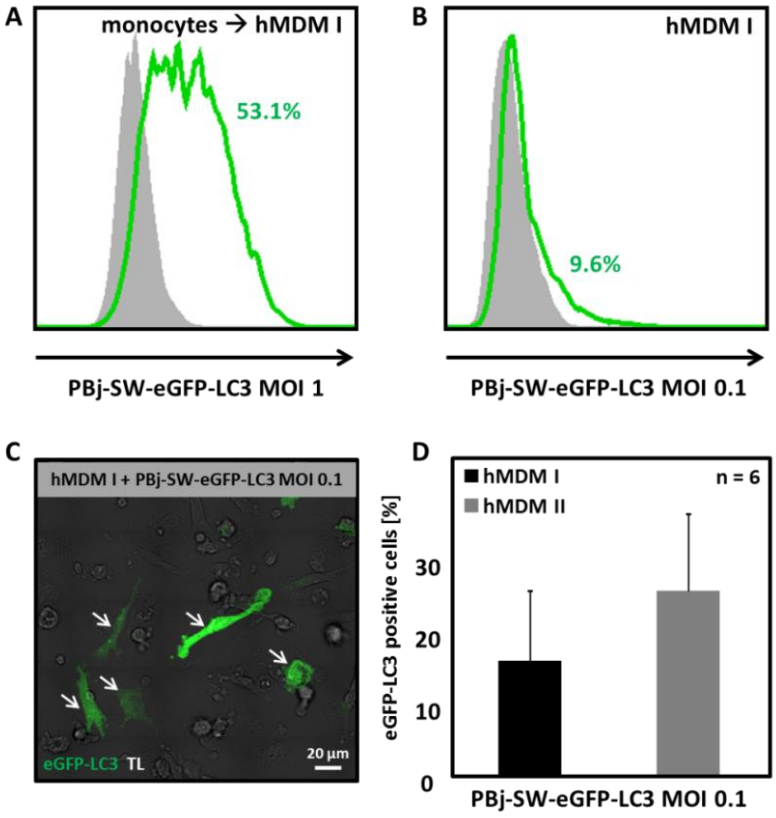

Figure 43: hMDM transduction efficiency of the lentiviral vector particle PBj-SW-eGFP-LC3. Primary human monocytes prior to macrophage differentiation (A) or hMDMs (B-D) were transduced with PBj-SW-eGFP-LC3 particles containing the accessory protein Vpx (MOI 1 or MOI 0.1). A) Transduction efficiency of monocyte transduced hMDM I analyzed by flow cytometry. B) Transduction efficiency of directly transduced hMDM I analyzed by flow cytometry. Preliminary FACS histograms are shown (n=2). PBj-SW-eGFP-LC3 transduced cells = green line, untransduced cells = grey area. C) Tile Scan micrograph of PBj-SW-eGFP-LC3 transduced hMDM I. Representative micrographs were taken on a Zeiss LSM 7 *Live*. White arrows indicate transduced cells. TL = transmitted light. Magnification: 63x oil objective with 10x ocular. Scale bar: as indicated. D) Quantification of eGFP-LC3 positive hMDM I and hMDM II using micrographs shown in (C). Data are shown as means of ± SD, n=6.

Moreover we transduced hMDM I and hMDM II with PBj-SW-eGFP-LC3 particles with a MOI of 0.1, and assessed eGFP-LC3 positive cells by combining transmitted light and fluorescent imaging (Figure 43 C). We found 16.3% ± 9.8 of hMDM I cells and 26.1% ± 10.6 of hMDM II cells to be eGFP-LC3 transduced (Figure 43 D). Transduction efficiencies strongly varied depending on different donors, but were in concordance with flow cytometry data. Both types of transduction (monocyte and macrophage) were used for further experiments.

3.3.4.5 Western Blot analysis of PBj-SW-eGFP-LC3 transduced hMDM

Using Western Blot analysis, we additionally demonstrated overexpression of eGFP-LC3 in hMDMs (Figure 44 A and B). In untransduced cells we were able to detect two forms of endogenous LC3 termed LC3-I and LC3-II (Lane 1, left panel, Figure 44 A and B). Treatment with the autophagy inducers rapamycin or AZD8055 resulted in increased LC3-II levels and thus autophagy induction (Lane 3 and 4, left panel, Figure 44 A and B). Co-incubation of hMDMs with *L. major* promastigotes also led to LC3-I to LC3-II conversion (Lane 2, left panel, Figure 44 A and B). We found less endogenous LC3 protein amounts in transduced cells (Lane 1-4, right panel, Figure 44 A and B). As a loading control we analyzed β-Actin. However, autophagy induction of endogenous LC3 in transduced cells was similar (Lane 1-4, right panel, Figure 44 A and B). In transduced cells we additionally could detect overexpressed eGFP-LC3 protein. There were high amounts of eGFP-LC3-I and only small amounts of eGFP-LC3-II detectable. Modulation of autophagy by autophagy inducers or parasite infection in terms of eGFP-LC3-I to eGFP-LC3-II conversion could not be demonstrated in Western Blot. Obtained results were similar for hMDM I and hMDM II (Figure 44 A and B).

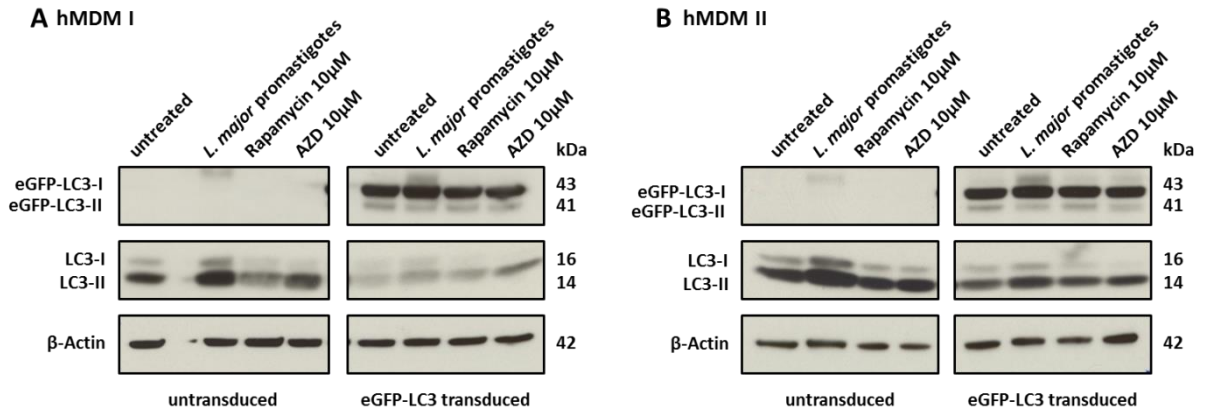

Figure 44: Western Blot analysis and autophagy modulation of PBj-SW-eGFP-LC3 transduced hMDMs. hMDM I (A) and hMDM II (B) were transduced with PBj-SW-eGFP-LC3 lentiviral vector particles, treated with *L. major* promastigotes, rapamycin or AZD8055 and separated on a 4-20% gradient gel prior to Western Blot Analysis. Endogenous LC3 was detected with a polyclonal rabbit LC3 antibody (Cell Signaling). Overexpressed eGFP-LC3 was detected using a polyclonal rabbit GFP antibody (abcam) and β-Actin as loading control was visualized with a monoclonal mouse antibody (Sigma). Appropriate HRP-coupled secondary antibodies were used. Overexpressed eGFP-LC3 is visible in transduced cells. LC3-I to LC3-II conversion can only be detected for endogenous protein levels.

3.3.5 Live cell imaging of *L. major* promastigotes inside LC3-positive and LC3-negative compartments using LC3 lentiviral vector particles

After we checked by flow cytometry and Western Blot analysis, that monocytes/macrophages can be transduced with PBj-SW-eGFP-LC3 lentiviral vector particles, we examined the development of LC3-positive compartments around the *L. major* promastigote containing PV by microscopy (Figure 46). Using live confocal fluorescence imaging we visualized the dynamics of LC3-positive and LC3-negative compartments. Therefore we stained stationary phase *L. major* promastigotes with the membrane dye PKH26 and the nucleus with DAPI and infected eGFP-LC3 transduced macrophages. Figure 45 shows compartment dynamics over time. One parasite remains in a LC3-negative compartment (white arrowhead) and a second parasite in a LC3-positive compartment (white arrow). The LC3-positive compartment can be followed for about 40 minutes until LC3 protein disappears from the *Leishmania* containing compartment. The duration of LC3 compartment stability strongly varies. The majority of compartments disappear after 3 to 4 hours, some even disappear after 5 to 15 minutes and some can be stable for up to 10 hours (data not shown). From this experimental setup we are not able to differentiate between viable and apoptotic promastigotes. However, we suggest that the LC3-positive compartment shown in Figure 45 harbors an apoptotic parasite, because preliminary LC3 immunofluorescence data have shown that only apoptotic promastigotes enter LC3-positive compartments (Crauwels et al., 2015).

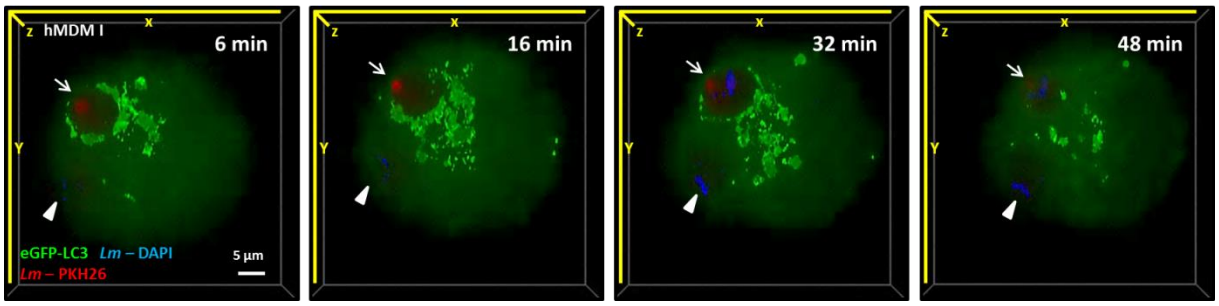

Figure 45: Live cell imaging of *L. major* promastigotes inside LC3-positive and LC3-negative compartments. Monocytes were transduced with PBj-SW-eGFP-LC3 lentiviral vector particles, differentiated into hMDM I and co-incubated with PHK26 and DAPI stained stationary phase promastigotes. Depicted is a parasite in a LC3-positive compartment (white arrow) disappearing over 40 minutes and a parasite remaining in a LC3-negative compartment (white arrowhead). Representative confocal fluorescent 3D images were generated on a Zeiss LSM7 *Live*. Magnification: 63x oil objective with 10x ocular. Scale bar: as indicated.

3.3.6 LC3 compartment quantification of eGFP-LC3 transduced and *L. major* promastigote infected hMDMs

To find differences between viable and apoptotic promastigotes we co-incubated the transduced cells with the virulent inoculum of a 8 days old parasite culture, with purified apoptotic promastigotes (PS+) or with purified viable parasites (PS-) (2.2.2), that were stained either with DAPI or Succinimidylester-AF647 (NHS-AF647) (Figure 46 A). In eGFP-LC3 transduced cells LC3-positive compartments (LC3 +), LC3-negative compartments (LC3 -) or compartments with LC3-dots developed around the parasites independently of used parasites, as it is shown in the micrographs of Figure 46 B. Quantification of LC3 compartments in hMDM I revealed, that about one third of the parasites enters LC3 -, LC3 + or LC3-dot compartments (Figure 46 C). There were no significantly differences between the infectious inoculum and the purified apoptotic or viable promastigotes. The results for transduced hMDM II were similar. Between 30% and 40% of the parasites enter LC3 - or LC3-dot compartments. Purified apoptotic parasites (d8 PS+) enter significantly more LC3 - compartments (36.57% ± 11.90) compared to LC3 + compartments (20.52% ± 3.54) in hMDM II. The same tendency can be observed for stationary phase parasites (d8) or viable parasites (d8 PS-). Less LC3 + compartments are formed in comparison to LC3 - or LC3-dot compartments, but the differences are not significant. There are also no significantly differences between hMDM I and hMDM II, only for apoptotic promastigotes (d8 PS+) in LC3 + compartments. Whereas in hMDM I 38.37% ± 11.02 compartments got LC3-positive in hMDM II only 20.52% ± 3.54 were LC3-positive.

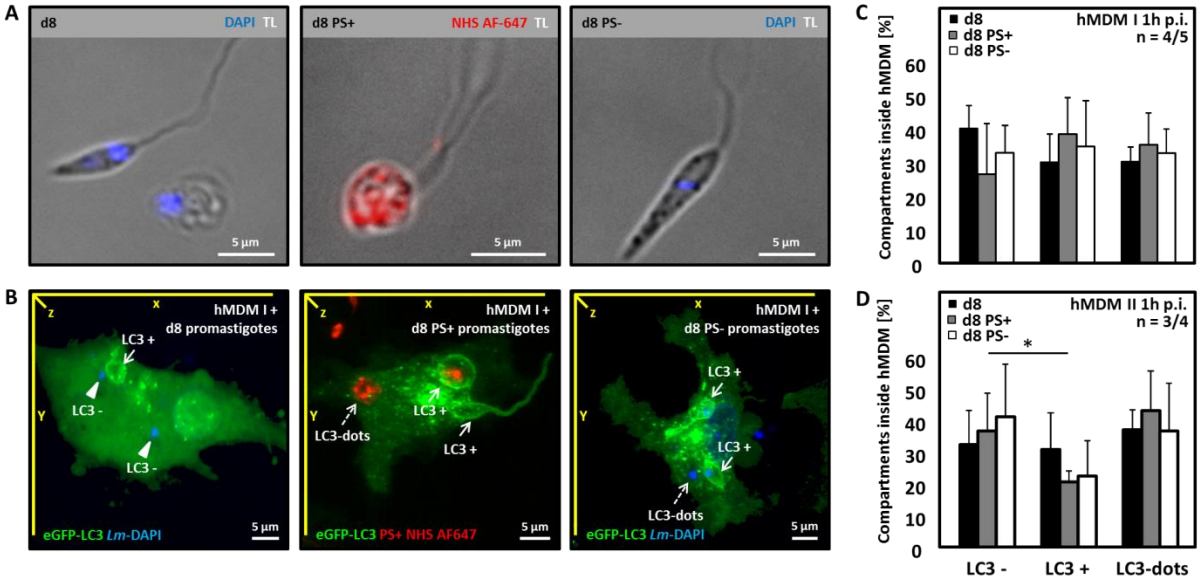

Figure 46: Apoptotic and viable *L. major* promastigotes enter LC3-positive compartments. hMDMs were transduced with PBj-SW-eGFP-LC3 lentiviral vector particles and co-incubated with stationary phase day 8 (d8) promastigotes, purified apoptotic or purified viable promastigotes prior to analysis by fluorescence microscopy. A) DAPI and Succinimidylester-AlexaFluor647 (NHS-AF647) staining of *L. major* promastigotes. B) Confocal fluorescent 3D micrographs of eGFP-LC3 transduced and parasite infected hMDMs. Representative micrographs of at least 3 independent experiments were taken on a Zeiss LSM 7 *Live*. Magnification: 63x oil objective with 10x ocular. Scale bar: as indicated. White arrowheads indicate LC3 - compartments, white arrows show LC3 + and white arrows with dashed line indicate LC3-dots. C+D) Quantification of *L. major* promastigote compartments in hMDM I (C) and hMDM II (D) using fluorescent micrographs shown in (B). Data are shown as means ± SD. n = 3-5.

3.3.7 Apoptotic *L. major* promastigotes are degraded in LC3-positive compartments

For analysis of compartment formation around apoptotic parasites, we stained purified PS+ promastigotes with NHS-AF647 (2.6.9) and infected eGFP-LC3 macrophages. With live confocal fluorescence imaging we visualized the uptake of apoptotic parasites and the formation and maturation of LC3-compartments (Figure 47). After half an hour of co-incubation we visualized two apoptotic parasites in LC3-negative compartments (Figure 47 A). One of the parasite compartments got LC3-positive after 2 hours (white arrow) and after another 3 hours the red parasite staining vanished, suggestive for degradation of the parasite, whereas the LC3-compartment disappeared 2 hours later. In contrast to that, the second PV (white arrowhead) just associated with some LC3-dots and was still visible after 8 hours. It finally disappeared after 15 hours (data not shown). A second example from the same cells is shown in Figure 47 B. One PV containing an apoptotic promastigote (white arrow) got LC3-positive after 1 hour, lost its red fluorescence after 4 hours and LC3 fluorescence disappeared after almost five hours. The parasite in the LC3-negative PV (white

arrowhead) was clearly identifiable during these five hours and finally disappeared after 11 hours (data not shown). So to summarize, apoptotic parasites in a LC3-positive compartment seem to be degraded faster than parasites in LC3-negative compartments.

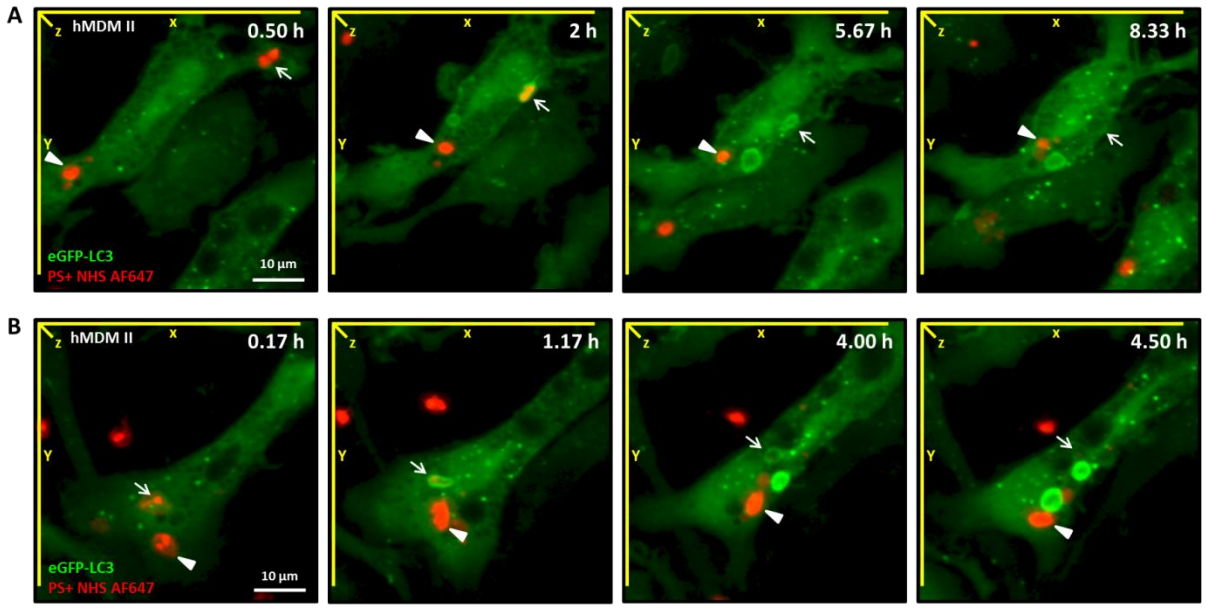

Figure 47: Live cell imaging of apoptotic *L. major* promastigotes. hMDM II were transduced with PBj-SW-eGFP-LC3 lentiviral vector particles and co-incubated with NHS-AF647 stained purified apoptotic promastigotes. A) and B) Depicted is an apoptotic parasite in a LC3-positive compartment (white arrow) with the parasite and compartment disappearing over time as well as an apoptotic parasite in a LC3-negative compartment (white arrowhead) remaining in the compartment. Representative confocal fluorescent 3D images were generated on a Zeiss LSM7 *Live*. Magnification: 63x oil objective with 10x ocular. Scale bar: as indicated.

3.3.8 Viable *L. major* promastigotes are targeted by LC3, but are able to escape the compartment

Quantification of LC3 compartments revealed, that contrary to previous immunofluorescence experiments not only apoptotic but also viable *L. major* promastigotes enter LC3-positive compartments. Similar as for apoptotic promastigotes we tried to image the compartment formation around viable parasites. Figure 48 A represents a viable promastigote in a LC3-negative compartment. We identified the parasite as a viable promastigote by its strong and powerful movements inside the cell. Over time LC3 protein accumulated at the PV to form a LC3-positive compartment after 1 hour. Another 30 minutes later the parasite escaped from the compartment being again in a LC3-negative PV. Additionally we visualized a promastigote escaping a LC3-positive compartment within 4 minutes (Figure 48 B). Summing

up, compartments containing viable *L. major* promastigotes can be targeted by LC3 protein, but the parasites are able to get rid of LC3 protein around the compartment.

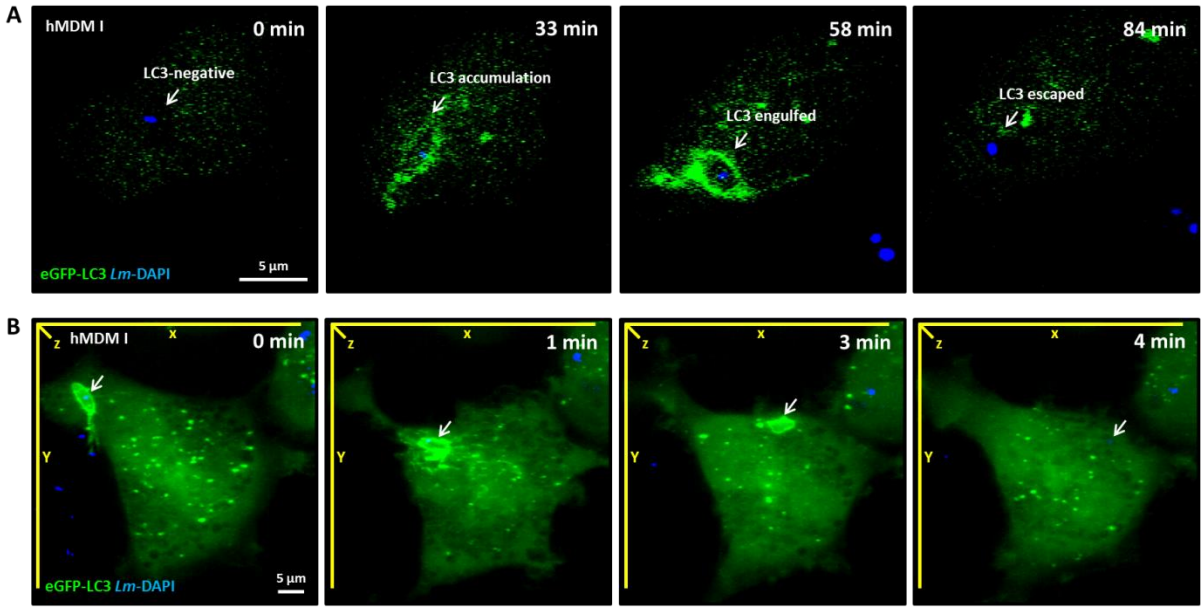

Figure 48: Live cell imaging of viable *L. major* promastigotes. Monocytes or hMDM I were transduced with PBj-SW-eGFP-LC3 lentiviral vector particles and co-incubated with DAPI stained stationary phase *L. major* promastigotes. A) and B) Depicted are viable promastigotes (white arrows) in LC3-positive compartments escaping LC3 engulfment over time. Representative confocal fluorescent single plane (A) or 3D images (B) were generated on a Zeiss LSM7 *Live*. Magnification: 63x oil objective with 10x ocular. Scale bar: as indicated.

3.3.9 Combining eGFP-fluorescence of LC3-positive compartments with the cellular ultrastructure using electron microscopy

In a next step we planned to combine LC3 fluorescence with electron microscopy using correlative approaches. Initial experiments using LC3-transduced macrophages on sapphire disks with an imprinted coordinate system were used for *L. major* promastigote infection and localization of infected transduced cells in both immunofluorescence microscopy (IF), followed by HPF and SEM analysis (Figure 49). We combined transmitted light (TL) images with fluorescence (FL) and SEM pictures and analyzed the macrophage surface to visualize parasite uptake into eGFP-LC3 transduced cells. We found parasites entering cells either via the parasite body (Figure 49 A) or with the flagellum first (Figure 49 B).

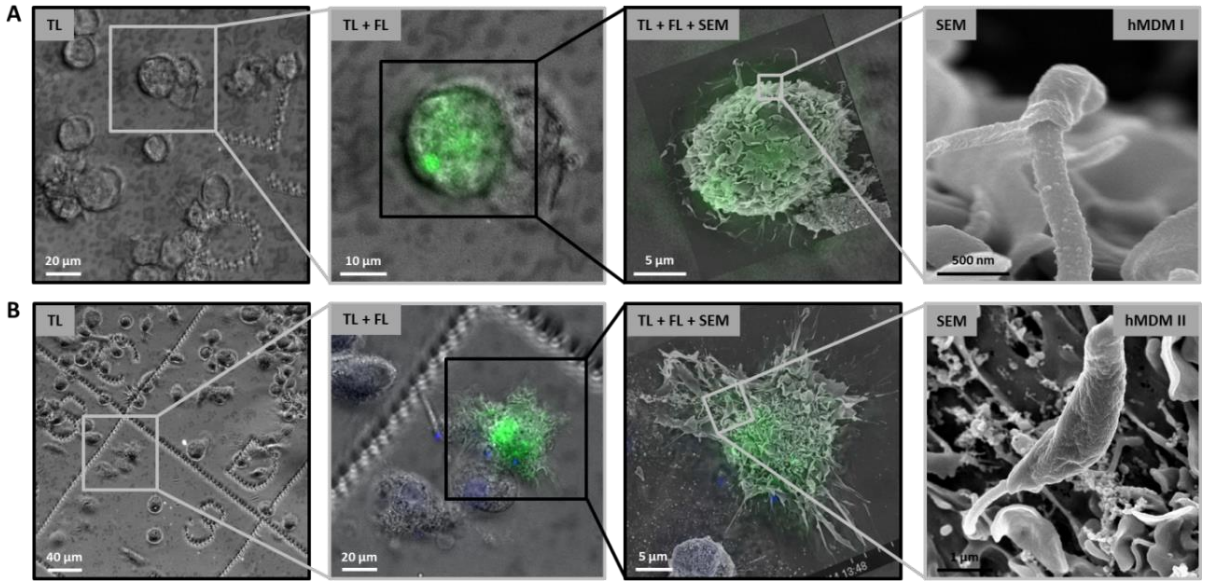

Figure 49: Combination of eGFP-LC3 fluorescence with scanning electron microscopy. hMDMs were transduced with PBj-SW-eGFP-LC3 lentiviral vector particles, co-incubated with (DAPI stained) stationary phase *L. major* promastigotes for 1h and analyzed by fluorescent light microscopy on sapphire disks with an imprinted coordinate system prior to SEM analysis. A) eGFP-LC3 transduced hMDM I taking up a promastigote with the parasite body first. B) eGFP-LC3 transduced hMDM II taking up a promastigote via the flagellum tip. Transmitted light (TL) and fluorescence (FL) micrographs were taken on a Zeiss Axio Observer Z1. SEM micrographs were taken on a Hitachi S-5200. Scale bar: as indicated.

However, to directly be able to combine IF information of an eGFP-LC3 staining with its surrounding ultrastructure, we decided to combine fluorescent light microscopy with focused ion beam / scanning electron microscopy (FIB/SEM) tomography (Figure 50, Figure 51, Figure 52).

Figure 50 shows an eGFP-LC3 transduced cell on a sapphire disk with an imprinted coordinate system (white arrowhead, left panel in A) containing a LC3-dot compartment (white arrow, right panel in A). During sample preparation the coordinate system is imprinted in the embedding medium and helps to find back the same cell in FIB/SEM (Figure 50 B). After FIB/SEM a black hole marks the milled region (white arrow, right panel in B).

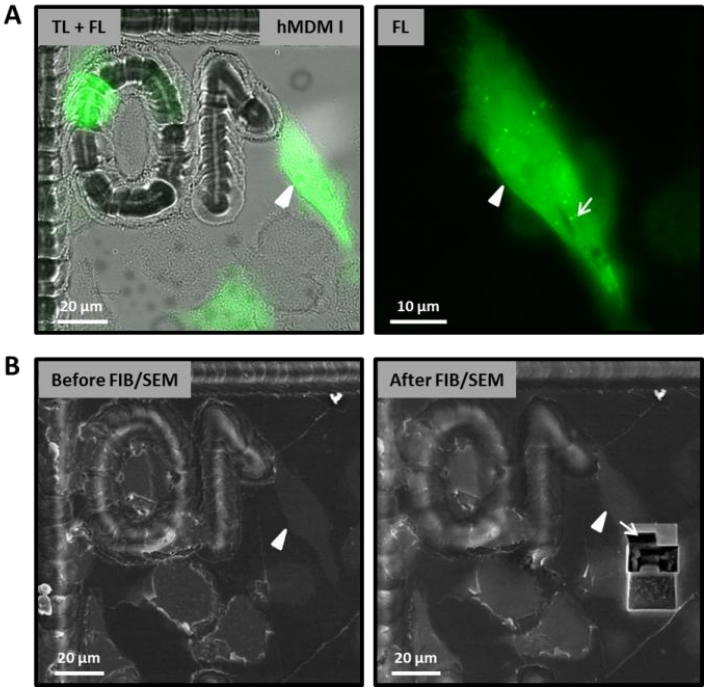

Figure 50: Area from where the tomographic dataset in Figure 51 has been obtained. hMDM I were transduced with PBj-SW-eGFP-LC3 lentiviral vector particles, co-incubated with stationary phase *L. major* promastigotes for 1h and analyzed by fluorescence microscopy on sapphire disks with an imprinted coordinate system prior to FIB/SEM tomography. A) eGFP-LC3 transduced cell (white arrowhead) with a LC3-dot compartment (white arrow). B) Same cell from A shown before and after FIB/SEM tomography. Transmitted light (TL) and fluorescence (FL) micrographs were taken on a Zeiss Axio Observer Z1. FIB/SEM overview micrographs were taken on a FEI Helios Nanolab 600 FIB/SEM. Scale bar: as indicated.

The acquired 3D datasets of the eGFP-LC3 transduced cell with the LC3-dot compartment is depicted in Figure 51. We identified a promastigote in a single-membrane compartment (Figure 51 A) by means of the nucleus in section 120 and the kinetoplast in section 2. Interestingly, in section 50 an opening of the PV to the outside was visible. It was the first time we got to see a connection of the parasite to the extracellular space and without 3D data we probably would not have recovered it.

Moreover we determined a lot of vesicle transport in terms of endo- and exocytosis (black arrowheads) of the infected macrophages (Figure 51 B). We observed vesicles (black arrow) fusing with the plasma membrane or rather being pinched off the membrane, as one would expect for phagocytic cells.

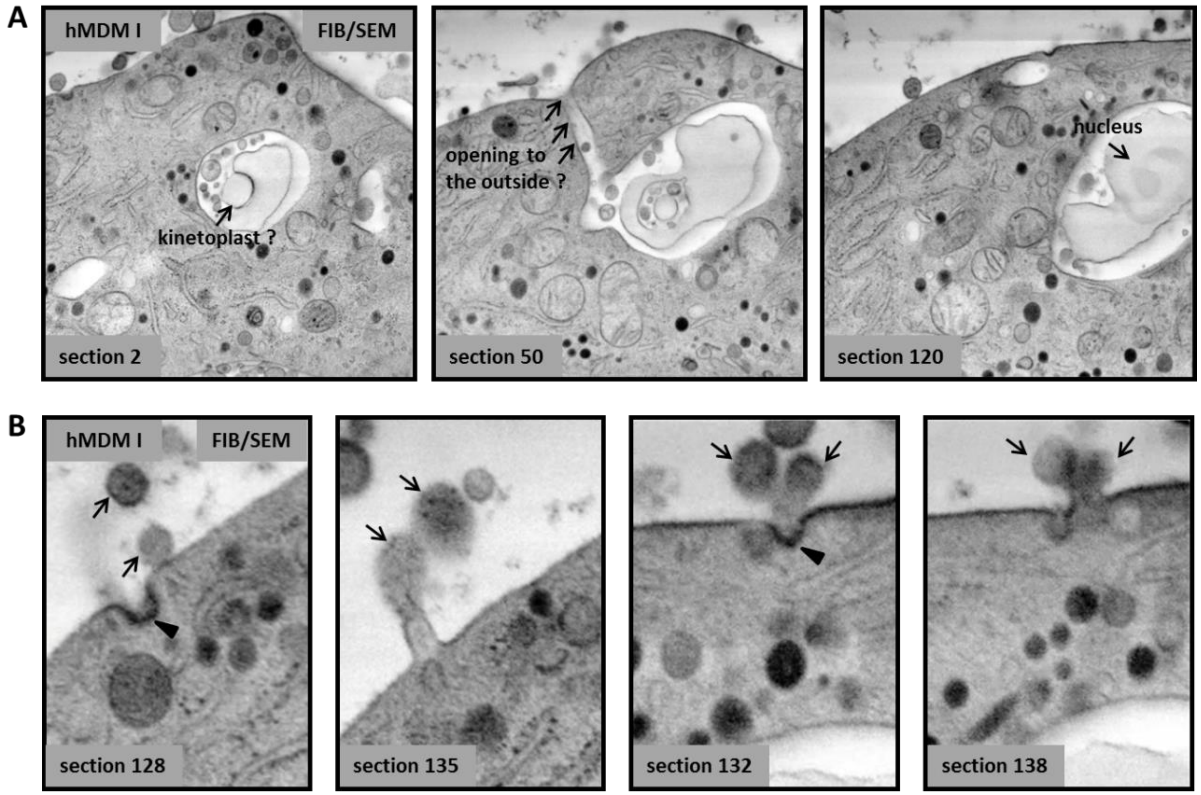

Figure 51: 3D dataset of a FIB/SEM tomography of a LC3-dot compartment. hMDM I were transduced with PBj-SW-eGFP-LC3 lentiviral vector particles, co-incubated with stationary phase *L. major* promastigotes for 1h and analyzed by 3D FIB/SEM tomography. A) 3D dataset of a parasite inside an eGFP-LC3 transduced macrophage showing a channel to the outside of the cell. B) 3D dataset of the vesicle transport of a *L. major* promastigote infected macrophage. FIB/SEM overview micrographs were taken on a FEI Helios Nanolab 600 FIB/SEM.

Next we analyzed a parasite in a LC3 + compartment by correlative fluorescence microscopy and FIB/SEM tomography (Figure 52). The position of the eGFP-LC3 transduced cell on the imprinted grid is shown in Figure 52 A (left picture, white arrowhead). The detailed fluorescence picture depicts a LC3 + compartment around the parasite body (white arrow) and the flagellum (white arrowhead). The FIB/SEM micrograph demonstrates that the milled region (black arrow) overlaps with the compartment of the parasite. Figure 52 B illustrates the acquired 3D dataset. Two parasites are visible indicated by characteristic structures like the flagellum (F), the kinetoplast (KP), the nucleus (N) and the mitochondrium (MT). The upper promastigote represents the parasite in the LC3 + compartment. In concordance with our TEM and STEM tomography data the parasite membrane (PM) is surrounded by a single parasitophorous vacuole (PV) indicating LC3-associated phagocytosis instead of autophagy.

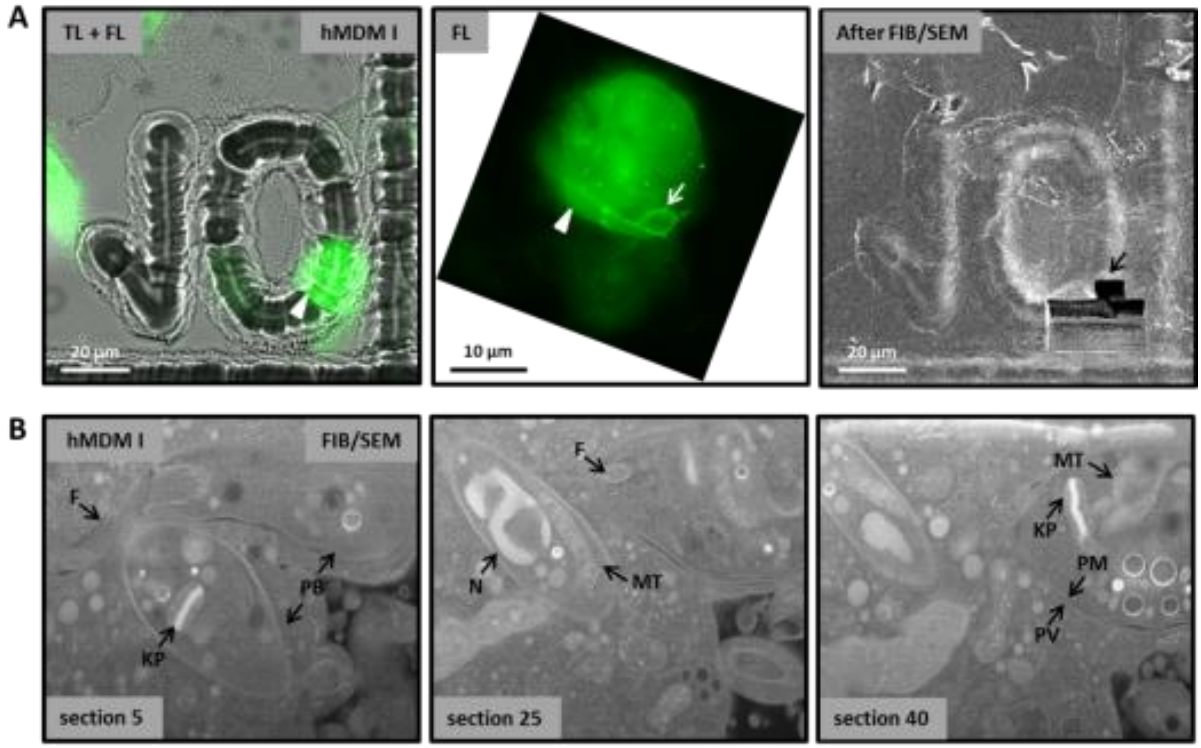

Figure 52: 3D dataset of correlative fluorescence microscopy and FIB/SEM tomography of a LC3-positive compartment. hMDM I were transduced with PBj-SW-eGFP-LC3 lentiviral vector particles, co-incubated with stationary phase L. major promastigotes for 1h and analyzed by 3D FIB/SEM tomography. A) eGFP-LC3 transduced cell (white arrowhead) with a LC3 + compartment (white arrow) before FIB/SEM and milled region after FIB/SEM. Transmitted light (TL) and fluorescence (FL) micrographs were taken on a Zeiss Axio Observer Z1. Scale bar: as indicated. B) 3D dataset of a parasite inside a single-membrane LC3 + compartment. FIB/SEM micrographs were taken on a FEI Helios Nanolab 600 FIB/SEM.

3.3.10 Analysis of *L. major* promastigote PV maturation using PBj-SW-LAMP2-mCherry lentiviral vector particles

To analyze compartment maturation leading to promastigote degradation, we transduced macrophages with PBj-SW-LAMP2-mCherry lentiviral vector particles. In previous experiments LAMP2 could be detected 3h and 24h p.i. around viable and apoptotic parasites (Dissertation Stefan Gottwalt). Thus we infected LAMP2-mCherry transduced cells and examined those 28h p.i. by fluorescence microscopy (Figure 53).

We were able to visualize LAMP2-mCherry positive compartments containing DAPI stained promastigotes (Figure 53, white arrows). However, the data are not representative, because only few cells expressed LAMP2-Cherry protein and it was not possible to reliably reproduce the data. Moreover imaging the development of the compartments over time was impossible since the LAMP2-mCherry signal was very weak and fluorescence quickly faded.

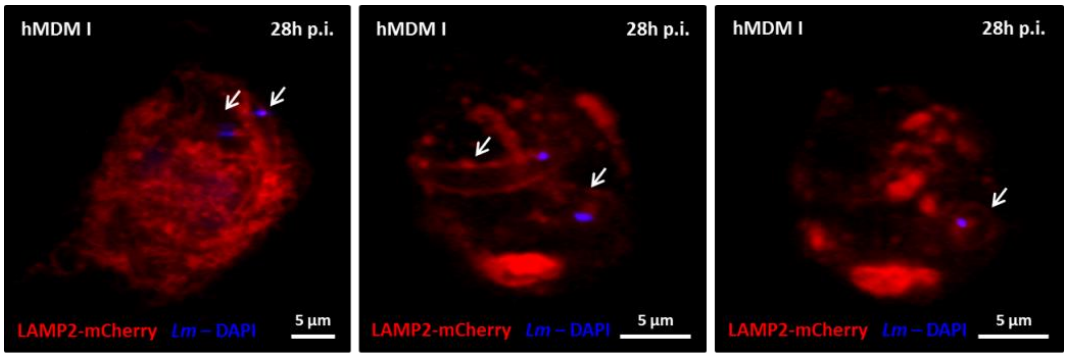

Figure 53: LAMP2 compartment analysis of LAMP2-mCherry transduced and *L. major* promastigote infected hMDMs. hMDM I were transduced with PBj-SW-LAMP2-mCherry lentiviral vector particles and co-incubated with DAPI stained stationary phase eGFP-expressing *L. major* promastigotes. Depicted are promastigotes in LAMP2-positve compartments (white arrows). Representative confocal fluorescent images were generated on a Zeiss LSM7 *Live*. Magnification: 63x oil objective with 10x ocular. Scale bar: as indicated.

3.3.11 Analysis of Phosphatidylinositol 3-phosphate generation using eGFP-2xFYVE transduced hMDMs

To analyze early events of compartment maturation we prepared PBj-SW-eGFP-2xFYVE lentiviral vector particles and analyzed generation of PI3P around the compartment by fluorescence microscopy (Figure 54 A). 15 min after co-incubation of macrophages with promastigotes we discovered FYVE negative (FYVE -) compartments (white arrowheads), FYVE positive (FYVE +) compartments (white arrow) and compartments with FYVE-dots (white arrow with dashed line). In hMDM I all three compartments developed in similar amounts (~30%) (Figure 54 C). In hMDM II less FYVE + compartments developed (Figure 54 D) compared to FYVE – and FYVE-dot compartments. Additionally, between 5% and 10% of analyzed PVs associated with small FYVE compartments (block arrow, Figure 54 A) in both macrophage types. These small FYVE compartments exhibit a size of approximately 1 µm and therefore match with the size of endosomes that varies between 60 nm up to 1 µm depending on the type of endocytosis (Conner and Schmid, 2003). We found no significant differences between stationary d8 promastigotes and purified PS+ parasites in both macrophage types (Figure 54 C and D).

Moreover we imaged FYVE compartment dynamics using live cell imaging (Figure 54 B). One promastigote (white arrow) entered an eGFP-2xFYVE transduced cell after 7 min. After 10 min the PV associated with FYVE-dots to become FYVE + after 13 min. After 16 min the PV was surrounded by FYVE-dots again. A second parasite (white arrow with dashed line) was taken up by the macrophage after 10 min, FYVE + after 13 min and FYVE - after 22 min (data not shown). A third parasite (white arrowhead) was in a FYVE + compartment during

the entire movie, in total 25 min. This data set demonstrates that we are able to image transiently generation of PI3P on the parasite containing compartment membrane of primary transduced macrophages in 3D over time.

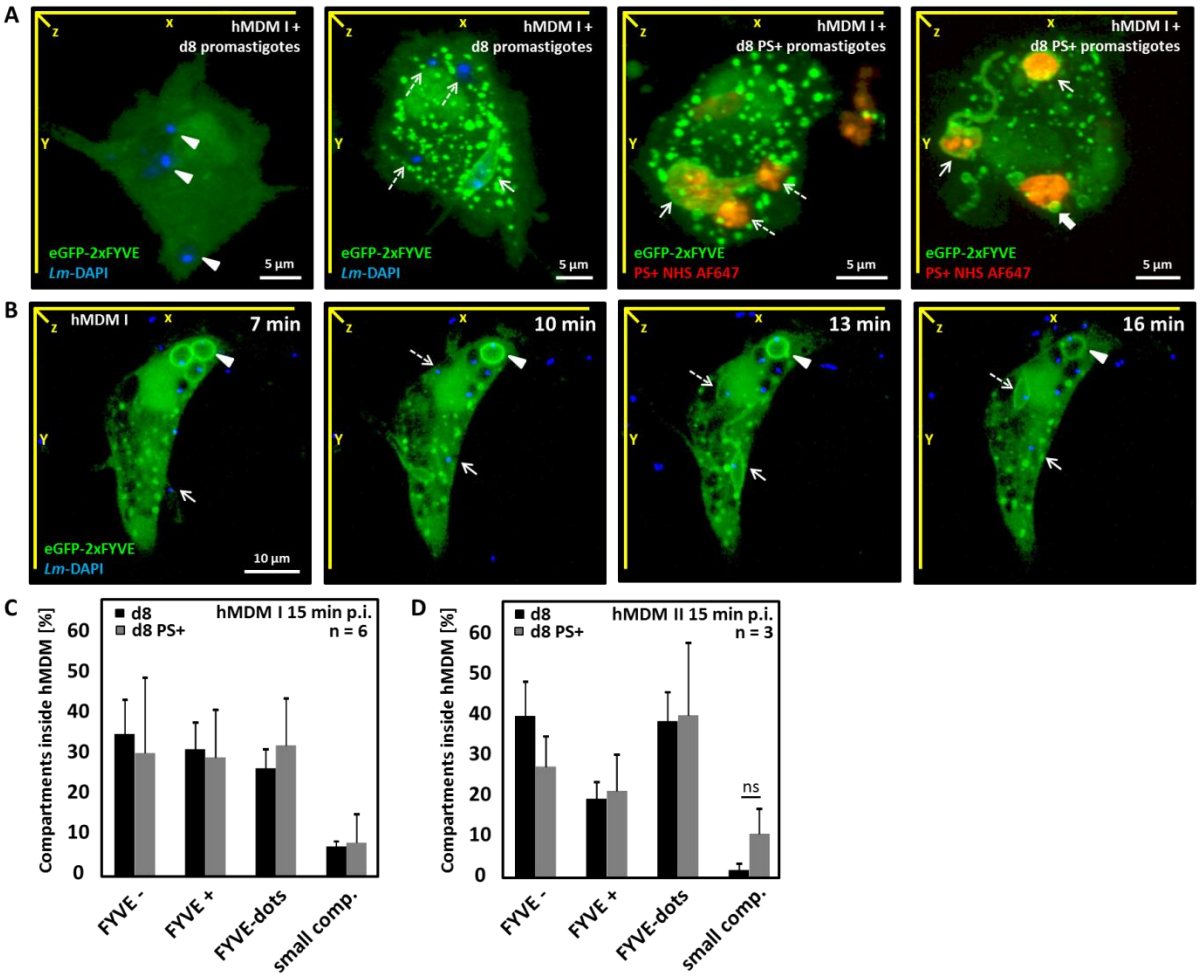

Figure 54: Quantification of PI3P generation using eGFP-2xFYVE transduced hMDMs. hMDMs were transduced with PBj-SW-eGFP-2xFYVE lentiviral vector particles and co-incubated with DAPI stained stationary phase day 8 (d8) or purified apoptotic promastigotes (PS+) prior to analysis by fluorescence microscopy. A) Confocal fluorescent 3D micrographs of eGFP-2xFYVE transduced and parasite infected hMDMs. White arrowheads indicate FYVE - compartments, white arrows show FYVE + and white arrows with dashed line indicate FYVE-dots compartments. The white block arrow points to small FYVE compartments. B) Live cell imaging of FYVE compartment dynamics. Representative 3D images were taken on a Zeiss LSM 7 *Live*. Magnification: 63x oil objective with 10x ocular. Scale bar: as indicated. C and D) Quantification of *L. major* promastigote compartments in hMDM I (C) and hMDM II (D) 15 min p.i. using fluorescent micrographs shown in (A). Data are shown as means ± SD. n = 6/3.

3.3.12 Analysis of EEA1 recruitment to promastigote-containing compartments early after parasite uptake

Via its FYVE domain, the early endosomal marker EEA1 is able to bind to PI3P and is therefore involved in early maturation events like the fusion of endosomes with phagosomes. Using EEA1 immunofluorescence analysis, we investigated the recruitment of EEA1 to promastigote-containing compartments in more detail. First of all we tested antibody specificities (Figure 55). For EEA1 staining we used a FITC-conjugated mouse antibody (BD Biosciences) (Figure 55 D). The corresponding isotype control was negative (Figure 55 A). Parasites were stained with an anti-*Leishmania* rabbit serum and an anti-rabbit AlexaFluor568 (AF568) conjugated secondary antibody (BD Biosciences). Control samples using only the secondary antibody or the secondary antibody together with a rabbit serum isotype control revealed that the anti-rabbit AF568 antibody already binds to the parasites (Figure 55 B and C). Due to the fact that we mainly focused on EEA1 recruitment, we nevertheless continued analyses.

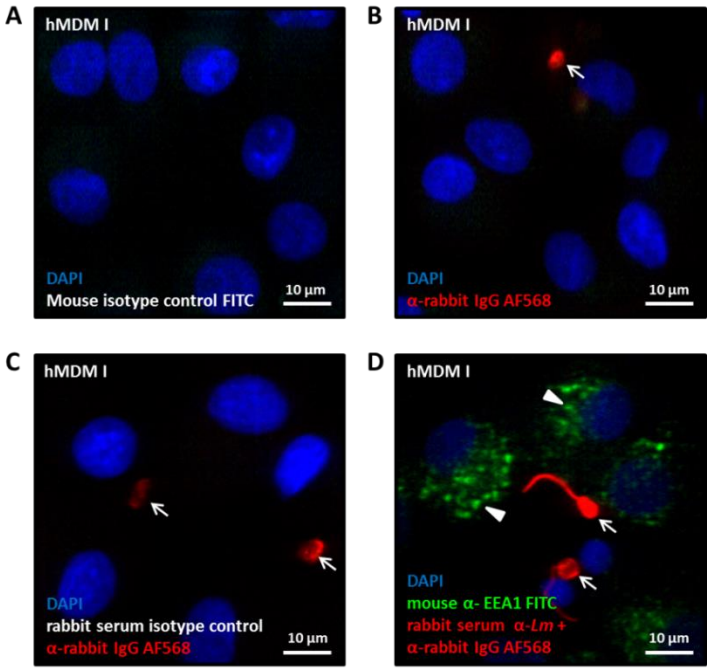

Figure 55: Antibody specificity of EEA1 immunofluorescence staining. hMDM I were co-incubated with 11 days old purified PS+ *L. major* promastigotes for 15 min, fixed and permeabilized prior to immunofluorescence staining. A) Control staining using DAPI and a mouse IgG1 FITC isotype control. B) Control staining using DAPI and a goat anti-rabbit AF568 secondary antibody. C) Control staining using DAPI, a rabbit serum isotype control and a goat anti-rabbit AF568 secondary antibody. D) Specific staining using DAPI (blue), a mouse anti-EEA1 FITC antibody (green) and an anti-*Leishmania* rabbit serum in combination with a goat anti-rabbit AF568 secondary antibody (red). Representative confocal micrographs of at least three independent experiments were taken on a Zeiss LSM 7 *Live*. White arrows indicate parasites, white arrowheads indicate EEA1 staining. Magnification: 63x oil objective with 10x ocular, Scale bar: as indicated.

Like for FYVE compartments we evaluated EEA1 recruitment to the *L. major* promastigote PV after an early time point (15 min p.i.). As shown by the immunofluorescence micrograph of Figure 56 A, parasites were either completely surrounded by EEA1 or rather associated with EEA1 dots designated as EEA1-positive compartments (EEA1 +, white arrow). Besides, parasites appeared in EEA1-negative compartments (EEA1 -, white arrowhead). Quantifying stationary phase (d8) harboring compartments in hMDM I resulted in 78.3% ± 20.7 EEA1 - compartments and 21.7% ± 20.7 EEA1 + compartments (Figure 56 B). Similar percentages (77.2% ± 7.5 in EEA - compartments, 22.8% ± 7.5 in EEA1 + compartments) were counted for purified PS+ promastigotes. We found no significantly differences between stationary phase and purified PS+ parasites. In hMDM II (Figure 56 C) the amount of EEA1 + compartments was around 20 %, too, both for stationary phase and PS+ parasites.

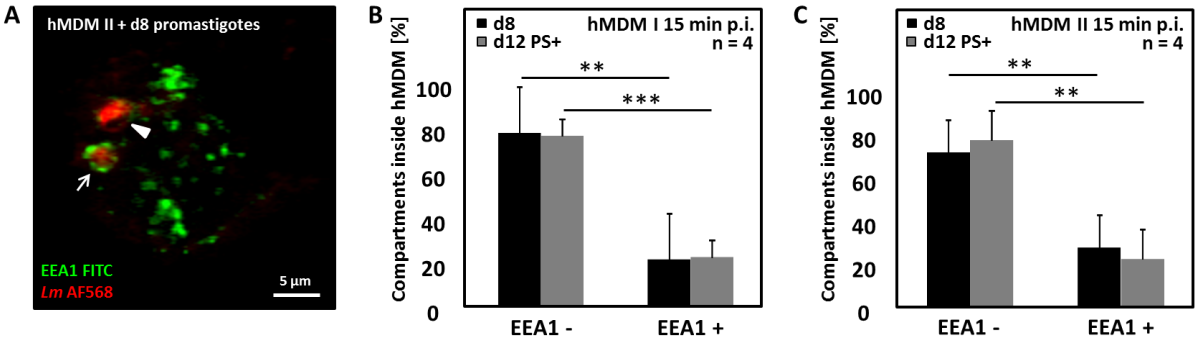

Figure 56: EEA1 recruitment to the *L. major* promastigote containing PV early after parasite uptake. hMDMs were co-incubated with stationary phase or d12 old purified PS+ promastigotes for 15 min, fixed and permeabilized prior to immunofluorescence staining. **A)** Confocal fluorescence micrograph of EEA1 and *Leishmania* stained hMDM II. For staining a mouse anti-EEA1 FITC antibody (green) and an anti-*Leishmania* rabbit serum in combination with a goat anti-rabbit AF568 secondary antibody (red) was used. The white arrowhead indicates an EEA1 - compartment and the white arrow shows an EEA1 + compartment. Representative images were taken on a Zeiss LSM 7 *Live*. Magnification: 63x oil objective with 10x ocular. Scale bar: as indicated. B and C) Quantification of *L. major* promastigote compartments in hMDM I (B) and hMDM II (C) 15 min p.i. using fluorescent micrographs shown in (A). Data are shown as means ± SD. n = 4.

3.3.13 Immuno-magnetic isolation of the *L. major* promastigote PV to identify maturation markers

Finally we were interested in the isolation of apoptotic *L. major* promastigote containing PVs for identification and analyses of additional compartment maturation markers. For the magnetic isolation approach, we used lipobiotin-labeled parasites that we incubated with streptavidin-coupled magnetic nanoparticles prior to co-incubation with macrophages and compartment isolation (2.5.3).

First of all we assessed lipobiotin labeling of purified PS+ promastigotes. Therefore promastigotes were incubated with increasing concentrations of lipobiotin subsequently labeled with AF647-conjugated streptavidin prior to flow cytometric analysis (Figure 57 A). We observed a dose-dependent labeling of the parasites with lipobiotin (Figure 57 B). However, with increasing lipobiotin concentrations we noticed events in the upper right corner of the dot blot suggestive for aggregate formation of the parasites (Figure 57 A). These aggregates additionally could be demonstrated using fluorescence microscopy. Figure 57 C depicts lipobiotin/ streptavidin AF647 labeled purified PS+ promastigotes. The white arrows point to single promastigotes, but most of the parasites appear associated in large aggregates (white arrowhead). Co-incubation of eGFP-LC3 transduced macrophages with lipobiotin/ streptavidin AF647 stained PS+ promastigotes demonstrates (Figure 57 D), that macrophages still take up stained parasites and form LC3 - (white arrowhead), LC3 + (white arrow) or LC3-dot (white arrow with dashed line) PVs. In conclusion we decided to use a 1:500 lipobiotin dilution for magnetic labeling, because only 13.0% aggregates arose and 83.6% parasites were stained.

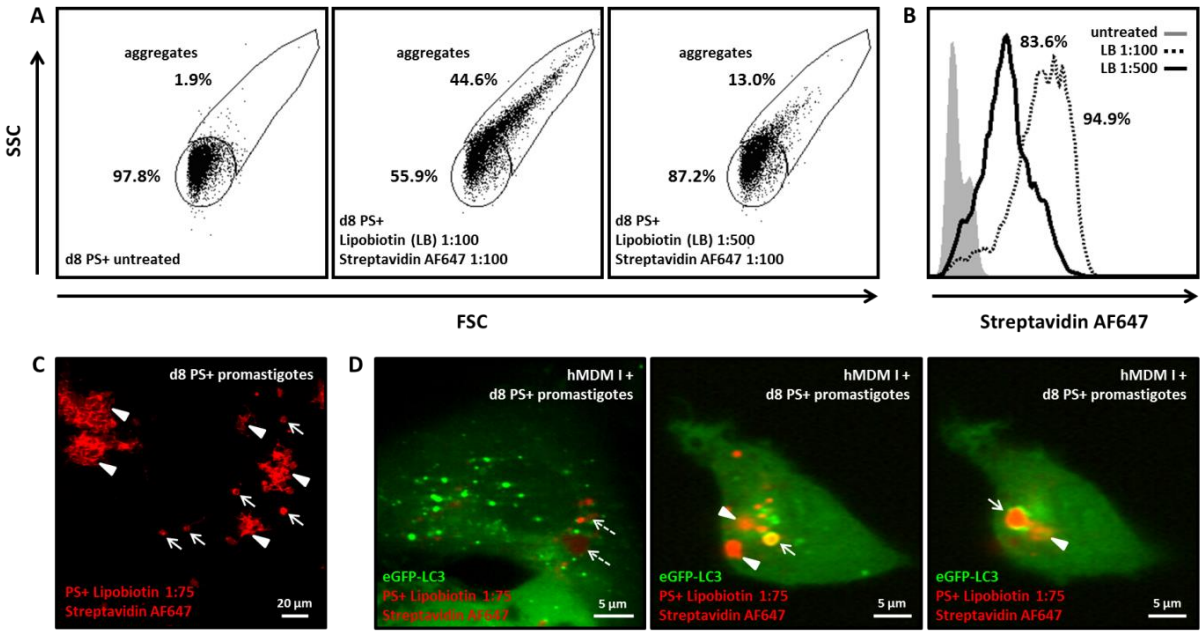

Figure 57: Labeling of apoptotic *L. major* promastigotes with lipobiotin leads to aggregate formation. PS+ purified stationary phase promastigotes were incubated with increasing lipobiotin concentrations and subsequently stained with streptavidinAF647. A) Aggregate formation of PS+ promastigotes after lipobiotin labeling visualized by flow cytometry. B) Lipobiotin labeling efficacy of PS+ promastigotes analyzed by flow cytometry. Representative FACS dot plots and histograms are shown (n=3). C) Aggregate formation of PS+ promastigotes after lipobiotin labeling analyzed by fluorescence microscopy. D) eGFP-LC3 transduced hMDM I take up lipobiotin labeled PS+ promastigotes and form LC3 – (white arrowhead), LC3 + (white arrow) and LC3-dot (white arrow with dashed line) compartments. Representative micrographs were taken on a Zeiss LSM 7 *Live*. Magnification: 63x oil objective with 10x ocular. Scale bar: as indicated.

Using streptavidin-conjugated magnetic nanoparticles (MagCellect streptavidin ferrofluid, R&D Systems) instead of streptavidin AF647 (2.6.11), we found that the parasites were not labeled efficiently with the magnetic beads. During labeling procedure we noticed two independent pellets, one belonging to the parasites and the second smaller one to the beads. Subsequent magnetic isolation process was also not successful (data not shown), so finally we looked for alternative magnetic beads.

Next we tested bionized nanoferrite (BNF)-Dextran beads harboring covalently bound lipobiotin on their surface for labeling of parasites. By tagging the lipobiotin-conjugated magnetic beads with streptavidin Cy5 we assessed labeling efficacy and formation of aggregates by flow cytometry (Figure 58 A). Using a 1:100 dilution of the beads, 62.4 % of the parasites were successfully labeled without the formation of aggregates. Subsequently, we infected labeled parasites, isolated compartments containing apoptotic promastigotes and analyzed isolated fractions by western blot (Figure 58 B). The magnetic fraction (M) showed accumulation of *Leishmania* proteins in contrast to the non-magnetic fraction (NM), the homogenized sample (H), the total lysate (TL) and uninfected hMDMs (ctrl). The purity of the magnetic fraction was addressed by soluble intracellular proteins like β-Actin and nuclear proteins such as the nuclear envelope protein complex Nucleoporin p62 that were depleted in the magnetic fraction (Figure 58 B). The mitochondrial protein Cox4 was enriched in the magnetic fraction indicating mitochondrial impurities (Figure 58 B). Taken together, data indicate an enrichment of *Leishmania* antigens in the magnetic fraction.

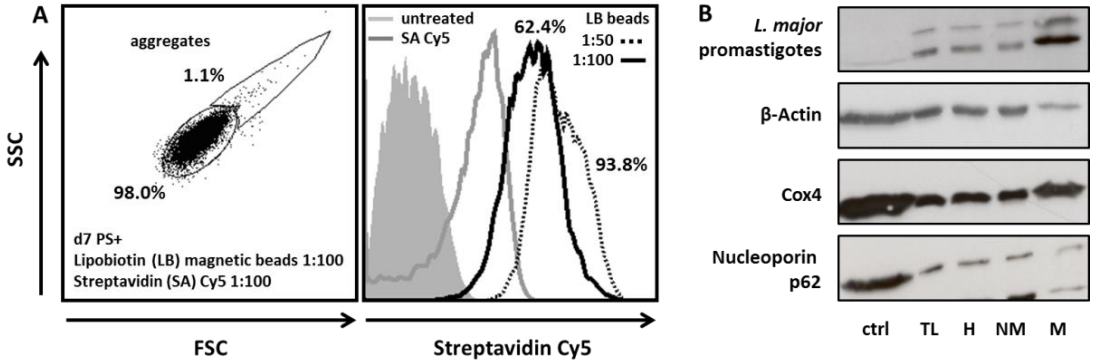

Figure 58: Immuno-magnetic isolation of apoptotic *L. major* promastigote containing compartments from hMDMs. PS+ purified stationary phase promastigotes were incubated with lipobiotin-conjugated magnetic beads for subsequent immuno-magnetic isolation of parasite containing compartments. A) Titration of lipobiotin-conjugated magnetic bead concentrations using streptavidin Cy5 labeling and flow cytometry. B) Western blot analysis of isolated apoptotic promastigote containing compartments from hMDM II. *L. major* promastigotes were detected using an anti-*Leishmania* mouse serum, β-Actin was visualized with a monoclonal mouse antibody (Sigma), Cox4 with a polyclonal rabbit antibody (Cell Signaling) and Nucleoporin p62 with a monoclonal mouse antibody (BD Transduction Laboratories). M = magnetic fraction, NM = non-magnetic fraction, H = homogenate, TL = total lysate, ctrl = uninfected hMDMs. Preliminary dot plots, histograms and Western blots are shown (n=1).

4 Discussion

In this thesis we were interested in the interaction of pro-inflammatory and anti-inflammatory primary human monocyte derived macrophages (hMDMs) with the protozoan parasite *L. major* and the development and composition of amastigote and promastigote parasitophorous vacuoles (PVs) inside hMDMs.

In the first part we concentrated on axenic *L. major* amastigote infections of hMDMs and hypothesized that amastigotes are able to escape from their compartment into the cytoplasm after re-infection of macrophages during disease development. First we compared two fixation methods for preparation of electron microscopic samples and found HPF in contrast to chemical fixation to better preserve the compartment membrane and therefore to be a suitable method for analysis of amastigote compartments. Furthermore we could demonstrate that axenic *L. major* amastigotes are surrounded by disrupted compartment membranes or are localized in the cytoplasm after direct infection of hMDMs. In addition, we visualized single amastigotes located in large PVs or multiple amastigotes laying in a common PV, what is untypical for *L. major* amastigotes, which are usually surrounded by single and tight-fitting vacuoles.

In the second part of this thesis, we focused on the *L. major* promastigote PV inside hMDMs. We hypothesized that apoptotic promastigotes are degraded in a LC3-positive autophagolysosome-like compartment, a process that might help the viable parasites to survive in the phagosome. First of all we analyzed the uptake process of viable and apoptotic parasites by hMDMs to evaluate whether differences in the uptake might lead to different compartment formation. We found that viable promastigotes are predominantly taken up via the flagellum tip whereas apoptotic promastigote are taken up with the parasite body first. Analyzing the apoptotic promastigote containing LC3-positive compartment in more detail, we found that it is a LAP compartment instead of a classical autophagosome, because the parasite was surrounded by a single-membrane and the ULK1 complex was dispensable for compartment formation. Overexpression of eGFP-LC3 using lentiviral transduction of hMDMs revealed that both viable and apoptotic promastigotes can recruit LC3 to their compartment and that apoptotic parasites are degraded rapidly in these compartments whereas viable parasites are able to get rid of LC3-protein. We started to establish a correlative approach to combine fluorescent signals with high-resolution ultrastructural information. Analyzing the maturation of parasite PVs, we found that the PV partially gets PI3P and EEA1 positive after early time points of infection. To evaluate compartment maturation in more detail, we isolated apoptotic promastigote PVs using an immuno-magnetic isolation protocol.

4.1 Part 1 – Development of *L. major* amastigote PVs inside hMDMs

So far, little is known about maturation of amastigote PVs in primary human macrophages. Since for a long time it was not possible to culture amastigotes *in vitro*, most studies are based on tissue amastigotes prepared from infected mice or short-term cultivation in peritoneal macrophages or macrophage cell lines (Gupta et al., 2001). Multiple studies in mouse macrophages have shown that *L. major* amastigotes reside in single and tight fitting vacuoles (Chang and Dwyer, 1978; Courret et al., 2002). Real and Mortara followed tight-fitting *L. major* DsRed amastigotes during parasite division in infected murine macrophages by time-lapse fluorescence microscopy (Real and Mortara, 2012) and could show that within 48 h parasites first divide inside the PVs followed by PV fission. Furthermore they observed two or three amastigotes in one PV in fixed macrophages after 48 h of infection, representing parasites that undergo division. These data are in concordance with our findings of two or four amastigotes in a tight, common PV after 144 h of infection. Interestingly, we also detected single amastigotes in loose compartments or multiple amastigotes (up to 12) in one communal, tight PV after 144 h of co-incubation with hMDM I. Up to now, multiple amastigotes in one large communal compartment were only reported for *L. amazonensis* amastigotes. Courret and colleagues (Courret et al., 2002) could demonstrate that *L. amazonensis* amastigotes first were located in relatively tight compartments, which due to fusion with endocytic compartments dilated to reach a large size and after later time points harbored numerous parasites. Similar results were obtained by Real and Mortara by time-lapse microscopy of murine macrophages infected with *L. amazonensis* amastigotes in the presence of the lysosomotropic probe Lysotracker. Lysotracker revealed that amastigotes are first lodged in tight-fitting PVs that increase in size and parasite numbers after 24 h (Real and Mortara, 2012). So far, none of the studies has investigated primary human cells or axenic amastigotes that are free of host-derived contaminants. Although in literature it is accepted that *L. major* amastigotes reside in single, tight-fitting PVs, it can be supposed that there exist differences between murine and human macrophages as well as between tissue and axenic amastigotes leading to different observations. Until now, we observed the phenomenon of large PVs harboring multiple *L. major* amastigotes only after late time points (120 h and 144 h) and only in hMDM I. It would be very interesting to increase the number of donors for this analysis as well as to analyze hMDM II and to figure out the function behind this phenomenon. Therefore it is important to analyze proteolytic activity of infected cells by assessing Cathepsins in Western Blot to prove whether multiple amastigotes in a common PV show better parasitic survival. To strengthen this hypothesis, it is eminent to perform studies on amastigote development after inhibition of acidification by chemically blocking V-

ATPase responsible for lowering the pH or by using cysteine protease inhibitors or siRNA knockdown approaches.

Using High-Pressure-Freezing (HPF) in combination with TEM analysis revealed damaged *L. major* amastigote PVs inside hMDMs. In addition, STEM tomography showed a parasite laying in the cytoplasm lacking the PV. In literature, it is only rarely mentioned how amastigotes spread to other cells during disease persistence. In 1980, Ridley was one of the first who studied *Leishmania* egress from the host cell and observed lysis of parasitized macrophages and the presence of amastigotes in the extracellular space (Ridley, 1980). Time-lapse microscopy of infected human peripheral blood monocytes illustrated numerous parasites that were released by the host cell in an exocytotic-like process (Rittig et al., 1998). Skin biopsies from patients with cutaneous leishmaniasis were analyzed on the ultrastructural level and revealed parasites in vacuoles or in the cytosol (M. Sandbank, 1976; Ridley and Wells, 1986; Rittig and Bogdan, 2000). At this time point it was controversial whether compartment membranes tightly enclosing the parasite can be resolved with the quality of electron microscopic pictures. In our studies we used state of the art HPF for excellent preservation of membrane details combined with a freeze-substitution procedure that was improved by varying the water content of the substitution medium for optimal contrasting and visibility of the membranes (Walther and Ziegler, 2002). HPF of pancreas tissue demonstrated that mitochondrial membranes are well preserved and that HPF does not destroy them (Walther and Ziegler, 2002). Using HPF, smaller intermembrane spaces have been observed than with chemical fixation using glutaraldehyde. HPF of *Saccharomyces cerevisiae* in combination with STEM tomography revealed that the membranes of mitochondrial cristae are in close proximity to each other (Höhn et al., 2011). Therefore HPF combined with STEM tomography is a powerful tool to analyze amastigote escape from the PV in a three-dimensional manner and we could clearly demonstrate an amastigote lacking the compartment membrane. Nevertheless, using static information from fixed samples, it is difficult to evaluate *Leishmania* egress (Florentino et al., 2014). Live cell imaging techniques are promising tools for investigation and evaluation of dynamic events like the parasite escape from the PV. For instance, using a LiveBLAzer system would enable us to measure amastigote outcome of the compartment by live cell imaging. This system contains a förster resonance energy transfer (FRET)-based fluorescent substrate for the enzyme β-lactamase that changes fluorescence after cleavage. In the absence of β-lactamase, excitation of coumarin (409nm) results in FRET to the fluorescein which emits a green fluorescent signal (520 nm). After cleavage, the two dyes are separated so that excitation of the coumarin now produces blue fluorescence (450nm). By linking β-lactamase to the surface of *L. major* amastigotes we could visualize compartment outbreak in real-time. Similar FRET experiments were performed by the working group of Albert Haas to analyze

phagolysosome formation of *Rhodococcus equi* containing compartments. Lysosomes of macrophages were preloaded with BSA rhodamine as acceptor-fluorophore and subsequently cells were infected with donor-fluorophore ATTO488 labeled bacteria (Von Bargen et al., 2009; Sydor et al., 2008, 2013).

To summarize, TEM and STEM analysis suggest that *L. major* amastigote PVs inside hMDMs are increasingly damaged and interrupted with time of infection leading to the escape of the amastigotes into the cytoplasm during re-infection of macrophages. Live cell imaging experiments are relevant to dynamically evaluate amastigote escape from the PV in real-time and to mechanistically understand amastigote development in human macrophages. Measuring proteolytic activity as well as inhibiting compartment acidification is important to understand the function of multiple amastigotes in a common PV and of amastigotes escaping into the cytoplasm.

4.2 Part 2 – Development of *L. major* promastigote PVs inside hMDMs

4.2.1 *L. major* promastigote uptake by hMDMs

Uptake of *L. major* parasites seems to be different depending on the parasite stage. Wenzel and colleagues could demonstrate in 2012 that axenic *L. major* amastigotes seem to sink into primary human macrophages by a mechanism involving CR3-mediated endocytosis. In contrast to that, *L. major* promastigotes were partly taken up by a CR1-mediated phagocytic mechanism of the macrophages starting at the tip of the flagellum (Wenzel et al., 2012). In literature promastigote uptake studies led to contradictory conclusions. Early studies investigating *L. donovani* promastigote uptake by hamster peritoneal macrophages using light microscopy claimed that the parasites attached in a random and non-orientated manner to the phagocytes prior to engulfment via pseudopods of the phagocytes (Chang, 1979). Besides, there exist several reports showing that promastigotes can enter their host cells either via the posterior or the anterior end. Studies using metacyclic *L. amazonensis* promastigotes and murine macrophages claim that promastigotes more often are phagocytosed with the cell body entering first (Courret et al., 2002). Pearson and colleagues quantified the orientation of *L. donovani* promastigotes attached to monocyte-derived macrophages and found that about 40% attached via the flagellum and 60% attached via the a-flagellar pole (Pearson et al., 1983). In another study, quantifying scanning and transmission electron microscopic pictures revealed that parasites can enter their host cell either “head-first” or “tail-first” and that both types occurred in equal frequency (Chang, 1979). These data fit to our suggestion that viable promastigotes enter the macrophage with

the flagellum first, whereas the apoptotic promastigotes enter macrophages with the body first. The infectious inoculum of *Leishmania* parasites consists of an equal mixture of viable and apoptotic promastigotes. This would explain the findings of Pearson and colleagues as well as of Chang that entry via the flagellum or the a-flagellar pole appeared in similar amounts. Separating viable from apoptotic promastigotes prior to infection would help to confirm our preliminary results suggesting differential uptake of viable and apoptotic promastigotes. Another study using *L. major* promastigotes quantified the attachment of the parasites to human monocytes and observed that they attached predominantly with the flagellar tip (~80%) and only occasionally with the flagellar base (~10%) or the posterior pole (~10%). Our findings suggest that this difference could be explained by their use of logarithmic/early stationary phase parasites that exhibit higher numbers of viable parasites compared to the infectious inoculum of late stationary parasites that we used.

Light-microscopy time-lapse imaging of the uptake process strongly indicates different orientation during uptake mechanisms of the parasites. Phagocytosis of the apoptotic promastigote via the cell body took about 12 min and the viable promastigote was engulfed during 20 min with the flagellar tip first. Similar results were reported by Forestier and colleagues (Forestier et al., 2011). They examined the interplay between metacyclic hamster-derived *L. donovani* promastigotes and primary bone-marrow-derived macrophages (BMDM) in real time as well. Engulfment from the flagellar tip towards the cell body took 10 to 20 min. They quantified 65% of the parasites entering via the flagellum tip, 29% entering via the flagellar base and 6% entering via the cell body. Additionally they could show that dead but morphologically intact promastigotes failed to be engulfed by macrophages. Courret and colleagues observed parasites that first interacted with the macrophage via the flagellum, but rapidly turned around and finally entered the macrophage with the cell body first. The phagocytic process took between 3 and 9 minutes (Courret et al., 2002). This data fit to our time-lapse movie visualizing the uptake of an apoptotic parasite. In our movie the parasite first attached to a macrophage via the flagellum tip, but in the end it was taken up with the cell body first by another macrophage. Duration of the phagocytic process was about 12 min.

Moreover live cell imaging and SEM analysis revealed macrophage membrane ruffles engulfing the viable promastigote at the flagellum tip and the formation of pseudopods enveloping first the flagellum and then the parasite body. Several investigations (Pearson et al., 1983; Zenian et al., 1979) discovered such funnel-like extensions of the phagocyte during parasite engulfment (Rittig and Bogdan, 2000). In contrast to that, in 2006 *L. chagasi* promastigote phagocytosis was reported to be associated with caveolae (Rodríguez et al.,

2006). Another study found that *L. major*, *L. donovani* and *L. aethiopica* promastigotes can be engulfed by coiling phagocytosis as well as by tubular protrusions (Rittig et al., 1998).

In conclusion it has to be mentioned that all reported studies just add some form of infectious inoculum to the macrophages. In contrast to that, we quantified viable and apoptotic populations within the infectious inoculum and specifically followed their uptake into the cells. Consideration of different promastigote forms could explain contradictory observations and results found in literature. Moreover high resolution live recordings of the host-pathogen interactions are important to reveal detailed aspects of the uptake process.

4.2.2 LC3 recruitment to the *L. major* promastigote PV inside hMDMs is meditated by LAP instead of autophagy

Recently, we could demonstrate that apoptotic *L. major* promastigotes enter LC3-positive compartments inside hMDMs (Crauwels et al., 2015). Based on these findings, in this thesis we wanted to evaluate the LC3-positive compartment in more detail focusing on the molecular mechanism and the involvement of the autophagy protein LC3.

Already in 2004 several studies implicated the autophagy machinery in elimination of intracellular pathogens that either disabled phagosomal maturation or escaped into the cytosol, a process termed xenophagy. Gutierrez and colleagues showed that induction of autophagy by starvation or rapamycin can overcome phagosomal maturation block during *Mycobacterium tuberculosis* infection (Gutierrez et al., 2004). *Streptococcus pyogenes* invades non-phagocytic cells and can escape from endosomes into the cytoplasm where they are enveloped by autophagosome-like compartments and are degraded after fusion with lysosomes (Nakagawa et al., 2004). Some pathogens like *Shigella flexneri* are able to escape the autophagy machinery through blocking the association with LC3-positive compartments by the virulence protein IscB (Levine, 2005; Ogawa et al., 2005). Besides, there exist parasites like *Toxoplasma gondii* that induce autophagy for parasite growth (Wang et al., 2009). Another example is *Trypanosoma cruzi*, where mammalian autophagy favors the colonization of the host cell (Romano et al., 2009). For *L. amazonensis* but not *L. major* promastigotes increasing infection rates in BALB/c macrophages were reported after autophagy induction (Pinheiro et al., 2009).

In this thesis, we found that *L. major* promastigotes are surrounded by a single-membrane compartment typical for LAP in both analyzed types of human macrophages (Crauwels et al., 2015). Recently, the working group of Frank Lafont investigated the role of vesicle-associated membrane proteins (VAMPs) that are key molecules of the vesicle fusion

machinery during *Yersinia pseudotuberculosis* infection. They focused on VAMP3 that had already been demonstrated to be required for the fusion of multivesicular bodies and autophagosomes to generate amphisomes (Fader et al., 2009). In their study they could show that VAMP3 only associated with single-membrane PVs in epithelial cells but not with double-membrane PVs in BMDMs. The number of lipid bilayers in these cells could be reversed by VAMP3 knockdown or VAMP3 overexpression, respectively. From this they concluded that VAMP3 is a marker for single-membrane LC3-positive compartments. Furthermore they found LC3 to be recruited to the vesicles by VAMP7 independent on single- or double-membranes (Ligeon et al., 2014). VAMP7 could previously be also associated with the fusion of autophagosomes with lysosomes (Fader et al., 2009). It has been reported, that VAMPs can be involved in different bacterial infections. One study demonstrated the kinetic of the recruitment of Vamp 3, 7 and 8 proteins to the *Coxiella burnetii* containing PV in HeLa cells (Campoy et al., 2013). Moreover, VAMP3 was shown to associate with *Mycobacterium tuberculosis* containing compartments and being proteolytically degraded with time of infection (Fratti et al., 2002). VAMP8 was demonstrated to play a role in *Leishmania* infection. The *Leishmania* surface metalloprotease gp63 was shown to cleave VAMP8 thereby inhibiting NADPH oxidase complex formation. Consequently, an altered pH in the PV led to a reduced T-cell activation (Matheoud et al., 2013). These studies demonstrate that VAMPs are associated to pathogen-containing phagosomes. Furthermore, VAMP3 had been demonstrated to localize to EEA1-positive early endosomes (Puri et al., 2014). Therefore it is necessary to clarify whether VAMP3 or other VAMPs also play a role in the formation of EEA1-/LC3-positive PVs around *L. major* promastigotes in hMDMs. Furthermore it is important to figure out whether there are differences between viable and apoptotic promastigotes leading to a different outcome of infection.

We could clearly demonstrate that ULK1 is not needed for *Leishmania* induced LC3-compartment formation. Consistent with our results, BMDM from wild-type or ULK1$^{-/-}$ mice displayed similar levels of GFP-LC3 translocation to phagosomes containing dead cells (Martinez et al., 2011). Similar, there were no differences between wild-type or ULK1$^{-/-}$ cells regarding LC3 recruitment to phagosomes containing DNA-IC-coupled beads (Henault et al., 2012). Furthermore, siRNA knockdown of FIP200, which is another protein of the preinitiation complex, resulted in equal levels compared to control cells of LC3-recruitment to compartments harboring apoptotic cells (Florey et al., 2011).

There is general agreement that LAP requires the Atg5-Atg12-Atg16L conjugation system during LC3 recruitment (Lai and Devenish, 2012). Loss of one of these components or loss of the E1-like enzyme Atg7, which is required to form this complex, demonstrated reduction

in LC3 recruitment to phagosomes containing either invading bacteria (Huang et al., 2009; Kageyama et al., 2011; Sanjuan et al., 2007), apoptotic bodies (Martinez et al., 2011) or live cells (Florey et al., 2011). Thus, knockdown of Atg5, Atg12, Atg16L and Atg7 in primary macrophages in combination with *Leishmania* infection is eminent to understand the molecular machinery involved in *Leishmania* induced LAP.

Concludingly, we could clearly show, that *Leishmania* induce LAP instead of autophagy. Now it is indispensable to analyze the involvement of further Atg proteins as well as VAMP proteins to understand the molecular mechanisms of compartment formation in more detail.

4.2.3 Analysis of *L. major* promastigote containing LAP compartments inside hMDMs using live cell imaging and correlative microscopy

Microscopy is the technique most commonly applied for studying autophagy (Karanasios et al., 2013; Klionsky, 2008). Autophagy proteins have been extensively studied by electron microscopy as well as by fluorescence microscopy. Kabeya and colleagues were the first who used immuno-electron microscopy and GFP-tagged LC3 in fixed cells to show that the mammalian homolog of Atg8 localizes on the autophagosome membrane (Kabeya et al., 2003). Furthermore, there exist several publications that either use cells transiently transfected with GFP-LC3 (Huang et al., 2009), cell lines stably expressing GFP-LC3 (Sanjuan et al., 2007) or mice derived GFP-LC3$^+$ cells (Martinez et al., 2011) for time-lapse microscopic imaging of autophagy. The problem with primary human monocyte derived macrophages is that they are hard to transfect by conventional transfection methods. Therefore we looked for alternative methods for overexpression of genetically modified proteins and established lentiviral transduction of primary human macrophages in collaboration with the group of Prof. Dr. Matthias Schweizer (Division of Medical Biotechnology, Paul-Ehrlich-Institute). Recently, EMD Millipore has also developed a technology to produce high-titer lentiviral particles encoding GFP-LC3 for fluorescent imaging of cells undergoing autophagy (Long et al., 2015). The advantage of lentiviral transduction is that it offers homogeneous protein expression compared to non-viral transfection methods and can be used for live cell fluorescent microscopy as well as in combination with fixation methods (Long et al., 2015). Using lentiviral transduction we were able to quantify LC3-compartment formation around *Leishmania* parasites in primary human macrophages. Similar like knockdown technologies, lentiviral transduction opens new experimental perspectives in primary human macrophages that otherwise would be dependent on cell lines or mouse cells. It would be of particular interest, whether primary human macrophages can be treated with siRNAs and lentiviral particles at the same time.

Using overexpressed fluorescent autophagy proteins enables us to get information about the autophagosome formation in 3 dimensions of space (Karanasios et al., 2013). Nevertheless, the fourth dimension – time, also provides important information and can be uncovered with real time imaging (Karanasios et al., 2013; Lippincott-Schwartz, 2011). Moreover, with live cell imaging autophagy proteins can be monitored in their natural environment without the need of fixation and permeabilization of the cells and the risk to create artifacts (Karanasios and Ktistakis, 2014). Yoshimori and colleagues were the first who studied autophagy using time-lapse video microscopy (Mizushima et al., 2001).

In our previous studies (Crauwels et al., 2015), LC3-compartment formation was assessed by immunofluorescence analysis and we could show that only apoptotic promastigotes enter LC3-compartments. Based on these results we came to our hypothesis of this thesis that only the apoptotic promastigotes associate with LC3 protein, a process that might somehow help the viable promastigotes to survive inside macrophages. This is contrasting to our current results demonstrating that LC3 also associates with PVs containing viable promastigotes. The question arises why viable promastigotes could previously not or only to a small amount be visualized in LC3-positive compartments (Crauwels et al., 2015). One explanation might be that we used different methods and time-points to analyze LC3-compartments. Previous experiments were performed on fixed samples using antibody staining 3 h p.i. whereas newly-created data arose from eGFP-LC3 transduced cells after 1 h of co-incubation. In addition, live cell imaging experiments have shown that viable promastigotes stay in LC3-positive compartments for only few minutes up to 1 h. Hence, the time point (3 h) analyzed in immunofluorescence stainings was too late to recover this information. In hMDM II less LC3-positive compartments formed around PS+ parasites compared to hMDM I. Furthermore, we observed the formation of significantly more LC3-negative than LC3-positive compartments in hMDM II after incubation with PS+ promastigotes. This was unexpected to us, since anti-inflammatory hMDM II are the macrophage cell type responsible for removing apoptotic cells and showing better survival rates of *Leishmania* parasites (Bank, 2012). Therefore, we expected hMDM II to take up increased numbers of PS+ parasites and the formation of increased LC3-positive compartments inside hMDM II. Nevertheless, hMDM II also seem to form less LC3-positive compartments around PS- parasites. Now we can speculate that apoptotic parasites are degraded by an additional mechanism in hMDM II, but the exact mechanism remains to be investigated. With regard to our hypothesis, we expected obvious differences in LC3 recruitment between viable and apoptotic promastigotes. Nevertheless, the results indicate a constant association of LC3 protein to the PV independent of the viability of the parasites.

Based on our quantification and supported by live cell imaging experiments we now propose a new hypothesis: viable promastigotes can be engulfed by membranes forming a PV containing LC3 protein as a marker, but are somehow able to get rid of LC3 protein. In contrast, LC3 recruitment to compartments containing apoptotic promastigotes promotes phagosome maturation and degradation of the parasites. Similar observations have been made for the pathogen *Plasmodium* causing malaria. The parasites are targeted by LC3 protein and only parasites that are able to get rid of the LC3 protein survive whereas the majority is degraded (Prof. Dr. Volker Heussler, unpublished). To prove the statement that viable promastigote PVs can get rid of LC3-protein, it would be interesting to analyze LC3-compartments in transduced macrophages after later timepoints. Due to the fact that in immunostaining experiments there were no viable promastigotes inside LC3-pos compartments 3h after co-incubation, 3h would represent an interesting time point. It would be very interesting to simultaneously visualize the uptake and maturation of differently labeled viable and apoptotic *Leishmania* promastigotes into LC3-compartments in real-time. Such an experimental setup could additionally prove our new drawn hypothesis.

Our results emphasize the importance of dynamic imaging of host-pathogen interactions. By only taking into account static information from fixed samples it is difficult to evaluate *Leishmania* compartment formation. Although live cell imaging has high analytical power it also shows some limitations (Karanasios et al., 2013). It has to be taken into account that during live cell imaging, cells are exposed to light for a prolonged period of time, what may result in altered physiological responses known as photo-toxicity (Karanasios et al., 2013). In addition, fluorescent live cell imaging is limited in the observation of detailed aspects because it lacks spatial resolution (Florentino et al., 2014). The resolution limit achieved by light microscopy is around 250 nm (Karanasios and Ktistakis, 2014). In the last decade the diffraction limit of fluorescence microscopy has been overcome (Lakadamyali, 2014) by the development of super-resolution microscopy methods. There exist different super-resolution microscopy methods like structured illumination microscopy (SIM) (Gustafsson, 2000), stimulated emission depletion microscopy (STED) (Klar et al., 2000), stochastic optical reconstruction microscopy (STORM) (Rust et al., 2006) or fluorescence photoactivation localization microscopy (fPALM) (Betzig et al., 2006). Whereas first super-resolution images had an acquisition time of several hours, the past decade has led to technological improvements and transformed super-resolution microscopes into powerful tools enabling to visualize dynamic processes in living cells (Lakadamyali, 2014). In 2014, the Nobel Prize in chemistry was awarded to the German scientist Prof. Dr. Stefan W. Hell, together with two US-American scientists, for his invention of STED microscopy. After excitation of a fluorophore, the fluorophore is forced back to its ground state using a depletion beam that resembles the shape of a doughnut enabling the molecules in the center to stay excited (Klar

et al., 2000; Lakadamyali, 2014). Using STED microscopy, a spatial resolution of up to 30 nm can be achieved (Lukinavičius et al., 2014; Schmidt et al., 2009). However, super-resolution of live cells is still in its early days and several parameters have to be carefully balanced against each other (Lakadamyali, 2014). Another promising tool to overcome limitations of light microscopy is a correlative approach that combines the information of fluorescent proteins with the high resolution of the ultrastructure (Karanasios and Ktistakis, 2014).

Razi and Tooze nicely have described correlative light and electron microscopy (CLEM) as a tool to understand the autophagy process (Razi and Tooze, 2009). Using HEK293 cells overexpressing eGFP-LC3 they were able to first analyze GFP-labeled structures by fluorescence microscopy followed by examination of the autophagic vacuoles by electron microscopy. CLEM application could also facilitate distinguishing between LAP and canonical autophagy (Lai and Devenish, 2012). To get detailed information about the ultrastructure, one can either analyze serial TEM sections or use three-dimensional methods like tomography or FIB/SEM. In 2009 the working group of Eskelinen demonstrated with the help of 3D electron microscopic tomograms that the phagophore membrane is connected to the ER what might give a hint for the origin of autophagosomal membranes (Ylä-Anttila et al., 2009). In this thesis we analyzed autophagy-like compartments containing *Leishmania* parasites by correlative approaches. For our question FIB/SEM is recommended in contrast to STEM tomography, because with FIB/SEM it is more easy and reliable to find back the cells of interest. We first visualized eGFP-LC3 protein by fluorescence microscopy followed by FIB/SEM. Thereby we identified the parasites in single-membrane compartments representative for LAP. Furthermore we obtained a parasite in a human macrophage with an opening to the outside. The imaging data suggest that this channel structure illustrates an uncompleted phagocytic process of the parasite, but the exact mechanism leading to the channel has to be investigated in more detail. Moreover we were able to observe vesicles fusing with the plasma membrane or rather being pinched off the membrane, as one would expect for phagocytic cells. We would not have been able to display this by conventional electron microscopy. Nevertheless, we came across some challenges using this correlative approach. Whereas fluorescence microscopy displays a horizontally section of the adherent cells, the FIB/SEM images are taken in an almost vertical direction. Therefore it is not possible to overlay single fluorescent with electron microscopic pictures. This emphasizes the importance to visualize the eGFP-LC3 fluorescence in 3D using fluorescence laser scanning microscopy that can be traced, compared and rendered with the 3D tomogram. Our working group now has a confocal laser scanning microscope that enables 3D recording over time, in close proximity to a HPF apparatus, which is needed for electron microscopic sample preparation. In concordance with the literature (McDonald, 2009), our data have shown, that cryo-fixation followed by freeze substitution are the methods of choice to preserve details in

living cells in comparison to conventional fixation methods. Combining confocal laser scanning microscopy with HPF and FIB/SEM will hopefully gain detailed information about the formation of LAP compartments around *Leishmania* parasites.

To sum up, lentiviral transduction is a powerful method for overexpression of fluorescent proteins of interest, making cell lines or mouse experiments dispensable. Furthermore lentiviral particles enable fluorescent imaging of live cells in three spacial dimensions over time. By combining 4D light microscopy imaging with high resolution 3D electron microscopy (FIB/SEM or STEM tomography) we are able to follow the dynamics of LAP compartment formation around *Leishmania* parasites with high resolution.

4.2.4 Maturation of *L. major* promastigote containing LAP compartments inside hMDMs

So far, there exists no pharmacological reagent that specifically acts against LAP, or a marker that is specific for LAP and can distinguish it from autophagy (Lai and Devenish, 2012). Although the working group of Lafont identified VAMP3 as a marker specific for single-membrane LAP compartments containing *Yersinia pseudotuberculosis* (Ligeon et al., 2014), VAMP3 association with other pathogens should be validated before it´s general accepted as a specific LAP marker. By means of live cell imaging experiments maturation markers of LAP compartments were time-dependently assessed. LAP uses maturation components of the autophagic pathway. Several publications (Florey et al., 2011; Henault et al., 2012; Sanjuan et al., 2007) are in agreement that in the first 5-20 min after infection the PI3K Vps34 is activated what leads to the production of the phospholipid PI3P in the compartment membrane. Already 10 min after infection, the phagosomes starts to become LC3 positive what lasts for 60-90 min. Finally, 40 min to 60 min after infection, the phagosomes are positive for the lysosomal marker LAMP1 or the lysosomotropic probe Lysotracker indicating acidification of the compartments. Acidification could be detected for a time period of about 2 h.

Generation of PI3P can either be detected by a PX-domain (Henault et al., 2012; Sanjuan et al., 2007) or a 2x-FYVE domain (Florey et al., 2011). Single FYVE domains could be shown to be insufficient for the use as probes in vivo, but tandem FYVE domains effectively bind to early endosomes, which are rich in PI3P (Gillooly et al., 2000; Vieira et al., 2001). We demonstrated that 3-5 min after infection the *Leishmania* PV gets FYVE-positive, what lasts for few minutes (5 min) up to half an hour. As described before, this is in agreement with data from literature. Moreover, Vieira and colleagues examined the role of PI3P in RAW macrophages transfected with chimeric GFP-FYVE constructs after phagocytosis of IgG

opsonized red blood cells. 4-5 min after addition of the erythrocytes FYVE-positive phagosomes formed, which lasted 7-10 min (Vieira et al., 2001). Quantification of FYVE compartments (FYVE -, FYVE +, FYVE-dots) resulted in no significant differences between stationary phase parasites or purified apoptotic promastigotes in both analyzed macrophage types. This indicates that recruitment of Vps34 to phagosomal membranes is a common process that is independent on phagosomal content. The same was observed for EEA1 positive compartments. There were no significantly differences between the infectious inoculum and purified apoptotic promastigotes indicating a permanent association of endosomes and phagosomes independent of the viability of the parasites. A similar assumption was drawn by Courret and colleagues, who suggested transient interactions of phagosomes and endosomes followed by rapid recycling of early endosome-associated molecules (Courret et al., 2002). It is likely, that the amount of FYVE + or EEA1 + compartments is underestimated, since phagocytosis does not occur synchronously in all cells and PI3P formation and degradation is a very fast process. Besides, small eGFP-2xFYVE positive compartments could be observed either associated with phagosomes or located in the cytoplasm. These compartments are obviously smaller than the PV indicating the visualization of PI3P on endosomes (Gillooly et al., 2001; Vieira et al., 2002). In addition, the size of these vesicles that is approximately 1 µm resembles the size of macropinocytic vesicles (Conner and Schmid, 2003) and the uptake of small particles or liquids occurs constitutive in cells independent from phagocytosis. To illuminate the role of PI3P in vesicle fusion and compartment maturation of *Leishmania* harboring LAP compartments, PI3P production could be manipulated. The class III PI3K Vps34, that is responsible for PI3P production, can be chemically inhibited by Wortmannin or 3-Methyladenine (Burman and Ktistakis, 2010). Nevertheless, this form of inhibition is unspecific since both inhibitors can also inhibit other class III PI3K or class I PI3K. Alternatively, Vps34 could be knocked down or the Vps34-specific phosphatases Jumpy or MTMR3 could be overexpressed (Vergne and Deretic, 2010) to modulate PI3P production during phagocytosis.

Acidification of *L. major* containing PVs can be assessed by the late endosomal/lysosomal marker proteins LAMP1 or LAMP2. In our study, we used lentiviral vector particles for overexpression of mCherry-conjugated LAMP2 protein. Unfortunately, we were not able to visualize LAMP2 recruitment to the PV in real time 24 h after infection. Most likely, the fluorescent probe is partially separated from the target protein or unstable under acidic conditions resulting in the weak fluorescent signals we observed. An alternative method to account for lysosomal maturation is the lysosomotropic probe Lysotracker, which is suited for live cells and is available in different colors. Furthermore, a mRFP-EGFP-LC3 (Kimura et al., 2007) chimeric protein is available that produces transient green fluorescence if autophagosomes have not fused with lysosomes, but shows a red fluorescence after EGFP

is degraded during acidification whereas mRFP (monomeric red fluorescent protein) is resistant to both acid and lysosomal proteases (Bauckman et al., 2014; Katayama et al., 2011). In 2011, a novel autophagy probe capable of monitoring the autophagy flux was established (Katayama et al., 2011). The coral-derived acid-stable fluorescent protein Keima emits different-colored signals at acidic and neutral pHs and can be visualized in conjunction with other green emitting fluorophores due to the large Stokes shift (Katayama et al., 2011). The time point to measure compartment acidification also has to be figured out in more detail, because in literature one finds different informations. High levels of LAMP1-positive *L. amazonensis* containing macrophages were observed half an hour after phagocytosis and were stable for 48 h (Courret et al., 2002). Another publication could show that *L. infantum chagasi* promastigote PVs can delay acquisition of LAMP1 from 20% at 1 h to 46% by 24 h (Rodríguez et al., 2011). In contrast to that other studies postulate that acidification can be detected during a time period of about 2 h (Florey et al., 2011; Sanjuan et al., 2007) and that autophagosome fusion with a lysosome occurs already few minutes (~10 min) after autophagosome formation (Karanasios et al., 2013).

The identification of further maturation markers and potential LAP specific markers will be facilitated by isolation of PVs containing apoptotic *L. major* promastigotes. In earlier studies, PVs that harbor *Leishmania* parasites were isolated by affinity selection via calnexin, a transmembrane protein that is present at the surface of the PV (Kima and Dunn, 2005). In our study, we successfully isolated *Leishmania* PVs, based on the immuno-magnetic isolation protocol of *Mycobacterium tuberculosis* containing compartments (Steinhäuser et al., 2013). We could demonstrate the enrichment of *Leishmania* proteins as well as a depletion of intracellular (β-Actin) and nuclear proteins (Nucleoporin p62). Nevertheless, it now would be interesting whether LAP maturation markers like PI3P, EEA1, LAMP2, VAMP3, LC3 and other Atg proteins are enriched on isolated compartments. However, mitochondrial proteins (Cox4) in the magnetic fraction indicate contaminations and relatively high protein amounts in the magnetic fraction give a hint that this fraction is still impure. For mass spectrometry analysis it therefore would be reasonable to insert a second purification step. Magnetic labeled parasites could be labeled fluorescently, so that the obtained magnetic fraction subsequently can be purified by fluorescence-activated cell sorting (FACS).

In summary, analyzing the maturation of *L. major* promastigote PVs inside hMDMs, we found that the PV partially gets PI3P and EEA1 positive after early time points of infection. Analysis of late maturation events like lysosomal maturation, so far was not successful using LAMP2-mCherry transferring lentiviral vector particles. Anyway, there exist plenty of alternative methods to assess acidification like Lysotracker, Keima or the tandem protein mRFP-GFP-LC3. The immuno-magnetic isolation protocol established in this thesis has to be improved,

but is a promising tool to identify new and hopefully specific LAP maturation markers by Western Blot or mass spectrometry.

4.3 Concluding remarks

Taken together, we conclude that *L. major* amastigotes enter different compartments in human macrophages as compared to *L. major* promastigotes. Whereas axenic amastigotes end up in interrupted compartments or are even localized in the cytosol (Figure 59), promastigotes enter LC3-positive compartments (Figure 60). We quantified that independent of the viability of the promastigotes 25% to 40% of the compartments get LC3-positive, but that there is significantly less LC3 compartment formation in hMDM II around apoptotic promastigotes compared to hMDM I. Analyzing LC3-positive compartments in more detail using lentiviral overexpression of eGFP-LC3 protein in primary human macrophages and live cell imaging, we come to the conclusion that apoptotic promastigotes are degraded in LC3-positive compartments whereas viable promastigotes are able to get rid of LC3-protein on their PV suggesting a role in parasite survival and/or development (Figure 60).

Furthermore, we demonstrated that viable promastigotes are taken up by human macrophages via the flagellum tip and that apoptotic promastigotes enter the cells with the parasite body first (Figure 60) likely resulting in different LC3-compartment maturation. Based on our findings, that LC3-positive compartments on the ultrastructural level consist of a single-membrane PV and that the protein kinase ULK1, which is involved in autophagy but not in LAP, is dispensable for LC3-compartment formation around *Leishmania* (Figure 60), we conclude that the LAP pathway is involved during *L. major* infection. We could quantify, that between 20% and 30% of *Leishmania* promastigote containing compartments get positive for the early maturation markers PI3P and EEA1 (Figure 60) and that this recruitment is independent from the analyzed human macrophage type (pro- or anti-inflammatory) as wells as from the viability of the promastigotes. The presented data demonstrate that lentiviral based fluorescent real time imaging in combination with HPF and high resolution 3D electron microscopy as well as immuno-magnetic compartment isolation represent powerful techniques (i) to analyze the dynamics of compartment formation around *Leishmania* parasites and (ii) to identify new targets that serve as potential biomarkers or therapeutic candidates. Understanding the dynamics and molecular mechanisms of parasite infection and parasite development in human host cells will contribute to combat and control this neglected but important infectious disease in the future.

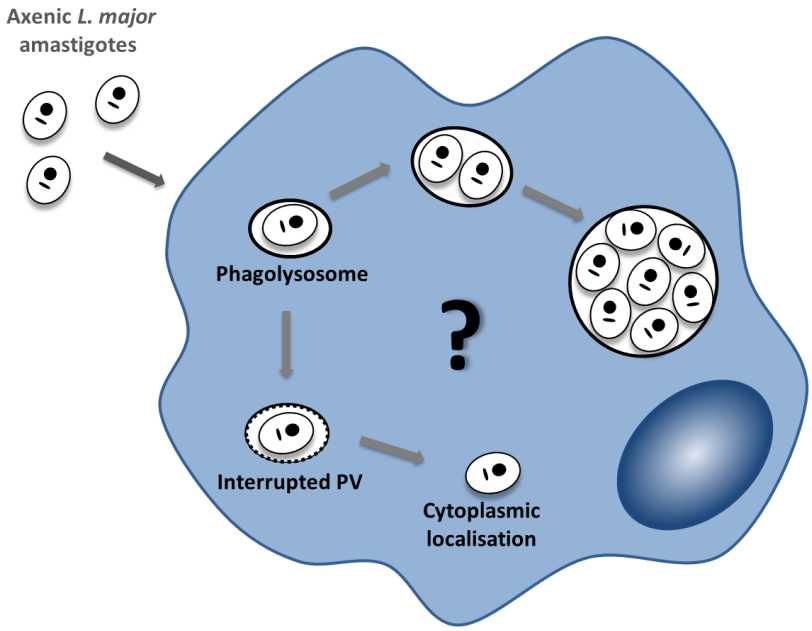

Figure 59: Infection of hMDMs with axenic *L. major* amastigotes. During re-infection of macrophages axenic *L. major* amastigotes enter a phagolysosome. We could demonstrate that some amastigotes are surrounded by a disrupted PV or are localized in the cytosol. Furthermore multiple amastigotes can be found in one large communal PV.

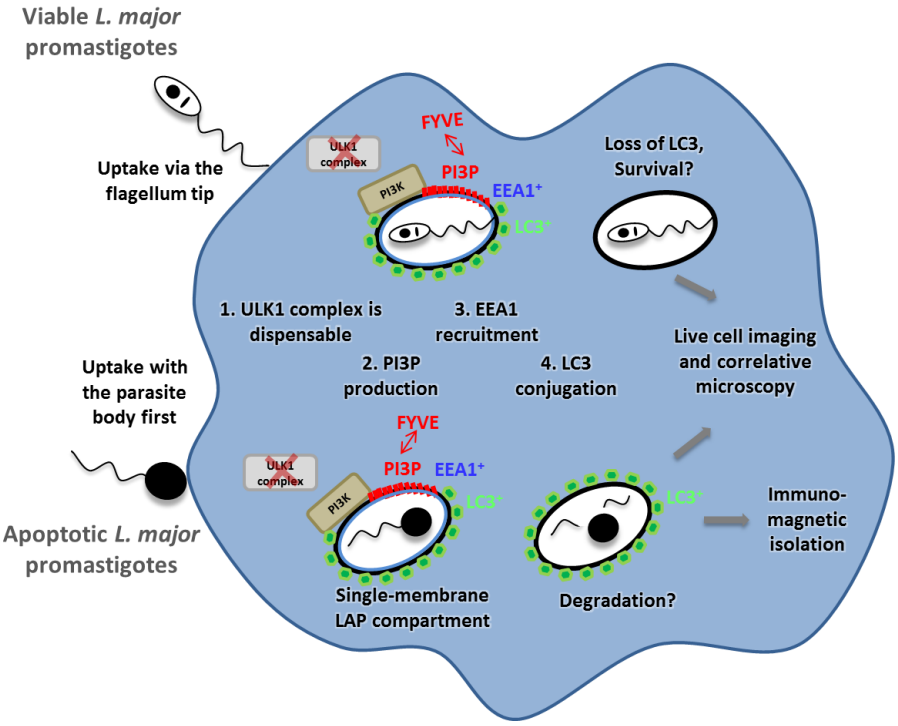

Figure 60: Infection of hMDMs with *L. major* promastigotes. Apoptotic promastigotes enter the macrophage with the parasite body first ending up in a single-membrane LAP compartment that gets positive for PI3P, EEA1 and LC3 finally leading to the degradation of the parasite. The ULK1 complex is dispensable for the formation of the LAP compartment. Viable promastigotes are taken up by the macrophage via the flagellum tip and similar like apoptotic promastigotes end up in a LC3-positive compartment, from which they somehow are able to escape.

5 References

Adams, D.O., and Hamilton, T.A. (1984). The cell biology of macrophage activation. Annu. Rev. Immunol. *2*, 283–318.

Aderem, a, and Underhill, D.M. (1999). Mechanisms of phagocytosis in macrophages. Annu. Rev. Immunol. *17*, 593–623.

Aiken, C. (1997). Pseudotyping human immunodeficiency virus type 1 (HIV-1) by the glycoprotein of vesicular stomatitis virus targets HIV-1 entry to an endocytic pathway and suppresses both the requirement for Nef and the sensitivity to cyclosporin A. J. Virol. *71*, 5871–5877.

Aliança, A., Anjos, K., de Vasconcelos Reis, T., Higino, T., Brelaz-de-Castro, M., Bianco, É., and de Figueiredo, R. (2014). The in Vitro Biological Activity of the Brazilian Brown Seaweed Dictyota mertensii against Leishmania amazonensis. Molecules *19*, 14052–14065.

Alvar, J., Yactayo, S., and Bern, C. (2006). Leishmaniasis and poverty. Trends Parasitol. *22*, 552–557.

Anderson, R.G. (1998). The caveolae membrane system. Annu. Rev. Biochem. *67*, 199–225.

Antoine, J.C., Prina, E., Jouanne, C., and Bongrand, P. (1990). Parasitophorous vacuoles of Leishmania amazonensis-infected macrophages maintain an acidic pH. Infect. Immun. *58*, 779–787.

Badaro, R., Lobo, I., Nakatani, M., Muiños, a, Netto, E.M., Coler, R.N., and Reed, S.G. (2001). Successful use of a defined antigen/GM-CSF adjuvant vaccine to treat mucosal Leishmaniasis refractory to antimony: A case report. Braz. J. Infect. Dis. *5*, 223–232.

Bahr, V., Stierhof, Y.D., Ilg, T., Demar, M., Quinten, M., and Overath, P. (1993). Expression of lipophosphoglycan, high-molecular weight phosphoglycan and glycoprotein 63 in promastigotes and amastigotes of Leishmania mexicana. Mol. Biochem. Parasitol. *58*, 107–122.

Ballou, L.M., and Lin, R.Z. (2008). Rapamycin and mTOR kinase inhibitors. J. Chem. Biol. *1*, 27–36.

Baltimore, D. (1970). RNA-dependent DNA polymerase in virions of RNA tumour viruses. Nature *226*, 1209–1211.

Bank, E. (2012). Leishmania major parasites and their interaction with human macrophages. Dissertation Johannes-Gutenberg University Mainz.

Von Bargen, K., Polidori, M., Becken, U., Huth, G., Prescott, J.F., and Haas, A. (2009). Rhodococcus equi virulence-associated protein A is required for diversion of phagosome biogenesis but not for cytotoxicity. Infect. Immun. *77*, 5676–5681.

Bauckman, K., Owusu-Boaitey, N., and Mysorekar, I. (2014). Selective autophagy: Xenophagy. Methods *75*, 120–127.

Beertsen, W., Willenborg, M., Everts, V., Zirogianni, A., Podschun, R., Schröder, B., Eskelinen, E.-L., and Saftig, P. (2008). Impaired phagosomal maturation in neutrophils leads

to periodontitis in lysosomal-associated membrane protein-2 knockout mice. J. Immunol. *180*, 475–482.

Berger, A., Sommer, A.F.R., Zwarg, J., Hamdorf, M., Welzel, K., Esly, N., Panitz, S., Reuter, A., Ramos, I., Jatiani, A., et al. (2011). SAMHD1-deficient CD14+ cells from individuals with Aicardi-Goutières syndrome are highly susceptible to HIV-1 infection. PLoS Pathog. *7*, 1–12.

Bertani, G. (1951). Studies on lysogenesis. I. The mode of phage liberation by lysogenic Escherichia coli. J. Bacteriol. *62*, 293–300.

Betzig, E., Patterson, G.H., Sougrat, R., Lindwasser, O.W., Olenych, S., Bonifacino, J.S., Davidson, M.W., Lippincott-Schwartz, J., and Hess, H.F. (2006). Imaging intracellular fluorescent proteins at nanometer resolution. Science *313*, 1642–1645.

Bogdan, C., and Röllinghoff, M. (1998). The immune response to Leishmania: Mechanisms of parasite control and evasion. Int. J. Parasitol. *28*, 121–134.

Bogdan, C., Rollinghoff, M., and Solbach, W. (1990). Evasion strategies of Leishmania parasites. Parasitol. Today *6*, 183–187.

Brittingham, A., and Mosser, D. (1996). Exploitation of the complement system by Leishmania promastigotes. Parasitol. Today *12*, 444–447.

Brittingham, A., Morrison, C.J., McMaster, W.R., McGwire, B.S., Chang, K.P., and Mosser, D.M. (1995). Role of the Leishmania surface protease gp63 in complement fixation, cell adhesion, and resistance to complement-mediated lysis. J. Immunol. *155*, 3102–3111.

Buechler, C., Ritter, M., Orsó, E., Langmann, T., Klucken, J., and Schmitz, G. (2000). Regulation of scavenger receptor CD163 expression in human monocytes and macrophages by pro- and antiinflammatory stimuli. J. Leukoc. Biol. *67*, 97–103.

Bumb, R.A., Prasad, N., Khandelwal, K., Aara, N., Mehta, R.D., Ghiya, B.C., Salotra, P., Wei, L., Peters, S., and Satoskar, A.R. (2013). Long-term efficacy of single-dose radiofrequency-induced heat therapy vs. intralesional antimonials for cutaneous leishmaniasis in India. Br. J. Dermatol. *168*, 1114–1119.

Burman, C., and Ktistakis, N.T. (2010). Regulation of autophagy by phosphatidylinositol 3-phosphate. FEBS Lett. *584*, 1302–1312.

Campoy, E.M., Mansilla, M.E., and Colombo, M.I. (2013). Endocytic SNAREs are involved in optimal Coxiella burnetii vacuole development. Cell. Microbiol. *15*, 922–941.

Cassol, E., Cassetta, L., Alfano, M., and Poli, G. (2010). Macrophage polarization and HIV-1 infection. J. Leukoc. Biol. *87*, 599–608.

Chakraborty, P., Sturgill-Koszycki, S., and Russell, D.G. (1994). Isolation and characterization of pathogen-containing phagosomes. Methods Cell Biol. *45*, 261–276.

Chan, J., Fujiwara, T., Brennan, P., McNeil, M., Turco, S.J., Sibille, J.C., Snapper, M., Aisen, P., and Bloom, B.R. (1989). Microbial glycolipids: possible virulence factors that scavenge oxygen radicals. Proc. Natl. Acad. Sci. U. S. A. *86*, 2453–2457.

Chang, K.P. (1979). Leishmania donovani: promastigote--macrophage surface interactions in vitro. Exp. Parasitol. *48*, 175–189.

Chang, K.P., and Dwyer, D.M. (1978). Leishmania donovani. Hamster macrophage interactions in vitro: cell entry, intracellular survival, and multiplication of amastigotes. J. Exp. Med. *147*, 515–530.

Chimini, G., and Chavrier, P. (2000). Function of Rho family proteins in actin dynamics during phagocytosis and engulfment. Nat. Cell Biol. *2*, E191–E196.

Chresta, C.M., Davies, B.R., Hickson, I., Harding, T., Cosulich, S., Critchlow, S.E., Vincent, J.P., Ellston, R., Jones, D., Sini, P., et al. (2010). AZD8055 is a potent, selective, and orally bioavailable ATP-competitive mammalian target of rapamycin kinase inhibitor with in vitro and in vivo antitumor activity. Cancer Res. *70*, 288–298.

Christoforidis, S., McBride, H.M., Burgoyne, R.D., and Zerial, M. (1999). The Rab5 effector EEA1 is a core component of endosome docking. Nature *397*, 621–625.

Conner, S.D., and Schmid, S.L. (2003). Regulated portals of entry into the cell. Nature *422*, 37–44.

Convit, J., Ulrich, M., Polegre, M.A., Avila, A., Rodríguez, N., Mazzedo, M.I., and Blanco, B. (2004). Therapy of Venezuelan patients with severe mucocutaneous or early lesions of diffuse cutaneous leishmaniasis with a vaccine containing pasteurized Leishmania promastigotes and Bacillus Calmette-Guerin - Preliminary report. Mem. Inst. Oswaldo Cruz *99*, 57–62.

Cottinet, S.L., Bergemer-Fouquet, A.M., Toutain, A., Sabourdy, F., Maakaroun-Vermesse, Z., Levade, T., Chantepie, A., and Labarthe, F. (2011). Danon disease: Intrafamilial phenotypic variability related to a novel LAMP-2 mutation. J. Inherit. Metab. Dis. *34*, 515–522.

Courret, N., Fréhel, C., Gouhier, N., Pouchelet, M., Prina, E., Roux, P., and Antoine, J.-C. (2002). Biogenesis of Leishmania-harbouring parasitophorous vacuoles following phagocytosis of the metacyclic promastigote or amastigote stages of the parasites. J. Cell Sci. *115*, 2303–2316.

Crauwels, P., Bohn, R., Thomas, M., Gottwalt, S., Jäckel, F., Krämer, S., Bank, E., Tenzer, S., Walther, P., Bastian, M., et al. (2015). Apoptotic-like Leishmania exploit the host´s autophagy machinery to reduce T-cell mediated parasite elimination. Autophagy *in press*.

Cuervo, A.M. (2010). The plasma membrane brings autophagosomes to life. Nat. Cell Biol. *12*, 735–737.

Danna, K., and Nathans, D. (1971). Specific cleavage of simian virus 40 DNA by restriction endonuclease of Hemophilus influenzae. Proc. Natl. Acad. Sci. U. S. A. *68*, 2913–2917.

Dermine, J.F., Scianimanico, S., Privé, C., Descoteaux, A., and Desjardins, M. (2000). Leishmania promastigotes require lipophosphoglycan to actively modulate the fusion properties of phagosomes at an early step of phagocytosis. Cell. Microbiol. *2*, 115–126.

Desjardins, M., and Descoteaux, a (1997). Inhibition of phagolysosomal biogenesis by the Leishmania lipophosphoglycan. J. Exp. Med. *185*, 2061–2068.

Dunn, J. (1990). Studies on the mechanisms of autophagy: formation of the vacuole. J. Cell Biol. *110*, 1923–1933.

Dunn, W.A. (1994). Autophagy and related mechanisms of lysosome-mediated protein degradation. Trends Cell Biol. *4*, 139–143.

Ellson, C.D., Anderson, K.E., Morgan, G., Chilvers, E.R., Lipp, P., Stephens, L.R., and Hawkins, P.T. (2001). Phosphatidylinositol 3-phosphate is generated in phagosomal membranes. Curr. Biol. *11*, 1631–1635.

Fader, C.M., Sánchez, D.G., Mestre, M.B., and Colombo, M.I. (2009). TI-VAMP/VAMP7 and VAMP3/cellubrevin: two v-SNARE proteins involved in specific steps of the autophagy/multivesicular body pathways. Biochim. Biophys. Acta - Mol. Cell Res. *1793*, 1901–1916.

Fletcher, T.M., Brichacek, B., Sharova, N., Newman, M. a, Stivahtis, G., Sharp, P.M., Emerman, M., Hahn, B.H., and Stevenson, M. (1996). Nuclear import and cell cycle arrest functions of the HIV-1 Vpr protein are encoded by two separate genes in HIV-2/SIV(SM). EMBO J. *15*, 6155–6165.

Florentino, P.T. V, Real, F., Bonfim-Melo, A., Orikaza, C.M., Ferreira, E.R., Pessoa, C.C., Lima, B.R., Sasso, G.R.S., and Mortara, R.A. (2014). An historical perspective on how advances in microscopic imaging contributed to understanding the leishmania Spp. and trypanosoma cruzi host-parasite relationship. Biomed Res. Int. *2014*, 565291.

Florey, O., and Overholtzer, M. (2012). Autophagy proteins in macroendocytic engulfment. Trends Cell Biol. *22*, 374–380.

Florey, O., Kim, S.E., Sandoval, C.P., Haynes, C.M., and Overholtzer, M. (2011). Autophagy machinery mediates macroendocytic processing and entotic cell death by targeting single membranes. Nat. Cell Biol. *13*, 1335–1343.

Forestier, C.L., MacHu, C., Loussert, C., Pescher, P., and Späth, G.F. (2011). Imaging host cell-leishmania interaction dynamics implicates parasite motility, lysosome recruitment, and host cell wounding in the infection process. Cell Host Microbe *9*, 319–330.

Fratti, R. a., Chua, J., and Deretic, V. (2002). Cellubrevin alterations and Mycobacterium tuberculosis phagosome maturation arrest. J. Biol. Chem. *277*, 17320–17326.

Fujita, N., Itoh, T., Omori, H., Fukuda, M., Noda, T., and Yoshimori, T. (2008). The Atg16L complex specifies the site of LC3 lipidation for membrane biogenesis in autophagy. Mol. Biol. Cell *19*, 2092–2100.

Fultz, P.N., McClure, H.M., Anderson, D.C., and Switzer, W.M. (1989). Identification and biologic characterization of an acutely lethal variant of simian immunodeficiency virus from sooty mangabeys (SIV/SMM). AIDS Res. Hum. Retroviruses *5*, 397–409.

Gaullier, J.M., Simonsen, a, D'Arrigo, a, Bremnes, B., Stenmark, H., and Aasland, R. (1998). FYVE fingers bind PtdIns(3)P. Nature *394*, 432–433.

Ge, L., and Schekman, R. (2014). The ER-Golgi intermediate compartment feeds the phagophore membrane. Autophagy *10*, 170–172.

Giannini, M.S. (1974). Effects of promastigote growth phase, frequency of subculture, and host age on promastigote-initiated infections with Leishmania donovani in the golden hamster. J. Protozool. *21*, 521–527.

Giepmans, B.N.G. (2008). Bridging fluorescence microscopy and electron microscopy. Histochem. Cell Biol. *130*, 211–217.

Gillooly, D.J., Morrow, I.C., Lindsay, M., Gould, R., Bryant, N.J., Gaullier, J.M., Parton, R.G., and Stenmark, H. (2000). Localization of phosphatidylinositol 3-phosphate in yeast and mammalian cells. EMBO J. *19*, 4577–4588.

Gillooly, D.J., Simonsen, A., and Stenmark, H. (2001). Cellular functions of phosphatidylinositol 3-phosphate and FYVE domain proteins. Biochem. J. *355*, 249–258.

Girolami, G. (2012). Osmium weighs in. Nat. Chem. *4*, 954–954.

Glaser, T. a, Moody, S.F., Handman, E., Bacic, a, and Spithill, T.W. (1991). An antigenically distinct lipophosphoglycan on amastigotes of Leishmania major. Mol. Biochem. Parasitol. *45*, 337–344.

Global Medicine (2015). http://globalmedicine.nl/issues/issue-6/leishmaniasis/. accessed on 15/01/2015.

Goerdt, S., Politz, O., Schledzewski, K., Birk, R., Gratchev, a, Guillot, P., Hakiy, N., Klemke, C.D., Dippel, E., Kodelja, V., et al. (1999). Alternative versus classical activation of macrophages. Pathobiology *67*, 222–226.

Gomes, L.C., and Dikic, I. (2014). Autophagy in antimicrobial immunity. Mol. Cell *54*, 224–233.

Goodridge, H.S., Wolf, A.J., and Underhill, D.M. (2009). Beta-glucan recognition by the innate immune system. Immunol. Rev. *230*, 38–50.

Gordon, S., and Taylor, P.R. (2005). Monocyte and macrophage heterogeneity. Nat. Rev. Immunol. *5*, 953–964.

Goto, H., and Lauletta Lindoso, J.A. (2012). Cutaneous and Mucocutaneous Leishmaniasis. Infect. Dis. Clin. North Am. *26*, 293–307.

Gottwalt, S. (2011). Apoptotische promastigote Leishmanien gelangen beim Eintritt in Makrophagen in ein Autophagie-Kompartiment. Dissertation Universität Ulm.

Granger, B.L., Green, S.A., Gabel, C.A., Howe, C.L., Mellman, I., and Helenius, A. (1990). Characterization and cloning of lgp110, a lysosomal membrane glycoprotein from mouse and rat cells. J. Biol. Chem. *265*, 12036–12043.

Griffith, F. (1928). The Significance of Pneumococcal Types. Journ. Hyg. *27*, 113–159.

Gupta, N., Goyal, N., and Rastogi, A.K. (2001). In vitro cultivation and characterization of axenic amastigotes of Leishmania. Trends Parasitol. *17*, 150–153.

Gustafsson, M.G. (2000). Surpassing the lateral resolution limit by a factor of two using structured illumination microscopy. J. Microsc. *198*, 82–87.

Gutierrez, M.G., Master, S.S., Singh, S.B., Taylor, G.A., Colombo, M.I., and Deretic, V. (2004). Autophagy is a defense mechanism inhibiting BCG and Mycobacterium tuberculosis survival in infected macrophages. Cell *119*, 753–766.

Guy, R.A., and Belosevic, M. (1993). Comparison of receptors required for entry of Leishmania major amastigotes into macrophages. Infect. Immun. *61*, 1553–1558.

Hailey, D.W., Rambold, A.S., Satpute-Krishnan, P., Mitra, K., Sougrat, R., Kim, P.K., and Lippincott-Schwartz, J. (2010). Mitochondria Supply Membranes for Autophagosome Biogenesis during Starvation. Cell *141*, 656–667.

Hara, T., Takamura, A., Kishi, C., Iemura, S.I., Natsume, T., Guan, J.L., and Mizushima, N. (2008). FIP200, a ULK-interacting protein, is required for autophagosome formation in mammalian cells. J. Cell Biol. *181*, 497–510.

Hawes, P., Netherton, C.L., Mueller, M., Wileman, T., and Monaghan, P. (2007). Rapid freeze-substitution preserves membranes in high-pressure frozen tissue culture cells. J. Microsc. *226*, 182–189.

Henault, J., Martinez, J., Riggs, J.M., Tian, J., Mehta, P., Clarke, L., Sasai, M., Latz, E., Brinkmann, M.M., Iwasaki, A., et al. (2012). Noncanonical Autophagy Is Required for Type I Interferon Secretion in Response to DNA-Immune Complexes. Immunity *37*, 986–997.

Hirsch, V.M., Sharkey, M.E., Brown, C.R., Brichacek, B., Goldstein, S., Wakefield, J., Byrum, R., Elkins, W.R., Hahn, B.H., Lifson, J.D., et al. (1998). Vpx is required for dissemination and pathogenesis of SIV(SM) PBj: evidence of macrophage-dependent viral amplification. Nat. Med. *4*, 1401–1408.

Hlavaty, J., Schittmayer, M., Stracke, A., Jandl, G., Knapp, E., Felber, B.K., Salmons, B., Günzburg, W.H., and Renner, M. (2005). Effect of posttranscriptional regulatory elements on transgene expression and virus production in the context of retrovirus vectors. Virology *341*, 1–11.

Höhn, K., Sailer, M., Wang, L., Lorenz, M., E. Schneider, M., and Walther, P. (2011). Preparation of cryofixed cells for improved 3D ultrastructure with scanning transmission electron tomography. Histochem. Cell Biol. *135*, 1–9.

Holness, C.L., and Simmons, D.L. (1993). Molecular cloning of CD68, a human macrophage marker related to lysosomal glycoproteins. Blood *81*, 1607–1613.

Hosokawa, N., Sasaki, T., Iemura, S.I., Natsume, T., Hara, T., and Mizushima, N. (2009). Atg101, a novel mammalian autophagy protein interacting with Atg13. Autophagy *5*, 973–979.

Hrecka, K., Hao, C., Gierszewska, M., Swanson, S.K., Kesik-Brodacka, M., Srivastava, S., Florens, L., Washburn, M.P., and Skowronski, J. (2011). Vpx relieves inhibition of HIV-1 infection of macrophages mediated by the SAMHD1 protein. Nature *474*, 658–661.

Huang, J., and Klionsky, D.J. (2007). Autophagy and human disease. Cell Cycle *6*, 1837–1849.

Huang, J., Canadien, V., Lam, G.Y., Steinberg, B.E., Dinauer, M.C., Magalhaes, M. a O., Glogauer, M., Grinstein, S., and Brumell, J.H. (2009). Activation of antibacterial autophagy by NADPH oxidases. Proc. Natl. Acad. Sci. U. S. A. *106*, 6226–6231.

Hunziker, W., and Geuze, H.J. (1996). Intracellular trafficking of lysosomal membrane proteins. Bioessays *18*, 379–389.

Huynh, M.L.N., Fadok, V.A., and Henson, P.M. (2002). Phosphatidylserine-dependent ingestion of apoptotic cells promotes TGF-beta1 secretion and the resolution of inflammation. J. Clin. Invest. *109*, 41–50.

Jäger, S., Bucci, C., Tanida, I., Ueno, T., Kominami, E., Saftig, P., and Eskelinen, E.-L. (2004). Role for Rab7 in maturation of late autophagic vacuoles. J. Cell Sci. *117*, 4837–4848.

Jamur, M.C., and Oliver, C. (2010). Permeabilization of cell membranes. Methods Mol. Biol. *588*, 63–66.

Janeway, C.A. (1992). The immune system evolved to discriminate infectious nonself from noninfectious self. Immunol. Today *13*, 11–16.

Jung, C.H., Jun, C.B., Ro, S.-H., Kim, Y.-M., Otto, N.M., Cao, J., Kundu, M., and Kim, D.-H. (2009). ULK-Atg13-FIP200 complexes mediate mTOR signaling to the autophagy machinery. Mol. Biol. Cell *20*, 1992–2003.

Kabeya, Y., Mizushima, N., Ueno, T., Yamamoto, A., Kirisako, T., Noda, T., Kominami, E., Ohsumi, Y., and Yoshimori, T. (2003). Erratum: LC3, a mammalian homolog of yeast Apg8p, is localized in autophagosome membranes after processing. EMBO J. *22*, 4577.

Kageyama, S., Omori, H., Saitoh, T., Sone, T., Guan, J.-L., Akira, S., Imamoto, F., Noda, T., and Yoshimori, T. (2011). The LC3 recruitment mechanism is separate from Atg9L1-dependent membrane formation in the autophagic response against Salmonella. Mol. Biol. Cell *22*, 2290–2300.

Karanasios, E., and Ktistakis, N.T. (2014). Live-cell imaging for the assessment of the dynamics of autophagosome formation: Focus on early steps. Methods *75*, 54–60.

Karanasios, E., Stapleton, E., Walker, S. a, Manifava, M., and Ktistakis, N.T. (2013). Live cell imaging of early autophagy events: omegasomes and beyond. J. Vis. Exp. 1–9.

Katayama, H., Kogure, T., Mizushima, N., Yoshimori, T., and Miyawaki, A. (2011). A sensitive and quantitative technique for detecting autophagic events based on lysosomal delivery. Chem. Biol. *18*, 1042–1052.

Kaye, P., and Scott, P. (2011). Leishmaniasis: complexity at the host-pathogen interface. Nat. Rev. Microbiol. *9*, 604–615.

Kima, P.E., and Dunn, W. (2005). Exploiting calnexin expression on phagosomes to isolate Leishmania parasitophorous vacuoles. Microb. Pathog. *38*, 139–145.

Kimura, S., Noda, T., and Yoshimori, T. (2007). Dissection of the autophagosome maturation process by a novel reporter protein, tandem fluorescent-tagged LC3. Autophagy *3*, 452–460.

Kiss, A.L. (2012). Caveolae and the regulation of endocytosis. Adv. Exp. Med. Biol. *729*, 14–28.

Klar, T. a, Jakobs, S., Dyba, M., Egner, a, and Hell, S.W. (2000). Fluorescence microscopy with diffraction resolution barrier broken by stimulated emission. Proc. Natl. Acad. Sci. U. S. A. *97*, 8206–8210.

Klionsky, D.J. (2008). Autophagy revisited: A conversation with Christian de Duve. Autophagy *4*, 740–743.

Kloke, B.P. (2009). Development of SIVsmmPBj- and HIV-2-derived lentiviral vector systems to correct gp91 phox gene defects in monocytes. Dissertation Johann Wolfgang Goethe-Universität.

Kloke, B.P., Schüle, S., Mühlebach, M.D., Wolfrum, N., Cichutek, K., and Schweizer, M. (2010). Functional HIV-2- and SIVsmmPBj- derived lentiviral vectors generated by a novel polymerase chain reaction-based approach. J. Gene Med. *12*, 446–452.

Kremer, J.R., Mastronarde, D.N., and McIntosh, J.R. (1996). Computer visualization of three-dimensional image data using IMOD. J. Struct. Biol. *116*, 71–76.

Kumar, P., Pai, K., Pandey, H.P., and Sundar, S. (2002). NADH-oxidase, NADPH-oxidase and myeloperoxidase activity of visceral leishmaniasis patients. J. Med. Microbiol. *51*, 832–836.

Kutateladze, T.G. (2006). Phosphatidylinositol 3-phosphate recognition and membrane docking by the FYVE domain. Biochim. Biophys. Acta - Mol. Cell Biol. Lipids *1761*, 868–877.

Laguette, N., Sobhian, B., Casartelli, N., Ringeard, M., Chable-Bessia, C., Ségéral, E., Yatim, A., Emiliani, S., Schwartz, O., and Benkirane, M. (2011). SAMHD1 is the dendritic- and myeloid-cell-specific HIV-1 restriction factor counteracted by Vpx. Nature *474*, 654–657.

Lai, S., and Devenish, R.J. (2012). LC3-Associated Phagocytosis (LAP): Connections with Host Autophagy. Cells *1*, 396–408.

Lakadamyali, M. (2014). Super-resolution microscopy: Going live and going fast. ChemPhysChem *15*, 630–636.

Lang, T., de Chastellier, C., Frehel, C., Hellio, R., Metezeau, P., Leao, S.D.S., and Antoine, J.C. (1994a). Distribution of MHC class I and of MHC class II molecules in macrophages infected with Leishmania amazonensis. J. Cell Sci. *107*, 69–82.

Lang, T., Hellio, R., Kaye, P.M., and Antoine, J.C. (1994b). Leishmania donovani-infected macrophages: characterization of the parasitophorous vacuole and potential role of this organelle in antigen presentation. J. Cell Sci. *107*, 2137–2150.

Laskay, T., van Zandbergen, G., and Solbach, W. (2003). Neutrophil granulocytes - Trojan horses for Leishmania major and other intracellular microbes? Trends Microbiol. *11*, 210–214.

Lauer, S., VanWye, J., Harrison, T., McManus, H., Samuel, B.U., Hiller, N.L., Mohandas, N., and Haldar, K. (2000). Vacuolar uptake of host components, and a role for cholesterol and sphingomyelin in malarial infection. EMBO J. *19*, 3556–3564.

Laufs, H., Müller, K., Fleischer, J., Jahnke, N., Jensenius, J.C., Solbach, W., Reiling, N., and Laskay, T. (2002). Intracellular Survival of Leishmania major in Neutrophil Granulocytes after Uptake in the Absence of Heat-Labile Serum Factors Intracellular Survival of Leishmania major in Neutrophil Granulocytes after Uptake in the Absence of Heat-Labile Serum Factors. Society *70*, 826–835.

Lee, B.-Y., Jethwaney, D., Schilling, B., Clemens, D.L., Gibson, B.W., and Horwitz, M.A. (2010). The Mycobacterium bovis bacille Calmette-Guerin phagosome proteome. Mol. Cell. Proteomics *9*, 32–53.

Leenen, P.J.M., De Bruijn, M.F.T.R., Voerman, J.S.A., Campbell, P.A., and Van Ewijk, W. (1994). Markers of mouse macrophage development detected by monoclonal antibodies. J. Immunol. Methods *174*, 5–19.

Leishman, W.B. (1901). The Application of Romanowsky's Stain in Malaria. Br. Med. J. *1*, 635–637.

Levine, B. (2005). Eating oneself and uninvited guests: Autophagy-related pathways in cellular defense. Cell *120*, 159–162.

Levine, B., and Deretic, V. (2007). Unveiling the roles of autophagy in innate and adaptive immunity. Nat. Rev. Immunol. *7*, 767–777.

Lewis, D.H., and Peters, W. (1977). The resistance of intracellular Leishmania parasites to digestion by lysosomal enzymes. Ann. Trop. Med. Parasitol. *71*, 295–312.

Liew, F.Y., Millott, S., Parkinson, C., Palmer, R.M., and Moncada, S. (1990). Macrophage killing of Leishmania parasite in vivo is mediated by nitric oxide from L-arginine. J. Immunol. *144*, 4794–4797.

Ligeon, L., Moreau, K., Barois, N., Bongiovanni, A., Lacorre, D., Werkmeister, E., Proux-Gillardeaux, V., Galli, T., and Lafont, F. (2014). Role of VAMP3 and VAMP7 in the commitment of Yersinia pseudotuberculosis to LC3-associated pathways involving single- or double-membrane vacuoles. *10*, 1588–1602.

Lippincott-Schwartz, J. (2011). Emerging in vivo analyses of cell function using fluorescence imaging. Annu. Rev. Biochem. *80*, 327–332.

Livak, K.J., and Schmittgen, T.D. (2001). Analysis of relative gene expression data using real-time quantitative PCR and the 2(-Delta Delta C(T)) Method. Methods *25*, 402–408.

Long, K., Mohan, C., Anderl, J., Huryn-Selvar, K., Liu, H., Su, K., Santos, M., Hsu, M., Armstrong, L., and Ma, J. (2015). Analysis of autophagosome formation using lentiviral biosensors for live fluorescent cellular imaging. Methods Mol Biol. 157–169.

Lukacs, G.L., Rotstein, O.D., and Grinstein, S. (1990). Phagosomal acidification is mediated by a vacuolar-type H+-ATPase in murine macrophages. J. Biol. Chem. *265*, 21099–21107.

Lukinavičius, G., Reymond, L., D'Este, E., Masharina, A., Göttfert, F., Ta, H., Güther, A., Fournier, M., Rizzo, S., Waldmann, H., et al. (2014). Fluorogenic probes for live-cell imaging of the cytoskeleton. Nat. Methods *11*, 731–733.

M. Sandbank (1976). Cutaneous leishmaniasis. Ultrastructural study of 3 cases. Arch Dermatol Res *257*, 195–201.

Ma, J., Becker, C., Reyes, C., and Underhill, D.M. (2014). Cutting edge: FYCO1 recruitment to dectin-1 phagosomes is accelerated by light chain 3 protein and regulates phagosome maturation and reactive oxygen production. J. Immunol. *192*, 1356–1360.

Mansour, M.K., Tam, J.M., Khan, N.S., Seward, M., Davids, P.J., Puranam, S., Sokolovska, A., Sykes, D.B., Dagher, Z., Becker, C., et al. (2013). Dectin-1 activation controls maturation of beta-1,3-glucan-containing phagosomes. J. Biol. Chem. *288*, 16043–16054.

Mantovani, A., Sica, A., Sozzani, S., Allavena, P., Vecchi, A., and Locati, M. (2004). The chemokine system in diverse forms of macrophage activation and polarization. Trends Immunol. *25*, 677–686.

Martinez, F.O., Helming, L., and Gordon, S. (2009). Alternative activation of macrophages: an immunologic functional perspective. Annu. Rev. Immunol. *27*, 451–483.

Martinez, J., Almendinger, J., Oberst, A., Ness, R., Dillon, C.P., Fitzgerald, P., Hengartner, M.O., and Green, D.R. (2011). Microtubule-associated protein 1 light chain 3 alpha (LC3)-associated phagocytosis is required for the efficient clearance of dead cells. Proc. Natl. Acad. Sci. *108*, 17396–17401.

Matheoud, D., Moradin, N., Bellemare-Pelletier, A., Shio, M.T., Hong, W.J., Olivier, M., Gagnon, É., Desjardins, M., and Descoteaux, A. (2013). Leishmania evades host immunity by inhibiting antigen cross-presentation through direct cleavage of the SNARE VAMP8. Cell Host Microbe *14*, 15–25.

McConville, M.J., and Blackwell, J.M. (1991). Developmental changes in the glycosylated phosphatidylinositols of Leishmania donovani. Characterization of the promastigote and amastigote glycolipids. J. Biol. Chem. *266*, 15170–15179.

McDonald, K.L. (2009). A review of high-pressure freezing preparation techniques for correlative light and electron microscopy of the same cells and tissues. J. Microsc. *235*, 273–281.

McGwire, B.S., and Satoskar, A.R. (2014). Leishmaniasis: clinical syndromes and treatment. QJM *107*, 7–14.

Meek, K.M., and Weiss, J.B. (1979). Differential fixation of poly(L-arginine) and poly(L-lysine) by tannic acid and its application to the fixation of collagen in electron microscopy. Biochim. Biophys. Acta *587*, 112–120.

Mehta, P., Henault, J., Kolbeck, R., and Sanjuan, M.A. (2014). Noncanonical autophagy: One small step for LC3, one giant leap for immunity. Curr. Opin. Immunol. *26*, 69–75.

Menck, K., Behme, D., Pantke, M., Reiling, N., Binder, C., Pukrop, T., and Klemm, F. (2014). Isolation of Human Monocytes by Double Gradient Centrifugation and Their Differentiation to Macrophages in Teflon-coated Cell Culture Bags. J. Vis. Exp. *9*, e51554.

Mills, C.D., Kincaid, K., Alt, J.M., Heilman, M.J., and Hill, A.M. (2000). M-1/M-2 macrophages and the Th1/Th2 paradigm. J. Immunol. *164*, 6166–6173.

Misra, S., and Hurley, J.H. (1999). Crystal structure of a phosphatidylinositol 3-phosphate-specific membrane-targeting motif, the FYVE domain of Vps27p. Cell *97*, 657–666.

Mißlitz, A., Mottram, J.C., Overath, P., and Aebischer, T. (2000). Targeted integration into a rRNA locus results in uniform and high level expression of transgenes in Leishmania amastigotes. Mol. Biochem. Parasitol. *107*, 251–261.

Miyoshi, H., Blömer, U., Takahashi, M., Gage, F.H., and Verma, I.M. (1998). Development of a self-inactivating lentivirus vector. J. Virol. *72*, 8150–8157.

Mizushima, N., and Levine, B. (2010). Autophagy in mammalian development and differentiation. Nat. Cell Biol. *12*, 823–830.

Mizushima, N., Yamamoto, A., Hatano, M., Kobayashi, Y., Kabey, Y., Suzuki, K., Tokuhis, T., Ohsumi, Y., and Yoshimori, T. (2001). Dissection of autophagosome formation using Apg5-deficient mouse embryonic stem cells. J. Cell Biol. *152*, 657–667.

Moestrup, S.K., and Møller, H.J. (2004). CD163: a regulated hemoglobin scavenger receptor with a role in the anti-inflammatory response. Ann. Med. *36*, 347–354.

Mosser, D.M., and Edwards, J.P. (2008). Exploring the full spectrum of macrophage activation. Nat. Rev. Immunol. *8*, 958–969.

Mu, F.T., Callaghan, J.M., Steele-Mortimer, O., Stenmark, H., Parton, R.G., Campbell, P.L., McCluskey, J., Yeo, J.P., Tock, E.P.C., and Toh, B.H. (1995). EEA1, an early endosome-associated protein: EEA1 is a conserved α-helical peripheral membrane protein flanked by cysteine “fingers” and contains a calmodulin-binding IQ motif. J. Biol. Chem. *270*, 13503–13511.

Mühlebach, M.D., Wolfrum, N., Schüle, S., Tschulena, U., Sanzenbacher, R., Flory, E., Cichutek, K., and Schweizer, M. (2005). Stable transduction of primary human monocytes by simian lentiviral vector PBj. Mol. Ther. *12*, 1206–1216.

Naderer, T., Vince, J.E., and McConville, M.J. (2004). Surface determinants of Leishmania parasites and their role in infectivity in the mammalian host. Curr. Mol. Med. *4*, 649–665.

Nakagawa, I., Amano, A., Mizushima, N., Yamamoto, A., Yamaguchi, H., Kamimoto, T., Nara, A., Funao, J., Nakata, M., Tsuda, K., et al. (2004). Autophagy defends cells against invading group A Streptococcus. Science *306*, 1037–1040.

Naldini, L., Blömer, U., Gallay, P., Ory, D., Mulligan, R., Gage, F.H., Verma, I.M., and Trono, D. (1996). In vivo gene delivery and stable transduction of nondividing cells by a lentiviral vector. Science *272*, 263–267.

Nathan, C.F. (1987). Secretory products of macrophage. J Clin Invest *79*, 319–326.

Negera, E., Gadisa, E., Hussein, J., Engers, H., Kuru, T., Gedamu, L., and Aseffa, A. (2012). Treatment response of cutaneous leishmaniasis due to Leishmania aethiopica to cryotherapy and generic sodium stibogluconate from patients in Silti, Ethiopia. Trans. R. Soc. Trop. Med. Hyg. *106*, 496–503.

Nichols, B. (2003). Caveosomes and endocytosis of lipid rafts. J. Cell Sci. *116*, 4707–4714.

Ogawa, M., Yoshimori, T., Suzuki, T., Sagara, H., Mizushima, N., and Sasakawa, C. (2005). Escape of intracellular Shigella from autophagy. Science *307*, 727–731.

Onofre, G., Kolácková, M., Jankovicová, K., and Krejsek, J. (2009). Scavenger receptor CD163 and its biological functions. Acta Medica (Hradec Kralove) *52*, 57–61.

Owen, D.J. (2004). Linking endocytic cargo to clathrin: structural and functional insights into coated vesicle formation. Biochem. Soc. Trans. *32*, 1–14.

Patki, V., Virbasius, J., Lane, W.S., Toh, B.H., Shpetner, H.S., and Corvera, S. (1997). Identification of an early endosomal protein regulated by phosphatidylinositol 3-kinase. Proc. Natl. Acad. Sci. U. S. A. *94*, 7326–7330.

Pearson, R.D., Sullivan, J. a., Roberts, D., Romito, R., and Mandell, G.L. (1983). Interaction of Leishmania donovani promastigotes with human phagocytes. Infect. Immun. *40*, 411–416.

Peters, N.C., Egen, J.G., Secundino, N., Debrabant, A., Kamhawi, S., Lawyer, P., Fay, M.P., Germain, R.N., and Sacks, D. (2008). In vivo imaging reveals an essential role for neutrophilis in Leishmaniasis transmitted by sand flies. Science (80-.). *321*, 970–974.

Pheiffer, B.H., and Zimmerman, S.B. (1983). Polymer-stimulated ligation: Enhanced blunt- or cohesive-end ligation of DNA or deoxyribooligonudcleotides by T4 DNA ugase in polymer solutions. Nucleic Acids Res. *11*, 7853–7871.

Pimenta, P.F.P., Saraiva, E.M.B., and Sacks, D.L. (1991). The comparative fine structure and surface glycoconjugate expression of three life stages of Leishmania major. Exp. Parasitol. *72*, 191–204.

Pinheiro, R.O., Nunes, M.P., Pinheiro, C.S., D'Avila, H., Bozza, P.T., Takiya, C.M., Côrte-Real, S., Freire-de-Lima, C.G., and DosReis, G.A. (2009). Induction of autophagy correlates with increased parasite load of Leishmania amazonensis in BALB/c but not C57BL/6 macrophages. Microbes Infect. *11*, 181–190.

Prina, E., Antoine, J.C., Wiederanders, B., and Kirschke, H. (1990). Localization and activity of various lysosomal proteases in Leishmania amazonensis-infected macrophages. Infect. Immun. *58*, 1730–1737.

Proudfoot, L., Nikolaev, A. V, Feng, G.J., Wei, W.Q., Ferguson, M.A., Brimacombe, J.S., and Liew, F.Y. (1996). Regulation of the expression of nitric oxide synthase and leishmanicidal activity by glycoconjugates of Leishmania lipophosphoglycan in murine macrophages. Proc. Natl. Acad. Sci. U. S. A. *93*, 10984–10989.

Puri, C., Renna, M., Bento, C.F., Moreau, K., and Rubinsztein, D.C. (2014). ATG16L1 meets ATG9 in recycling endosomes additional roles for the plasma membrane and endocytosis in autophagosome biogenesis. Autophagy *10*, 182–184.

Ravikumar, B., Moreau, K., Jahreiss, L., Puri, C., and Rubinsztein, D.C. (2010). Plasma membrane contributes to the formation of pre-autophagosomal structures. Nat. Cell Biol. *12*, 747–757.

Razi, M., and Tooze, S. (2009). Correlative light and electron microscopy. Methods Enzymol. *452*, 261–275.

Real, F., and Mortara, R. (2012). The diverse and dynamic nature of leishmania parasitophorous vacuoles studied by multidimensional imaging. PLoS Negl. Trop. Dis. *6*, e1518.

Real, F., Pouchelet, M., and Rabinovitch, M. (2008). Leishmania (L.) amazonensis: Fusion between parasitophorous vacuoles in infected bone-marrow derived mouse macrophages. Exp. Parasitol. *119*, 15–23.

Reiling, N., Blumenthal, a, Flad, H.D., Ernst, M., and Ehlers, S. (2001). Mycobacteria-induced TNF-alpha and IL-10 formation by human macrophages is differentially regulated at the level of mitogen-activated protein kinase activity. J. Immunol. *167*, 3339–3345.

Ridley, D.S. (1980). A histological classification of cutaneous leishmaniasis and its geographical expression. Trans. R. Soc. Trop. Med. Hyg. *74*, 515–521.

Ridley, M.J., and Wells, C.W. (1986). Macrophage-parasite interaction in the lesions of cutaneous leishmaniasis. An ultrastructural study. Am. J. Pathol. *123*, 79–85.

Rittig, M.G., and Bogdan, C. (2000). Leishmania-host-cell interaction: Complexities and alternative views. Parasitol. Today *16*, 292–297.

Rittig, M.G., Schröppel, K., Seack, K.H., Sander, U., N'Diaye, E.N., Maridonneau-Parini, I., Solbach, W., and Bogdan, C. (1998). Coiling phagocytosis of trypanosomatids and fungal cells. Infect. Immun. *66*, 4331–4339.

Rizvi, F.S., Ouaissi, M.A., Marty, B., Santoro, F., and Capron, A. (1988). The major surface protein of Leishmania promastigotes is a fibronectin-like molecule. Eur. J. Immunol. *18*, 473–476.

Rodman, J.S., Levy, M. a, Diment, S., and Stahl, P.D. (1990). Immunolocalization of endosomal cathepsin D in rabbit alveolar macrophages. J. Leukoc. Biol. *48*, 116–122.

Rodríguez, N.E., Gaur, U., and Wilson, M.E. (2006). Role of caveolae in Leishmania chagasi phagocytosis and intracellular survival in macrophages. Cell. Microbiol. *8*, 1106–1120.

Rodríguez, N.E., Dixit, U., Allen, L. a H., and Wilson, M.E. (2011). Stage-specific pathways of Leishmania infantum chagasi entry and phagosome maturation in macrophages. PLoS One *6*.

Romano, P.S., Arboit, M.A., Vázquez, C.L., and Colombo, M.I. (2009). The autophagic pathway is a key component in the lysosomal dependent entry of Trypanosoma cruzi into the host cell. Autophagy *5*, 6–18.

Rosenthal, L. a., Sutterwala, F.S., Kehrli, M.E., and Mosser, D.M. (1996). Leishmania major-human macrophage interactions: Cooperation between Mac-1 (CD11b/CD18) and complement receptor type 1 (CD35) in promastigote adhesion. Infect. Immun. *64*, 2206–2215.

Russell, D.G., and Wilhelm, H. (1986). The involvement of the major surface glycoprotein (gp63) of Leishmania promastigotes in attachment to macrophages. J. Immunol. *136*, 2613–2620.

Russell, D.G., and Wright, S.D. (1988). Complement receptor type 3 (CR3) binds to an Arg-Gly-Asp-containing region of the major surface glycoprotein, gp63, of Leishmania promastigotes. J. Exp. Med. *168*, 279–292.

Russell, D.G., Xu, S., and Chakraborty, P. (1992). Intracellular trafficking and the parasitophorous vacuole of Leishmania mexicana-infected macrophages. J. Cell Sci. *103*, 1193–1210.

Rust, M.J., Bates, M., and Zhuang, X. (2006). Sub-diffraction-limit imaging by stochastic optical reconstruction microscopy (STORM). Nat. Methods *3*, 793–795.

Sacks, D.L., and Perkins, P. V (1984). Identification of an infective stage of Leishmania promastigotes. Science *223*, 1417–1419.

Sanjuan, M. a, Dillon, C.P., Tait, S.W.G., Moshiach, S., Dorsey, F., Connell, S., Komatsu, M., Tanaka, K., Cleveland, J.L., Withoff, S., et al. (2007). Toll-like receptor signalling in macrophages links the autophagy pathway to phagocytosis. Nature *450*, 1253–1257.

Sannes, P.L., Katsuyama, T., and Spicer, S.S. (1978). Tannic acid-metal salt sequences for light and electron microscopic localization of complex carbohydrates. J. Histochem. Cytochem. *26*, 55–61.

Schmidt, R., Wurm, C.A., Punge, A., Egner, A., Jakobs, S., and Hell, S.W. (2009). Mitochondrial cristae revealed with focused light. Nano Lett. *9*, 2508–2510.

Schütze et al. (2003). Vorrichtung zur Isolierung von an magnetischen Partikeln gebundenem biologischen Material in einem Magnetfeld.

Shintani, T., and Klionsky, D.J. (2004). Autophagy in health and disease: a double-edged sword. Science *306*, 990–995.

Da Silva, R.P., Hall, B.F., Joiner, K. a., and Sacks, D.L. (1988). CR1 mediates binding of L. major metacyclic promastigotes to human macrophages. Mem. Inst. Oswaldo Cruz *83 Suppl 1*, 459–463.

Sini, P., James, D., Chresta, C., and Guichard, S. (2010). Simultaneous inhibition of mTORC1 and mTORC2 by mTOR kinase inhibitor AZD8055 induces autophagy and cell death in cancer cells. Autophagy *6*, 553–554.

Smith, H.O., and Welcox, K.W. (1970). A Restriction enzyme from Hemophilus influenzae. J. Mol. Biol. *51*, 379–391.

Smith, W., Feldmann, M., and Londei, M. (1998). Human macrophages induced in vitro by macrophage colony-stimulating factor are deficient in IL-12 production. Eur. J. Immunol. *28*, 2498–2507.

Solovjov, D. a., Pluskota, E., and Plow, E.F. (2005). Distinct roles for the alpha and beta subunits in the functions of integrin alphaMbeta2. J. Biol. Chem. *280*, 1336–1345.

Srivastava, S., Swanson, S.K., Manel, N., Florens, L., Washburn, M.P., and Skowronski, J. (2008). Lentiviral Vpx accessory factor targets VprBP/DCAF1 substrate adaptor for cullin 4 E3 ubiquitin ligase to enable macrophage infection. PLoS Pathog. *4*, e1000059.

Von Stebut, E. (2007). Immunology of cutaneous leishmaniasis: The role of mast cells, phagocytes and dendritic cells for protective immunity. Eur. J. Dermatology *17*, 115–122.

Steinhäuser, C., Heigl, U., Tchikov, V., Schwarz, J., Gutsmann, T., Seeger, K., Brandenburg, J., Fritsch, J., Schroeder, J., Wiesmüller, K.H., et al. (2013). Lipid-Labeling facilitates a novel magnetic isolation procedure to characterize pathogen-containing phagosomes. Traffic *14*, 321–336.

Steinhäuser, C., Dallenga, T., Tchikov, V., Schaible, U.E., Schütze, S., and Reiling, N. (2014). Immunomagnetic isolation of pathogen-containing phagosomes and apoptotic blebs from primary phagocytes. Curr. Protoc. Immunol. *105*, 14.36.1–14.36.26.

Stenmark, H., Aasland, R., Toh, B.H., and D'Arrigo, A. (1996). Endosomal localization of the autoantigen EEA1 is mediated by a zinc- binding FYVE finger. J. Biol. Chem. *271*, 24048–24054.

Stout, R.D., and Suttles, J. (2004). Functional plasticity of macrophages: reversible adaptation to changing microenvironments. J. Leukoc. Biol. *76*, 509–513.

Swanson, J.A., and Baer, S.C. (1995). Phagocytosis by zippers and triggers. Trends Cell Biol. *5*, 89–93.

Sydor, T., von Bargen, K., Becken, U., Spuerck, S., Nicholson, V.M., Prescott, J.F., and Haas, A. (2008). A mycolyl transferase mutant of Rhodococcus equi lacking capsule integrity is fully virulent. Vet. Microbiol. *128*, 327–341.

Sydor, T., von Bargen, K., Hsu, F.F., Huth, G., Holst, O., Wohlmann, J., Becken, U., Dykstra, T., Söhl, K., Lindner, B., et al. (2013). Diversion of phagosome trafficking by pathogenic Rhodococcus equi depends on mycolic acid chain length. Cell. Microbiol. *15*, 458–473.

Tanaka, Y., Guhde, G., Suter, a, Eskelinen, E.L., Hartmann, D., Lüllmann-Rauch, R., Janssen, P.M., Blanz, J., von Figura, K., and Saftig, P. (2000). Accumulation of autophagic vacuoles and cardiomyopathy in LAMP-2-deficient mice. Nature *406*, 902–906.

Tanida, I., Minematsu-Ikeguchi, N., Ueno, T., and Kominami, E. (2005). Lysosomal turnover, but not a cellular level, of endogenous LC3 is a marker for autophagy. Autophagy *1*, 84–91.

Tchikov, V., and Schütze, S. (2008). Chapter Five Immunomagnetic Isolation of Tumor Necrosis Factor Receptosomes. Methods Enzymol. *442*, 101–123.

Tchikov, V., Fritsch, J., and Schütze, S. (2014). Separation of magnetically isolated TNF receptosomes from mitochondria. Methods Enzymol. *535*, 327–349.

Temin, H.M., and Mizutani, S. (1970). RNA-dependent DNA polymerase in virions of Rous sarcoma virus. Nature *226*, 1211–1213.

Tokuyasu, K.T. (1973). A technique for ultracryotomy of cell suspensions and tissues. J. Cell Biol. *57*, 551–565.

Towbin, H., Staehelin, T., and Gordon, J. (1979). Electrophoretic transfer of proteins from polyacrylamide gels to nitrocellulose sheets: procedure and some applications. Proc. Natl. Acad. Sci. U. S. A. *76*, 4350–4354.

Tsanev, R. (1965). Direct spectrophotometric analysis of ribonucleic acid fractionation by agar-gel electrophoresis. Biochim. Biophys. Acta *103*, 374–382.

Tulchin, N., Ornstein, L., and Davis, B.J. (1976). A microgel system for disc electrophoresis. Anal. Biochem. *72*, 485–490.

Turco, S.J., and Sacks, D.L. (1991). Expression of a stage-specific lipophosphoglycan in Leishmania major amastigotes. Mol. Biochem. Parasitol. *45*, 91–99.

Turco, S.J., Späth, G.F., and Beverley, S.M. (2001). Is lipophosphoglycan a virulence factor? A surprising diversity between Leishmania species. Trends Parasitol. *17*, 223–226.

Vergne, I., and Deretic, V. (2010). The role of PI3P phosphatases in the regulation of autophagy. FEBS Lett. *584*, 1313–1318.

Vermes, I., Haanen, C., Steffens-Nakken, H., and Reutelingsperger, C.P. (1995). A novel assay for apoptosis. Flow cytometric detection of phosphatidylserine expression on early apoptotic cells using fluorescein labelled Annexin V. J. Immunol. Methods *184*, 39–51.

Verreck, F.A.W., de Boer, T., Langenberg, D.M.L., Hoeve, M.A., Kramer, M., Vaisberg, E., Kastelein, R., Kolk, A., de Waal-Malefyt, R., and Ottenhoff, T.H.M. (2004). Human IL-23-producing type 1 macrophages promote but IL-10-producing type 2 macrophages subvert immunity to (myco)bacteria. Proc. Natl. Acad. Sci. U. S. A. *101*, 4560–4565.

Verreck, F.A.W., Boer, T. De, Langenberg, D.M.L., Zanden, L. Van Der, and Ottenhoff, T.H.M. (2006). Phenotypic and functional pro ling of human proin ammatory type-1 and anti-in ammatory type-2 macrophages in response to microbial antigens and IFN-□- and CD40L-mediated costimulation. J. Leukoc. Biol. *79*, 285–293.

Vieira, O. V, Botelho, R.J., and Grinstein, S. (2002). Phagosome maturation: aging gracefully. Biochem. J. *366*, 689–704.

Vieira, O. V., Botelho, R.J., Rameh, L., Brachmann, S.M., Matsuo, T., Davidson, H.W., Schreiber, A., Backer, J.M., Cantley, L.C., and Grinstein, S. (2001). Distinct roles of class I and class III phosphatidylinositol 3-kinases in phagosome formation and maturation. J. Cell Biol. *155*, 19–25.

Villinger, C., Gregorius, H., Kranz, C., Höhn, K., Münzberg, C., Von Wichert, G., Mizaikoff, B., Wanner, G., and Walther, P. (2012). FIB/SEM tomography with TEM-like resolution for 3D imaging of high-pressure frozen cells. Histochem. Cell Biol. *138*, 549–556.

Vinet, A.F., Fukuda, M., Turco, S.J., and Descoteaux, A. (2009). The Leishmania donovani lipophosphoglycan excludes the vesicular proton-ATPase from phagosomes by impairing the recruitment of Synaptotagmin V. PLoS Pathog. *5*, e1000628.

Waldo, S.W., Li, Y., Buono, C., Zhao, B., Billings, E.M., Chang, J., and Kruth, H.S. (2008). Heterogeneity of human macrophages in culture and in atherosclerotic plaques. Am. J. Pathol. *172*, 1112–1126.

Walther, P., and Ziegler, A. (2002). Freeze substitution of high-pressure frozen samples: The visibility of biological membranes is improved when the substitution medium contains water. J. Microsc. *208*, 3–10.

Walther, P., Wehrli, E., Hermann, R., and Müller, M. (1995). Double-layer coating for high-resolution low-temperature scanning electron microscopy. J. Microsc. *179*, 229–237.

Wanderley, J.L.M., da Silva, L.H.P., Deolindo, P., Soong, L., Borges, V.M., Prates, D.B., de Souza, A.P.A., Barral, A., de Freitas Balanco, J.M., do Nascimento, M.T.C., et al. (2009). Cooperation between apoptotic and viable metacyclics enhances the pathogenesis of leishmaniasis. PLoS One *4*, 1–11.

Wang, Y., Weiss, L.M., and Orlofsky, A. (2009). Host cell autophagy Is induced by toxoplasma gondii and contributes to parasite growth. J. Biol. Chem. *284*, 1694–1701.

Warburg and Schlein (1986). The effect of post-bloodmeal nutrition of Phlebotomus papatasi on the transmission of Leishmania major. Am J Trop Med Hyg. *35*, 926–930.

Wenzel, U.A., Bank, E., Florian, C., Forster, S., Zimara, N., Steinacker, J., Klinger, M., Reiling, N., Ritter, U., and van Zandbergen, G. (2012). Leishmania major parasite stage-dependent host cell invasion and immune evasion. FASEB J. *26*, 29–39.

WHO (2015). http://www.who.int/leishmaniasis/en/. accessed on 15/01/2015.

Wilson, M.E., and Pearson, R.D. (1986). Evidence that Leishmania donovani utilizes a mannose receptor on human mononuclear phagocytes to establish intracellular parasitism. J. Immunol. *136*, 4681–4688.

Wolfrum, N., Mühlebach, M.D., Schüle, S., Kaiser, J.K., Kloke, B.P., Cichutek, K., and Schweizer, M. (2007). Impact of viral accessory proteins of SIVsmmPBj on early steps of infection of quiescent cells. Virology *364*, 330–341.

World Health Organization (2010). Control of the leishmaniases. World Health Organ. Tech. Rep. Ser. 22–26.

Xu, W., Roos, A., Schlagwein, N., Woltman, A.M., Daha, M.R., and Van Kooten, C. (2006). IL-10-producing macrophages preferentially clear early apoptotic cells. Blood *107*, 4930–4937.

Xu, W., Schlagwein, N., Roos, A., van den Berg, T.K., Daha, M.R., and van Kooten, C. (2007). Human peritoneal macrophages show functional characteristics of M-CSF-driven anti-inflammatory type 2 macrophages. Eur. J. Immunol. *37*, 1594–1599.

Yang, Z., and Klionsky, D.J. (2010). Mammalian autophagy: Core molecular machinery and signaling regulation. Curr. Opin. Cell Biol. *22*, 124–131.

Ylä-Anttila, P., Vihinen, H., Jokitalo, E., and Eskelinen, E.L. (2009). 3D tomography reveals connections between the phagophore and endoplasmic reticulum. Autophagy *5*, 1180–1185.

Van Zandbergen, G., Hermann, N., Laufs, H., Solbach, W., and Laskay, T. (2002). Leishmania promastigotes release a granulocyte chemotactic factor and induce interleukin-8 release but inhibit gamma interferon-inducible protein 10 production by neutrophil granulocytes. Infect. Immun. *70*, 4177–4184.

Van Zandbergen, G., Klinger, M., Mueller, A., Dannenberg, S., Gebert, A., Solbach, W., and Laskay, T. (2004). Cutting edge: neutrophil granulocyte serves as a vector for Leishmania entry into macrophages. J. Immunol. *173*, 6521–6525.

Van Zandbergen, G., Bollinger, A., Wenzel, A., Kamhawi, S., Voll, R., Klinger, M., Müller, A., Hölscher, C., Herrmann, M., Sacks, D., et al. (2006). Leishmania disease development depends on the presence of apoptotic promastigotes in the virulent inoculum. Proc. Natl. Acad. Sci. U. S. A. *103*, 13837–13842.

Van Zandbergen, G., Solbach, W., and Laskay, T. (2007). Apoptosis driven infection. Autoimmunity *40*, 349–352.

Zenian, a, Rowles, P., and Gingell, D. (1979). Scanning electron-microscopic study of the uptake of Leishmania parasites by macrophages. J. Cell Sci. *39*, 187–199.

Zijlstra, E.E., Musa, A.M., Khalil, E.A.G., El Hassan, I.M., and El-Hassan, A.M. (2003). Post-kala-azar dermal leishmaniasis. Lancet Infect. Dis. *3*, 87–98.

Zilberstein, D., and Shapira, M. (1994). The role of pH and temperature in the development of Leishmania parasites. Annu. Rev. Microbiol. *48*, 449–470.

Zufferey, R., Nagy, D., Mandel, R.J., Naldini, L., and Trono, D. (1997). Multiply attenuated lentiviral vector achieves efficient gene delivery in vivo. Nat. Biotechnol. *15*, 871–875.

Zufferey, R., Dull, T., Mandel, R.J., Bukovsky, a, Quiroz, D., Naldini, L., and Trono, D. (1998). Self-inactivating lentivirus vector for safe and efficient in vivo gene delivery. J. Virol. *72*, 9873–9880.

Zufferey, R., Donello, J.E., Trono, D., and Hope, T.J. (1999). Woodchuck hepatitis virus posttranscriptional regulatory element enhances expression of transgenes delivered by retroviral vectors. J. Virol. *73*, 2886–2892.

Acronyms and Abbreviations

A	absorption
AF	aggregation factor
APIC	ULK pre-initiation complex
ATG	autophagy-related genes
ATP	adenosine triphosphate
AVd	degradative or late autophagic vacuoles
AVi	initial or early autophagic vacuoles
BHI agar	Brain Heart Infusion agar
BMDM	bone-marrow-derived macrophages
BNF	bionized nanoferrite
bp	basepairs
BCA	bicinchoninic acid
BCG	bacillus Calmette-Guerin
C3b	complement component C3b
C3bi	complement protein fragment C3bi
CD	cluster of differentiation
cDNA	complementary DNA
CDS	coding sequence
CIP	Calf Intestinal Alkaline Phosphatase
CL	cutaneous leishmaniasis
CLEM	correlative light and electron microscopy
cm^2	square centimeter
CMV	cytomegalovirus
CO_2	carbon dioxide
COX4	cytochrome c oxidase subunit 4
CPD	critical point drying
CR1	complement receptor 1 / CD35
CR3	complement receptor 3 / CD11b / CD18
CT-value	cycle threshold
DIC	differential interference contrast
DMEM	Dulbecco´s Modified Eagle Medium
DMSO	Dimethylsulfoxid
DNA	deoxyribonucleic acid
E	efficiency
ECE	Electrical Current Exclusion
EEA1	early endosome antigen 1
eGFP	enhanced green fluorescent protein
F	flagellum
FACS	fluorescence activated cell sorting
FcR	Fc receptors
FCS	fetal calf serum
FIB/SEM	focused ion beam/scanning electron microscopy
FIP200	focal adhesion kinase-interacting protein of 200 kDa
FL	fluorescence
for	forward
FRET	förster resonance energy transfer

FSC	forward scatter
FP	flagellum pocket
fPALM	fluorescence photoactivation localization microscopy
FYVE domain	zinc finger domain named after Fab1, YOTB, Vac1 and EEA1
g	gravitational force
G	gram
GA	glutaraldehyde
GAPDH	glyceraldehyde 3-phosphate dehydrogenase
GILPs	glycoinositolphospholipids
GM-CSF	granulocyte-macrophage colony-stimulating factor
gp63	glycoprotein 63
GPI	glycosylphosphatidylinositol
h	hour
H	homogenate
H_2O_2	hydrogen peroxide
HEK cells	human embryonic kidney cells
HIV	human immunodeficiency virus
hMDM I	human monocyte derived macrophages type I
hMDM II	human monocyte derived macrophages type II
HPF	High-Pressure-Freezing
HRP	horseradish peroxidase
IF	immunofluorescence
IG	immunogold
IL	interleukin
IN	integrase
INF	interferon
iNOS	inducible nitric oxide synthase
kb	kilobase
kDa	kilo dalton
KP	kinetoplast
L	liter
LAP	LC3-associated phagocytosis
LAMP	Lysosomal-associated membrane protein
LB	lipobiotin
LB medium	Lysogeny Broth medium
LC3	microtubule-associated protein 1A/B-light chain 3
LC3-I	cytosolic form of LC3
LC3-II	lipidated form of LC3
LCF	*Leishmania* chemotactic factor
LL37	antimicrobial peptide cathelicidin
Lm medium	*Leishmania* medium
L. major	*Leishmania major*
LPG	lipophosphoglycan
LTR	long-terminal-repeat
LSM	leukocyte separation medium
m	meter
M	magnetic fraction
M	microtubuli
M	molar

mA	milliampere
MACS	magnetic activated cell sorting
MCL	mucocutaneous leishmaniasis
M-CSF	macrophage colony-stimulating factor
MDM	monocyte-derived macrophages
MFs	macrophages
MHC	major histocompatibility complex
min	minute
MIP1-β	macrophage inflammatory protein 1 beta, also known as CCL4
mL	milliliter
mm	millimeter
mM	millimolar
MOI	multiplicity of infection
mRFP	monomeric red fluorescent protein
MT	mitochondrium
mTOR	mammalian target of rapamycin
MTMR3	myotubularin-related protein 3
N	nucleus
NADPH oxidase	nicotinamide adenine dinucleotide phosphate-oxidase
NEB	New England Biolabs
ng	nanogram
nm	nanometer
nM	nanomolar
NM	non-magnetic fraction
NNN medium	Novy, McNeal, Nicolle medium
NHS AF647	Succinimidylester AlexaFluor647
NO	nitrogen oxide
O2·-	hyperoxide anion / superoxide
PAMPs	pathogen-associated molecular patterns
PB	parasite body
PBMC	peripheral blood mononuclear cells
PCR	polymerase chain reaction
PE	phosphatidylethanolamine
PFA	paraformaldehyde
pg	picogramm
p.i.	post infection
PI	phosphatidylinositol
PI3P	phosphatidylinositol 3-phosphate
PtdIns3K	phosphatidylinositol 3-kinase
PKDL	post-kala-azar dermal leishmaniasis
PM	parasite membrane
PMN	polymorphonuclear neutrophil granulocytes
PRRs	pattern recognition receptors
PS	phosphatidylserine
PS-	phosphatidylserine-negative
PS+	phosphatidylserine-positive
P/S	penicillin/streptomycin
PtdIns3K/PI3K	phosphatidylinositol 3-kinase
PV	parasitophorous vacuole

PVDF	polyvinylidene fluoride
PX domain	phox homology domain
qPCR	quantitative real-time PCR
Rab	rabenosyn
rev	reverse
RT	room temperature
RT	reverse transcriptase
RNA	ribonucleic acid
ROI	reactive oxygen intermediates
ROS	reactive oxygen species
rpm	rotations per minute
S	SFFV promotor
SAMHD1	SAM domain and HD domain-containing protein 1
SD	standard deviation
SDS-PAGE	sodium dodecyl sulfate polyacrylamide gel electrophoresis
sec / s	second
SEM	scanning electron microscopy
SFFV	spleen focus-forming virus
SIM	structured illumination microscopy
SIN	self-inactivating
siRNA	small interfering RNA
SNARE	soluble N-ethylmaleimide-sensitive-factor attachment receptor
SSC	sideward scatter
STED	stimulated emission depletion microscopy
STEM	scanning transmission electron microscopy
STORM	stochastic optical reconstruction microscopy
TEM	transmission electron microscopy
TfR	transferrin receptor, also known as CD71
TGF- β	transforming growth factor beta
TIM4	T cell immunoglobulin domain and mucin domain protein-4
TL	total lysate
TL	transmitted light
TLRs	toll-like-receptors
Tm	melting point
TNF-α	tumor necrose factor alpha
TU/mL	transducing units per mL
U	unit
Ub-I/Ub-II	ubiquitin-like conjugation system
ULK1	unc-51 like autophagy activating kinase 1
UV	ultraviolet
V	Volt
VAMPs	vesicle-associated membrane proteins
V-ATPase	vacuolar-type H^+-ATPase
VL	visceral leishmaniasis
VLP	virus-like particle
v/v	volume per volume %
W	WPRE element
WB	Western Blot
WHO	world health organization

WPRE	woodchuck hepatitis virus posttranscriptional regulatory element
w/v	mass per volume %
µg	microgram
µL	microliter
µM	micromolar
°C	degree celsius
%	percent

List of figures

List of tables

Declaration/Erklärung

Hiermit versichere ich, dass ich die vorgelegte Dissertation mit dem Titel

„*Leishmania major* promastigote entry of an autophagy-like compartment and amastigote escape from the parasitophorous vacuole“

selbstständig verfasst und keine anderen als die angegebenen Quellen und Hilfsmittel verwendet habe. Die Stellen der Dissertation, die anderen Werken und Veröffentlichungen dem Wortlaut oder dem Sinn nach entnommen wurden, sind durch Quellenangaben gekennzeichnet.

Die Dissertation wurde in der jetzigen oder in ähnlicher Form noch an keiner anderen Hochschule eingereicht und hat noch keinen sonstigen Prüfungszwecken gedient.

Langen, 30. Juni 2015

M. Thomas

(Meike Thomas)

Copyright

Acknowledgements

I would like to thank…